Diss. ETH Nr. 16519

Multiscalar porosity structure of a Miocene reefal carbonate complex

A dissertation submitted to the

SWISS FEDERAL INSTITUTE OF TECHNOLOGY (ETH)

ZÜRICH

For the degree of

DOCTOR OF NATURAL SCIENCE

presented by

DAVID JAEGGI

Dipl. Geologe

Swiss Federal Institute of Technology (ETH) Zürich

born September 2nd 1974

Mümliswil-Ramiswil (Solothurn)

Accepted on the recommendation of

Prof. Dr. Simon Löw, examiner

Dr. Martin Herfort, co-examiner

Prof. Dr. Flavio Anselmetti, co-examiner

Dr. Philippe Pézard, co-examiner

2006

A)   Acknowledgments

This work has been conducted at the chair of Engineering Geology ETH Zurich in the framework of a European Union project called ALIANCE (Advanced logging investigations of aquifers in coastal environments) led by Dr. Philippe Pézard (University of Montpellier). I thank my supervisor Professor Simon Löw for his support and for giving me the opportunity to work with an excellent equipment and professional infrastructure within such an interesting geological environment. With Dr. Nathalie Van Meir I learnt to do borehole logging and to perform pumping tests under extreme climatic and geological conditions. The collaboration with Nathalie was extremely fruitful and on Mallorca she taught me lots of useful things about the Spanish mentality and language. Furthermore, I want to thank my co-examiner Dr. Martin Herfort who was not only of indispensable help in the field but as well extensively supported me during data analysis and the final stages of my thesis when I had to bring all this to paper. Besides the scientific support for my doctorate thesis he could motivate me additionally for a new hobby – speleology in active karstic systems.

Furthermore, I would like to thank our collaborators within the Project namely Dr. Philippe Pézard, who supported me as co-examiner, Dr. Gerard Lods and all people I know from University of Montpellier for providing me with excellent logging data and for advising me during my doctorate thesis in the field and per email. Professor Modesto Montoto and his right hand Felix Mateos I thank for their introduction into digital image analysis and their enthusiasm for my work. This work would never have been possible, if there were not the Gobiern Balear, which supported our project on Mallorca with manpower and finally with a 28 ton state of the art drilling machine. Among numerous people from the Gobiern Balear to whom I had contact, I want to emphasize the two hydrogeologists Concha Gonzalez and Alfredo Baron, the man who knows every well on Mallorca, Ramon and the driller with the sunglasses Juan Antonio. All those people were always very helpful in the field and found time despite their full agenda.

For a Swiss geologist Miocene reefal carbonates are exotic geology, which is not present in our country. However, with Professor Luis Pomar I had support from a man who has been working almost 30 years on the platform of Llucmajor and who knows almost everything about it. I could enjoy his excursions and courses, which built together an excellent introduction for the geology at our test site near Campos. At ETH Zurich I got further support in determining facies from thin sections and rock samples by Dr. Heinz Furrer, whose course about paleoecology of reefs was ideal for better understanding the geology of my study area. Professor Flavio Anselmetti helped me determining porosity and pore types of these carbonate rocks. With his experience in carbonate rocks he could give me many useful hints about how to solve specific technical and scientific problems. Furthermore, he agreed to be a co-examiner of my thesis.

Thin sections built an important part of my work. I thank Frowin Pirovino for the preparation of dozens of thin sections and the photographer Urs Gerber for scanning them all. He furthermore introduced me into professional photography, which I directly applied on the semi-industrial core photography (imaging 500 m of cored material). Furthermore, I would like to thank Gabriele Peschke from the institute of building materials for the ESEM-images, which she made with both interest and high precision. Professor Renee Heilbronner from University of Basel provided me with software for digital image analysis and helped me

B) Table of contents

C)   List of figures

D)   List of tables

E)   Abstract – Zusammenfassung

Abstract

In this thesis the porosity structure of a Miocene reefal carbonate complex was investigated on three different scales of investigation. The variety of datasets and different investigation methods, which directly or indirectly image the pore space, led to a comprehensive image of the subsurface. Heterogeneity at different scales can only be understood correctly if there is a sound knowledge about the depositional and post-depositional history of the whole carbonate platform.

At the rock-matrix-scale an extensive sampling program was performed, which targeted on the detailed characterization of pore structure and sedimentology of stratigraphic elements, such as lithofacies types and their subtypes. Digital image analysis on thin sections and physical measurements of porosity respectively permeability on 1inch mini-cores were performed. For each individual lithofacies type diagnostic features of the pore structure were found. High permeability was recorded in outer lagoon and proximal talus, which is mainly due to well connected moldic porosity. Especially within proximal talus large and elongated molds with large shape factors are leading to a prominent depositional anisotropy. In parts of the upper proximal talus in addition to the depositional anisotropy a diagenetic anisotropy could be detected, however restricted to smaller pore size classes and thus less important for permeability. In distal talus porosity can reach very high amounts but the small and round shaped molds are barely interconnected within the micritic matrix and thus permeability is low. Samples with a bimodal pore size distribution observed in outer lagoon and parts of proximal talus do not follow the common correlations between permeability and parameters describing the pore geometry. In these unsorted sediments, with mostly complex pore size distributions, averaged pore size parameters are not useful for characterizing permeability, since a few extreme poreshapes and -sizes can have a large impact on permeability. Thus, unlike proposed by many authors no pore size-dependent correlation of porosity versus permeability could be observed. The energetic milieu and location within the former carbonate factory significantly defines the primary parameters, like grain size distribution, sorting, sedimentary anisotropy and mud content. Permeability of the rock matrix is not only dependent on these primary factors but also on secondary processes. The subsequent diagenetic overprint led to remarkable changes of the rock properties, like formation of moldic porosity, recrystallization of the coral framework and partial occlusion of pore space by blocky spar. The latter two processes in reef core at least partly can be related to karst processes.

Heterogeneity at the borehole-scale is known to be an important control on reservoir behavior and has been investigated extensively with wireline borehole logs. It could be shown, that an important part of the total reservoir porosity is of a vuggy pore type. Lithofacies types control the primary pore structure and to a certain degree guide post-depositional processes. Reef core is the most heterogeneous lithofacies type, where primary and secondary pores can be remarkably enlarged and interconnected to channels, if supported by karst. The channel-system, which is developed at the bottom of the reef core proved to be the most permeable feature of the reef complex. Large dissolution cavities and the interconnecting channels are associated with dense and recrystallized rock, leading to high porosity contrasts. To a certain degree sequence boundaries and as well residual clays may locally act as seals. The non-standard method of scanning the acoustic travel-time image revealed cyclicity of vuggy pores

>1 cm within proximal talus and made it possible to determine REV's of each individual lithofacies type, if the dataset was long enough. One of the most prominent boundaries, with an abrupt change of the pore structure, is doubtless the transition proximal/distal talus. Here especially the sonic tool revealed a change in pore structure from large and elongated moldic pores to small and round shaped molds within a micritic, framework-like matrix, leading to a remarkable reduction of permeability at equal total porosity at the rock-matrix-scale.

At the crosshole-scale sequence stratigraphy in combination with outcrop analogues and geophysical investigations, such as electrical resistivity tomography and seismic tomography, have been applied. From the observations made at the test site it can be stated that the geometry and sedimentary structure is comparable to the Cap Blanc reefs at the well exposed cliff coast. The main focus was set on the crosshole lateral and vertical distribution of large scale heterogeneity, such as karst, zones of high electrical resistivity and high seismic velocity, their evolution and internal pore structure. The high resistivity contrasts observed at several levels in the reef core display the complexity of the distribution of large scale primary and secondary porosity, which acted as a nucleus for karstic processes at certain levels. Results have shown that a complex and lateral continuous network of karstic channels is present within reef core, which leads to extremely permeable features at several distinct horizons. It could be shown, that the high velocity zone is only partly controlled by the extension of the reef core. Other controls are diagenetic, of which sea level stillstands are the most important. The role of sea level stillstands is discussed with a special emphasis on the Younger Dryas-event, which overlaps with the lower part of the high velocity zone. The upper parts are mainly caused by the neomorphosed coral framework and diagenetically altered rock in the vicinity of karstified horizons. Low resistivity zones are correlated with karstified horizons and can be traced laterally. A channeling is present, which interconnects larger primary and secondary pores. These pores are unevenly distributed on the karstified horizons, which leads to complex traces of the channels in the horizontal direction.

The integration of information originating from smaller scales was performed permanently during the analysis of the pore structure at larger scales. The investigations have shown that in most lithofacies types, porosity at the rock-matrix-scale builds a significant fraction of the overall porosity. The reef core exhibits a pronounced scale dependency concerning permeability. Permeability at the rock-matrix-scale is very low, whereas at larger scales it is highest. The high permeability of the karstic system within the reef core in combination with the pore structure at the rock-matrix-scale in the adjacent lithofacies types is crucial for an enhanced water management on the Llucmajor platform. Zones of high electrical resistivity respectively high seismic velocity have been recorded within reef core and the upper proximal talus. These zones have been recognized by different methods at all three scales of investigation and they are controlled by sea level stillstands, which affected the entire platform. The impact of these stillstands on the pore space could be studied at the rock-matrix-scale, where cements occluded the pore space of smaller pore classes and led to secondary anisotropy. The pore structure within outer lagoon and proximal talus as well allows for a good productivity of the aquifer, however, orders of magnitudes lower than the karst-system. A remarkable change of the pore structure from moldic-intergranular to framework-like moldic is present at the transition proximal/distal talus, resulting in low permeability at high porosity.

Zusammenfassung

In der vorliegenden Dissertation wurde die Porositäts-Struktur eines Miozänen Riffkarbonates auf drei unterschiedlichen Untersuchungsmassstäben behandelt. Die Vielfalt von Datensätzen und unterschiedlichen Methoden, welche direkt oder indirekt den Porenraum abbilden, führte zu einem umfassenden Verständnis des geologischen Untergrundes. Heterogenität auf unterschiedlichsten Skalenbereichen kann nur verstanden werden, wenn die Ablagerungs-geschichte und die diagenetischen Prozesse der ganzen Riffplattform exakt bekannt sind.

Auf dem Massstab der Gesteinsmatrix wurden umfangreiche Proben genommen, welche auf die detaillierte Erfassung der Porenstruktur und Sedimentologie von stratigraphischen Elementen, wie Lithofaziestypen und ihre Subtypen, abzielten. Digitale Bildanalyse an Dünnschliffen und physikalische Messungen von Porosität und Permeabilität an 1inch Mini-Kernen wurden in umfangreichem Masse durchgeführt. Für jeden einzelnen Lithofaziestyp wurden diagnostische Merkmale erfasst. Hohe Permeabilitäten wurden in der äusseren Lagune und im proximalen Talus gemessen, was hauptsächlich eine Folge der gut verbundenen Molds ist. Insbesondere im proximalen Talus führen grosse und längliche Molds mit grossen shape-Faktoren zu einer wichtigen sedimentären Anisotropie. In Teilen des oberen proximalen Talus tritt zusätzlich eine diagenetische Anisotropie auf, welche jedoch nur auf kleinere Porengrössenklassen beschränkt ist. Folgedessen ist diagenetische Anisotropie weniger wichtig für die Permeabilität. Im distalen Talus werden hohe Porositäten erreicht aber die kleinen und rundlichen Molds in mikritischer Matrix sind untereinander kaum verbunden, und deshalb ist die Permeabilität vergleichsweise gering. Proben mit einer bimodalen Porengrössenverteilung sind typisch für die äussere Lagune und den proximalen Talus. Diese folgen nicht den allgemeinen Korrelationen zwischen Permeabilität und Porenparametern, welche die Porengeometrie beschreiben. Darüber hinaus sind in diesen unsortierten Sedimenten mit meist komplexen Porengrössenverteilungen durchschnittliche Porenparameter nicht brauchbar, um die Permeabilität zu charakterisieren, da im Allgemeinen wenige extreme Porenformen und Porengrössen permeablitätsbestimmend sind. Folglich kann die von vielen Autoren vorgeschlagene porengrössenabhängige Korrelation zwischen Porosität und Permeabilität nicht beobachtet werden. Das energetische Milieu und der genaue Standort innerhalb der „Karbonat-Fabrik" definieren zusammen die primären Parameter wie Porengrössenverteilung, Sortierung, sedimentäre Anisotropie und Gehalt an Karbonat-schlamm. Die Permeabilität der Gesteinmatrix ist nicht nur von diesen primären Faktoren abhängig, sondern auch von sekundären Prozessen. Die nachfolgende Diagenese führte zu wichtigen Veränderungen der Gesteinseigenschaften, wie z.B. die Bildung von Molds, die Rekristallisation der Korallenstruktur und die Reduktion des Porenraumes durch sparitischen Zement. Die beiden letztgenannten Prozesse können im Riffkern zumindest teilweise mit Karst in Verbindung gebracht werden.

Heterogenität auf dem Bohrloch-Massstab bildet einen wichtigen Faktor für das hydraulische Verhalten eines Reservoirs und wurde deshalb in der vorliegenden Arbeit intensiv mit Hilfe von Bohrloch-Messverfahren untersucht. Es konnte gezeigt werden, dass ein wichtiger Teil der totalen Reservoirporosität Lösungsporen sind. Die Lithofaziestypen kontrollieren die primäre Porenstruktur und beeinflussen den Verlauf der sekundären Prozesse bis zu einem gewissen Grad. Der Riffkern ist der heterogenste Lithofaziestyp, wo, falls Karst im Spiel ist, primäre und sekundäre Poren stark vergrössert und zu regelrechten Kanälen verbunden sein können. Das System von Kanälen, welches sich am Grund des Riffkerns entwickelt hat, ist bei weitem die durchlässigste Zone des Riffkomplexes. Grosse Lösungshohlräume und die verbindenden Kanäle treten zusammen mit dichtem und rekristallisiertem Gestein auf, was zu einem hohen Porositätskontrast führt. Sequenzgrenzen und residuale Lehme können lokal als Stauer wirken. Die neue Methode des Akkustik-Laufzeiten-Scans führte zur Entdeckung der

Zyklizität von Lösungsporen >1 cm im proximalen Talus und ermöglichte zusätzlich bei genügend langen Datensätzen die Bestimmung des repräsentativen Elementarvolumens jedes einzelnen Lithofaziestyps. Eine der auffälligsten Grenzen mit einem abrupten Wechsel der Porenstruktur ist zweifellos der Übergang vom proximalen zum distalen Talus. Insbesondere mit dem Sonic-Messverfahren wurde der Wechsel der Porenstruktur von grossen und länglichen zu kleinen und rundlichen moldic-Poren, eingebettet in einer mikritischen und gerüstähnlichen Matrix, erfasst. Dieser Wechsel führt zu einem markanten Rückgang der Permeabilität bei gleich bleibender totaler Porosität auf dem Massstab der Gesteinsmatrix.

Auf dem Massstab des Teststandorts wurde Sequenz-Stratigraphie in Kombination mit Erfahrungen aus analogen Aufschlüssen von der Küste und geophysikalischen Untersuchungsmethoden, wie elektrische und seismische Tomographie, angewandt. Aufgrund der Beobachtungen, welche am Teststandort gemacht wurden kann eindeutig gesagt werden, dass die Geometrie und die sedimentäre Struktur den Cap Blanc Riffen an der Küste sehr ähnlich ist. Das Hauptaugenmerk wurde in diesem Teil auf die laterale und vertikale Verteilung von Karst und Hochwiderstands- resp. Hochgeschwindigkeitszonen, ihre Entstehung und interne Porenstruktur gelegt. Die starken Widerstandsunterschiede, welche auf verschiedenen Niveaus im Riffkern beobachtet wurden, zeigen die Komplexität der Verteilung von grossskaliger primärer und sekundärer Porosität, welche als Initialkern für Karstprozesse fungierte. Die Resultate haben gezeigt, dass im Riffkern ein komplexes und lateral kontinuierliches Netzwerk von verkarsteten Kanälen vorhanden ist, welches auf verschiedenen Niveaus zu permeablen Zonen führt. Im Weiteren konnte gezeigt werden, dass die Hochgeschwindigkeitszone nur teilweise durch die Ausdehnung des Riffkerns kontrolliert ist. Andere Einflussfaktoren sind diagenetischer Art, von denen die Meeresspiegelstillstände am wichtigsten sind. Die Rolle dieser Stillstände wird unter spezieller Betrachtung des Younger Dryas-Ereignisses diskutiert, welches mit dem unteren Teil der beobachteten Hochgeschwindigkeitszone übereinstimmt. Die oberen Teile dieser Zone können vor allem durch neomorphosierte Korallen und diagenetisch verändertes Gestein unmittelbar bei Karsthorizonten erklärt werden. Zonen mit tiefem elektrischem Widerstand korrelieren mit Karsthorizonten und können lateral verfolgt werden. Die Karst-Kanäle verbinden grössere primäre und sekundäre Poren. Diese Poren sind im Riffkern ungleichmässig verteilt, was zu einem komplexen Verlauf dieser Kanäle in horizontaler Richtung führt.

Die Integration von Information aus kleinen Skalenbereichen wurde während der Analyse der Porenstruktur auf grösseren Untersuchungsmassstäben permanent durchgeführt. Die Untersuchungen haben gezeigt, dass die Porosität auf dem Massstab der Gesteinsmatrix bei den meisten Lithofaziestypen einen signifikanten Teil der Gesamtporosität bildet. Der Riffkern weist bezüglich der Permeabilität eine ausgeprägte Skalenabhängigkeit auf. Auf dem Massstab der Gesteinsteinsmatrix ist die Permeabilität sehr gering, auf grösseren Massstäben hingegen ist sie am höchsten. Die Kenntnis der hohen Permeabilität des Karstsystems innerhalb des Riffkerns und der Porenstruktur der Gesteinsmatrix in den angrenzenden Lithofaziestypen ist wichtig für eine nachhaltige Wasserbewirtschaftung auf der Llucmajor Plattform. Zonen mit hohem elektrischem Widerstand, resp. hoher seismischer Geschwindigkeit wurden im Riffkern und im oberen proximalen Talus beobachtet. Diese Zonen wurden mit unterschiedlichen Methoden auf allen drei Untersuchungsmassstäben erkannt und sind die Folge von früheren Meeresspiegelstillständen, welche die ganze Plattform beeinflussten. Der Einfluss dieser Meeresspiegel auf den Porenraum konnte auf dem Massstab der Gesteinsmatrix studiert werden, wo Zemente den Porenraum von kleineren Porenklassen verschlossen und so zu einer sekundären Anisotropie führten. Die Porenstruktur in der äusseren Lagune und im proximalen Talus ist auch verantwortlich für die hohe Ergiebigkeit des Aquifers, jedoch anteilsmässig viel geringer als das Karstsystem. Ein

bemerkenswerter Wechsel der Porenstruktur von moldic-intergranular zu gerüstähnlich-moldic tritt an der Grenze von proximalem und distalem Talus auf, was zu einer geringen Permeabilität bei hoher Porosität führt.

1. Introduction

1.1. Objective and scientific approach

The objective of this thesis is the development of a multiscalar 3D-porosity-model of a reefal carbonate complex, which is based on geological data, such as core material and data from outcrop analogues and petrophysical data, such as wireline logs and lab tests. For a full understanding of the porosity structure at the µm- to decameter-scale, depositional and post-depositional processes and their impact on the porosity structure have been studied.

In 2002, a project called ALIANCE was initiated with EU funding to develop diagnostic technologies for use in characterizing aquifers suffering from salt water intrusion. Consequently 2003 and 2004 a test site was developed on the island of Mallorca, Spain. The test site is located on the Miocene reefal platform of Llucmajor, about 6 km off the coast near the town of Campos (Figure 1). Miocene reefal carbonates provide an important percentage of the worlds exploited oil reservoirs. The Miocene reefal platform of Llucmajor has reached a world reputation due to its readily accessible outcrops at the cliff coast. Especially the coastal part of the platform has been investigated extensively by numerous scientists regarding reef architecture, sedimentology, sequence stratigraphy and reef genesis and led to its status of a world wide reference site for Miocene prograding reefal platforms. Furthermore, the Llucmajor platform builds an aquifer of high socio-economic relevance for the island of Mallorca. Water is pumped out of the aquifer mainly for irrigation. Due to a missing regulative water management, at some locations piezometric levels have been dropping considerably during the last 20 years. As a consequence dramatic salt water intrusion took place, affecting even pumping wells, which are located far inland. Thus, a comprehensive understanding of geological and petrophysical aquifer parameters is indispensable and must build the basis for sustainable water-management.
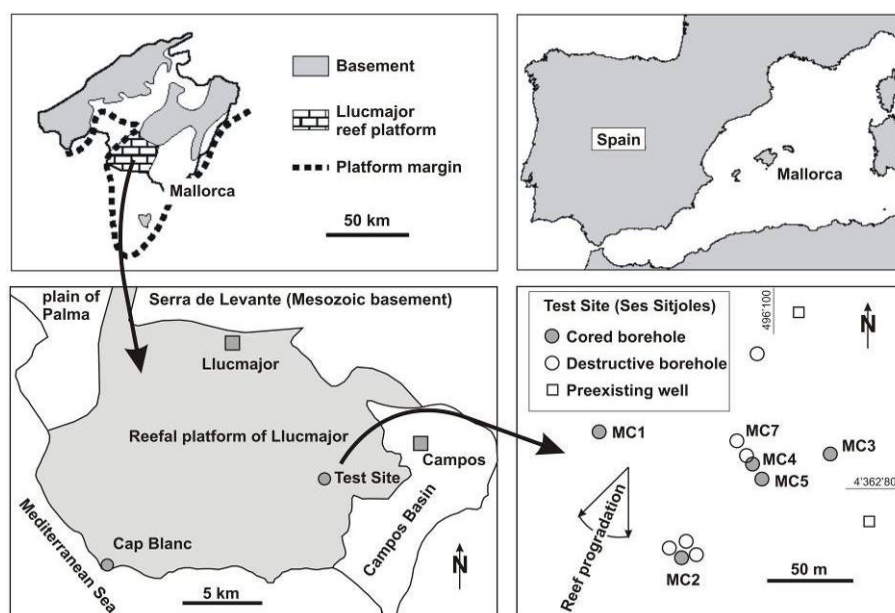
Figure 1:   The test site is located on the reefal platform of Llucmajor on the island of Mallorca, Spain (modified after Pomar & Ward, 1995).

Despite the importance of the Llucmajor carbonate platform up to now no comprehensive characterization of the pore- and permeability structure has been performed. Most work on this platform has been concentrated on large scale sequence stratigraphical concepts, platform evolution and distribution of architectural elements (1993; Pomar and Ward, 1995; 1999). Furthermore, sedimentology is well known (Pomar et al., 2004a; Pomar et al., 1996) and along the coast some studies about karstic phenomena have been performed (Ardila and Pomar, 2000; Baron et al., 1995; Gines and Gines, 1995). The pore structure is briefly mentioned in one publication, which mainly concentrates on reservoir-scale heterogeneity (Pomar and Ward, 1999).

The site called Ses Sitjoles comprises 5 fully cored 100 m deep boreholes (MC1-MC5) and 1 destructive borehole (MC7) on a cultivated field of 100x100 m (Figure 1). All boreholes were extensively logged with standard wireline logs and a dense sampling program was performed for lab tests. Furthermore, sophisticated single-hole and crosshole geophysics, such as electrical resistivity tomography and seismic tomography, were performed. The resulting huge dataset allowed for analyzing the complex 3D-pore structure of the reefal carbonate complex on three main scales of investigation (Figure 2). The rock-matrix-scale covers microporosity, which is only accessible by scanning electron microscopes up to moldic pores of a few mm size, captured by thin section scans. Digital image analysis and lab measurements on 1inch mini-cores provide the possibility to assess numerous pore parameters, which describe porosity and permeability. At the borehole-scale wireline logs capture information about the pore space at a scale of cm to m. The crosshole-scale is accessed by outcrop analogues, sequence stratigraphy on cored boreholes and through single-hole and crosshole tomography.
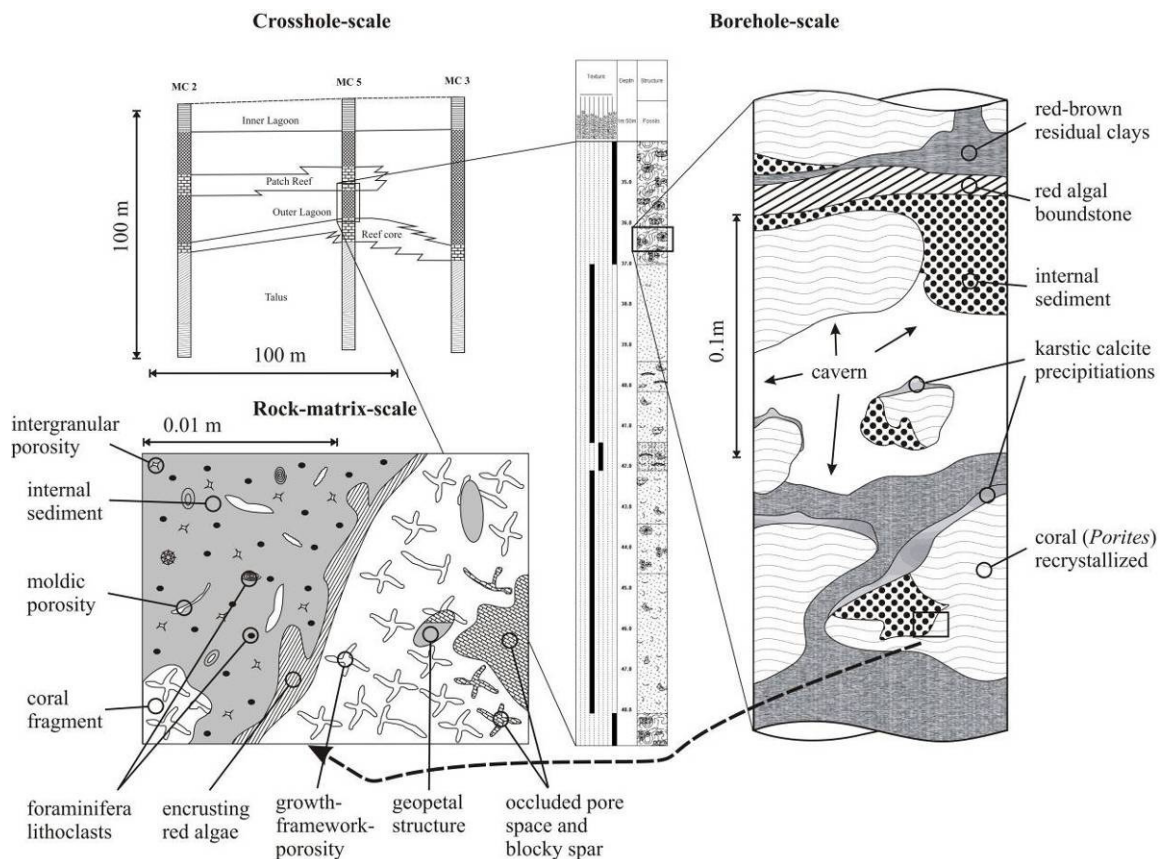
Figure 2:   Illustration of the multiscalar approach used in this study.

Building a multiscalar porosity model includes the combined interpretation of geological observations made on cored boreholes and petrophysical measurements performed in the boreholes themselves. A sound understanding of the depositional and post-depositional processes, which formed respectively modified the rockmass under investigation, is crucial for a correct interpretation of petrophysical signals. The borehole core samples are spot checks of the unaltered in situ fresh rock mass, which provided a more or less unbiased insight. Lots of investigation methods have been applied in order to capture as much independent data on different scales focusing on different petrophysical parameters as possible in order to get a comprehensive image of the subsurface. Many standard investigation methods, such as acoustic televiewer log, sonic log, induction log and impeller flowmeter imply the existence of a thick saturated zone. At Ses Sitjoles about 60 m of the boreholes are saturated. Also the single-hole and crosshole geophysical methods like electrical resistivity tomography (ERT) and seismic crosshole tomography were conducted within the saturated zone, yielding excellent images of the large-scale porosity structure.

This thesis contributes to a better understanding of the 3D-porosity structure of young and unburied carbonate hydrocarbon reservoirs and aquifers on the µm- to decameter-scale. It furthermore stresses the important role of depositional and post-depositional processes such as karst and the resulting impact on the entire porosity- and permeability system. In addition to the unique borehole cluster with extremely low borehole spacing of several meters to a few tens of meters, acoustic travel-time scan, ERT and seismic tomography have been applied successfully, methods which are not standard in reservoir characterization.

1.2.   Geological and hydrogeological outline

The investigation area lies on the upper Miocene Llucmajor platform in the south western part of the island. The flat lying and trough tectonical flexure slightly emerged reef complex is about 20 km wide and 100 m thick. Steep sea cliffs, which display in exquisite detail the facies architecture of the reefal unit, build the western and southern margins of the platform. To the east the Campos basin, which seems to have subsided only during Pleistocene time and to the north the Mesozoic basement of the Serra de Levante to which the platform onlaps build the borders (Figure 1). The platform prograded on a gentle depositional profile towards the south and southwest. It shows the characteristic features of a prograding reefal complex with aggradation and progradation. The upper Miocene was a time of tectonic stability and low terrigeneous influx, consequently reefal architecture and distribution of lithofacies are mainly controlled by sea level fluctuations of 4th to 7th order.

From top to bottom five main lithofacies types, namely inner lagoon, outer lagoon, reef core, proximal and distal talus have been encountered at Ses Sitjoles. They have been recognized in all cored boreholes, however their thickness varies considerably. Inner lagoon is characterized by layered shallow marine sediments and intermittent continental influence. Oolithes, packstones to grainstones with mangrove roots and calcrete horizons are more abundant in the upper part and layers of shallow marine packstones to wackestones and intercalated mudstones in the lower part of this lithofacies type. Below outer lagoon is present, which consists of bioclastic grainstones with a high amount of moldic porosity. Rudstone layers as well as single coral colonies or even small patch reefs are present within this lithofacies. The coral framework of the reef core builds the most heterogeneous part of the reefal complex. Here dense recrystallized corals of very low matrix porosity and dm-scale karstified pores are present, leading to pronounced porosity- and permeability contrasts. Between individual coral colonies internal sediment can be present, built of bioclastic material. Within proximal talus

below, layers of grainstones to rudstones are present, building clinobeds steeply dipping in the direction of reef-progradation. The clinobeds as well as the entire lithofacies type coarsen upwards. Distal talus consists of homogeneous mud-dominated packstones, which are extensively burrowed and gently dipping towards the basin.

Most of this flat lying platform has been buried no more than several tens of meters (Pomar and Ward, 1999). The platform was only slightly deformed by Pliocene-Pleistocene uplift, faulting and gentle flexure. Minor burial compaction and scarcity of pervasive cementation has preserved much of the primary porosity, which can reach man-size. Moldic porosity is the most important pore type on the platform. Karst plays an important role, especially within the coral framework of the reef core. These characteristics make the Llucmajor platform an excellent example for analyzing pre-deep-burial stratigraphic and diagenetic heterogeneities and thus it can serve as a model for other prograding platforms.

The Llucmajor platform builds an important aquifer that is bordered in the southern and western part by the Mediterranean Sea. The plain of Palma and the Campos basin are water divide boundaries and the Serra de Llevante provides some recharge to the platform (Figure 1). The aquifer's main recharge, however, comes from direct precipitation. The few cemented young reefal limestones are highly porous, reaching values at the rock-matrix-scale up to 55% and especially karstified sections within the reef core cause the high transmissivity, which is $120 \, m^2/s$ for the reefal complex (Van Meir et al., 2005). The test site is located within an agricultural region, where water levels are only slightly above sea level and hydraulic gradients are very low. As a consequence, large parts of the aquifer, that has a surface area of about 420 km^2, are already polluted with seawater. Due to excessive irrigation, saltwater intrusion is important, especially in the adjacent Campos basin. At Ses Sitjoles the water level lies roughly at 40 m below ground level. Freshwater is present till a depth of about 60 m. From 60 to 80 m the mixing-zone occurs, where conductivity rises from 5'000 µS/cm to more than 35'000 µS/cm. Below 80 m a fluid conductivity equal to that of sea water is reached. Generally the reef core lithofacies type is regarded as the most permeable zone within the reef complex, which is mainly due to extensive karst. As well outer lagoon and proximal talus are highly permeable, however, the hydraulic contrast to the reef core is still considerable.

1.3.   Contents of the thesis

This work consists of 3 main parts, chapters 2, 3 and 4. These chapters are written in manuscript form for later submission to journals. Chapter 2 deals with the rock-matrix-scale porosity structure. Here an appropriate sampling strategy is elaborated and the different scales of heterogeneity defined, so that lab measurements and field-scale data can be compared correctly. Geology observed on core material and thin sections are described and the pore space is characterized by data out of thin sections and measurements of porosity and permeability on standard 1inch mini-cores. The latter build the physical basis for the digital image analysis, which we used as the main tool for assessing the pore structure at the rock-matrix-scale. Digital image analysis here in contrast to studies of other authors will be performed on a combination of images from entire thin sections and images shot with an environmental scanning electron microscope. This method allows for analyzing the pore space at a much larger range than from single thin section images only. The optical measurements from digital image analysis were cross-checked with the physical measurements on 1inch mini-cores. In the end of the first part, a comparative analysis between petrophysical data obtained from the measurements and geological observations

made on thin sections and half core pieces will be given, in order to provide a genetic interpretation for the observed present state poro-perm-system at the rock-matrix-scale.

Chapter 3 deals with the borehole-scale porosity structure. It starts with the geology, which was observed on core material with a special emphasis on the porosity structure and sedimentary textures. Then the applied investigation methods will briefly be introduced. Here mainly the new method of the acoustic travel-time scan will be presented in more detail. This method proved to be very useful for determining borehole-scale porosity, where a significant percentage of total porosity is moldic or cavernous. Furthermore, by having full control about the scale of investigation, REV's and the periodicity of coarsening upward cycles within proximal talus can be studied. Together with the results from standard logs, data is integrated and for each lithofacies type the pore structure will be discussed individually and a clear distinction between primary or depositional porosity, secondary porosity, which is the result of diagenetic processes and tertiary karst porosity will be made. Finally based on the observations made on the pore structure, possible implications for the hydraulic behavior of the reservoir will be discussed.

Chapter 4 is about the crosshole-scale porosity structure. First the geological setting and the parameters, which control the crosshole-scale heterogeneity are presented in short. Then the three main applied methods, namely sequence stratigraphy on boreholes in combination with outcrop analogues, electrical resistivity tomography and seismic tomography are presented and their results are discussed subsequently. In this chapter special emphasis is put on the development and distribution of karst and the possibilities to correlate resistivity- and velocity anomalies between the boreholes. In the discussion of chapter 4 the role of sea level stillstands, such as the Younger Dryas event, are discussed and their impact on the pore structure of the reefal complex studied. It is shown that the high-velocity- and high-resistivity-zone is of a composite origin, which in the lower part is influenced by the sea level stillstand of the Younger Dryas and in the upper part by recrystallized coral colonies and karst-related cementation and precipitation. Furthermore, large scale reservoir heterogeneity is characterized and the implications for the reservoir behavior discussed.

A brief overall synthesis together with some conclusions and perspectives is developed in chapter 5.

2. Rock-Matrix-Scale Porosity Structure of a Miocene Reefal Carbonate, Mallorca (Spain)

D. Jaeggi, M. Herfort, S. Löw

Abstract

The objective of this chapter is to describe and to understand the 3D-porosity structure of the Miocene reefal limestones, which have been investigated on the Ses Sitjoles test site (Llucmajor platform, Mallorca, Spain) at the rock-matrix-scale (µm-cm-scale). In order to achieve this goal, an extensive sampling program was performed, which targeted on representative stratigraphic elements, such as lithofacies types and their subtypes of three fully cored 100 m deep boreholes MC2, MC3 and MC5. On these samples a variety of methods, which allow for determining optical and physical parameters with very different approaches have been used such as a visual description and interpretation of thin sections, porosity and permeability measurements on 1inch mini-cores and an extensive digital image analysis on thin sections including determination of total optical porosity (TOP), heterogeneity and anisotropy from the autocorrelation function (ACF) and an analysis of the 3D-pore size distribution. All of these methods provide an insight into a part of the pore structure and finally the synthesis of all these investigation methods together with elaborated cross-checks has led to the overall understanding of the 3D-porosity- and permeability structure at the rock-matrix-scale. The exact definition of which part of the pore system information is captured with an individual investigation method is crucial for a correct interpretation of the petrophysical signals. In a highly heterogeneous environment like the Llucmajor reefal platform, the final output of a measurement is strongly scale-dependent and reliable data is achievable only if sound geological knowledge is combined with geostatistical concepts. For each lithofacies type and its subtypes a geological description will be given and typical porosity-values and pore size distribution-curves will be presented together with descriptions of isotropy and heterogeneity of the investigated samples. The relationship between observed pore structure and measured permeability will be discussed. The occurring pore types and their spatial distribution are described and an integrated interpretation of geological and petrophysical data is provided together with a discussion of the depositional and post-depositional processes, which led to the present state of the poro-perm-system at the rock-matrix-scale. The investigations have shown that the division of the reefal unit into 5 main lithofacies types is correct and diagnostic features of the pore structure at the rock-matrix-scale could be found. Samples with a bimodal pore size distribution were found to be important controls on the permeability behavior of the rock matrix especially within outer lagoon and the lower part of proximal talus. Furthermore, a primary sedimentary and a secondary diagenetic anisotropy were found of which only the primary one is important for the fluid flow. The highly porous pore structure of the mud-dominated distal talus consists of small and round shaped moldic pores in a recrystallized micritic matrix building a rigid framework, which is of little permeability.

2.1.   Introduction

About 45% of the known hydrocarbon reserves in build-ups originate from Miocene rocks and lots of productive reservoirs especially in the Middle East are located within Miocene formations. In contrast to siliziclastics carbonates are essentially autochthonous, as they form very close to the final depositional sites. The initial texture is more dependent on the nature of the skeletal grains than on external influences. Biofacies and lithofacies often correlate or in other words, organisms produce typical lithofacies and are controlled by substrates. In such environments porosity structure is related to both deposition and the post-depositional processes, summed up as diagenesis. Reefal structures exhibit complex lateral variation in porosity and permeability distribution. As observed by many authors overall porosity increases with increasing abundance of skeletal material and microporosity contributes significantly to total porosity, however, is ineffective, since the smallest pores have very high capillary pressures (e.g., Bliefnick and Kaldi, 1996; Montgomery et al., 1999).

In the Mediterranean lots of Miocene reefal carbonate platforms are present among which the Llucmajor platform on the Balearic Island Mallorca is one of the largest. The present work will focus on the porosity structure at the rock-matrix-scale (µm-cm-scale) as initial part of the comprehensive reservoir characterization performed at the test site near Campos (Friedel et al., 2004). The small-scale porosity structure of a Miocene reef in the Mediterranean has been described by Armstrong et al. (1980). They described the pore structure qualitatively and mainly addressed the processes, which led to the observed present-day porosity. Carozzi (1995) discussed depositional models and the reservoir properties of Miocene reefs, however, as well rather in a descriptive manner and mainly based on observations on thin sections. Work, which focused more on the petrophysical properties of the rock and the impact of the pore system on the permeability behavior has been carried out by (Anselmetti et al., 1998) who performed a quantitative characterization of Miocene carbonate pore systems by using mostly optical methods. They introduced a new method for the assessment of the total optical porosity by combining images from the electron microscope with images of the optical microscope and found the pore shape to be an important control of permeability. Lucia (1999) made the distinction between carbonates with separate vugs and carbonates with touching vugs and compared their poro-perm relationships to samples with intergranular porosity. One of his main statements is that permeability increases with decreasing separate-vug porosity. Melim et al. (2001a) stress as well the significance of the specific pore type for the control of permeability. Furthermore, they distinguished between low-k and high-k carbonates and found that high-k carbonates show a direct correlation to intergranular porosity whereas in low-k samples as well molds are important for permeability. The degree of interconnection between molds and the intergranular pore space depends to a high degree on factors controlled by diagenesis. Several authors stress the importance of pore size distribution on permeability (e.g., Anselmetti et al., 1998; e.g., Nelson, 1994; Tiab and Donaldson, 2004). Empirical evaluations on the relationship between porosity and permeability are mostly based on the Carman-Kozeny equation, which has been adapted by many authors (Flint and Selker, 2003). The main outcome of these attempts in finding a permeability predictor is that pore size distribution, pore shape and portion of pores that contribute to flow have to be identified and considered in order to have a control on permeability.

The reefal platform of Llucmajor, Mallorca, has been described in numerous papers by L. Pomar (Pomar, 1993; , 2001a; Pomar and Ward, 1999; Pomar et al., 1996). His work mainly focused on the geological evolution and the geometry of the reef complex and only briefly mentioned porosity structure and petrophysical relationships. He found that moldic porosity from dissolution of aragonitic constituents is the main pore type. Primary porosity like

framework- and intergranular porosity is related to the distribution and proportion of lithofacies, which vary between systems tracts (Pomar and Ward, 1999). Framework pores occur mainly in the reef core of the aggradational systems tract (AST) and intergranular primary porosity in outer lagoon and proximal talus of the AST. Especially along the coast dolomitisation produced much of the secondary porosity. Porosity reduction through vadose and phreatic calcite cements was incomplete. Besides this qualitative description of the porosity types encountered no further indications for reservoir productivity were given. Furthermore, former workers mainly focused on the marginal parts of the Llucmajor platform, which is nicely exposed at the cliff coast. The knowledge about the central parts of the platform was based on a few cored boreholes with non-continuous core recovery. The present study will therefore focus on the qualitative and quantitative characterization of the 3D-pore structure of the test site at the inner part of the reefal platform (located about 6 km from the coast) and try to explain the observed features with the geological knowledge about the depositional and post-depositional processes.

At the test site near Campos on a cultivated field of 100x100 m five fully cored 100 m deep boreholes were drilled, from which 3 representative boreholes have been sampled for the present investigation. The main approach of this study is to integrate many different investigation methods with their inherent scale of investigation and the individual petrophysical relationship to the pore space into a comprehensive qualitative model of the porosity structure at the rock-matrix-scale. The first step consists in the elaboration of an appropriate sampling strategy for the physical measurements, which is very important for representing the reservoir in highly heterogeneous cases, like a reefal limestone (Al-Hanai et al., 2004). It is important to understand and define the different scales of heterogeneity so that lab measurements and field-scale data can be compared correctly. Directional measurements of the properties on core plugs are important, which means that plugs should be aligned with the sedimentary stratification in the formation. The next step is to describe the observed geology and to characterize the pore space together with standard petrophysical measurements on 1inch mini-cores, like porosity and permeability. These physical measurements build the basis for a modern reservoir characterization at the rock-matrix-scale (Anselmetti et al., 1998; Jackson et al., 1998) and are despite the fact that the scale of investigation is much lower still widely used as a calibration tool for wire-line logs (e.g., Bristow and Williamson, 1998; Lucia, 1999; Russell et al., 2002). In the third step the pore space is quantified optically using digital image analysis (DIA) on thin sections, which is a well known and widely used technique (e.g., Ehrlich et al., 1991a; e.g., Ehrlich and Crabtree, 1984; Ehrlich et al., 1991b; McCreesh et al., 1991). Many DIA-techniques used in this work have been refined recently (e.g., Heilbronner, 1988; , 1992; , 2000; , 2002a; Heilbronner and Bruhn, 1998) and proved to be valuable tools in assessing the 3D-porosity and permeability structure of such a complex reefal carbonate. Most methods however are somehow limited, because they use images only at a finer or larger scale. The method of DIA, which covers a wide range of pore sizes over several orders of magnitude by integrating porosities measured at smaller scales into the values assessed at larger scales is relatively new (Anselmetti et al., 1998). They found that permeability appears to be mainly controlled by the macropore shape in high-permeability samples and by the amount of intrinsic microporosity in the low-permeability samples. A large range of scales from micropores up to larger pores can alternatively be assessed by using mercury injection capillary pressure (MICP) as done by many authors but is a very time consuming process (e.g., Bliefnick and Kaldi, 1996; Montoto, 2004).

In order to cover the whole range of scales up to the next larger borehole-scale, within the framework of this chapter, thin section scans will be introduced additionally. Thin section scans allow for gathering information about the pore structure, which is of a comparable scale

as data from 1inch mini-cores. Digital image analysis on thin section scans thus enables us to cross-check permanently the data obtained optically with physical measurements on 1inch mini-cores. The fourth and final step will then be a comparative analysis between petrophysical data obtained from the measurements and geological observations made on thin sections and half core pieces in order to provide a genetic interpretation for the observed present state poro-perm-system at the rock-matrix-scale.

Whereas the main focus of the present study is the rock-matrix-scale, porosity structure at the borehole-scale respectively the cross-hole-scale will be discussed in chapters 3 and 4.

2.2.   Geological outline of the study area

2.2.1.   Regional overview and previous work
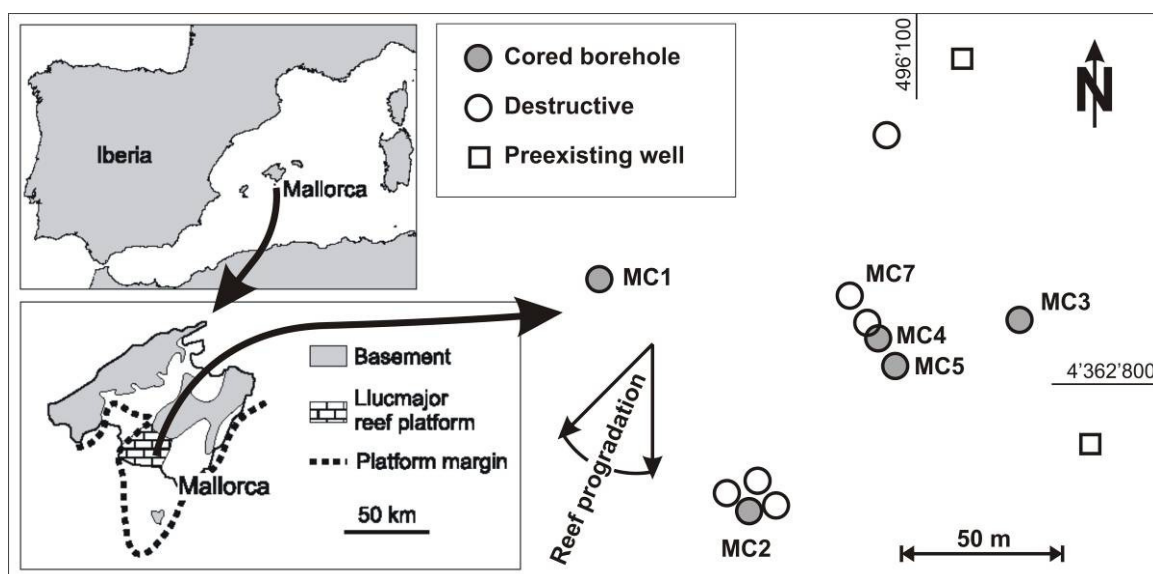
Figure 3:   The Campos site lies on the late Miocene reefal carbonate platform of Llucmajor about 6 km from the cliff coast and consists of 5 fully cored and 5 destructive 100 m long boreholes (modified after Pomar & Ward, 1995).

The investigation area lies on the upper Miocene Llucmajor platform in the south western part of the island Mallorca (Figure 3). The flat lying and through tectonical flexure slightly emerged reef complex is about 20 km wide and 100 m thick. It first has been recognized as a reefal platform about 30 years ago (Esteban, 1979; Esteban et al., 1978). A more detailed facies analysis was given by Pomar et al. (1983). The steep sea cliffs, which display in exquisite detail the facies architecture and the high-frequency depositional sequences of the reefal unit build the western and southern margins of the platform and have been extensively described during the last 15 years (e.g., Pomar, 1993; Pomar and Ward, 1999; Pomar et al., 1996). To the east the Campos basin, which seems to have subsided only during Pleistocene time (Jenkyns et al., 1990) and to the north the Mesozoic basement of the Serra de Levante to which the platform onlaps, build the borders. The platform prograded on a gentle depositional profile towards south and south west and shows the characteristic highly complex architecture, driven by eustatic sea level changes with aggradation and progradation but without backstepping. The latter is missing, since the rate of carbonate production could keep

up with the rate of creation of accommodation space (Pomar and Ward, 1995). The upper Miocene was a time of tectonic stability and low terrigenous influx, consequently reefal architecture and distribution of lithofacies are mainly controlled by sea level fluctuations of 4th to 7th order. According to Pomar and Ward (1999) most of this flat lying platform has been buried no more than several tens of meters. The platform was only slightly deformed by Pliocene-Pleistocene uplift, faulting and gentle flexure. Minor burial compaction and scarcity of pervasive cementation has preserved much of the primary porosity, which can reach man-size. Moldic porosity is the most important pore type on the platform. Especially the coral framework was subjected to extensive leaching and the location, where karst predominantly developed. From the Cap Blanc area karst has been reported in the aggrading systems tract (AST) of the reefal complex, which developed presumably during lowstands of sea level at the water table in the reef front and the coral patches of the lagoonal beds (Ardila and Pomar, 2000). Thus, karst and diagenesis both are strongly related to post-depositional sea level changes and significantly affected the porosity structure of the reef complex.

These characteristics make the Llucmajor platform an extraordinary example for analyzing pre-deep-burial stratigraphic and diagenetic heterogeneities and thus can serve as a model for other progradational platforms. The architectural concepts, which have been reported extensively from the splendid outcrops at the cliff coast around Cap Blanc can act to a certain degree as an analog model for our test site. Most of the lithofacies types reported by the aforementioned authors have been recognized on the core material, even though some important differences are present.

2.2.2.   Pore types encountered at the test site

Before the characteristics of the lithofacies types are presented, the main pore types encountered on the core material have to be defined. Pore types were divided into primary and secondary pores in order to distinguish between depositional and diagenetic fabrics. Furthermore, a distinction was made between macro- and microporosity. The separation between macropores and micropores was chosen at the resolution limit of thin section petrography: micropores are those <20 µm all the others are called macropores. Primary porosity, such as intergrain, intrafossil or growth-framework porosity has been directly inherited from the original sedimentary fabric. These porosity types can be strongly modified by cementation with blocky spar (Figure 4D and E). Secondary porosity per definition evolved after deposition of the sediment and is part of the post-depositional processes summed up as diagenesis (Pomar and Ward, 1999). The most important secondary porosity type is the moldic porosity, which develops through dissolution of aragonitic constituents, mostly corals and shells of bivalves and gastropods. If the aragonite is not replaced by calcite the hollow space of the original fossil remains and forms a moldic pore. Two types of moldic porosity have been observed in the study area. Large and elongated molds originating from shells and coral debris are typical for rudstones and coarse grained, grain-dominated deposits in general (Figure 4A). Small and round shaped molds are due to leached out peloids and rounded bioclasts, which are typical for fine grained, mud-dominated grainstones and packstones. In some parts of the reefal unit such molds build a highly porous framework-like structure, which presumably is not very permeable (Figure 4A and B). Molds are per definition part of the fabric-selective vuggy porosity, since they are restricted to the original shape of the bioclast, which has been dissolved. Furthermore, following the definition of Lucia (1999) molds belong to the separate-vug pore space, which is interconnected only through the interparticle porosity (Figure 4C and F). In contrast to separate vugs, touching-

vug pore systems are defined as pore space, which is significantly larger than the particle size and non-fabric-selective.
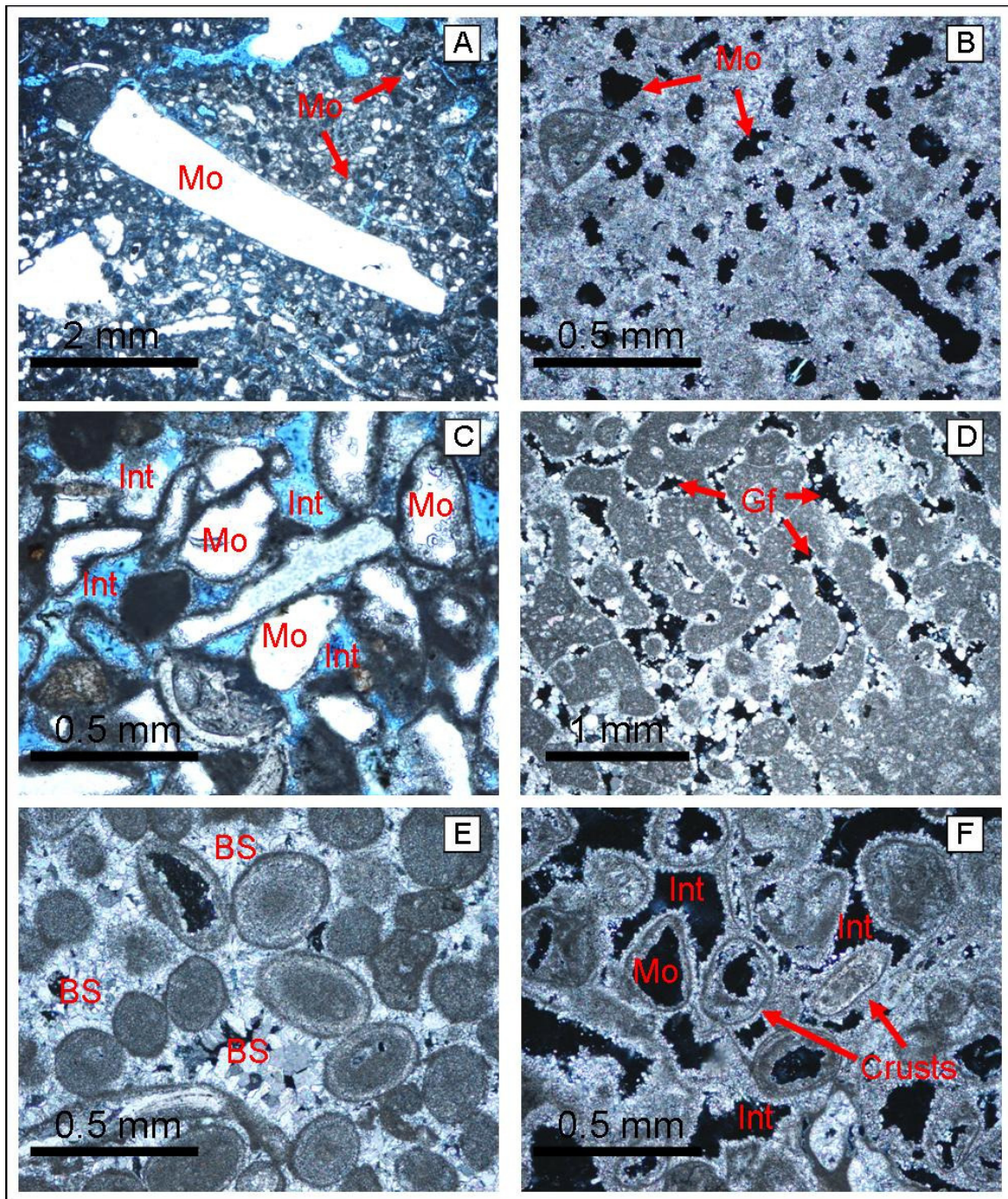
Figure 4:   Photomicrographs showing pore space and degree of cementation (A,C non-polarized, B,D,E,F plane polarized light): (A) MC3 (85.65 m) grainstone-rudstone from basis of proximal talus with large, elongated and small, round shaped molds (Mo), (B) MC5 (84.65 m) mud-dominated packstone with small round-shaped molds (Mo), (C) MC5 (15.13 m) bioclastic grainstone with moldic (Mo) and intergrain (Int) porosity. Blue resin indicates that intergranular porosity is open, (D) MC2 (56.68 m) framestone with partly occluded growth-framework porosity (Gf). Structure is preserved by the micritic mud, which fills the coral-framework, (E) MC2 (1.66 m) blocky spar (BS), which cements an oolithic grainstone. Some intra- and intergranular porosity is present, (F) MC2 (11.45 m) grain-dominated packstone with micritic crusts surrounded by fine micritic cements. A well developed intergranular porosity (Int) and few molds (Mo) at an initial stage are present.

Solution enlarged fractures and caverns belong to this group, which builds interconnected pore systems of significant extent. Since they occur mainly at scales larger than rock-matrix-scale, they will not be discussed in the present study. Karst is defined here as tertiary porosity and although present at larger scales, will be briefly discussed, since karstic processes have a pronounced influence on the adjacent rock matrix. As mentioned above, karst mainly developed in zones, where larger primary pores were present or in zones of secondary porosity, where coral colonies have been leached. During sea level lowstands the subsequent karst interconnected these heterogeneities building an interconnected channel system. As a consequence of karst, calcite precipitations, residual clays and vadose cements could form, which occluded large amounts of the framework-porosity of preserved corals. Thus, karst though building larger scale heterogeneities, locally is very important for the porosity-and permeability structure at the rock-matrix-scale.

2.2.3.   Lithofacies types and diagenesis at the test site

In order to give an overview of the geological situation encountered at the test site, results from the geological investigation are already presented below allowing for a better understanding of the phenomena presented and discussed in chapters 2.4 respectively 2.5. Cored drillings at Ses Sitjoles yielded in general good core recovery for MC2-MC5 between 86 and 94%, except for MC1 with only 33%. Core losses can be explained in most cases by karstic cavities or poorly cemented material, phenomenon, which have been recorded in all boreholes, however, poor core recovery in MC1 is due to inadequate drilling technique. Large scale heterogeneity is mostly controlled by the architectural pattern, which is comparable to the cliff coast near Cap Blanc. From top to bottom five main lithofacies types, namely inner lagoon, outer lagoon, reef core, proximal talus and distal talus have been encountered at the test site (Figure 27). The deposition of sediment within a reefal carbonate complex is the complex interaction between depth-dependent carbonate production, depositional profile, accommodation space, encrusting and carbonate producing biota, hydrodynamic situation and the sea level history, which influences the rates of production and the subsequent amount of erosion. Low energy and ecologically zoned lagoons with patch reefs behind the barriers graded into mangrove tidal flats and communicated with the open sea through numerous tidal passes, cutting across the barrier systems. Loose-grain sediment accumulation in the lagoon was dependent on the hydrodynamic action at wave base and could be mud- or grain-dominated fabric in addition to predominant deep-water oligophotic carbonate production, which mainly led to mud-dominated sedimentary fabrics like observed in distal talus (Pomar, 2001b) In the reef core and in patch reefs, framework producing organisms were able to grow above wave base, in addition to the predominant shallow-water euphotic carbonate production. In the high energy zone of reef core and outer lagoon finer skeletal components can be easily winnowed away and shed seawards to accumulate on a depositional slope. Especially during storm events large amounts of peloidal and skeletal grainstones and rudstones from the outer lagoon and reef rubble from reef core and patch reefs were shed on the slopes of the proximal talus, building lenticular layers rich in peloids, shells and coral debris. Due to the wave action in shallow parts of the outer lagoon, rather well sorted and grain-dominated fabrics are present. In outer lagoon lots of encrusting organisms like byozoans, red algae and encrusting forams are present, which in addition to the protection by the reef barrier led to a high depositional profile. Thus, sediment accumulation within outer lagoon is also possible above wave base level building large coarse grained sediment depots, which are partly transported towards the talus during intermittent storms. Depending on the hydraulic regime, fine- to coarse-sand-grained bioclasts may be shed off the platform, building out a depositional slope, whereas gravel-sized skeletons will mostly remain on the

platform top. According to Pomar (2001b) these large clasts mainly act as a zone of hydraulic energy dissipation.

The lithofacies types reported by Pomar et al. (1996) have been recognized in all cored boreholes, however their thickness varies considerably. In none of the cores pervasive dolomite has been encountered except for two thin layers in the talus. The whole complex has been subjected only to meteoric diagenesis, no marine cements have been encountered. The main diagenetic influence were most probably sea level changes, which lifted the fresh water lens from one peak to the other and which overprinted the whole reef complex several times. Starting at the top, the observed lithofacies types are as follows:

Inner lagoon (IL) with observed thickness of 10-13 m consists from top to bottom of oolithic grainstones (Figure 5 A), dense calcrete hardpans and layers with continental influence, such as black pebbles, followed by relatively soft marly limestones with root structures and some karstified levels. Within the capping oolithic grainstones, vadose blocky cements occlude most of the intergrain pore space. Furthermore, sedimentary texture of inner lagoon is often dominated by micritic crusts. The marly limestones are mostly poorly cemented and porosity is low and of intrafossil or intergrain type. Below an alternation of dense, recrystallized, quartz-grain-bearing limestones, siltstones and dm-thick clays occurs. The clays are without internal lamination and maybe partly products of microkarst or weathered volcanic ashes, which also have been reported and dated at Cap Blanc (Pomar et al., 1996). Among the forams milliolids are predominant and some red-algae and molluscs occur as well. This lithofacies type without doubt represents several transgression and regression cycles, consisting of a succession of shallowing-upwards cycles, with some very shallow water marine deposits merging gradually into continental deposits. The low diversity of the observed biota points to a restricted facies, which intermittently was lacking direct connection to the open marine environment and ran dry.

Outer lagoon (OL) with observed thickness of 30-46 m consists of skeletal grainstones (Figure 5 B) and packstones with variable cementation, which exhibit a high and non-restricted biodiversity consisting of red algae, lots of different sessile and benthic foram genus, echinoids, molluscs among which oysters are quite abundant, small single coral heads and crabs (*Daira speciosa*). Bellow 30 m depth the hyaline shells of planctonic forams can be found. In the upper region peloids occur and cross-stratification indicates a deposition above wave base level. Micritic vadose cements (vadose silt) seem to dominate but also patchy blocky spar is present in some samples at its initial stage. Isopachous cements are typical for outer lagoon and have been found in samples between 15 and 40 m mainly, indicating a phreatic milieu. Porosity seems to be very high and consists to a large extent of molds from shells and other dissolved aragonitic organisms. Sequence boundaries within this unit are composed of wackestones, which results in a sharp gamma signal. The arenitic rock is mostly poorly cemented. Within this unit isolated patch reefs mostly consisting of *Porites* with extensive sponge and bivalve (*Lithophaga*) borings occur. Some of the partly with carbonate mud filled holes build geopetal structures. Aragonitic constituents, like corals and shells of bivalves and gastropods, have been neomorphosed to calcite or leached out and are the main reason for the extensive moldic porosity. The patch reefs form dense, commonly well cemented and diagenetically altered heterogeneities within the quite uniform bioclastic rock and megapores with diameters up to 30 cm are common. The sediments of outer lagoon are mostly bioturbated and small accumulations of the shells from molluscs and reef debris in up to 1 m thick lenses are abundant. These rudstones originate most likely from storm events, which shoveled material from the reef crest into the shallow and protected depressions behind, if no tidal channel or grove was close, which could transfer the material towards the

sea. Thus, the main pore type within outer lagoon is moldic porosity built of mostly large and elongated shapes and intergranular porosity only reaches values of 20-30% of the macroporosity.
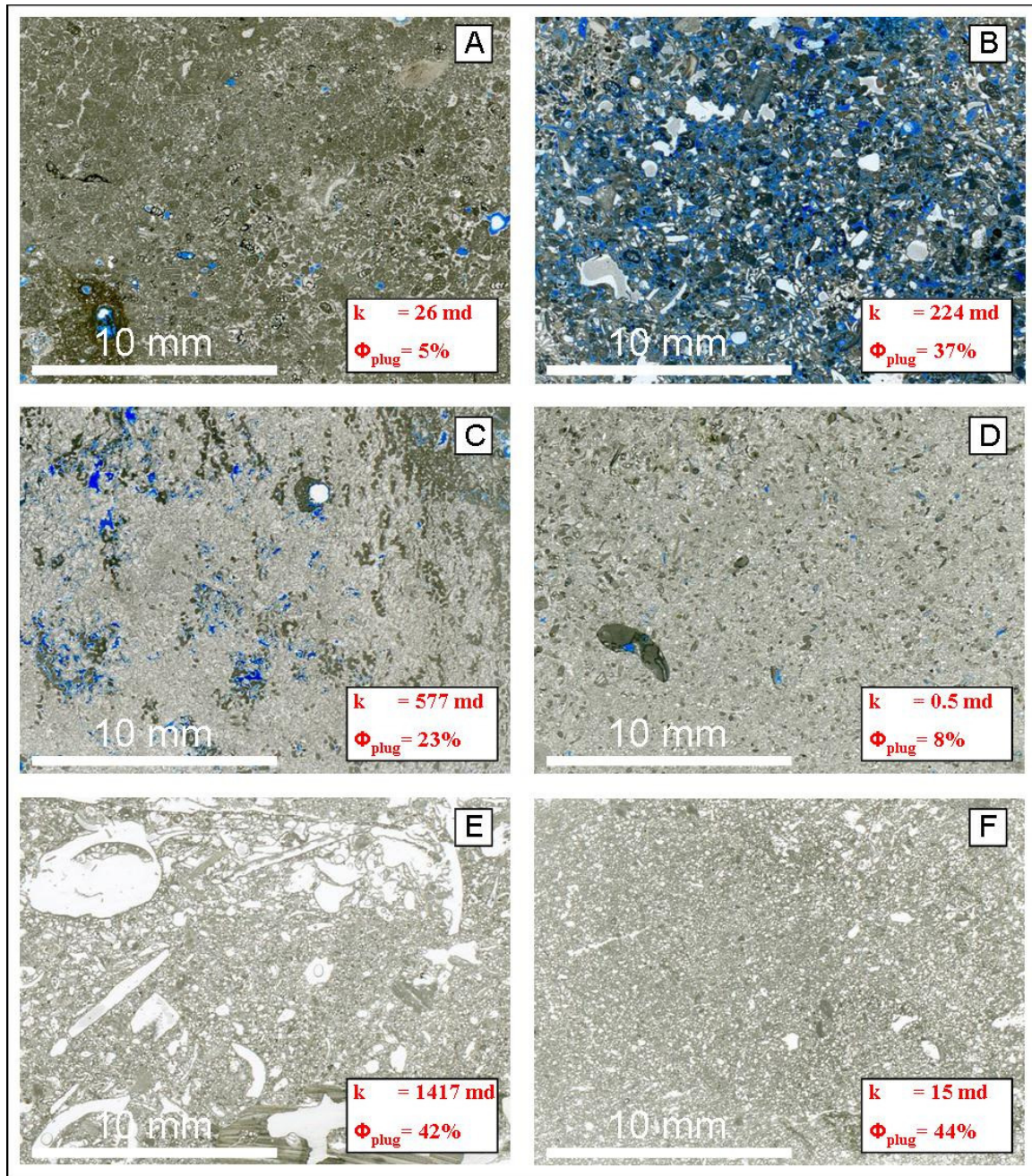
Figure 5:   Photomicrographs of typical sedimentary fabrics (optical microscope, non-polarized light): (A) MC5 (2.60 m) inner lagoon oolithic and peloidal grainstone, recrystallized, porosity mostly intrafossil, (B) MC5 (15.13 m) outer lagoon bioclastic grainstone, micritic crusts, porosity moldic and intergrain, (C) MC3 (60.44 m) reef core recrystallized framestone, growth-framework porosity, (D) MC5 (59.52 m) proximal talus packstone with some blocky spar, porosity moldic and intergrain, (E) MC5 (84.65 m) proximal talus grainstone to rudstone, micritic cement, large elongated molds, (F) MC5 (91.53 m) distal talus packstone, micritic cement, small round shaped moldic pores.

The reef core (RC) with thickness of 4-19 m consists of framestones (Figure 5 C) and grainstones to packstones, which act as internal sediment and subordinated also some red

algal bindstones occur. The internal sediment fills up most cavities between the massive coral heads and furthermore fills the large channels within the reef core. These channels build a direct connection between lagoon and open sea, the so called spurs and grooves-zone. Moldic and non-fabric-selective vuggy pores are typical, which is supported by the originally aragonitic corals. Especially the lower part of the reef core is usually karstified and a channeling is present. The rock affected by karst is dense and recrystallized and blocky spar occludes part of the growth-framework porosity (see chapter 2.2.2). The internal sediment builds a significant part of this lithofacies type and consists mainly of grainstones and packstones with coral debris and single coral heads, large gastropods (*Murex spinicosta*), bivalves and a microfauna comparable to outer lagoon sediments but additionally with pelagic forams. Micritic crusts and encrustations of red algae, forams, bryozoans and worm tubes are very common. The most important pore types of the internal sediment are moldic and intergranular porosity. The mostly recrystallized coral framework exhibits low matrix porosities, but at a larger scale permeabilities are highest, due to extensive channeling (chapter 2). As will be seen later on, porosity, especially open porosity at the rock-matrix-scale can be close to zero. The corals initially were filled with carbonate mud, which later on recrystallized to micrite or microspar (Figure 4D). The originally aragonitic coral-structure was either leached out or neomorposed to the more stable calcite, which is documented by some preserved ghosts of the original structure. Growth-framework porosity, which is present in zones, where the original structure of mud-filled corals has been removed completely, especially close to karstified sections can be occluded by blocky spar. Erosional surfaces or emersion horizons, which have been observed directly below or above the reef core and also within lagoonal sediments predominantely consist of wackestones, with abundant red algal fauna. The thickness can reach up to 2 m and their presence is clearly marked in the gamma log by high amplitudes. They are not only crucial for the geometrical interpretation but could also act as low permeability zones for groundwater flow at larger scales than investigated here (Melim et al., 2001a).

Proximal talus (PT) with thickness of 20-30 m consists of white, bioclastic and intraclastic, intensively bioturbated packstones (Figure 5 D) to rudstones, which are steeply bedded (10-30°). Lenticular layers of coral rubble and skeletal debris-flow rudstones are common, which were deposited during intermittent storm events (Figure 5 E). Coarsening upwards cycles can be interpreted as clinobeds, which are the basinward continuation of interfingering prograding reef core sigmoids. Parts where rhodoliths occur are designated as floatstones or rudstones. The rock is better cemented in the upper part adjacent to reef core, where patchy blocky spar is present. The lower part is mostly poorly cemented and micritic cements or crusts are common. Fractures are unlike in other lithofacies types a typical feature for proximal talus and occur especially towards the overlying reef core. This unit is slightly anisotropic due to steeply dipping beds and coarse grained layers in between. Porosity, which is mainly moldic decreases towards the reef core. Within proximal talus two types of moldic porosity occur. The large and elongated molds, which are typical for rudstones and the dissolved shell debris in the grainstones and the small and round-shaped molds originating from the dissolution of peloids and small rounded bioclasts (Figure 4A).

Fabric-selective vugs like molds are present throughout the whole reef complex, however, in the lower part approximately below 65 m much more grains have been dissolved completely to molds (about 60 to 80%) than in the upper part (about 5 to 40%). Furthermore, in the lower part of the reef components and matrix are sometimes not distinguishable any more, since recrystallization to micrite or microspar of both components and matrix was very complete. Recrystallization of the matrix from the original mud to microspar has been observed throughout the whole reef complex.

Distal talus (DT) builds the lowermost unit encountered at the test site and consists of white, strongly bioturbated, gently dipping (less than 10°) and fine grained packstones and grainstones (Figure 5 F). Micritic cements and crusts are common. The rock is very homogeneous and mostly lacks macrofossils. The poorly sorted and fine grained mud-dominated packstones in contrast to proximal talus sediments are rather affected by vertical and slow deposition because they are deposited below wave base level and within a zone, where oligophotic carbonate production builds a significant contribution. Distal talus exhibits a high amount of small, well sorted spherical moldic pores but since an effective intergranular porosity is not present, the connectivity between pores is low and therefore also permeability is expected to be rather low (Figure 4B).

2.3. Methods

2.3.1. Sampling strategy

In the present study the explicit sampling strategy has been applied, which samples the core material at discrete depths, which allows a much better control of scale disparity than with implicit sampling (Worthington, 1998). The specific rock measurements were targeted on representative sedimentological features like stratal patterns and architectural elements. This method, which is called genetic petrophysics (Corbett et al., 1998) assures that no sampling close to Nyqvist frequency occurs, which would bias the reconstruction of the petrophysical signal. Following the strategy of genetic petrophysics the database of this study was acquired mainly of core material from the three 100 m long boreholes MC2, MC3 and MC5, which have been chosen due to their high core recovery and the availability within the framework of the project.
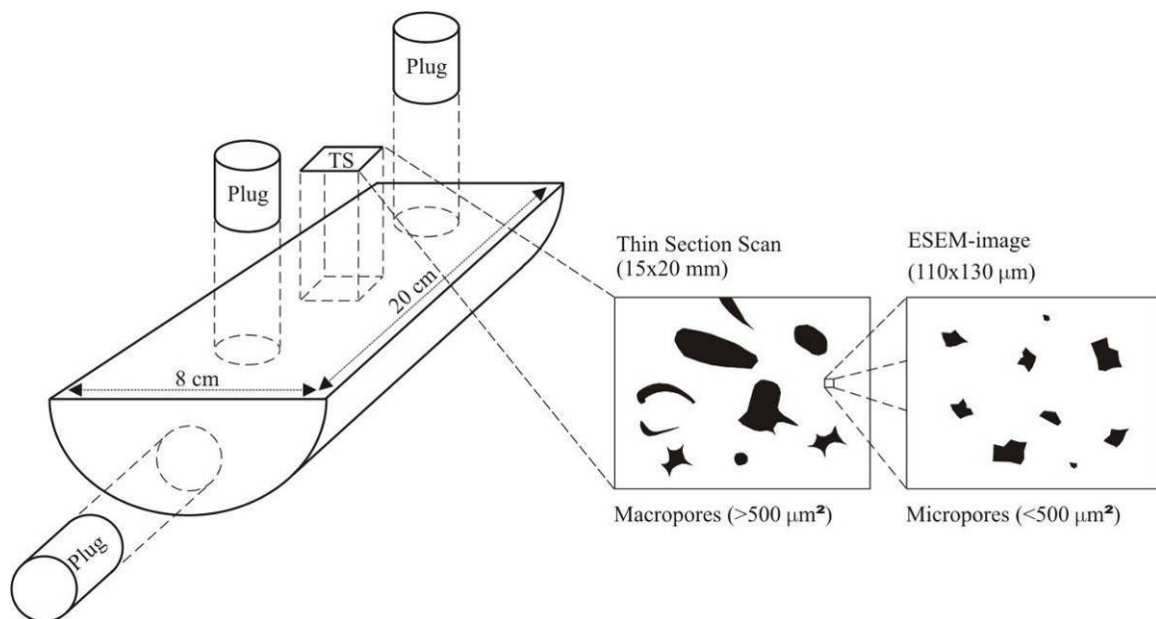
Figure 6:   Illustration of sampling strategy on half cores with extraction of horizontal and vertical plugs and a thin section for further optical analysis. Thin section scan is analyzed for macropores on the optical microscope, micropores are assessed by ESEM-images from the rock matrix.

During the visual core description up to 20 cm long core pieces have been extracted at about 100 locations and cut into half in order to get a working- and an archive half. Out of the working half 1inch mini-cores with a length of 3-4 cm have been drilled mostly perpendicular to the borehole axis in order to capture as much information from single beds as possible. Additionally a plug parallel to the borehole axis has been extracted from each core half, in order to be able to check for anisotropy of permeability (Figure 6). For the comparison of physically measured properties like porosity and permeability on the plugs with optical and processed data from digital image analysis (DIA) a representative thin section (1.5x2 cm) has been made. If the field of view for the DIA is representative of the entire sample, then total optical porosity should be in the same order as the total porosity measured on the corresponding plug. The thin section represents a vertical section and consequently an unfocussed plane parallel to the borehole axis, which assesses the pore space at a scale comparable to 1-inch plugs. In samples, which are homogenous at cm- to dm-scale, data from these two methods should be comparable.

2.3.2.   Measurements on 1 inch mini-cores

From the sampling campaign a total of 140 horizontal and vertical mini-cores resulted, which were all analyzed on porosity. Preliminary to the analysis, samples were dried at 80° during several days and afterwards volume and dry weight were measured, which result in the bulk density. The density of the matrix was determined by staining the rock with alizarin red, which differentiates between calcite and dolomite. From the bulk density and the matrix density total porosity could be calculated. The data was then verified with the he-pycnometer accupyc 1330 from Micrometrics. Normally the he-pycnometer can be used to determine the closed porosity of the rock but for the few cemented Miocene carbonates of Mallorca in general the whole pore space including closed pores is accessible by helium. These measurements thus were used to confirm the total porosity determined by weighing. The large dataset of plugs was mainly analyzed on porosity changes between and within individual lithofacies types and to study the porosity changes with depth over the whole borehole length.

Permeability measurements were focused on totally 40 plugs of 25 representative half cores. The plugs were first saturated with tap water and then put into a standard falling head permeability-cell (e.g., Lang et al., 2003). Permeability for each sample was determined by using graphical fitting on a semilog-plot (see appendix).

2.3.3.   Digital image analysis on thin sections (Scan, ESEM)

Digital image analysis (DIA) is a powerful tool for the quantitative assessment of the pore space, thus many techniques are described in literature (Anselmetti et al., 1998; Ehrlich and Crabtree, 1984; Heilbronner, 1988; 1992; 2002a; Lang et al., 2003). DIA on thin sections enables us to evaluate total optical porosity (TOP), anisotropy and heterogeneity of the pore space, pore shape factors and pore size distribution, which all together result in a better understanding of the 3D-pore structure at the rock-matrix-scale (cm-µm). The investigation scale of plugs (2.54x3.5 cm) and thin section scans (TSS) (1.5x2 cm) is approximately the same, however the plug is an average over a cylindrical volume and the thin section is a planar measurement (Figure 6). The TSS used in this study takes an average over an area 100x larger than commonly used TS-images (e.g., Anselmetti et al., 1998), which increases at the same time the investigated pore scale by one order of magnitude (Figure 7).

Table 1: Data of the 25 samples used in the present study. Abbreviations are explained in the text.

Facies	Depth [m]	Sample No	Fabric Dunham	Pore type main	Pore structure (ACF)	DPS [mm]	OM [%]	ESEM [%]	TOP [%]	y_{TS}	y_{int}	Mean [µm]	Median [µm]	StDev [µm]	CV	Skew	S_{sp} [m²/cm³]	Φ-plug [%]	k-plug [md]
IL	2.60	5_1	grainstone	intrafossil	bit patchy	0.099	1.3	5.7	6.9	1.62	1.83	180	94	36	0.20	3	0.25	5.2	26.41
OL	15.13	5_10	grainstone	moldic long	homo	0.105	34.7	9.7	41.0	2.27	2.23	301	153	44	0.15	11	0.33	36.9	224.35
	17.15	5_11	grainstone	moldic long	hetero, aniso	0.096	36.5	13.6	45.1	2.96	2.76	348	215	43	0.12	6	0.47	40.0	1369.27
	22.56	5_12	grainstone	moldic long	hetero	0.099	19.4	28.2	42.1	1.82	2.44	153	79	30	0.19	15	0.83	30.8	282.51
	31.18	3_15	grainstone	moldic long	hetero	0.295	31.3	37	56.7	2.04	2.56	674	374	73	0.11	3	0.89	43.3	252.60
	34.23	5_17	wackestone	moldic long	hetero, aniso	0.274	1.9	11.4	13.1	2.12	2.15	409	434	51	0.12	0	0.36	12.8	10.73
	41.29	3_19	packstone	moldic round	hetero, aniso	0.162	43.8	6.7	47.6	3.39	3.25	949	737	77	0.08	2	0.31	49.5	7741.98
	41.77	5_19	packstone	moldic long	hetero, aniso	0.228	24.2	13.1	34.1	2.05	2.05	435	276	54	0.12	7	0.56	30.0	1518.08
RC	55.29	5_23	rudstone	moldic long	hetero	0.321	21.4	7.4	27.2	1.65	1.69	413	330	44	0.11	4	0.30	17.2	0.39
	57.69	5_24	grainstone	intergrain	bit patchy	0.098	0.5	2.7	3.2	1.57	1.64	88	57	19	0.22	2	0.12	10.7	60.41
	60.44	3_26	framestone	framework	bit patchy	0.084	5.1	9.3	13.9	1.6	1.79	91	39	23	0.25	8	0.22	23.2	577.18
	63.58	3_27	packstone	intergrain	homo	0.072	8.7	7.1	15.2	1.45	1.67	75	45	15	0.20	13	0.24	20.2	10.32
PT	59.52	5_26	packstone	moldic round	homo, aniso	0.049	6.4	6.6	12.6	1.28	1.59	43	27	7	0.15	8	0.23	8.4	0.50
	60.94	5_27	grainstone	intergrain	homo	0.072	16.8	14.7	29.0	1.79	1.99	122	56	25	0.21	12	0.52	32.9	192.26
	65.42	5_32	packstone	moldic round	homo, aniso	0.058	22.4	12.1	31.8	1.61	1.73	90	52	18	0.21	15	0.50	38.4	562.69
	69.85	5_35	packstone	intergrain	homo, aniso	0.058	18.6	12.5	28.8	1.72	1.84	99	45	23	0.23	12	0.44	45.8	1163.06
	74.92	3_31	floatstone	moldic round	hetero	0.130	10.2	12.3	21.2	1.75	1.96	277	66	49	0.18	8	0.45	25.1	0.15
	78.85	5_37	grainstone	moldic round	bit patchy	0.067	4.4	30.1	33.2	1.41	2.59	71	27	19	0.27	10	0.63	36.9	161.34
	80.31	3_33	packstone	moldic round	homo, aniso	0.058	9.4	20.7	28.2	1.36	2.08	56	35	11	0.20	12	0.58	18.1	17.42
	84.66	5_39	grainstone	moldic long	hetero, aniso	0.278	32.5	13.5	41.6	2.04	2.15	576	505	60	0.10	5	0.41	42.4	1416.59
	85.65	3_35	rudstone	moldic long	hetero, aniso	0.519	23.4	16.2	35.8	2.29	2.27	867	659	83	0.10	3	0.51	33.8	704.23
DT	88.75	2_35	packstone	moldic round	homo, aniso	0.064	9.6	38.2	44.1	1.37	2.32	62	36	12	0.20	11	0.60	41.2	19.04
	91.53	5_40	packstone	moldic round	homo, aniso	0.067	25.6	33.4	50.4	1.75	2.21	133	60	28	0.21	19	0.56	43.6	14.63
	98.66	5_41	packstone	intergrain	homo	0.055	16.1	26	37.9	1.49	2.01	73	40	16	0.22	17	0.61	42.0	107.93
	99.68	3_38	packstone	moldic round	homo, aniso	0.058	12.5	29.3	38.1	1.49	2.22	58	35	11	0.18	9	0.50	46.1	190.97

Furthermore, concerning scale its TOP can more easily be compared to 1inch mini-cores and thus helps in keeping scale-disparity low.

For the evaluation of the porosity structure and its attributes at the rock-matrix-scale more than 50 thin sections have been prepared of which finally 25 have been chosen from the most representative zones of the boreholes MC2, MC3 and MC5 and which build the main data set used in this study (Table 1). Only one representative sample is available from inner lagoon, since this lithofacies type is entirely located in the vadose zone. From the thin sections non-polarized scans were made, using a commercially available flatbed scanner EPSON Perfection 3200 Photo. The resolution chosen here is 2400 dpi, which yields an absolute pixel size of 10.6 µm. Microporosity was assessed by an environmental scanning electron microscope (ESEM) FEI Quanta 600. With the ESEM 3 representative composition contrast images have been taken per thin section. Each image was acquired with a magnification of 1000x and the size of the image was set to 110x130 µm. The real resolution of these images is 399'000 dpi, which yields a pixel size of less than 0.1 µm.
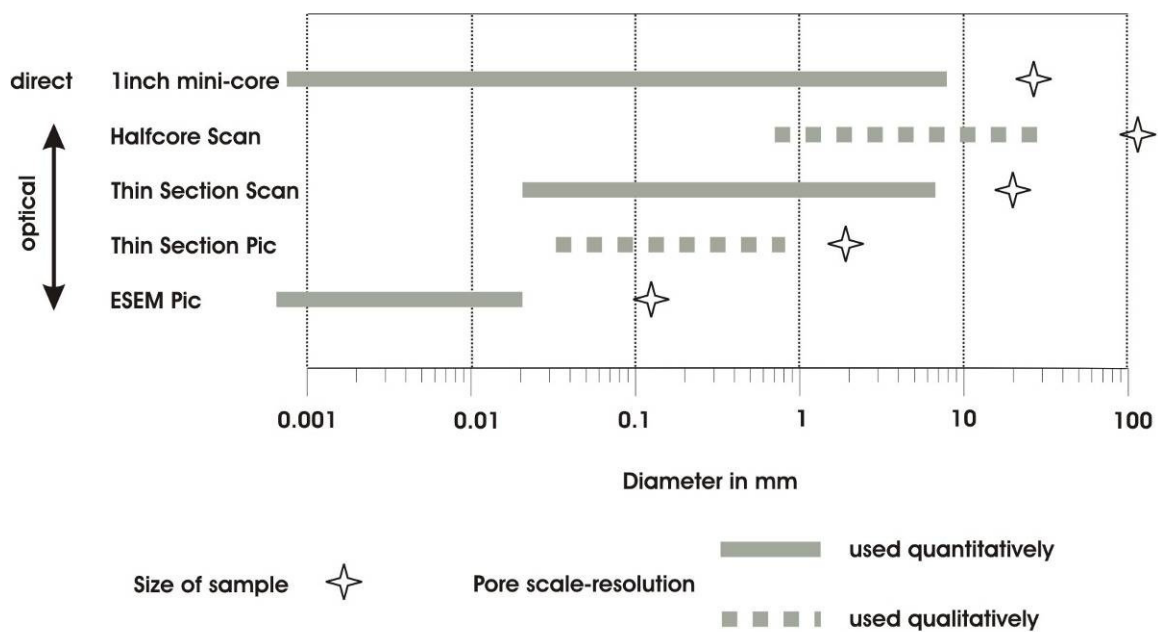
Figure 7:   Overview of the optical data acquisition system with information about their sample size and the covered pore-scale and a comparison to 1inch mini-cores. Data from standard flatbed-scanner are halfcore scan (8x15 cm) and thin section scan (15x20 mm). Images from optical microscope are denoted as thin section pic (1x2 mm) and images from the environmental scanning electron microscope as ESEM pic (110x130 µm).

2.3.3.1.   Segmentation of TSS and ESEM-images

Segmentation has been performed with two software-programs, which are available in the public domain namely *ImageJ*, which runs on PC-systems and *SXM175* for mac-based systems. *ImageJ* has been chosen for standard DIA like segmentation, pore size distributions and orientation imaging, whereas the more sophisticated *SXM175* has been used for calculating the autocorrelation functions. An extensive description of the classical segmentation procedure on digital images is given in Ehrlich et al. (1984). Images from the optical microscope show a bimodal brightness distribution and thus have been segmented manually, yielding a reproducibility of about ±10%. However for ESEM-images the brightness distribution commonly is very flat, allowing for an automated segmentation

procedure, which yielded excellent results (see chapter 2.4.3). After the subsequent filtering a suite of standard measurements has been performed on the pores, such as pore area, perimeter, orientation and axial ratio of the fitted ellipse.

With this technique pores down to a diameter of 20 μ have been analyzed, consisting of at least 4 pixels. This small amount of pixels is sufficient for the analysis of total optical porosity (TOP) but leads to erroneous values for directional- and shape measurements. This is due to the point density of a square lattice, which is not constant for all directions resulting that not all directions can be represented equally well. It has been shown that pores consisting of less than 16 pixels led to significant errors in the evaluation of the pore-orientation. Elliptical envelopes of small pores whose sizes are close to the resolution limit tend to preferred orientations. This phenomenon is a consequence of the squared shape of a single pixel and has already been addressed by Heilbronner (1988). By neglecting pores smaller than 16 pixels even more complex shapes are quite well represented.

2.3.3.2.   The integrated approach of TOP
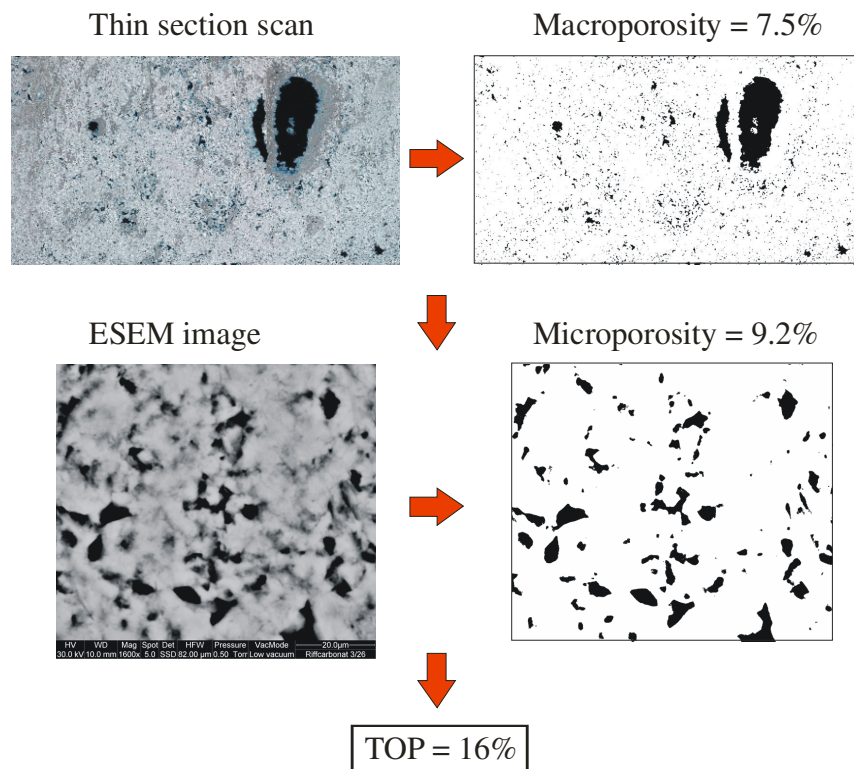
Figure 8:   Procedure of the integrated approach for TOP-evaluation on thin sections. Original images are shown on the left and binary images of the pore space on the right hand side.

Porosity quantification from thin section images only is limited by the resolution of the optical microscope (OM). Its resolution is controlled by the thickness of the thin section, which is about 30 μm. In samples where the microporosity (<20 μm) is significant, porosity from OM-images only is strongly underestimated (Figure 8). In order to be able to compare optical data to measured total porosity on 1inch mini-cores, the microporosity has to be incorporated into TOP. This is done by using a method first described by Anselmetti et al. (1998), where macropores from the optical microscope and micropores from the ESEM are used both to determine TOP. In order to calculate the total porosity Φ_{tot} of the analyzed

sample, one has to correct the intrinsic microporosity by a factor of (1- Φ_{mac}), which accounts for the lack of intrinsic microporosity within the macropores Φ_{mac}:

$$\phi_{tot} = \phi_{mac} + \phi_{mic} * (1 - \phi_{mac})$$

If the field of view for the image analysis is representative of the entire sample, then Φ_{tot} should be in the same order as the total porosity measured on the corresponding 1inch mini-core (Figure 6).

But even if the scale of investigation seems to be in the same order and results are comparable to each other, one has to keep in mind the restrictions of both methods, the optical and the physical one. Optically it is not possible to measure microporosity, which is smaller than 0.1 μm in diameter due to the weak electrical conductance of the thin section-glass. Furthermore, at too high magnifications it becomes more difficult to distinguish grain boundaries from pore space. According to DeMarsily (1986) between 0.1 and 0.5 μm there exists a transition zone in which the forces of molecular attraction are still not negligible. Beyond 0.5 μm the water is said to be free. The widely used kinematic porosity is defined as the porosity in which the water is able to circulate. Thus, the lower bound of resolved microporosity is as well a lower bound for the kinematic porosity. Consequently the microporosity is rather underestimated however the lost information might not be of hydrodynamic significance.

2.3.3.3.   Anisotropy and heterogeneity

Anisotropy of the pore structure can be the result of a preferred orientation during sedimentation of the grains or of elongated fossil debris, e.g. through currents, gravity, topography or the result of a directional growth of cement within the primary pore space due to fluid gradients or gravitational forces (vadose cements). The anisotropy of the rock matrix can have a large influence on the flow behavior of a porous medium (e.g., Anderson et al., 1994; Freeze and Cherry, 1979). Especially in combination with large shape factors an anisotropic pore structure is supposed to be more permeable than others for a given total porosity. In order to check these effects from the DIA-data a set of angles with the following constraints has been extracted: Particles must exhibit a minimum size of 16 pixels and all edge particles are excluded. The measured angle describes the orientation of the large axis of an ellipse fitted to a single pore. The angle measurement, which is performed within the software *ImageJ* for each individual pore is based on the mathematical system, which means from east (0°) to west (180°) in a counter-clockwise sense.

All measured angles of one TSS are then plotted as a rose diagram with class sizes of generally 10°. Though partially oriented lines theoretically do not form an ellipse (Underwood, 1970), the rose diagrams obtained in most cases can be approximated by an ellipse whose shape is a measure for the anisotropy of the rock concerning preferred pore orientation (Figure 9). The fitting of the ellipse has been performed within *ImageJ*, where the automated fitting procedure assures a certain consistency in the parameter estimation. The factor of isotropy is given by the axial ratio of the ellipse, thus anisotropy is expressed by factors <1. In general anisotropy was measured for pore sizes ranging from 10-0.05 mm, which are the pores covered by the TS-scan and for pore sizes ranging from 0.02-0.0003 mm, which are those covered by the ESEM-image. In order to check whether anisotropy is different for different pore sizes, anisotropy has been determined for 4 different pore size

classes namely 10-0.05 mm, 10-1 mm, 1-0.1 mm and 0.1-0.05 mm for the thin section scan and for 1 pore size class 0.02-0.0003 mm for the ESEM-image.
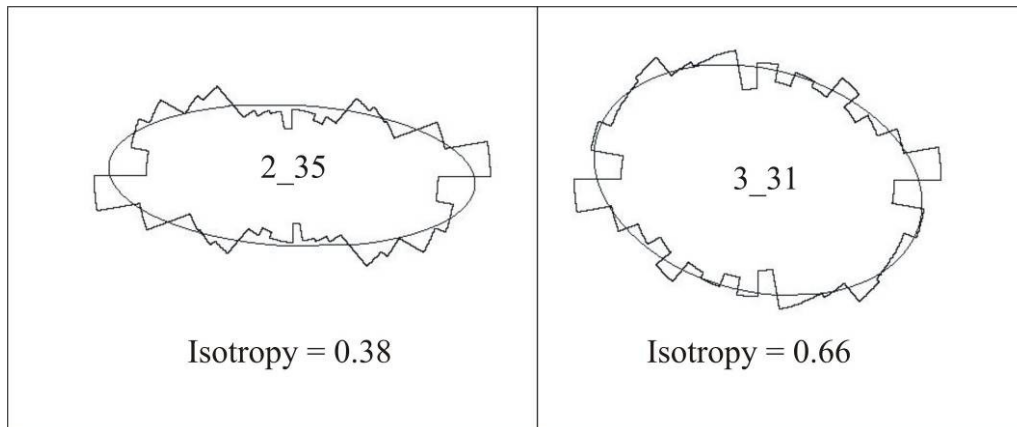
Figure 9:   Determination of anisotropy from plotting angles of large axis from fit-ellipse in a rose diagram. The shape of a rose diagram can reasonably well be approximated by an ellipse, whose axial ratio describes the degree of anisotropy.
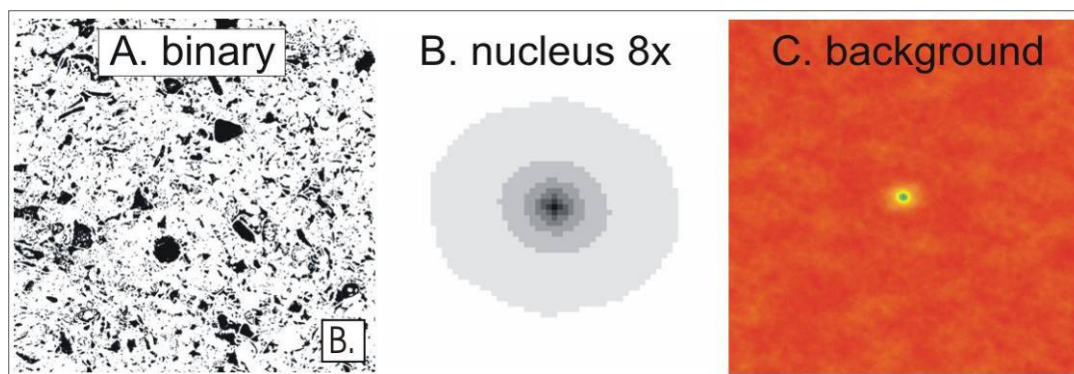
Figure 10:   The binary image of the thin section (1) with an inset, which shows the relative size of the ACF (2) where the nucleus is displayed at a magnification of 8x in an 8 gray color table-representation. On the right hand side the non-magnified ACF is displayed (3) with a spectrum color table, which highlights the background.

Anisotropy can alternatively be assessed by using the autocorrelation function (ACF) (Heilbronner, 1992). In cases where the fabric consists of ellipses or is otherwise anisotropic, the rate of decay of the ACF away from the center is not the same in all directions. The ACF remains high along directions parallel to the preferred orientation, which could be long feature extension or low spatial frequencies. The contour lines of the ACF become elongated in the direction of maximum correlation. The interpretation of the resulting image is not always straight forward because the ACF provides a simultaneous quantitative description of geometry at all scales of the image. It has to be compared with other data, e.g. anisotropy data from angle rose-diagrams. The use of the ACF for analyzing microstructure variations has been described in Heilbronner (1992) and Heilbronner (2002a) who stated that ACF is especially useful for the detection of subtle microstructures, like for example weak anisotropies and for large datasets. In this study the ACF has been used for the determination of anisotropy, heterogeneity and dominant (average) pore size (DPS). The analysis was performed with scaled images in order to determine the dominant pore size metrically. Starting from the binary image (Figure 10A), investigations were concentrated on the nucleus at a magnification of 8x for the evaluation of pore fabric-anisotropy and the dominant pore

sizes and –shapes (Figure 10B) and on the analysis of the background, which represents the degree of heterogeneity at the rock-matrix-scale (Figure 10C). The analysis includes the shape and size of the nucleus, which is characteristic for the average pore size and pore shape and furthermore indicates, whether a sample is anisotropic or not. The background of the ACF-image provides us with information whether the pore distribution within the regarded area is rather homogeneous or heterogeneous. The contour of the dominant pore shape and size can be evaluated by thresholding the ACF at 39% (Heilbronner, 1992). The axial ratio b/a and the orientation of the contour at 39% are a measure for the axial ratio and the preferred orientation of the fabric anisotropy. Since for non-elliptical pores the shape-relation between ACF contours and shapes of fabric components ceases to be one of geometrical similarity, the shapes will not be considered in the discussion.

2.3.3.4.   Pore shape factor

Not only the amount of porosity, but also the pore geometry affects the physical properties of rocks (Anselmetti and Eberli, 1993; Ehrlich et al., 1991b; Lucia et al., 1994). Samples with the same amount of total porosity but with different pore shapes and pore connections can exhibit very different permeability. A study of Anselmetti et al. (1998) mostly on carbonate samples of the Great Bahama Bank has shown that permeability rather correlates to macropore geometry than to the amount of macroporosity. The pore-shape factor y is therefore at least as important as macroporosity. Early studies have shown that elongated pores have different effects on physical properties than do round pores (Brie et al., 1985; Wilkens et al., 1991). A measure of the pore shape is needed in order to describe the connectivity of the pores and to have an idea about the range of permeability. There exist many parameters, which describe in one or another way the pore shape. A widely used shape factor is the dimensionless shape factor y, which derives as follows:

$$y = \frac{P}{2\sqrt{\pi * A}}$$

P designates the pore perimeter and A the pore area. The value of y is equal to 1, if the pore is perfectly circular (in 2D) and it is larger than 1 for elongated pores. This pore shape factor is supposed to be correlated with the connectivity of the pores and therefore with the permeability of the rock at the investigated scale. Branching and elongated pores with a large perimeter compared to a relatively small area result in a high y-value. Such pores tend to contribute more to permeability than isometric pores. For isometric pores the probability to be isolated and non-touching is higher than for branching or elongated pores. But of course permeability and connectivity of the pores also depends strongly on the relative sizes and the abundance. Therefore the shape factor y has to be weighted and summed up in order to get a reliable and representative value for a whole sample. The weighing procedure used in this study is as follows:

$$\overline{y} = \frac{\sum_{i}(A_i * y_i)}{\sum_{i}A_i}$$

where for each individual pore the shape factor y_i is weighed with its area A_i. This procedure avoids a high number of insignificant, small pores with specific geometries, dominating a few

larger pores with different geometry, which due to their size are much more important for the properties of the whole rock (Anselmetti et al., 1998).

In addition to the standard analysis performed in most studies about the pore space, we have also incorporated data from the ESEM-images into the shape factor. The resulting shape factor is designated as y_{int} or integrated shape factor. For micropores the shape is not that well defined, because the depth information from the ESEM-images leads to some bias in the area- and shape-detection but it contributes significantly to the weighted pore shape factor as integrated calculations have shown. For the calculation of the integrated shape factor the much smaller area of investigation of ESEM-images has to be taken into account. These images have to be weighted appropriately in order to fully account for their statistical abundance. Each ESEM-image contributes the following weighing factor:

$$W = \left(\frac{1 - \phi_{mac}}{\#images} \right) * \left(\frac{A_{TSS}}{A_{ESEM}} \right)$$

For each detected ESEM-pore the value ($A_i * y_i$) and the area (A_i) are multiplied with the above calculated factor W before the summation, which finally yields the weighted and integrated shape factor y_{int}. The advantage of the integrated approach is that porosity-structure is considered on a much larger range and it allows for comparison to the integrated TOP-value and permeability- and porosity-measurements from 1inch mini-cores.

The macroporosity data set is calculated for pores down to a size of 16 pixels excluding edge particles. Therefore the lower limit diameter is 50 μm. However, tests have shown that the shape factor does not change significantly if all pores down to a size of 4 pixels are used for the calculations. For ESEM-images the dataset consisting of pores down to 1 pixel excluding the edge particles has been used. Here as well the shape factor does not change significantly (less than 1%), if a cut is made at 16 pixels. Thus, the pores considered for the integrated shape factor range from 10 mm till 50 μm and from 20 μm till 0.1 μm.

2.3.3.5.   Pore size distribution

The 3D pore size distribution is a critical parameter for many physical processes that take place in rocks. Methods, which are capable of determining the pore size distribution and its effects on permeability are important in petroleum industry and among them mercury injection capillary pressure (MICP) is the most widely used, however, it fairly accurately provides a reservoir analog when calibrated to measured values of reservoir fluid properties (Bliefnick and Kaldi, 1996). Instead of the time consuming procedure of MICP, pore size distribution was analyzed by using data from DIA. The pore size distribution of a rock provides us with information about distribution of pore types, storage capacity and permeability of the rock. The binary image of the TSS-pore space is a 2D-representation, which should provide us with information about the 3D-pore space. In order to get a real 3D-representation of the pore size distribution a relation between the size distribution of sectional circles h(r) measured on a thin section and the corresponding size distribution of spheres h(R) in the solid has to be found. Here a modified routine based on the public domain program *StripStar* is used, which has been described in Heilbronner and Bruhn (1998) and Heilbronner (2000; 2002a). This simple program applied to a given set of input returns the same result as the Schwartz-Saltykov method, which is best described in Underwood (1970). The theory underlying the StripStar program and the Schwartz-Saltykov method is the same. With StripStar the 3D-volumetric histogram V(R) is calculated, which is much more useful for

physical interpretation than a numerical density histogram only. Possible negative occurrences in the resulting 3D-histograms (so called anti-spheres) are not neglected but used as additional information. If the pores are interconnected like tubes, or if the pore size distribution is extremely well graded, the applied method is not valid anymore. None of these restrictions is occurring at the present dataset, however for very anisotropic pore structures one has to keep in mind the dependence of the pore size distribution on the relative orientation of the thin section.

In general the original distribution of measured circles on the thin section and the calculated volumetric distribution of spheres show a different behavior, which stresses the importance of this procedure. The volumetric distribution of the pores was calculated for all pores from the TSS down to a size of 4 pixels, with bin sizes of 2 pixels in order to get comparable histograms. The whole range of pore sizes (>20 µm) has been analyzed by adapting the number of bins for every individual sample. Data from ESEM-images has not been incorporated into the dataset, because it would disturb the distribution in a non convenient way, such as total overflow of the small pore classes. Data from ESEM-images has been analyzed in a similar way like TSS but separately.

2.3.3.6.   Specific surface area

The specific surface area is a dominant parameter in models for permeability and the transport properties of species that can adsorb on mineral surfaces. It is defined as the pore-surface area per unit grain volume and its unit is m^2/cm^3 or m^2/g. The specific surface area has been estimated optically, a method which takes advantage of the relationship between pore perimeter and pore area. For the estimation of the specific surface area from segmented 2D-binary images of thin sections several methods are available from literature. Underwood (1970) discusses several equations like Tomkeiff's eq., which uses the concept of intercept length, being based on the equivalent diameter of a particle and the relationship from Chalkey, which calculates the surface to volume ratio from the two parameters pore-perimeter and pore-area. Tiab and Donaldson (2004) provide a similar relationship that can be used to estimate specific surface area from 2D-binary pore images:

$$S_{sp} = \frac{4 \sum L_p}{\pi(A_{tot} - A_p)}$$

where S_{sp} designates the specific pore surface, L_p the pore perimeter, A_{tot} the area of the measurement window and A_p the area of all pores. The formula keeps the same ratio for the unit (m/m^2) as for the specific surface area (m^2/m^3). The S_{sp} calculated here comprises data from TSS as well as data from ESEM-images. The latter had to be multiplied with an appropriate factor, like done for the shape factor, in order to account for the smaller sample size of the ESEM-image (see chapter 2.3.3.4).

2.4.   Results and their interpretation

The aim of this study is the characterization of the pore structure at the rock-matrix-scale and its interpretation concerning depositional and post-depositional geological processes (see chapter 2.5.1). Furthermore, the impact of the observed pore structure on the hydraulic behavior of the rock matrix will be discussed (see chapter 2.5.3). The discussion is based on a

suite of purposeful basic results, which will be presented below. We start with the physically measured values on 1inch mini-cores like porosity and permeability, continue then with the optically measured porosity and cross-check them with plug porosity. Thereafter parameters from post-processed DIA-data will be presented, which best describe the pore structure like anisotropy, heterogeneity, shape factor, pore size distribution and specific pore area. Thereby a special emphasis will be set on the distribution of the parameters within individual lithofacies types and on the comparison of the parameters with porosity and permeability.

2.4.1. Porosity from 1inch mini-cores

Measurements of total plug porosity are available for 140 samples of boreholes MC2, MC3 and MC5 and will be discussed in the following section with regard to the evolution with depth and the characteristic values of individual lithofacies types. The spread for samples taken from the same half-core is an indication for the heterogeneity of porosity at the rock-matrix-scale. In MC2 measured values are highest in distal talus, above 40% and proximal talus, slightly below 40% (Figure 11A). The recrystallized reef core exhibits very low values between 5 and 15%. At MC3 reef core again exhibits lower porosities, which lie around 20% (Figure 11B). In the proximal talus values ranges from 15 to 45% and distal talus exhibits values at a higher level. 78 measurements are available for borehole MC5, where the embedded patch reef shows much lower porosities (10-40%) than the outer lagoon (Figure 11C). This is due to the partly recrystallized rock material (coral patches), which is filled in between with grainstones from the outer lagoon. Reef core again exhibits values between 15 and 20%. Surprisingly below the reef in the adjacent proximal talus even lower values are recorded (below 10%). The lower part of the proximal talus again exhibits high porosity in the range of 30-50%. Values in distal talus are very uniformly lying within a narrow band (40-45%).
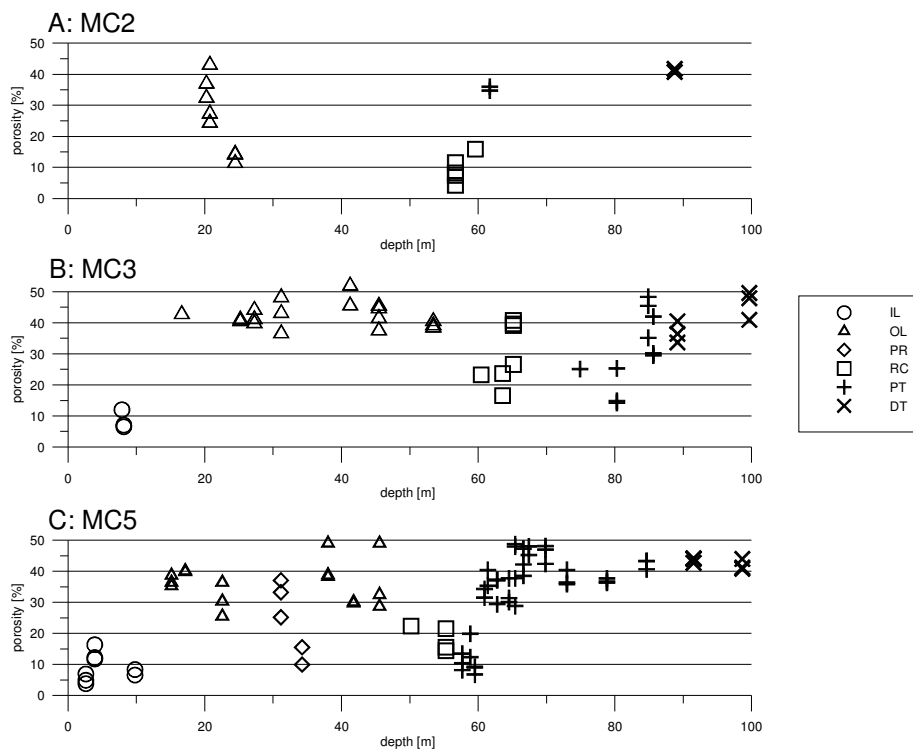
Figure 11:   Plug porosities measured on 140 samples for boreholes MC2, MC3 and MC5 and their evolution with depth.

For the evaluation of typical parameters for individual lithofacies types a simple statistical procedure has been applied. Each borehole has been divided into its lithofacies types and for each individual type the average of the measurements made, the standard deviation and the number of measurements has been calculated. The most outstanding observations are the high variability of the lithofacies types outer lagoon including patch reefs and reef core between individual boreholes. At the same time the trends of average plug porosity are absolutely equal but on different levels (Figure 12A). For these two lithofacies types including the subtype patch reef, lowest average plug porosities are measured in borehole MC2 followed by much higher values in MC5 and MC3. The two lithofacies types proximal and distal talus in contrast exhibit identical average plug porosities among individual boreholes. The standard deviation of values, which comprise an average value is very low for distal talus and thus an indication for the high homogeneity of this lithofacies type (Figure 12B). It is most probably not coincidence that for the lithofacies types outer lagoon and reef core, which belong to the most dynamic zone of the reefal complex in direction of reef-progradation (MC3-5-2), average plug porosities consistently become smaller. A direct link of the average plug porosity not only to depositional but also post-depositional processes can be supposed, since reef core at MC2 and MC5 is much more affected by erosional events and their related diagenetic overprint than at MC3, where the reef core is at a lowstand position. High standard deviations of the plug porosities in outer lagoon and proximal talus are explained by rudstones originating from storm events, which typically consist of reef debris and shell fragments. In the reef core large standard deviations originate from the unevenly distributed few cemented internal sediment, which has intruded into the strongly recrystallized framework of the coral heads.
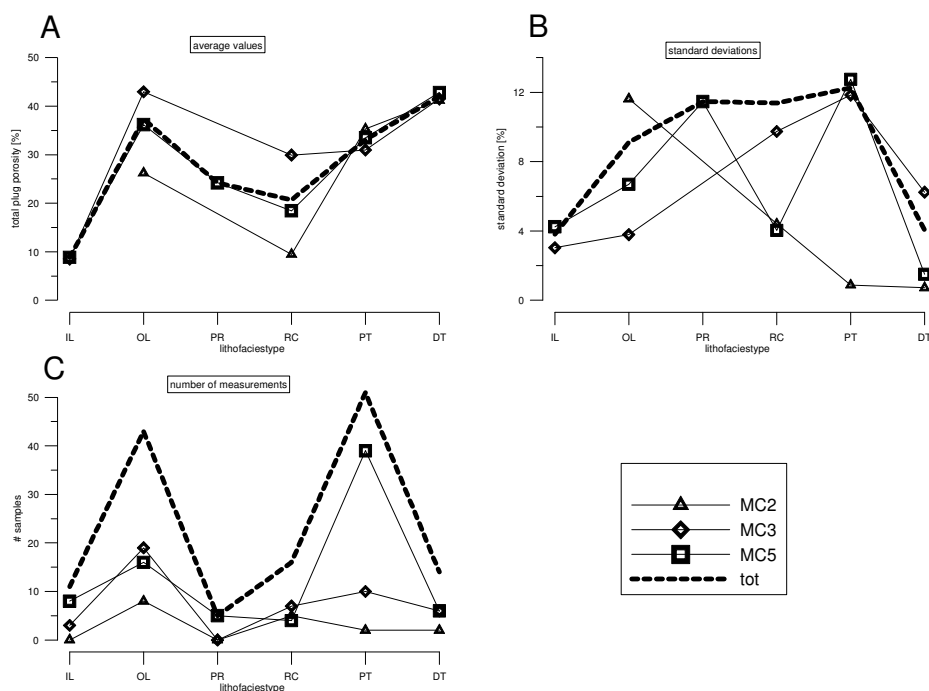
Figure 12:   Representation of the statistical parameters average, standard deviation and number of measurements from all 140 plug measurements. Values are calculated for each lithofacies type separately including the subtype patch reef (PR).

In order to study the distribution of plug porosities within individual lithofacies types, all measurements per type have been plotted into histograms. For outer lagoon a wide range with classes up to 55% has been recorded, however, about 90% of the samples exhibit porosities

larger than 25% (Figure 13B), which is similar to observations made for proximal talus. Both lithofacies types show a bimodal porosity distribution, however, with a dominant peak on the high porosity side. Low porosities of outer lagoon are mostly originating from framestones of patch reefs and wackestones or mud-dominated packstones of sequence boundaries. In proximal talus as well sequence boundaries are present, however, much more important is the low porosity zone right below the reef core, which is present at MC5 (see chapter 2.5.2). For the reef core, which is sandwiched in between it is the other way round. Almost 90% of the plugs showed values lower than 30% indicating a different depositional and diagenetic milieu (Figure 13C). In distal talus a very narrow spike is present at the porosity-class 40-45%, comprising about 75% of the measured values (Figure 13E). Its presence stresses the homogeneous distribution of porosity at the rock-matrix-scale and is typical for a distal environment, which is not influenced anymore too much by coarse grained reef rubble, being shed off the reef-top during intermittent storm events.
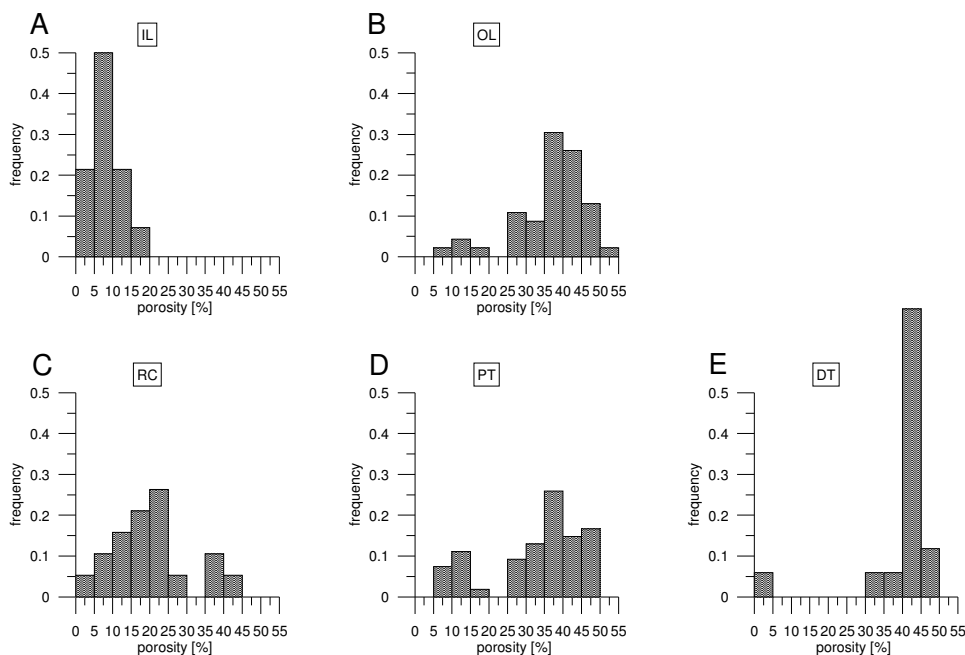
Figure 13:   Histograms of the measured plug porosities for each lithofacies type.

2.4.2.   Permeability from 1inch mini-cores

The permeability measurements, which have been performed on 40 1inch mini-cores originate from 25 representative half-core samples (Figure 14). From outer lagoon 13 measurements are available with a geometrical mean of 440 md. 5 samples have been extracted from reef core with the lowest geometrical mean of only 9 md. Most data is available from proximal talus, where 15 measurements yield a geometrical mean of 185 md. In distal talus 6 measurements have been made and yielded values with a geometrical mean of 50 md. The absolute minimum of 0.01 md was measured in reef core and the maximum of 7742 md in outer lagoon. This results in a very high range of almost 6 orders of magnitude, which is typical for matrix permeabilities of young unburied carbonates. Constantly high permeabilities have been recorded for outer lagoon and rather low values for reef core. Only few examples exist, where horizontal permeability is greater than the vertical one. The most remarkable hydraulic anisotropy has been recorded for one sample of the reef core, where k_h/k_v is approximately 1000. This is not surprising, since the rock matrix of the reef core is

mostly strongly recrystallized and thus depending on whether a touching vug is hit or not, a high variation in measured permeabilities is likely. Consequently as well ratios of 0.001 could occur within this lithofacies type. Proximal talus exhibits mostly high values, which are located in the range of outer lagoon, however, in addition very low values occur, which are related to mud-dominated packstones to wackestones and rhodalgal floatstones of erosional horizons and condensed intervals. Distal talus, which mostly consists of mud-dominated packstones, exhibits a much lower variability and lower permeabilities, which is due to the weak interconnection of the small and round shaped moldic pores. Even at similar total porosity compared to a sample of proximal talus, permeability can be two orders of magnitude lower (Figure 5E and F).
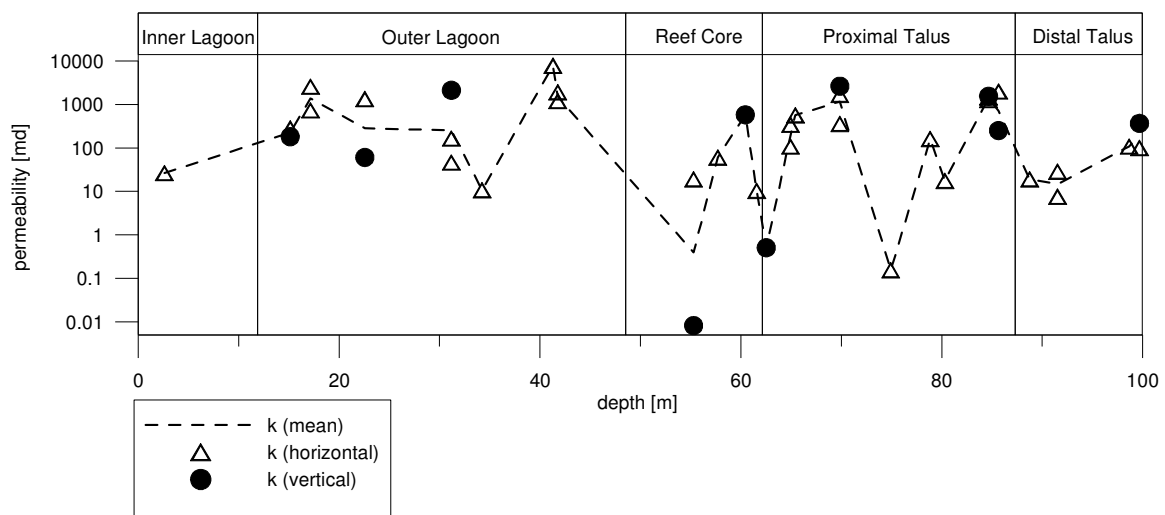
Figure 14:   Measured plug permeabilities for horizontal and vertical permeability. Dashed line marks geometrical mean of all measured plugs per sample.

2.4.3. TOP, pore types and their distribution with depth

Before a post-processing of data from DIA is performed, its validity and reliability has to be evaluated with a cross-check to measured plug porosity. The cross-plot TOP versus plug-porosity shows, that the right approach has been chosen (Figure 15). There is no overestimation of TOP at low porosities and no underestimation at high porosities as commonly reported from carbonate rocks (e.g., Anselmetti et al., 1998). The fields of view under the microscopes were therefore representative for the pore structure of the individual samples. In Anselmetti et al. (1998) thin sections have been taken from the plugs directly however the spread of the data is not significantly lower than in the present study. We think that this is due to the scale disparity, which occurs when TOP determined from 1x2 mm thin section images is compared to the porosity of 1inch mini-cores. The use of TSS's, which are of a similar scale than plugs, is surely a big advantage of the approach chosen here. The correct determination of the intrinsic microporosity from ESEM-images proved to be a challenging task. Based on the overall average of plug porosity (31%) and the assumption, that macroporosity has been evaluated correctly, a unique threshold for the ESEM-images can be chosen such that TOP equals plug porosity. It is important to state that the use of an overall and invariant threshold value is only possible because the composition contrast images all exhibit the same illumination and the same magnification. The resulting threshold is 115 for which an R^2 of 0.74 was achieved (Figure 15). Most part of the misfit between plug and thin section data is likely to be caused by the heterogeneity of the rock. The DIA-data set thus

provides a well defined and thoroughly elaborated basis for further data analysis, like evaluation of anisotropy, heterogeneity, shape factor, pore size distribution and specific surface area.
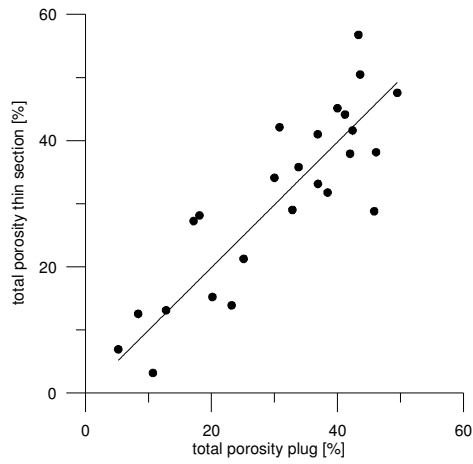
Figure 15:   Crossplot plug porosity versus TOP with a fairly high R^2 of 0.74 indicating that the correct approach was chosen for DIA on TSS.
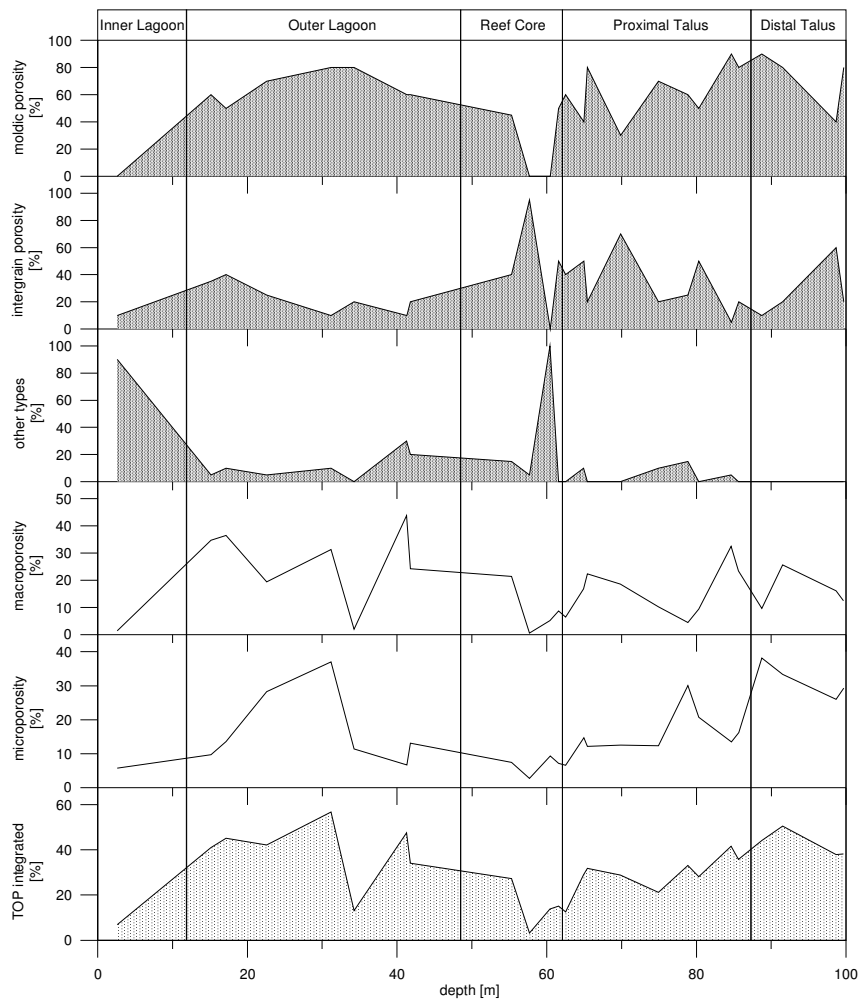
Figure 16:   Synthesis of poretypes and porosity acquired at the different scales. The upper 3 graphs are relative porosities and the lower 3 graphs are absolute porosities.

Since the validity of DIA has been proven and pore types have been defined already in chapter 2.2.2, the distribution of the different porosity types can be presented now, starting with the relative porosties of individual pore types, which comprise macroporosity. Moldic porosity is the most important porosity type occurring in the reefal unit of Llucmajor (Pomar and Ward, 1999). Observations made on core material from the test site revealed that in outer lagoon 60-80% of the macroporosity consists of large, mostly elongated moldic pores and only 10-40% of intergrain porosity, which builds the rest of the pore space (Figure 16). Within reef core intergrain porosity builds 40-95% of macroporosity and is especially typical for the internal sediment in between the coral framework. Some coral heads exhibit 100% framework porosity, which can be very low due to incomplete occlusion with blocky spar. In some samples vugs reach up to 40% of the macroporosity. Moldic porosity is again dominating in proximal talus lithofacies where a clear increase with depth from 40% to about 90% can be observed. Intergrain porosity accordingly decreases from about 60% down to not more than 5%. The quite heterogeneous rock built of rudstones, grainstones and packstones consists in contrast to outer lagoon mostly of small and round shaped molds. Exceptions are the rudstones at the bottom of this lithofacies type, which additionally exhibit large and elongated molds from shells of gastropods and bivalves and reef debris. In distal talus again small and round shaped moldic pores are predominant, accounting 40-90% to macroporosity; intergrain pores build the rest, which is 10-60%.

The intrinsic microporosity is in general high for talus sediments, where it contributes significantly to TOP. Highest values are recorded in distal talus with 30-40%. For a few samples around 30 m in outer lagoon microporosity can reach the same percentage but in most parts of outer lagoon, the whole reef core and the upper parts of proximal talus 15% are barely reached. TOP is highest in parts of the outer lagoon with values of 40-55% and the whole distal talus where porosity constantly lies at 40-50%. Within talus TOP increases gradually from 10% at he top to 50% at the bottom. This increase is mainly controlled by the increase of intrinsic microporosity between 60 and 100 m depth, which in turn is controlled by the more mud-dominated sedimentary fabrics in the lower part of talus. Furthermore, within talus generally the cementation decreases with depth and cements change from coarse grained and blocky at the top to micritic and disperse at the bottom.

2.4.4.   Assessment of anisotropy by rose plots

The binary images of the pore space contain information about anisotropy and heterogeneity, which are important for the petrophysical behavior of the rock matrix. First results from rose plots of the pore orientations will be analyzed and in the next chapter ACF-images of the pore space are presented, which in addition to anisotropy provide a possibility of characterizing the heterogeneity.

The possibilities of the interpretation of rose plots will be illustrated by the two examples 5_27 and 5_40 first (Figure 17) and thereafter the whole dataset will be analyzed. Sample 5_27 is quite an isotropic sample, especially for the pore size class 0.1-1 mm with an isotropy of 0.92. The smaller pore size class 0.05-0.1 mm is with an isotropy of 0.73 more anisotropic and the angle between the two preferred orientations is about 40°. The angle of the preferred orientations between two different populations indicates how the individual anisotropies account for the overall anisotropy. If the angle is large, intrinsic anisotropy of an individual pore size class can be significantly different from the overall anisotropy. On the other hand sample 5_40 is highly anisotropic at all displayed pore scales. For all three pore-size classes isotropy is only about 0.4 and the angle is close to zero. The angle of anisotropy between the

two populations can be of primary or secondary origin. Large elongated, moldic pores can have a different orientation than small intergranular pores, which is a fully depositional process and which is dependent on the energy of the sedimentary environment. Smaller pores can show a preferred orientation if a directional diagenetic modification of the pore space has occurred, to which smaller pores are more sensitive.
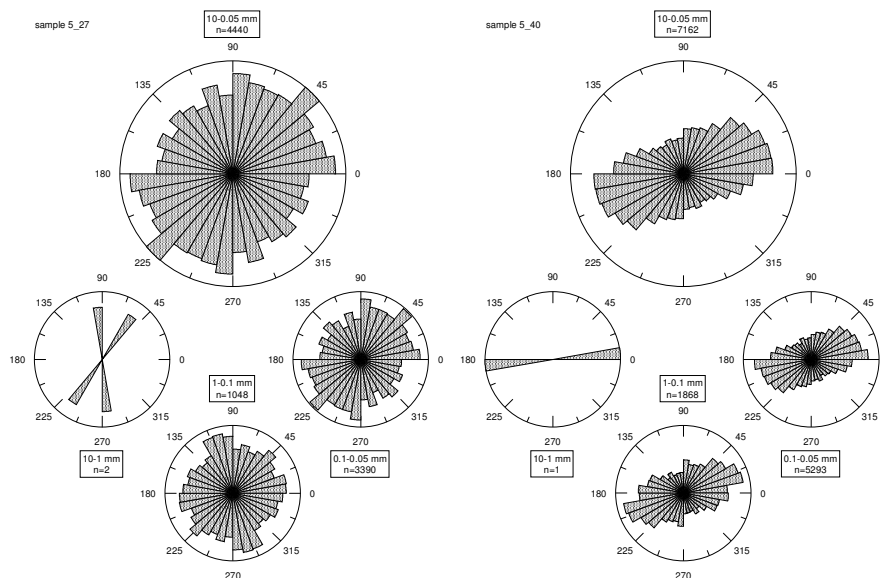
Figure 17:   Two examples for pore-orientation-based anisotropy assessment. The sample on the left side exhibits a high degree of isotropy for all pore size classes, whereas the sample on the right hand side is anisotropic for all investigated pore size classes.

For all 25 samples factors of isotropy have been calculated for the pore classes mentioned above together with the angle of the preferred orientations between the two smaller pore size classes (Figure 18). Within outer lagoon with 0.35 for class 0.1-1 mm the lowest isotropy values of the whole reef complex are measured. This fact highlights the complex sedimentary environment within outer lagoon, where certain inner reef currents and also intermittent storm events have led to highly anisotropic fabrics of the carbonate sands, consisting mainly of coarse grained bioclastic debris. Isotropy of the reef core lies on an intermediate level, ranging from 0.5-0.65 only. The angles show large variations from 5 up to 40°. Similar observations can be made in the underlying proximal talus, where the angles vary in the same range, however, variability of isotropy is much higher. Very low variability for both angle and isotropy at low levels is typical for distal talus and once again expresses its homogeneous character.

The larger pore class in general is more anisotropic than the smaller pore class, which can be explained by the fact that larger grains (initial stage of moldic pores) commonly have more elongated shapes and are more prone to be deposited in a preferred orientation. Smaller molds originating from peloids, ooids and small rounded bioclasts together with intergrain porosity are less sensitive to sedimentation-driven anisotropy. However for the lower part of the reef core and especially in the upper part of proximal talus, smaller pore classes are more anisotropic than larger ones, which cannot be explained by the sedimentary environment. The anisotropy of the smaller pores must be controlled by a secondary process, which is supposedly due to a post-depositional vadose cementation. Gravitation, which affects the direction of cement precipitation, could have led to the observed anisotropy. Smaller molds and intergranular pores of course are more sensitive to directed modifications of the pore

shape originating from incomplete occlusion and recristallization within the pore space than larger pores. Extensive investigations dividing the datasets into 5 different pore size classes showed that only samples from upper proximal talus gradually increase isotropy with increasing pore class. We suppose that a strong diagenetic overprint, such as vadose cementation or directional cement growth, e.g. driven by a fluid front (mixing-zone environment, paleo-waterlevel), led especially in the upper part of the proximal talus to an inverse trend. According to G. Eberli (personal communication) in any case the upper part of the proximal talus is a zone with a peculiar diagenetic history and thus such a secondary anisotropy seems to be a plausible explanation.
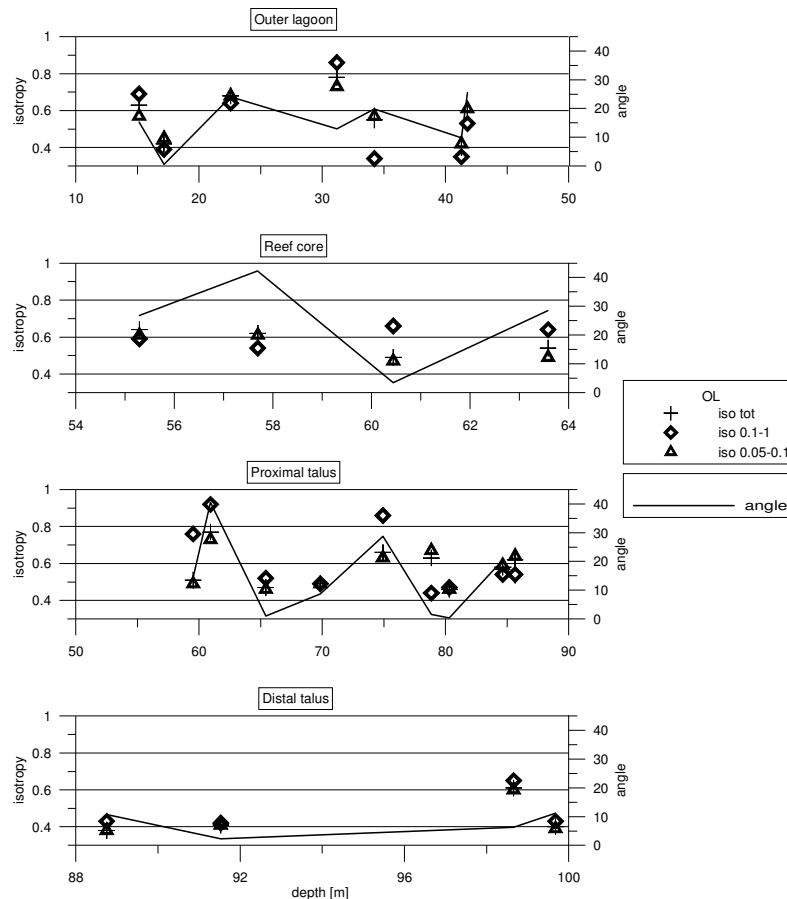
Figure 18:   The behavior of pore space anisotropy for two different pore size classes of individual lithofacies types. The solid curve represents the angle of anisotropy between these two populations.

2.4.5.   Anisotropy and heterogeneity by using ACF

In the following section the results obtained from the ACF-technique will be presented, which provides us with a first real measure about heterogeneity of the pore space. Three different cases of heterogeneity have been observed on the main dataset:

Homogeneous pore-fabrics have mainly been found in the lower part of the reef complex, where distal talus is outstanding (Figure 19A). The dominant pore size (DPS) is small. Such samples normally lack large moldic or vuggy pores, since at this scale of investigation they would automatically lead to a heterogeneous fabric. Some of the samples show a patchy behavior of the pore-fabric, which is typical for reef core (Figure 19B). This is in most cases due to a homogeneous background, which is disturbed by some sporadically occurring

macropores, being unevenly distributed over the plane of investigation. In many samples of the reef complex, especially in outer lagoon and the rudstones in proximal talus a heterogeneous fabric at this scale of investigation is present (Figure 19C). Large moldic pores and non-fabric selective vugs are typical for heterogeneous fabrics. The background image shows clearly autocorrelation at certain zones, which is expressed by larger and unevenly distributed patches. Samples with a heterogeneous pore fabric exhibit larger standard deviations for plug parameters, such as porosity and permeability. In some samples the nucleus extends to concentric elliptical shapes, which build a remarkable part of the whole image. The pore structure of these samples is additionally anisotropic and/or it represents the average grain shape. As investigations have shown, the anisotropy determined by the ACF-technique is comparable to the one assessed by rose-diagrams, however, the nucleus of the ACF-image seems to be more sensitive to large and elongated pores. The ACF-procedure has also been applied on ESEM-images and showed that for the applied magnification (2000x) the pore structure is heterogeneous in all samples and no trends could be detected for individual lithofacies types.

Dominant pore size (DPS) is indicating the average pore size and is high in outer lagoon and in some coarse grained sediment in the proximal talus. In the rest of proximal and distal talus DPS is very low. Homogeneous fabric and low DPS in the lower part of the reef complex reflect the low energy environment, which is typical for distal talus and parts of the proximal talus. In lithofacies types where DPS is large, permeability is large and vice versa. However, no good correlation between DPS and permeability was found. This result is not very surprising, since DPS yields average information about the whole macro-porespace of a thin section image and does not take into account single large pores and complicated pore shapes. The DPS furthermore is only affected by the pore size but not by its shape. However as investigations have shown, if the large macropores, which consist mainly of large elongated molds and vugs are removed from the dataset, a certain correlation with permeability is present.
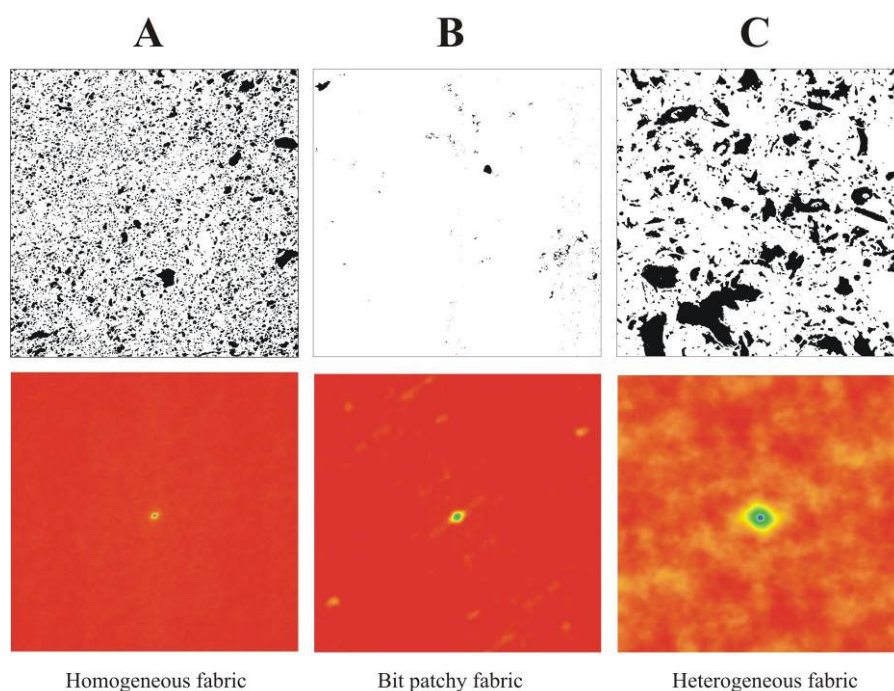
Figure 19:   Binary images and their ACF-equivalents of 3 representative samples of borehole MC5 at 91.53 m (A) at 57.69 m (B) and 55.29 m (C) are given. Side length of squared images is 1 cm.

2.4.6.   Genetic interpretation of anisotropy and heterogeneity

The pore structure of outer lagoon grainstones and packstones for macroporosity is mostly heterogeneous and can exhibit a remarkable anisotropy. The amount of moldic porosity is increased within this lithofacies type. A carbonate production, which is controlled by sea level fluctuations and a deposition, which is strongly affected by intermittent storm-events (Pomar, 2001a), together with extensive subsequent leaching of aragonitic bioclasts are the main factors, leading to the observed heterogeneity. Sediments in outer lagoon range from storm induced rudstone-lenses over cross-stratified oolithic carbonate sands till isolated coral build-ups like coral patch reefs. Bivalves and gastropods are very abundant within outer lagoon and the molds of their shells build a main factor of the pore shapes observed there. In grainy sediments anisotropy can develop through the surface parallel deposition of elongated grains. In this case the primary intergrain porosity as well as a probable secondary moldic porosity build together an anisotropic pore structure. This could be the case for sediments, which are deposited in outer lagoon or distal talus, where the deposition happens below the wave base or is not influenced by submarine currents. In outer lagoon some coarse grained sediments, which have been deposited above the wave base level show cross-stratification and are mostly well sorted and anisotropic, especially for larger pores. These sediments predominantly consist of bioclasts, such as shell fragments and pieces of corals.

Within reef core all kinds of sediments seem to be present. The reef core consisting of framestones, which are filled in between with internal sediment (bioclastic packstones to rudstones) builds a basis for all variations. The coarse grained sediments (rudstones, grainstones) are rather heterogeneous and the finegrained sediments rather homogeneous (packstones, framestones).

Proximal talus is mostly homogeneous, except for rudstones and grainstones, which have been deposited during storm events, when reef debris and coarse grained sands from the outer lagoon have been deposited on the slopes of proximal talus. In this lithofacies type again moldic porosity is the dominant pore type but its shape in general is different from the one observed in outer lagoon. Here the molds are mostly circular and small and only the rudstones with molds from shells have large and elongated shapes. The latter lead to the anisotropy observed for the lowermost samples. In parts of the proximal talus, where turbidity currents induced for example by storm events or slope instabilities occur, a certain inclined deposition of elongated particles is possible, however, in most cases the fabric there is isotropic at rock-matrix-scale due to turbulent and very fast deposition of a non-sorted sediment. The high energy milieu is rather indicated by isotropic behavior and high angles since the angle varies a lot if both classes are almost isotropic. In the upper part of proximal talus as mentioned in chapter 2.4.4, secondary processes affected the pore space such that anisotropy shows an anomalous behavior, which is unique for the reefal complex.

The packstones of distal talus are homogeneous and in the mud-dominated sediment a remarkable anisotropy of the pore-fabric is present. The low isotropy values here could be explained by the fact that the particles sedimented slowly in a non-turbulent and mud-dominated environment. Small round shaped molds and intergranular pores build together a highly anisotropic pore structure, which is probably due to early dissolution of aragonitic constituents and the subsequent compaction of the mud-dominated sediment together with a recrystallization of the matrix to micrite and microspar. Samples of these low energy sedimentary environments mostly exhibit low isotropy at low angles.

2.4.7.   Pore shape

This paragraph deals with the important shape factor, which resulted from the post-processed DIA-data. Shape factors of TS-images only (y_{TS}) yield values between 1.28 and 3.39, integrated shape factors (y_{int}), which are including data of the ESEM-images yield values ranging from 1.59-3.25. In general y_{int} is larger than the y_{TS} (Figure 20). Especially for low to moderate shape factors the integrated one is clearly higher than the single one only. For the largest factors it seems to be the other way round. In general the shape factor including all pores down to 0.1 µm size is larger, because microporosity, which mainly consists of intergranular and intercrystal porosity accounts significantly to the integrated shape factor. Samples from outer lagoon exhibit the highest shape factors, lying within a wide range. Samples from proximal talus as well occur on a large range, but the shape factors in general are much lower than for the outer lagoon samples. For reef core samples integration of ESEM-information does not change the shape factor significantly. Although only 4 samples are available the values all lie in a very narrow range. The same is true for the distal talus samples, which describe as well a dense cloud but the y_{int} values are much larger, than the y_{TS} values. The density respectively the size of these clouds is a measure for the heterogeneity on the regarded scale. Outer lagoon and proximal talus thus are more heterogeneous than reef core and distal talus.
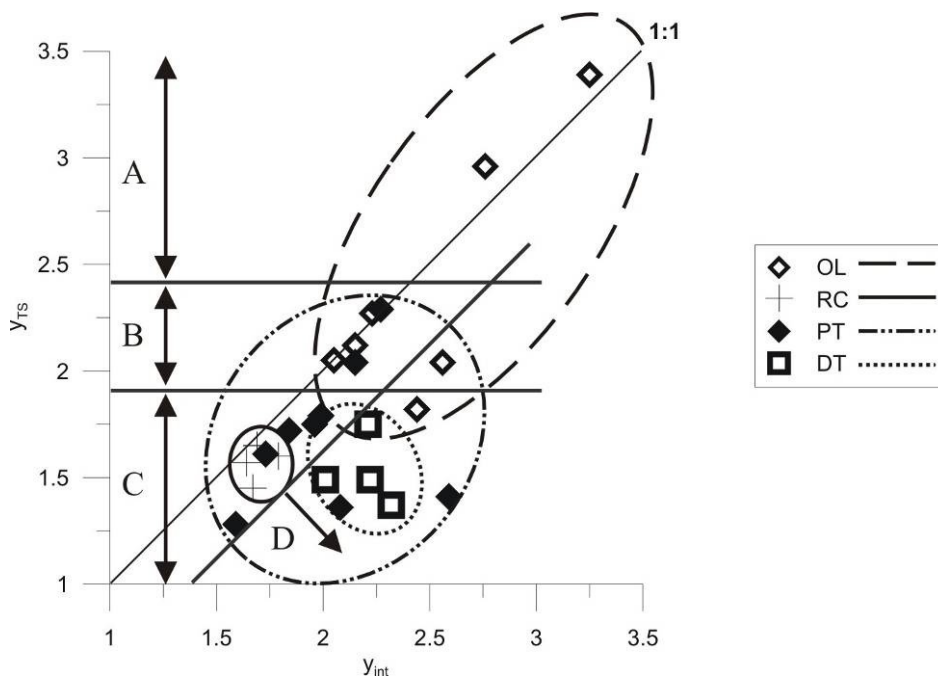
Figure 20:   Shape factor of the macropores versus the integrated shape factor. Elliptical envelopes mark the heterogeneity of the lithofacies types concerning observed pore shapes, respectively the spread of the data within individual lithofacies types. Zones A, B, C and D are discussed in the text.

Within zone A very high macroporosity (>35%) has been recorded, consisting mainly of large branching moldic and vuggy pores. The intrinsic microporosity is low and shapes are rather circular than branching. Zone B is typical for Lumachella-limestones. The micropores are mostly non-branching and still rather circular. Zone C is characterized by small round pores, which are mostly of moldic origin, like dissolved peloids and round shaped bioclasts. Zone D consists of samples with a very high intrinsic microporosity (>20%). These samples exhibit small, round shaped mostly moldic macropores and a very large intrinsic microporosity,

which includes large branching pores forming a mesh-like pore-network. We can state that the pore-structure and total amount of intrinsic microporosity determines the degree of misfit between the two shape factors. Furthermore, the weighted pore shapes y_{TS} and y_{int} are functions of the pore types, which are assembled within a sample. But each pore type occurs on a large range of pore sizes and thus a shape factor alone does not directly determine an individual pore type. It is therefore important to check the behavior of the shape factor for different pore size classes of individual samples.
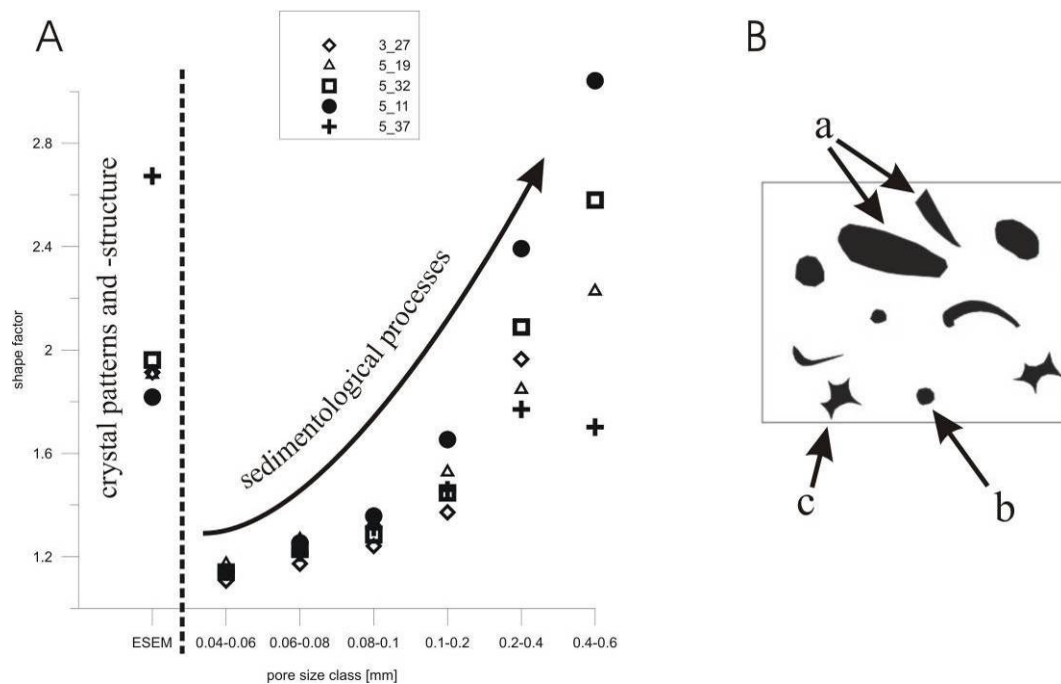
Figure 21:   Relationship of pore size and TS-shape factor for 5 different samples (A) and synthetic example of common poreshapes (B).

Larger pores or pore size classes generally yield larger shape factors for the macroporosity (Figure 21A). Furthermore, shape factors of ESEM-images lie in the range of these from larger macropores. The pronounced step between the smallest macropore class and the micropore class is mainly due to the fact that the ESEM operates in the subgrain-domain displaying crystal patterns and internal structures in contrast to the macropores, which are part of the grain-domain, mainly being controlled by depositional processes. If the pore structure of a sample consists of small isolated pores of moldic origin, which commonly are surrounded by thin micritic crusts and an intergrain porosity, which mostly has been occluded by calcite cements, the shape factors remain small and no larger aggregates of pores can form. However, if the pore structure is very dense, e.g. consisting of lots of moldic and intergrain pores, which have undergone only minor cementation, larger pores can be present with more complex shapes. Therefore especially for samples with a dense pore-pattern a clear increase of the shape factor from smaller pore classes towards larger pore classes can be observed. But of course there is also a genetic aspect, which has to be taken into account if one tries to explain the pore size dependence of the shape factor (Figure 21B). Moldic pores (a) originating from the dissolution of aragonitic shells, shell fragments and reef rubble are generally large and so are their shape factors (1.6-2.2 in the synthetic example). Spherical pores are in general small and of moldic origin, e.g. from the dissolution of peloids (b). These pores exhibit very low shape factors, which in the synthetic example range from 1.0-1.3. Intergranular pores (c) are

also rather small, but there exists the tendency to form larger aggregates, if occlusion of the pore space through calcite cement was minor. Shape factors there are on an intermediate level, ranging from 1.7-1.9. It is therefore not correct to state that larger pores exhibit larger shape factors, since aggregates of lots of small pores within a dense pore pattern as well as small intergrain pores, which are not occluded by calcite cement, can reach high values.

For both shape factors a clear dependency on the lithofacies type can be observed (Figure 22). Like for many other petrophysical properties, the proximal talus is the only lithofacies type where a clear trend with depth can be observed. The difference between the two shape factors is minor but the trend from low factors around 1.5 in the upper part right below reef core up to 2.5 in the lower part close to distal talus can be observed on both graphs and is undoubtedly outstanding. ESEM-images clearly show that microporosity increases with depth and that the micro-pore network gets more complex and connected as one approaches the distal talus (Figure 16). The increase in microporosity towards the bottom of this lithofacies type is presumably a result of the fact that more distally located sediments are rather mud-dominated. The increase of microporosity with depth is the main factor for the observed trend of y_{int} with depth in proximal talus. The higher y_{TS} at the bottom of proximal talus can be explained by the rudstones occurring there, containing lots of large and elongated molds and which contribute due to their size significantly to y_{TS}.
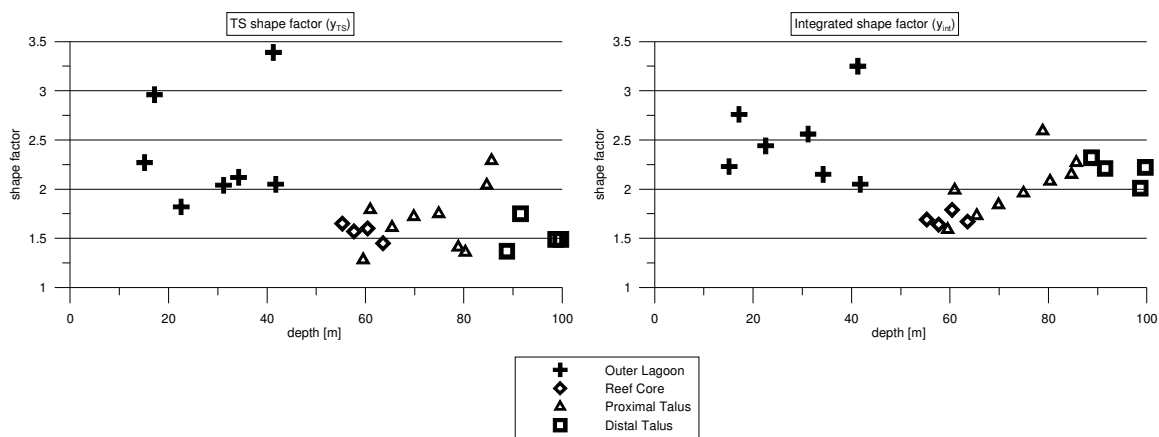
Figure 22:   TS- and integrated shape factor versus depth with distinction of the different lithofacies types.

2.4.8. Statistical parameters of pore size distributions

Porosity of sediments often follows a lognormal distribution with highest frequencies at low pore sizes. However, the ideal model of lognormally distributed pores or particles is hardly achieved in carbonates with a complex depositional and post-depositional history. Despite the fact that for carbonates no generalized distribution model can be found, the statistical parameters have a certain meaning for the pore structure, without the basis of a statistical model.

Mean and median of the volumetric pore size distribution have been weighted concerning their volumetric abundance. Low median values (<60 μm) are generally obtained for distributions, which resemble lognormal-distributions or, which at least lack larger pore-classes with high volumetric percentage. Thus, there is a concentration of small pores with no dominating larger pores. In general for median values >60 μm or mean values >100 μm a significant amount of macropores with r_{eq} larger than 500 μm is present. For the mean as for

the median a positive correlation can be observed, if the data is plotted versus macroporosity excluding samples with bimodal pore size distribution (Figure 23A+B). The scattered points belong to samples with bimodal distribution and those, which can be fitted, belong to samples with unimodal or pseudo-lognormal pore size distribution. These bimodal distributions are typical for grainstones and rudstones with large moldic or vuggy pores as they occur in outer lagoon and some rudstones of proximal talus. A similar observation was made concerning permeability, where as well for both mean and median data points from bimodal distributions plot outside the much smaller range defined by unimodal pore size distributions (Figure 23D). Two observations are outstanding: Mean and median both do not seem to have a large impact on the permeability and for samples with large macropores, like large elongated molds or vugs it is very difficult to estimate the permeability from these two parameters only. The fact that samples with dominant large macropores exhibit a different petrophysical behavior than samples, which lack these macropores, has been shown by Anselmetti et al. (1998) on Miocene reefal carbonates from the Great Bahama Bank.
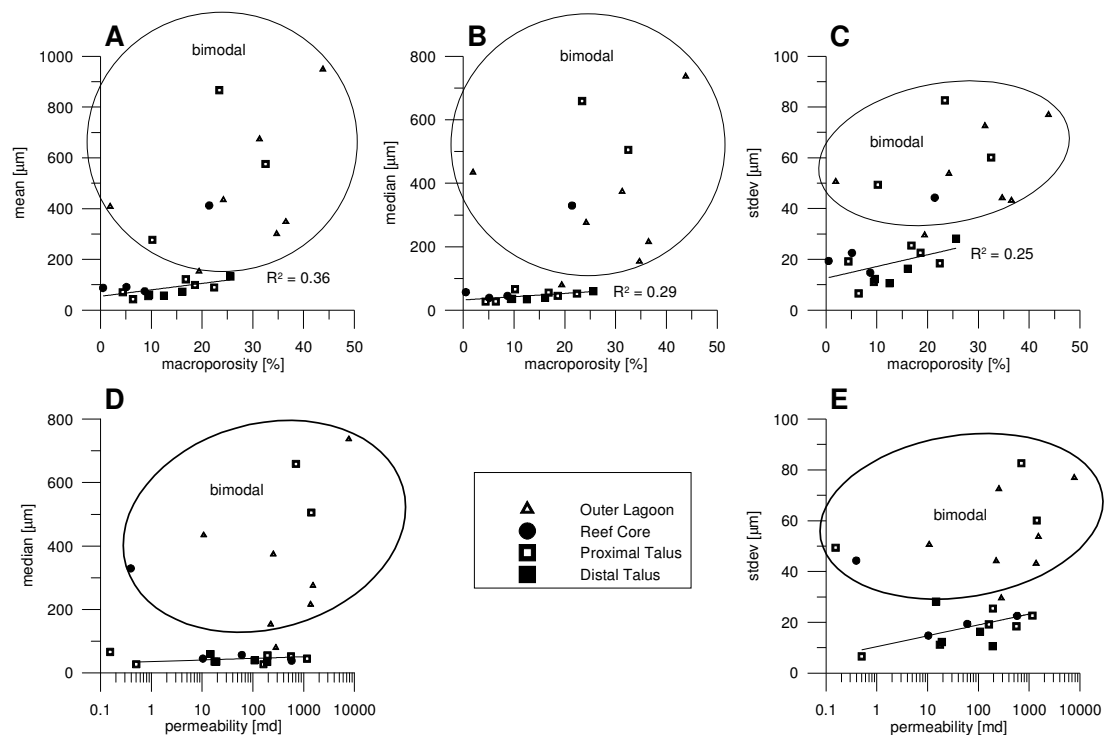
Figure 23:   Crossplots of macroporosity respectively permeability versus statistical parameters from volumetric pore size distributions. Bimodal samples mostly plot outside the unimodal range.

For the data set of the present study, an increase in standard deviation with increasing macroporosity is present (Figure 23C). High standard deviations for the porosity distribution implies a well graded pore space, which means that all different pores sizes are abundant and contribute to macroporosity, whereas low standard deviations point to well sorted pore populations with less macroporosity and rather isolated or non-connected pores. It can be seen from Poiseuille's equation and Carman-Kozeny that the flow passes easier through larger pores. Furthermore, a well graded pore space is rather interconnected and thus permeability in general behaves similar to macroporosity - it is larger for larger standard deviations and samples with a bimodal pore size distribution deviate strongly from the others (Figure 23E).

The statistical parameters of the pore size distributions have shown that there are major differences between samples with large moldic or vuggy macropores and samples, which lack such pores outside the pseudo-lognormal pore size distribution. It could furthermore be shown, that these differences in the shape of the distribution have major impacts on permeability, which will be investigated in more detail below by analyzing the individual histograms.

2.4.9.   Pore size distributions and implications for permeability

In this paragraph the histograms of volumetric pore size distribution V(R) obtained for the 25 samples will be discussed. The outer lagoon is in general dominated by high mean and median and rather high standard deviations (Figure 24A). Mean and median increase towards the bottom and the CV decreases slightly, which are indicators of higher permeability at the bottom (Figure 25). The moldic pore type is important in all samples from outer lagoon and intergrain porosity slightly decreases towards the bottom. A high permeability at the rock-matrix-scale can be postulated for this lithofacies type. Generally in outer lagoon the equivalent radius r(eq) of the pore sizes shows a distribution, which resembles a bit the lognormal distribution for smaller macropores till approximately 800 µm. But in all samples isolated moldic macropores, which are at least double the size occur and account significantly to the volumetric percentage V(R), leading to bimodal distributions. Some non-fabric selective vugs are present as well. These two types of large pores, which lead to high values for mean and median, are supposed to be important controls of the fluid flow through the rock matrix. In addition to their large size they mostly are elongated within outer lagoon lithofacies. As has been demonstrated in chapter 2.4.7, large pores generally exhibit larger shape factors than smaller ones. Therefore even if there is no pronounced anisotropy present, samples with such macropores should yield increased values for permeability, which was confirmed by the permeability measurements, yielding for outer lagoon values between 10 and 7742 md.
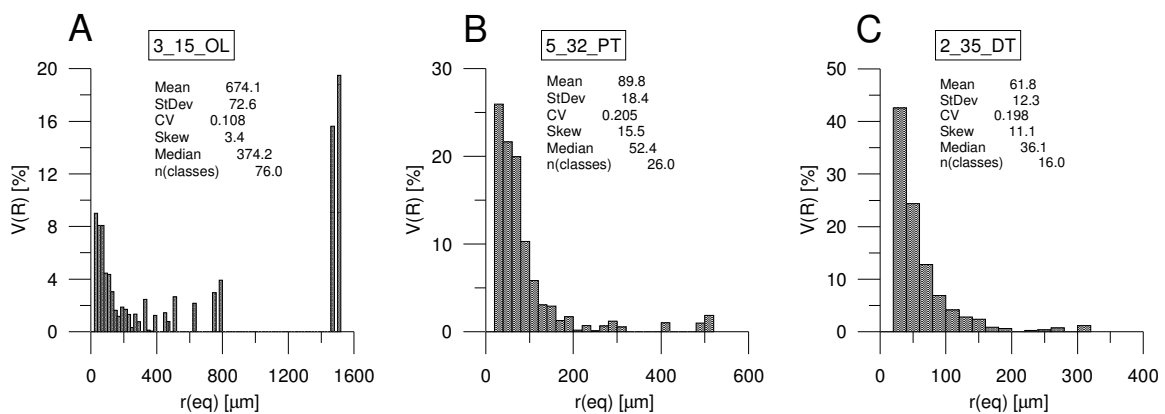
Figure 24:   Examples of typical pore size distributions for outer lagoon (left), proximal talus (middle) and distal talus (right).

Samples from the reef core show different characteristics. No typical example can be given because the distributions observed there are too diverse. Some samples seem to follow a uniform distribution and others the lognormal distribution. The reef core is quite heterogeneous at the rock-matrix-scale, since recrystallized framestones associated with coral heads can occur as well as internal sediment consisting of rudstones, bioclastic grainstones

and packstones with grain compositions comparable to those of outer lagoon. For most samples the median is low, with maximal r(eq) not exceeding 400 µm. This is due to the dominating intergranular pores, which in general are smaller (Figure 25). Permeabilities measured here range between 0.01 and 580 md.
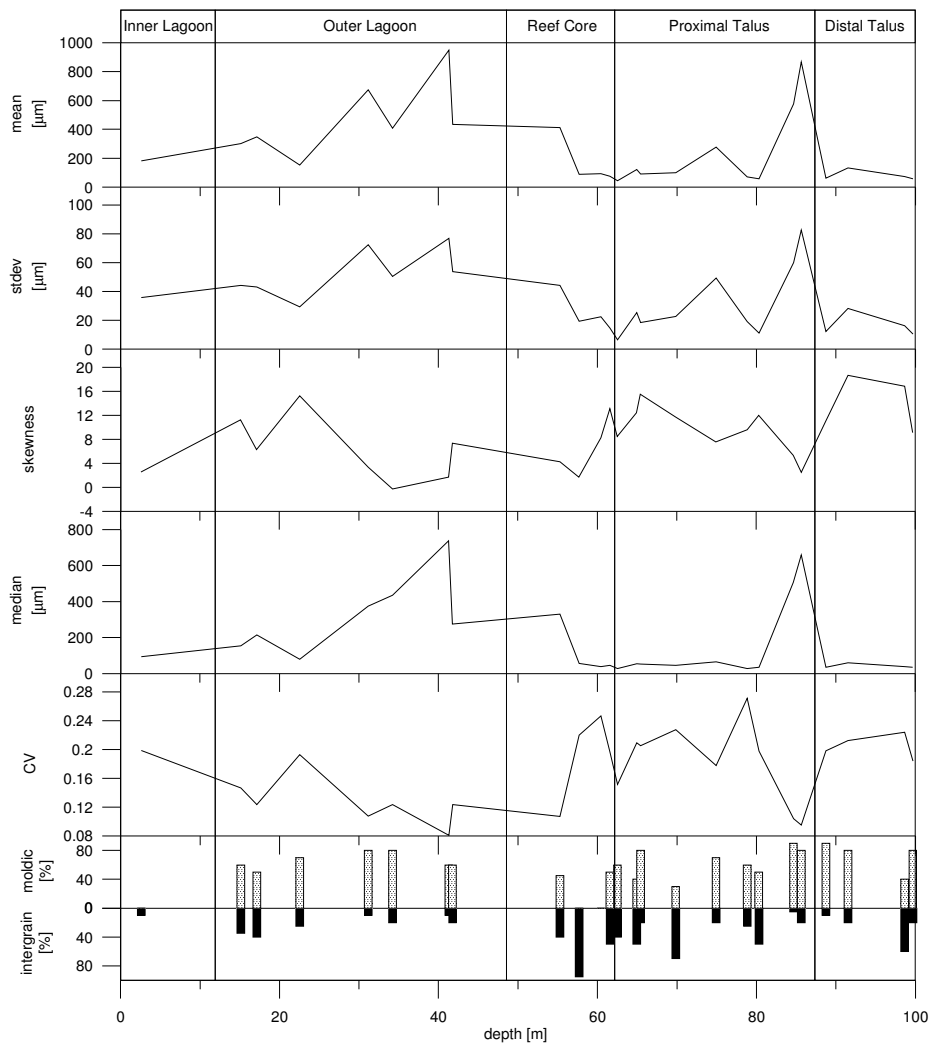
Figure 25:   Statistical parameters of pore size distributions are plotted as a function of depth together with the relative amounts of the two most important pore types moldic- respectively intergrain-porosity.

Pore size distributions for proximal talus samples show in most cases a lognormal shape, at least for the smaller pores (Figure 24B). Intermittent storm events and its location very close to the main carbonate factory led to a bioclastic sediment, with a variety of grain sizes, which consisting of lots of aragonitic fragments, led to a mainly moldic porosity structure with a large range of pore sizes. For larger pores V(R) often disagrees with the lognormal model. Mean and median are much smaller than for outer lagoon, mostly below 100 µm for r(eq). Large and elongated molds only occur at the bottom of proximal talus (Figure 25). The round and small molds are typical for distal talus as well. They build a framework-like pore structure, which exhibits a low pore-interconnection. The relative percentage of intergranular porosity, which is high in the reef core, decreases with depth within the talus. Permeabilities measured on 1inch mini-cores from proximal talus yielded values ranging from 0.15-2620 md.

Mean, median and standard deviation are low for distal talus lithofacies, thus the porespace mostly consists of well sorted small pores, which in turn express the distal sedimentary environment within the reef complex (Figure 25). Moldic porosity is even higher than for proximal talus. Permeability measurements yielded constant values ranging from 7 to 370 md only. The distribution is commonly pseudo-lognormal (Figure 24C). There is a high concentration of pores at small classes and significant macropores outside the pseudo-lognormal distribution are lacking. The similar shapes of the distributions for the individual samples stress the homogeneous pore structure even at this small scale of investigation.

Pore size distributions of ESEM-images were calculated as well and yielded uniform distributions for most of the samples. Microporosity significantly accounts to total porosity but is rather unimportant for the fluid flow through the rock matrix. An increase in microporosity counters permeability but the statistical parameters of the pore size distribution will not yield any useful correlation or information. The main reason for this is that microporosity mainly occurs in the subgrain domain and its pore size distribution therefore is not directly controlled by grain size distribution any more. The abundance, size and shape of micropores are rather controlled by the types of grains, their internal structure and the degree and type of cementation.

2.4.10. Specific surface area

The final parameter presented, which describes an important property of the pore space is the specific surface area S_{sp}. The determined values of S_{sp} are rather rough estimates, which can be compared relative to the others. For the Mallorca samples values ranging from 0.1 to 1.0 m^2/cm^3 have been found, which compared to the values given in literature (e.g., Tiab and Donaldson, 2004) seem to be reasonable for the S_{sp} (solid) of young unburied carbonates. A positive correlation between S_{sp} (solid) and TOP could be found (Figure 26A). In addition to the importance of the surface/volume-ratio to adsorption on porous media, the ratio of surface to pore volume is an important parameter in models of permeability (Hearst et al., 2000). S_{sp} (pore) yields a negative correlation with TOP indicating that larger porosities lead to a lower surface/pore-volume ratio (Figure 26B). Thus, samples with low TOP exhibit more complicated pore structures, yielding a much higher relative surface area per pore volume. Large pores, which account significantly to TOP yield only a minor percentage to the specific surface area. For permeability we would suppose to get an inverse proportional relationship to S_{sp}. The theory implies that large S_{sp}-values should correlate with low permeability values because at a large S_{sp} a lot of water is trapped in small pores and more adhesive water is abundant. The ratio surface to pore volume is not dependent on the amount of TOP any more and is really a characteristic parameter for the pore space of an individual sample (Figure 26B). The theory that in general for small S_{sp} permeability should be higher is confirmed by the plot and thus the relationship S_{sp} versus permeability is clearly a function of pore structure and not directly of the total amount of macroporosity (Figure 26C). Samples where the macroporosity is very low plot outside the common trend. Here the few pore volume, which is available, is mainly built of small macropores and micorporosity with a much higher surface/pore volume-ratio than other samples.

High values of S_{sp} (solid) have been recorded for distal talus (Figure 26D), where the fine grained and mud-dominated sediments built the basis for a pore structure, which consists of small intergrain and small spherical moldic pores and additionally for two samples in outer lagoon, where microporosity reaches values of 30-40%. Proximal talus samples as well yield intermediate to high values for S_{sp}. Lowest values are recorded in the reef core, which is due

to very low microporosity of 2-10% only. If the specific surface area for each sample is plotted versus depth, a decrease within outer lagoon towards its bottom can be picked out (Figure 26D). In talus in contrast an increase towards its bottom was recorded. A low S_{sp} (solid) not only correlates to a low TOP but is also dependent on the pore sizes, which tend to be rather large in such samples. The gradual increase of S_{sp} in talus and the high values in outer lagoon are mainly controlled by the amount of microporosity.
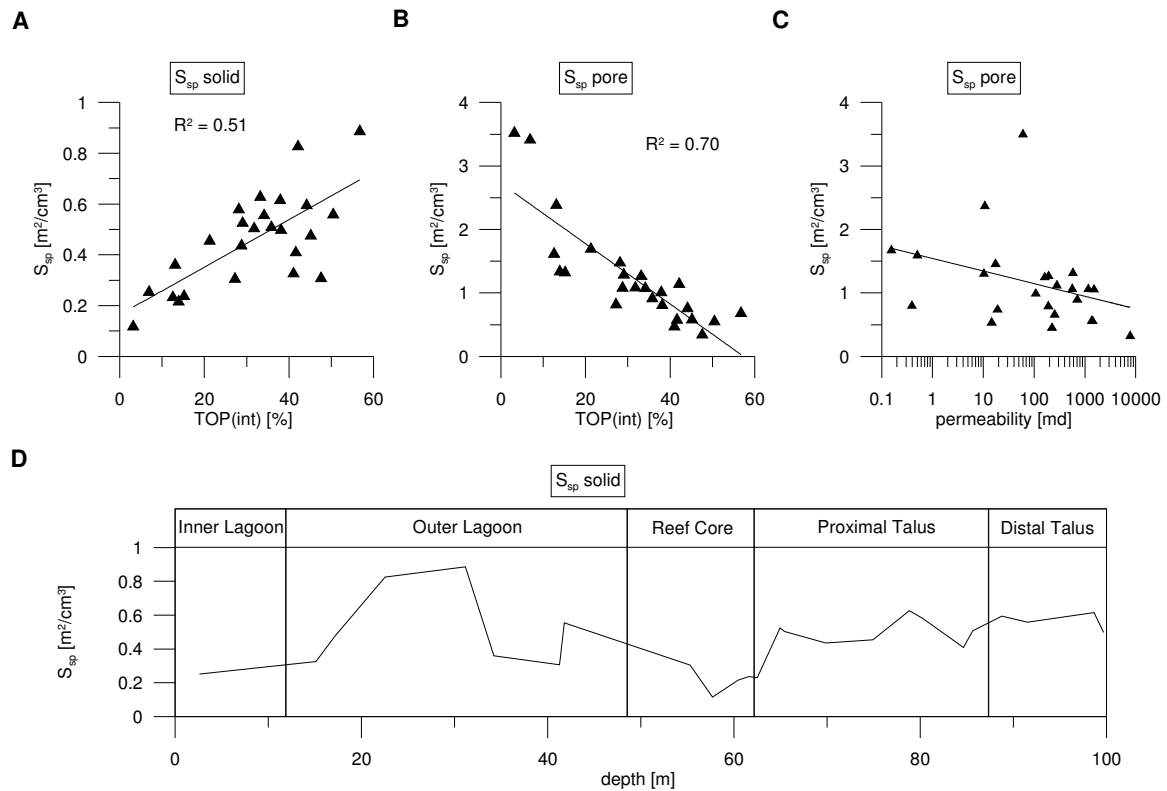
Figure 26:   Crossplots of TOP(int) versus S_{sp} (solid) (A), TOP(int) versus S_{sp} (pore) (B), permeability versus S_{sp} (pore) (C) and evolution of S_{sp} (solid) with depth with indication of lithofacies types (D).

2.5. Discussion

2.5.1. Geological interpretation of the observed pore structure and its distribution within lithofacies types and subtypes

The evaluation of the pore structure for every single lithofacies type has shown that characteristic values can be given. However, there still exist some remarkable differences within individual lithofacies types. This is mainly due to some typical architectural elements like patch reefs or rudstones whose distribution and occurrence is strongly dependent on the local reef setting (Table 2).

According to Pomar (2001b) the outer lagoon is a sedimentary environment with a high euphotic carbonate production, since in the shallow and protected water behind the reef barrier a diverse biota is present. Channels through the reefal barrier and tidal channels led to a well developed water circulation, which provided nutrients and oxygen rich water for the lagoonal inhabitants and which allow sediment to be efficiently transferred from the lagoon to

the off-reef slope settings (Pomar et al., 1996). Coral patch reefs with boring and encrusting organisms built local heights and were separated by depressions of bioclastic carbonate sands. The bioclastic carbonate sands and the storm induced rudstone lenses contained lots of large fragments of bivalves, gastropods and coral rubble, which after deposition, since mostly aragonitic, have been leached out and finally led to large and elongated moldic pores. Furthermore, an important percentage of the primary pore space has been preserved as intergranular porosity. The sedimentary environment of the outer lagoon was both high energy and low energy, dependent on storms and the location relative to channels and protecting reefs. Bioclastic grainstones deposited above wave base level are well sorted and show a remarkable anisotropy of the pore space due to cross-stratification. Thus, for most parameters describing the pore structure samples from outer lagoon show the highest range of the whole reef complex. Due to the high energy environment sedimentary fabrics are well sorted or at least coarse grained and mostly grain-dominated. Carbonate mud is missing, since it was winnowed by tidal currents and storm events and shed seawards on the gentle slopes of the talus. However, since the wave base level is quite shallow in protected areas according to Pomar (2001b) oligophotic biota, like red algae, larger forams or even photic-independent biota like bryozoans, sponges and crinoids may produce up to gravel sized clasts below the base of wave action. In this setting even fine grained sediments may remain in place, building up a depositional relief composed of unsorted sediments (mudstone-wackestone) until they reach the level on which according to the hydraulic competence particles start to be moved and sorted to produce packstone and grainstone. Anisotropy as well as porosity (40-55%) and shape factors are highest leading to highest measured permeabilities on plugs (up to 7742 md). Among the architectural elements within this lithofacies type, largest permeabilities occur in the rudstones, followed by grainstones to packstones and the lowest in recrystallized patch reefs. The patch reefs build low porosity- and permeability zones, since the original aragonitic corals mostly neomorposed to calcite and furthermore parts of the growth-framework pore space and the adjacent intergranular pore space were occluded by vadose blocky spar (Figure 27). Heterogeneity, which is given for example by the spread of the porosity measurements, is high in outer lagoon.

Lithofazies	Subtypes	Porosity range [%]	Permeability range [md]	Observations on pore space
Outer lagoon	Grainstones-packstones Rudstones Patch reef	20-**55** 10-30	10-**7740** Mean: 440	- **large elongated molds**, which are interconnected through intergranular porosity - rudstones above wave base show significant **anisotropy** and very **high shape factors** - framework porosity is mostly occluded by blocky spar
Reef core	Framestone Internal sediment	**0**-30 20-40	**0.01**-580 Mean: 9	- **framework porosity**, which is patchy occluded, some **non-fabric selective vugs**, few molds - **intergranular porosity** – partly occluded by **blocky spar**, few molds
Proximal talus	Grainstones Rudstones (MC5: 58-68 m)	25-50 40-50 5-30	0.15-2620 Mean: 185	- **moldic** and a high amount of intergranular porosity on top and round shaped molds, low intergranular and high microporosity at the bottom - **large elongated molds** and small round shaped molds, strongly anisotropic, high shape factors
Distal talus	mud-dom. Packstones	40-45	7-370 Mean: 50	- **small and round shaped molds** building framework-like fabric, **mud-dominated** fabric with high amount of **microporosity**

Table 2:   Important characteristics of the pore space for lithofacies types and subtypes.

The sedimentary archive of outer lagoon by far is not complete, since erosional events removed big parts of it. This is one of the main reasons for its remarkable heterogeneity because transgression and regression cycles sometimes separated by microkarst build the

main part of this lithofacies type. From the pore size distributions we learn that a remarkable volumetric percentage lies outside the pseudo-lognormal distribution, which goes up to 800 µm. Pore size classes at 1600 µm and higher typically form bimodal pore size distributions in outer lagoon samples. The smaller molds together with the intergranular pores build the gap-less distribution, which interconnects the large molds outside the distribution. The special petrophysical behavior of these large pores will be discussed in chapter 2.5.3.
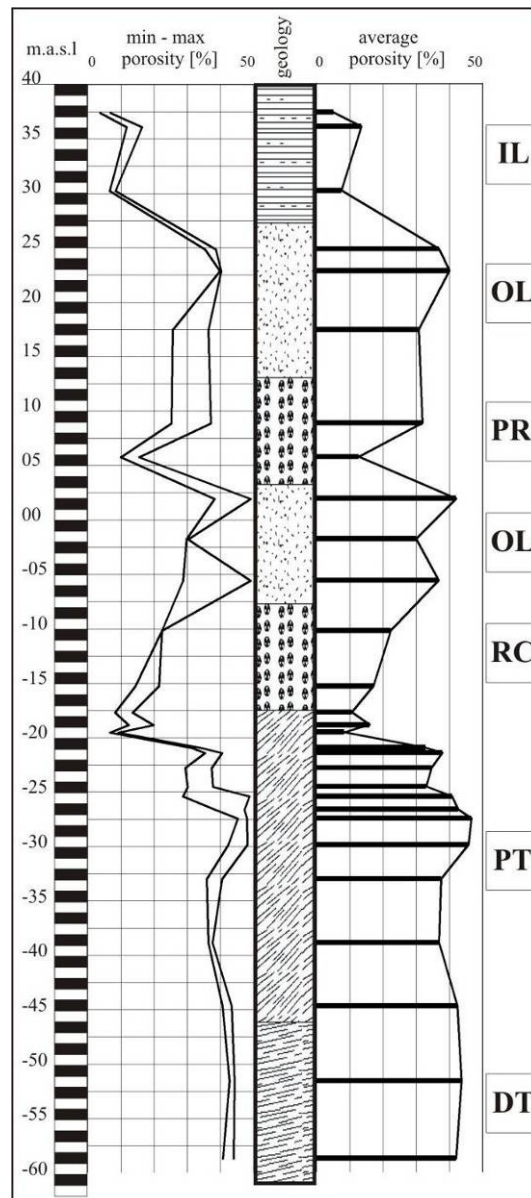
Figure 27:   Representation of measured plug porosities at borehole MC5. Indicated are from left to right depth in m.a.s.l., the measured bandwidth of plug porosities with min and max value, a simplified geological profile of the main lithofacies types and the position of the samples with the average plug porosities.

The transition to reef core in most cases is sharply bound. However, an erosional surface is not always present on core material. In general the well recrystallized reefal framestones are easily distinguishable from outer lagoon and proximal talus. Difficulties occur only, if internal sediment is present. In the reef core framework-producing organisms were able to grow above wave base, in addition to the predominant shallow-water euphotic carbonate production. The reef core is the most dynamic and formative genetic unit of the reef complex, controlling

sediment thickness and -composition within lagoon and talus. Furthermore, at scales larger than rock-matrix-scale it exhibits extensive primary and secondary pore space, which is due to coral growth, respectively leached corals, which influenced by several sealevel lowstands were subjected to extensive karst. Especially in the vicinity of such karst further leaching and recrystallization through neomorphism led to a very dense but discontinuous rock matrix. Especially the well recrystallized framestones contain besides a certain framework-porosity non-fabric selective vugs. Intergranular porosity is the most important pore type. However, in the vicinity of abundant karstic cavities most of it, as for the framework-porosity, is occluded by blocky spar. Plug porosities with 5-15% as well as measured permeabilities with mean of 9 md can be very low. Thus, despite the fact that large solution enlarged pores and the interconnecting intergranular porosity are present, permeability is low and consequently at the rock-matrix-scale reef core is not a reservoir rock. Similar results were found on samples from the Great Bahama Bank, where meteoric diagenesis led to low matrix permeability and permeability is controlled by vugs and caverns, however at a larger scale (Melim et al., 2001b). Furthermore, within this lithofacies type microporosity is lowest, since no mud could accumulate in such a high energy setting. Even the internal sediment is mostly mud-free and well sorted, which is in contrast to observations from other authors (e.g., Carozzi, 1995), who attested the constructional framework sufficient internal protection, to allow deposition of fine, interstitial matrix material.

Isotropy for all measured samples lies constantly at 0.6, however, the angle between individual classes is variable. Furthermore, shape factors are low and again very similar for all measured samples. However no typical pore size distribution could be evaluated and thus pore fabrics are rather variable indicating heterogeneity at the rock-matrix-scale. Microporosity is below 10% and its internal structure is not interconnected leading to the lowest specific surface area of the whole reef complex.

From the permeability measurements we learnt that here hydraulic anisotropy expressed by the ratio k_h/k_v can be equal to 1000 or 0.001, which is extremely variable. From plug measurements it is known that about 80% of all samples from reef core exhibit porosities lower than 25%, which is exactly the other way round than in the two adjacent lithofacies outer lagoon and proximal talus. Thus, there is a remarkable porosity-contrast at the upper and the lower bound.

At its bottom reef core interfingers with mostly non-recrystallized grainstones to rudstones of proximal talus. Especially the aggrading reef led to the accumulation of thick talus sediments, which are composed of grainstones intercalated with lenses of reef rubble. Anisotropy of the pore space is very variable indicating the depositional cyclicity of clinobeds and storm induced rudstone lenses. Whereas molds of leached reef rubble are more abundant in the upper part of talus, a trend of higher porosity at greater depth exists. As one moves away from the high energy environment of the reef core into deeper settings below the wave base, sediments become more and more mud-dominated. The increase in mud, which has been recrystallized to microspar or micrite is enhancing the porosity of these samples, since intrinsic microporosity can reach up to 40%. This is also the main reason for the increasing integrated shape factors with depth. As one approaches distal talus the micropore network in addition to the increase of its absolute amount gets more interconnected. Furthermore, intergranular porosity decreases with depth and the moldic porosity increases, however, the shape of the molds is different than observed in outer lagoon. Towards the bottom of proximal talus small and round shaped molds are more and more common. There molds formed through fabric selective dissolution of peloids and other well rounded bioclasts. Besides the planctic carbonate production during sea level highstands through the spurs and groves-zone

peloidal-skeletal carbonate-sands were transported from outer lagoon to the slopes of talus (Kenter et al., 2001). As well Pomar et al. (1999) report that carbonate-sediment shedding is volumetrically important, when the platform tops are flooded. At sea level lowstands carbonate production moved seawards and mostly skeletal sediments and lithoclasts were sedimented originating from the reef core and the uppermost talus. The originally high amount of carbonate mud has been reworked especially in the upper part by contour currents, like proposed by the authors above. Amalgamated rhodalgal biostromes mark winnowing during sea level lowstands on the shallow shelf, where only coarse sediment, rich in red algae remained in situ. The finer sediment was transported to the lower talus and slope. Red algal deposits furthermore only developed, where the basin floor was not too deep to allow sufficient light penetration.

The remarkable behavior of the proximal talus right next to the reef core will be discussed in a separate section below. Two sediment types are typical for proximal talus namely packstones to grainstones, which build the background sedimentation and lenticular rudstones, which are typical deposits shed off the parts above storm base during intermittent storm events. The rudstones especially occur in the upper part as a result of the interfingering with reef core, where coral fragments and other larger bioclasts are present. Furthermore, rudstones are concentrated at the basis of proximal talus, however with a different composition. There, much more shells of bivalves and gastropods are present and coral fragments are rare. In addition to the small and round shaped molds in the lower part of proximal talus, in these rudstones large and elongated molds leading to a significant anisotropy of the rock matrix are present (Figure 4A). Mean and median of the pore size distribution, which in proximal talus in general do not significantly exceed 100 µm, reach 500-800 µm within these basal rudstones (Figure 25). Consequently there measured permeabilities with 700-1400 md are among the highest of the whole reef complex. Recalling the increase of mud with depth and the geometrical mean of 185 md for measurements of proximal talus, this is a remarkable hydraulic contrast. Thus, despite the fact that they form lenticular layers of limited extent, a significant hydraulic anisotropy is present in a rather mud-dominated geological setting. The spread of different plug porosities measured at distinct depths reduces towards the bottom of this lithofacies type, indicated by the much smaller range of values (Figure 27).

Geologically the transition between proximal and distal talus is set below the basal rudstone, which has been observed in all boreholes. Packstones to grainstones of distal talus are mud-dominated and round-shaped small moldic pores originating from the dissolution of peloids are the most important pore type. Microporosity with values of 25-40% is highest of the whole reef complex and mostly due to the mud-dominated sedimentary fabric. Unlike observed in outer lagoon and the upper part of talus, there is almost a total lack of larger and elongated molds. The original carbonate mud, which originates from shedding off the lagoon and which as well formed in situ, e.g. by sediment feeders, recrystallized to microspar or micrite. Micritic crusts, which enclose the small moldic pores, impede a productive interaction between individual pores and most of the interparticle pore space is filled with microspar. The resulting pore structure is framework-like and compared to the high porosity rather of low permeability (Figure 5E+F). Melim et al. (2001a) state that in low k-samples as well moldic pores are important for permeability. However, if micritic crusts or else a dense cementation are present, molds are not interconnected.

Besides the high porosity of 40-50% and relatively low permeability of 7-370 md, digital image analysis revealed a clear anisotropy of the pore space of grainstones and packstones of distal talus. However, unlike in outer lagoon, where primary processes like water dynamics

above or at the wave base level led to a preferred orientation of elongated grains, anisotropy in distal talus is clearly of a secondary origin (see chapter 2.4.6). In distal talus particles were deposited slowly in a non-turbulent and mud-dominated sedimentary environment. Presumably the primary pore structure was isotropic, which was supported by extensive burrowing, which can either enhance or undo depositional anisotropy (Anderson et al., 1994; Gingras et al., 2004). Early dissolution of aragonitic constituents together with the subsequent compaction and recrystallization of the mud to microspar and micrite led to the observed anisotropy of the pore structure recorded at every single pore size class (Figure 18). The volumetric pore size distribution of distal talus is pseudo-lognormal and unimodal, without an isolated species of larger pores. Mean and median are lowest of the whole reef complex, barely exceeding 100 µm and maximal pore sizes only reach 400 µm, which expresses the high degree of homogeneity. The homogeneity is furthermore expressed by the fact that 80% of the plug porosities from this lithofacies type lie within the porosity-class 40-45%, which creates a narrow bandwidth of occurring porosities (Figure 27). The autocorrelation function, which is supposed to yield information about anisotropy and heterogeneity, even of very subtle features of the porosity structure, confirmed the results by smooth and regular backgrounds. The high amount of intrinsic microporosity in combination with a complex pore structure leads to enhanced specific surface area. Furthermore, integrated shapes are mainly controlled by the high amount of microporosity, which exhibits complex shapes and patterns. Thus, the integrated shape factor is remarkably higher than the one of macroporosity only.

2.5.2. Depositional and post-depositional interactions between lithofacies types

In this section we want to focus on the interactions between different lithofacies types. The heterogeneity of the reef core does not follow chronostratigraphical boundaries. Architectural elements, like reef core or proximal talus build lithostratigraphical units, which mainly control the distribution of heterogeneity. A further control on the distribution of heterogeneity are the secondary processes like formation of moldic porosity, vadose cements and the formation of extensive tertiary porosity with the accompanying alteration of the rock matrix in the adjacent rock. Important controls on diagenesis in carbonates are the original lithology, the depositional environment and the sea level history (Melim et al., 2001b). Primary porosity and its distribution within a lithofacies type furthermore are controlled by the local reef geometry and the evolutionary stage of the reef complex. For inner lagoon, proximal- and distal talus the latter seems not as important as for outer lagoon and reef core (Figure 12A). As for example averaged porosities, measured on 1inch mini-cores showed among different boreholes, remarkable differences in the average plug porosity can occur, which could be the result of different stages during reef genesis. In borehole MC3 porosities of outer lagoon and reef core are generally high, in MC5 including patch reef, they lie on an intermediate level and in MC2 porosities are lowest. The averaged porosity trends remain the same for each borehole, however on different levels. The question arises, whether this phenomenon is due to a primary depositional process or the result of a secondary diagenetic overprint.

On the profile MC3-5-2, which is located along the dip-section, reef-progradation occurred from MC3 over MC5 towards MC2 (Figure 3). Reef core at MC3 belongs to a lowstand systems tract, which later on becomes part of an aggradational systems tract at MC5 and finally part of an offlapping systems tract at MC2. The geological cross-section and the local reef evolution are analyzed in more detail in chapter 4. The offlapping and contemporaneous down-stepping between MC5 and MC2 was produced by a high order sea level fall, which led to exposure of the platform top and erosion within outer lagoon of MC3 and top of reef core

at MC5 and MC2. Additionally in MC3 outer lagoon is very thick and not capped by a patch reef. In MC5 and MC2 a patch reef could develop most probably behind a lower order aggradational stack, which is located towards the sea. Thus, the much higher average porosity at MC3 could be explained by the aggradational stack at MC5, which protected the low lying reef core of the lowstand systems tract at MC3 to be affected by subaerial exposure of the aforementioned erosional event. The reefal stack at MC5 was too thick to be fully removed by erosion and at MC2 the thin reef core was intensively recrystallized by karstic processes. However, as reported in chapter 3, reef core in borehole MC3 additionally was subjected to extensive post-depositional karstification, which is related to younger sea level lowstands. For outer lagoon at MC2 and MC5 the sandwiched position between reef core and patch reef could have led to lower porosities and at MC3 lots of rudstones have been recorded with high to very high porosity. Thus, whereas the differences of porosity between individual reef core parts can clearly be explained by reef geometry and subsequent diagenetic overprint, in outer lagoon differences in porosity are rather of depositional and thus primary origin. Porosity distributions within lithofacies types below the reef core are much less affected by local reef geometry and thus more homogeneous. Proximal talus in general shows similar averages for all boreholes but also very high standard deviations. Due to the depositional cyclicity with storm events and background sedimentation, building coarsening upwards clinobeds and lenticular rudstone layers, a sufficient number of measurements are needed in order to get similar average values for the lithofacies-sections between individual boreholes.

The main exception builds the uppermost proximal talus at borehole MC5 where a strange porosity behavior could be delineated. The outlines of the lithofacies boundaries are not always displayed correctly by the petrophysical data. The geological transition reef core/proximal talus lies higher than would be predicted from porosity data only (Figure 27). A closer inspection of the transition reveals that unlike expected, lowest porosities are not measured within the recrystallized framestones of the reef core but 2-3 m below in the top part of proximal talus. Furthermore, from this local minimum of about 5%, porosity increases downwards gradually to almost 50% about 8 m below. This zone, where the reef core is interfingering with talus is characterized by a low moldic porosity of about 40%, which increases towards the bottom and a high intergranular porosity of 60%, which in turn decreases towards the bottom. The rock at the transition is better cemented and coarse grained blocky spar with a patchy distribution is abundant. Within proximal talus towards the bottom an overall change of the cements to fine grained and micritic can be observed. Furthermore, an increase in microporosity towards the bottom of talus was recorded, which is mainly due to the rather mud-dominated sedimentary fabrics there. Another parameter, which illustrates the different petrophysical behavior at the top of proximal talus in borehole MC5, is anisotropy (Figure 18). As demonstrated already (see chapter 2.4.4) within the section of interest smaller pore classes are more anisotropic than larger ones, which is most probably due to a secondary process, like a post-depositional vadose cementation, which mostly affected the sensitive smaller pore classes. Since this zone seems to be restricted to MC5, a direct influence of the capping reef core is rather unlikely, however, the strong overprinting might have blurred former diagenetic effects and thus they cannot be discarded. Eberli et al. (2001) observed a strong relation between diagenesis and changes in facies, however noted that changes in sea level also influence the diageneitc processes. Consequently the considered zone at MC5 cannot be classified as a subtype, since it is of secondary origin and most probably not directly controlled by lithostratigraphy.

2.5.3. Implications for the hydraulic behavior of the reservoir

Despite the fact that a crossplot of permeability versus plug porosity will not yield a quantitative relationship (Enos and Sawatsky, 1981; Lucia, 1999; Melim et al., 2001a), it can improve the knowledge about the pore structure and highlight differences among samples from individual lithofacies types (Figure 28). Each lithofacies type has its own porosity-permeability relationship, which is dependent on the individual pore structure, which by Lucia et al., (1999) were designated as permeability fields. Samples from distal talus exhibit high plug porosities but permeability is relatively low. For the reef core plug porosities are much lower but permeability can be very similar to as observed for distal talus, which stresses the much better connectivity of the few large pores at the reef core, which are mostly non-fabric selective and touching through the intergranular pore space. Good fits on the crossplot can be observed for proximal talus and outer lagoon samples where the coefficient of determination is almost 0.7. Due to the similar behavior in the crossplot, pore structure of these two lithofacies types might be comparable. Like observed by Melim et al. (2001a), the predominant moldic pore type is connected in a continuous pore network, contributing significantly to permeability. The sedimentary fabric, which influences the pore structure a lot, builds together with secondary processes the main control of the porosity-permeability relationship. A mud-dominated fabric like, observed in distal talus results in much higher porosity compared to permeability than a grain-dominated fabric like observed for reef core. Grainy fabrics of high energy sedimentary environments like the reef core, outer lagoon and parts of the proximal talus have mostly undergone a winnowing, which washed the mud component out. The high porosity of small and round shaped moldic pores in distal talus is barely interconnected, since the original mud within the intergranular pore space recrystallized to microspar and micrite, leading to a framework-like pore structure.
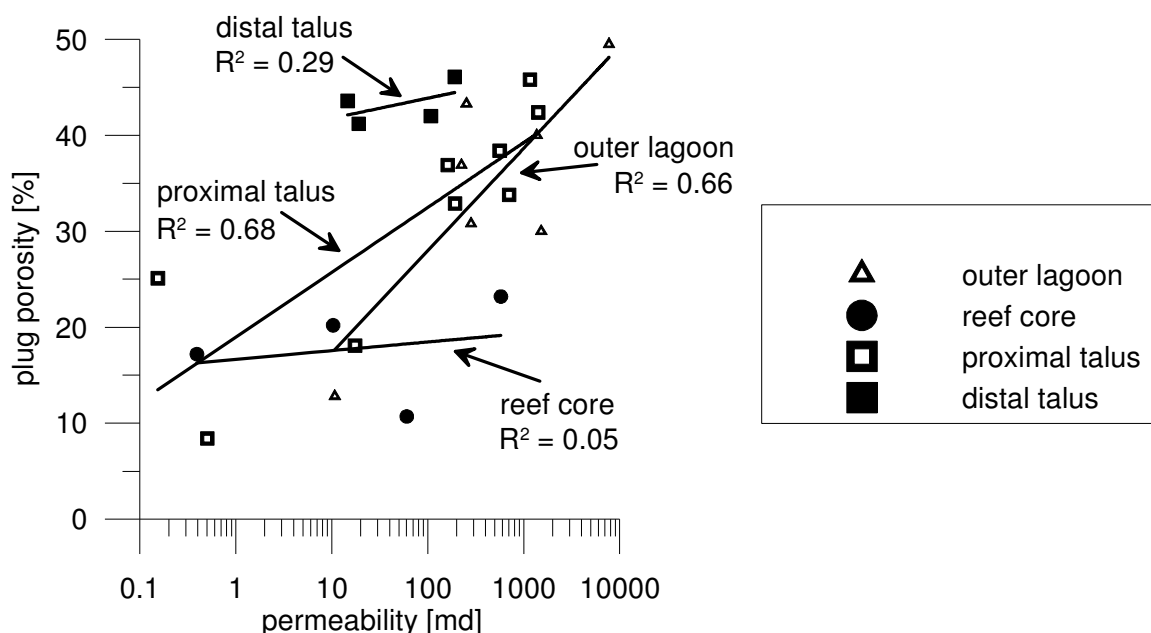
Figure 28:   Crossplot of permeability versus plug porosity with fits for each individual lithofacies type and indication about the coefficient of determination.

However, it is known that for example microporosity contributes to total porosity but in most cases is ineffective, since the smallest pores have very high capillary pressures (Bliefnick and Kaldi, 1996; Montoto, 2004). Crossplots of the different porosity types versus permeability

did not yield significant correlations, however it clearly appeared that permeability is rather controlled by macroporosity than by micorporosity. Already earlier studies (e.g., Anselmetti et al., 1998) showed that especially for larger macroporosities a weak correlation can be observed between macroporosity and permeability. For macroporosity lower than 4% they postulated a better correlation for microporosity with permeability. Since only 3 samples of the present study accomplish this requirement, this assumption cannot be verified here. Furthermore, it is known that permeability of a rock depends on its effective porosity (Flint and Selker, 2003), consequently it is affected by arrangement of the pores (anisotropy), pore shape, pore size and pore size distribution (Tiab and Donaldson, 2004). These major controls on permeability will be discussed below:

In a carbonate setting, which besides its complex, sea level driven architecture has been subjected to several stages of overprinting diagenesis, which at least partly was driven by the original architectural structure, a prediction of fluid flow within the rock matrix of the reservoir is fairly complicated. We found that anisotropy of the rock matrix can be split into primary anisotropy inherited from the sedimentary fabric and secondary anisotropy, which evolved through diagenetic processes. Since among other controlling factors there is a clear dependency on the absolute pore size, whether a pore was subjected to secondary anisotropy or not, we suppose that mainly sedimentary anisotropy can significantly contribute to the fluid flow within the rock matrix. Large elongated moldic pores, which are aligned lead to a directional orientation of the fluid pathways. It is questionable whether an overall isotropy dominates the hydraulic behavior of a rock, if the largest partial pore class is anisotropic. Larger pores should dominate the smaller ones concerning contribution to fluid flow, especially in connection with large shape factors, since large shape factors enhance the probability that pores are interconnected.

From the comparison of y_{TS} and y_{int} we predicted high permeability and lower storage capacity for samples from zones A and B to which most samples from outer lagoon and some samples from proximal talus belong (Figure 20). Large moldic pores and a small amount of rather circular and non-branching micropores lead to the observed shape factors there. In order to investigate more on the differences between the two shape factors and their influence on permeability, these data have been compared to porosity- and permeability measurements on the core plugs (Figure 29).

These crossplots tell us that there exists a good correlation for y_{TS} versus macroporosity, which is even better than for y_{int} versus TOP. Furthermore, a correlation could be observed for y_{TS} versus permeability, which again is slightly better than for y_{int}. The plots show that the fit doesn't get any better if ESEM-data is included. Since the shape factor is weighted for the pore size, large pores with a branching shape have a much bigger impact than do smaller ones. Most samples from zones A and B with low microporosity but high shape factors as expected plot at high permeability. Outstanding are the two samples from zone A, which plot outside the main trend at very high permeability. These two samples belong to outer lagoon and exhibit an extremely well connected pore space at a high moldic porosity. Obviously an upper border exists, where pore structure is not capable of enhancing the permeability any more and thus an exponential fit would be suspected for the relationship shape factor versus permeability. Samples with a high amount of small round shaped moldic pores, like observed in distal talus thus plot rather below the fitted straight line, because their shape factor is low with respect to the amount of porosity. Some samples from outer lagoon in contrast exhibit large and elongated touching pores, whose shape factor is high with respect to the amount of porosity or permeability. However, for the two lithofacies types reef core and distal talus permeability does not seem to be controlled by the shape factor too much. This is most

probably due to the non-touching and framework-like pore structure observed at these two lithofacies types. Isolated pores independent of their pore shape do not contribute significantly to permeability. Anselmetti et al. (1998) reported a good correlation of permeability with pore shape and concluded that permeability is controlled by macropore geometry rather than by macropore amount. For the dataset of the present study if the correlation is applied on the whole dataset, this statement can be supported. However, separate correlations for outer lagoon, distal- and proximal talus show better correlations to plug-porosity than to macropore geometry.
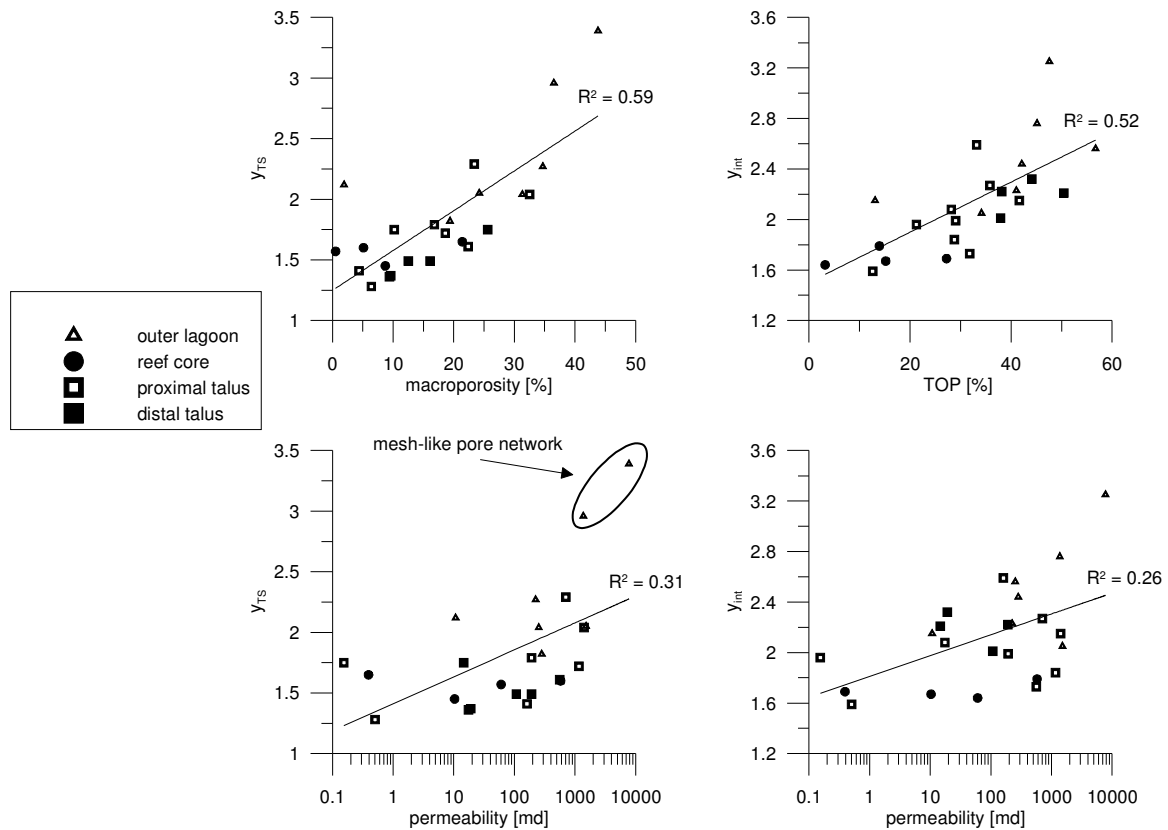
Figure 29:   Crossplots of y_{TS} and y_{int} versus optical porosity and permeability.

From literature it is well known that there is no direct correlation between porosity and permeability, unless pore size is not considered (Hearst et al., 2000; Lucia, 1983; Nelson, 1994; Serra, 1984). However, in this study crossplots of macroporosity versus permeability under consideration of the pore size like mean, median and DPS yielded only weak correlations. Mean, median and DPS are averaged parameters, which do not determine permeability. The division into pore size classes, which has been proposed by the authors above, is obviously not valid for carbonates with non-sorted pores and thus more complex pore size distributions. Extreme pore sizes, which are not considered by average values, have a significant impact on permeability. A small number of large pores can have a significant effect on the volumetric pore size distribution. As we learnt from shape factor analysis and determination of total optical porosity, large interconnected pores can strongly affect plug permeability. Whether the pores indicated at larger pore classes are connected or not cannot be stated from the pore size distribution directly but in general larger and elongated pores tend to enhance the permeability of the rock matrix considerably, especially if they are part of an anisotropic fabric or well interconnected through intergranular porosity. It was found that permeability correlates to median and standard deviation of the pore size distributions, if

samples with bimodal distributions were not considered. Samples with bimodal pore size distribution mostly originate from outer lagoon and the basal rudstones of proximal talus. Large pores, which build bimodal pore size distributions, enhance porosity and average pore sizes much more than permeability. But they as well are part of the interconnected pore network, which is bridged through the intergranular pore space.

The relationship of Carman-Kozeny relates porosity to permeability over the particle diameter. The equation has been adapted by Beard and Weyl (1973) in order to consider as well the standard deviation of the pore size distribution. For the dataset of the present study calculated permeability versus measured permeability yielded a good correlation, which proves that permeability is being controlled by the pore structure as we have seen it from the investigation of the pore space. At lower permeability a larger spread of the data was observed, which is not surprising, since here small scale heterogeneities can have a significant influence on the measured and calculated parameters.

Despite the difficult prediction of permeability from samples with bimodal pore size distribution rather high permeabilities at rock-matrix-scale have been measured for outer lagoon and rather low values for lower talus sediments. The boundaries of individual lithofacies types are not always precisely displayed (Figure 25 + Figure 27) but some outstanding characteristics of each lithofacies type were found and they show that the basic approach of dividing the geology into 5 main lithofacies types in order to characterize the 3-D-porosity-and permeability structure of the reefal carbonate complex was correct.

2.6. Conclusions

For each individual lithofacies type diagnostic features of the pore structure at the rock-matrix-scale were found. High permeability was recorded in outer lagoon and proximal talus, which is mainly due to well connected moldic porosity, which consists of large and elongated molds with large shape factors, leading to a prominent depositional anisotropy. In the upper proximal talus of borehole MC5 in addition to the depositional anisotropy a diagenetic anisotropy could be detected, however restricted to smaller pore size classes and thus less important for fluid flow. Reef core lithofacies is characterized by the lowest porosity- and permeability values of the whole reef complex. The intergranular poretype is the most important one, connecting the rare non-fabric selective pores. However, occlusion with blocky spar in zones of karst-influence is common. In distal talus porosity can reach very high amounts, however the small and round shaped molds are barely interconnected within the micritic matrix and thus permeability is low. In these mud-dominated packstones and grainstones high values of microporosity have been recorded, which is mostly ineffective for permeability.

It was found, that samples with a bimodal pore size distribution observed in outer lagoon and parts of proximal talus do not follow the common correlations between pore parameters and it is barely possible to predict permeability from parameters only. Furthermore, in these unsorted sediments, with mostly complex pore size distributions, averaged pore size parameters are not useful for characterizing permeability, since a few extreme poreshapes and -sizes can have a large impact on permeability. Thus, unlike proposed by many authors no pore size-dependent correlation of porosity versus permeability could be observed.

It has been shown that differences of the porosity- and permeability behavior within lithofacies types exist and some subtypes can be defined, being controlled as well by local

reef geometry. The diagenetic overprint, which as well was driven by lithostratigraphical contrasts, led to remarkable changes of the reservoir properties like formation of moldic porosity, recrystallization of the coral framework, partial occlusion of pore space by blocky spar within outer lagoon, reef core and proximal talus, which especially in reef core can be related to karst and recrystallization of mud to microspar or micrite in the shallow marine diagenetic milieu.

The energy-milieu and location within the former carbonate factory significantly defines the primary parameters, like grain size distribution, sorting, sedimentary anisotropy and mud content. Permeability of the rock matrix is not only dependent on these primary factors but also on secondary processes like leaching, neomorphism, blocky spar cementation and micritization.

The investigation of the reefal carbonate complex at the rock-matrix-scale showed, that the division into 5 main lithofacies types like reported by several authors from the Cap Blanc area, despite the fact that secondary processes blurred boundaries of architectural elements, was correct and thus on the basis of this first chapter about the rock-matrix-scale of the reefal complex further research can be focused on larger scales.

3. Borehole-Scale Porosity Structure of a Miocene Reefal Carbonate, Mallorca (Spain)

D. Jaeggi, M. Herfort, N. Van Meir, P. Pézard, S. Löw

Abstract

This study about the porosity structure of the Miocene reefal carbonate platform of Llucmajor on the island of Mallorca concentrates on the borehole-scale (cm-m-scale). Heterogeneities along the borehole at this intermediate scale are known to be important controls on reservoir behavior and have been investigated extensively with wireline borehole logs. Heterogeneity recorded along the borehole is strongly affected by the applied investigation method. Thus, for each logging tool, the exact knowledge of the investigation volume, resolution power and physical meaning of the measured petrophysical parameter is crucial for a correct geological interpretation. The main approach of this study is to integrate a sufficient number of different investigation methods with their inherent scale of investigation and their individual petrophysical relationship to the pore space into a comprehensive qualitative model of the porosity structure at the borehole-scale. Towards this aim the objective is not simply to compare data, but to constrain and characterize geological processes or effects that controlled the development of porosity and permeability.

In 2002, a project was initiated with EU funding, to develop diagnostic technologies for use in characterizing aquifers, suffering from salt water intrusion. At the test site near Campos on a cultivated field of 100x100 m, 5 fully cored 100 m deep boreholes (MC1-MC5) and 1 destructive borehole (MC7) were drilled, on which numerous standard logs provided insight into the variation of petrophysical and geological parameters along the vertical borehole axis. The main focus has been set on data from acoustic travel-time log, induction- and sonic log. Additionally impeller-flow-meter logs were run in order to localize the hydraulically active zones at the borehole-scale. The scan of acoustic travel-time as an optical high resolution method (1cm-resolution) is used for evaluating heterogeneity within the formation lithofacies types. With this method, the fine-scale sedimentary structures, which are known to be important controls of reservoir behavior, can be adequately characterized. Furthermore, the variability of heterogeneity can be expressed as a function of variable window-sizes.

Within the young, unburied reefal limestone of the Llucmajor platform, an important part of the total reservoir porosity is of a vuggy porosity type, like moldic-, intraparticle-, cavernous- and solution enlarged fracture-porosity. Lithofacies types control the primary pore structure and to a certain degree guide post-depositional processes, like blocky spar-cementation, dissolution of aragonitic constituents and neomorphism, which are mostly the result of numerous changes of the diagenetic conditions from vadose over freshwater phreatic to marin. At some locations within the reefal complex these processes blur the lithofacies boundaries, leading to complex log-responses. Within reef core primary pores and secondary porosity, which originate from the dissolution of aragonitic constituents, can be remarkably enlarged and interconnected to channels, if supported by karst. The channel-system, which is developed at the bottom of the reef core proved to be the most permeable heterogeneity of the reef complex. In addition to the integrated interpretation of borehole-scale pore structure, in this chapter quantitative porosities will be given and qualified carefully for each part of the

reef and the observed porosity structure will be related to depositional and post-depositional processes.

3.1. Introduction

This study is the second part of the multi-scalar reservoir characterization, performed on a 100x100 m test site, situated on the Miocene Llucmajor reefal carbonate platform on the island of Mallorca. In this chapter we will concentrate on the borehole-scale porosity- and heterogeneity, which has been accessed by a suite of standard wire-line logs. Whereas the first part of this thesis dealt with the description and geological interpretation of the porosity-structure at the rock-matrix-scale (chapter 2), here the rock massive scale (cm-m) (Montoto, 2004) will be investigated, a scale at which the rock matrix (µm-cm) can be viewed as homogeneous (Gueguen et al., 1996). Other authors designate the scale of well logs as mesoscopic scale (e.g., Tiab and Donaldson, 2004). In order to impede confusion with other scales of investigation, here the term borehole-scale will be used.

Subsurface characterization and assessment of the borehole-scale heterogeneity- and porosity distribution by wireline logs is a widely used approach and has been developed mainly by oil industry for hydrocarbon reservoir characterization. Numerous reservoir characterizations in carbonates have been performed so far, which in general showed that the utilization of different data sources recorded at different scales in general remarkably improves the knowledge about the pore structure and generates more reliable images about reservoir heterogeneity (e.g., Lucia, 1999; Montgomery, 1996; Montgomery et al., 1999; Saller et al., 1999). In aquifers the use of flowmeter logs is indispensable for the characterization of the hydrodynamical behavior of individual lithofacies types (Muldoon et al., 2001). Their integrated approach focused mainly on the correlation of downhole measurements with stratigraphy. Changes in stratigraphy, namely the distribution of individual lithofacies types, have a large impact on the reservoir behavior. Furthermore, small scale sedimentary structures within stratigraphical units or lithofacies types are known to be important controls on the reservoir behavior (Russell et al., 2002). Thus, logs, which are capable of resolving the stratigraphy to a high degree, such as image logs, play an important role in modern reservoir characterization.

For the correct interpretation of the sedimentary patterns and in order to have an idea about the architectural elements, their associated secondary heterogeneity and lateral extension, an appropriate architectural model of the subsurface is needed. The use of outcrop analogues for the assessment of heterogeneity of carbonate reservoirs has proved to be important, since facies-based porosity models result in the better definition of porosity distribution both vertically and laterally compared to models, where the facies-control is neglected (e.g., Kerans et al., 1994; Khalifah and Makkawi, 2002; Mace and Hovorka, 2000; Pomar and Ward, 1999). This is especially important in carbonate rocks, where stratigraphic complexity and distribution of primary porosity are the result of a sea level-driven hierarchical stacking of accretional units.

Since about 45% of the commercial hydrocarbon reservoirs in build-ups are of Miocene age, many intensive reservoir characterizations have been performed in such environments. However, most of these studies are about build-ups, which have undergone intense burial diagenesis and thus outcrop analogues are scarce. A depositional model of a Miocene reefal carbonate on the Philippines is given in Carrozzi (1995). There most of the commercial reservoirs developed in the complex barrier systems and atolls, in the frontal bioclastic talus

and in pinnacle reefs. Occlusion of the pore space was recorded mainly at the edges of the reefal build-ups. Extensive investigations on the Great Bahama bank with a suite of investigation methods, including lab measurements, wire-line logs and seismic lines, led to a geologically well constraint model of the multiscalar heterogeneity of the Miocene to Holocene sediments (Anselmetti and Eberli, 2001; Eberli et al., 2001; Eberli and Ginsburg, 1989; Warzeski et al., 2001). Some major log-responses, which are typical for the sedimentary patterns of Miocene reefal carbonates were derived there and will be compared to the investigation site of this study, under consideration of the different diagenetic history.

The best basis for outcrop analogues of the present study is the well exposed cliff coast of the Llucmajor reefal platform of Mallorca, which has been described in numerous papers (Pomar, 1993; 2001a; Pomar and Ward, 1999; Pomar et al., 1996). Early studies mainly focused on sedimentology, the geological evolution and the geometry of the reef complex and only briefly mentioned porosity structure and petrophysical relationships. However, some fundamental reservoir properties were given and will be discussed for the situation encountered at the test site near Campos. Already early studies revealed that the reefal structure and its architectural elements at the interior of the platform can be quite different from the extensively described Cap Blanc section (Pomar et al., 1996). Thus, certain care has to be taken when using outcrop analogues of the Cap Blanc section. Furthermore, most of the work done on the Llucmajor platform up to now was based on the well exposed outcrops at the cliff coast or on core material, originating from prospection-drillings from the interior of the platform, with poor core recovery and -quality.

The present study is based on a comprehensive suite of wire-line logs, performed in 5 fully cored 100 m long boreholes with perfect core recovery and -quality. Due to the complex sea level-driven architecture observed on dip-sections at the cliff coast, 6 km from the test site, the boreholes were drilled, such that borehole spacing lie in the order of meters to tens of meters. Besides the complex architecture of the reef complex and the distribution of depositional and post-depositional heterogeneity, karst is known to be an important control on reservoir behavior. Reservoirs can be compartmentalized significantly by karst modification (e.g., White, 2003; Worthington et al., 1999; Worthington, 2003; Worthington and Ford, 1997). For the Llucmajor platform karst collapse structures have been reported in the reef core and back-reef settings of the aggrading systems tracts (Ardila and Pomar, 2000). The development of groundwater conduits or even a mega-scale channeling is therefore possible and must be considered in the reservoir model. Thus, the tools used to assess heterogeneity at the borehole-scale must be chosen very carefully. The main approach of this study is to integrate a sufficient number of different investigation methods with their inherent scale of investigation and their individual petrophysical relationship to the pore space into a comprehensive qualitative model of the porosity structure at the borehole-scale. Towards this aim the objective is not simply to compare data but to constrain and characterize geological processes or effects that controlled the development of porosity and permeability.

Chapter 3.2 discusses the geology observed on core material, with a main emphasis on the porosity structure and the sedimentary textures. In chapter 3.3 the applied investigation methods are presented. A new method, which even allows for varying the scale of investigation, is the acoustic travel-time scan (ATS). Up to now automated scanning of the porosity distribution along binary images has been performed mostly at much smaller scales, like halfcore scans or thin sections (e.g., Van der Berg et al., 2003), however, barely at the borehole-scale and not from acoustic images. Here a new high-resolution method will be introduced and applied for the first time for the evaluation of the borehole-scale heterogeneity within the formation and the inherent scales of heterogeneity for each lithofacies type. By

varying the scale of investigation gradually, REV's can be assessed by statistically analyzing the obtained datasets. In addition, with this tool the fine-scale sedimentary structures, which are important controls of reservoir behavior, can be adequately characterized (Jackson et al., 1998). Thus, for the evaluation of cm-m-scale heterogeneities along the borehole, the acoustic travel-time scan provides a valuable alternative to imaging tools, like FMI and FMS, which have been used in lots of recent studies (e.g., Russell et al., 2002).

Impeller flowmeter logs have been run in order to detect major preferential pathways in the highly porous reefal carbonate. These logs allowed for a direct measurement of flow and the productivity of the reservoir, whereas pumping tests did not yield any measurable drawdown. The standard gamma log was indispensable for detecting sequence boundaries and having a control about the clay content of the formation. Induction logs were run in combination with temperature-conductivity logs for the assessment of the formation factor. The sonic tool records the velocity distribution along the borehole and its signal is known to be affected by the pore type and thus yields information about the down-hole porosity structure (Anselmetti and Eberli, 1999; 2001).

In chapter 3.6 by integrating all available data, for each lithofacies type the pore structure will be discussed individually and a clear distinction between primary or depositional porosity, secondary porosity, which is the result of diagenetic processes and tertiary karst-porosity will be made. Furthermore, effects of sea level stillstands and processes, which occur in the mixing-zone, will be addressed and their impact on the porosity structure discussed. In chapter 3.7 based on the observations made on the pore structure, possible implications for the hydraulic behavior of the reservoir will be discussed.

3.2.   Geological setting and parameters controlling the borehole-scale porosity structure

3.2.1.   Regional overview and previous work

The investigation area lies on the upper Miocene prograding reefal platform of Llucmajor in the south western part of the island Mallorca about 6 km inland from the well exposed cliff-coast, the so called Cap Blanc section. The steep sea cliffs, which display in exquisite detail the facies architecture and the high-frequency depositional sequences of the reefal unit, build the western and southern margins of the platform and have been extensively described in the last 15 years (e.g., Pomar, 1993; Pomar and Ward, 1999; Pomar et al., 1996). To the east the Campos basin, which seems to have subsided only during Pleistocene time (Jenkyns et al., 1990) and to the north the Mesozoic basement of the Serra de Levante, to which the platform onlaps build the borders. During late Tortonian and early Messinian time the platform prograded on a gentle depositional profile about 20 km towards south and south west and shows a highly complex architecture, driven by eustatic sea level changes with aggradation and progradation but without backstepping. Transgressive retrogradation is missing, because the rate of carbonate production could keep up with the rate of creation of accommodation space (Pomar and Ward, 1995). The upper Miocene was a time of tectonic stability and low terrigeneous influx, consequently reefal architecture and distribution of lithofacies are mainly controlled by sea level fluctuations of 4th to 7th order. According to Pomar and Ward (1999), most of this flat lying platform has been buried no more than several tens of meters. The platform was only slightly deformed by Pliocene-Pleistocene uplift, faulting and gentle flexure. Minor burial compaction and scarcity of pervasive cementation has preserved much

of the primary porosity. The platform was overprinted by complex patterns of dolomite and secondary porosity that are related to probable third- and fourth-order sea level fluctuations.

The Cap Blanc section can doubtless act to a certain degree as analogue model for the inner parts of the platform, however at least 3 different reef morphologies have been described along the exposed cliff coast (Pomar et al., 1996). Oldest reefs are the mound-like Vallgornera reefs, which are constructed of massive and columnar colonies of *Tarbellastraea* and *Porites*. Channels cutting perpendicular to the reef tract are filled with red algal grainstone. The Cala Beltran reefs are composed of the same coral assemblages but lack the mound-like morphology and the reef rock there is pervasively dolomitized. These reefs are elongated perpendicular to the direction of reef-progradation and as well separated by 2-3 m wide basin-ward channels. Cap Blanc reefs are predominantly build of *Porites* and show a well developed morphology of aggrading and prograding sequences. Coral morphology shows a clear zonation, which is related to paleo-bathymetry. From the mapped reef tracts it is not possible to determine to which of these reef types the reef of the present study belongs to but it is certainly much older than the outcrops described along the coast.

3.2.2. Borehole-scale heterogeneity and local reef architecture

The test site near Campos lies about 6 km inland from the splendid outcrops of the well exposed cliff coast, about 40 m above present-day sea level. In 2003 and 2004 on a squared agricultural field with 150 m side length, five fully cored and five destructive boreholes, each 100 m deep have been drilled with diameters ranging from 100-300 mm. Furthermore, two large diameter pumping-wells and a 270 m deep prospection-borehole, which were preexisting at the beginning of the campaign, are available (Figure 30). Generally the uppermost 40 m of the boreholes are dry, followed by a freshwater lens, which is about 20 m thick. Below from 60 to 80 m the mixing-zone is present, which in this study is defined as the transitional part between fresh water above and sea water below, with conductivities of 5'000-35'000 µS/cm. The water level lies about 1.5 m above sea level and the very low hydraulic gradient points towards the sea.
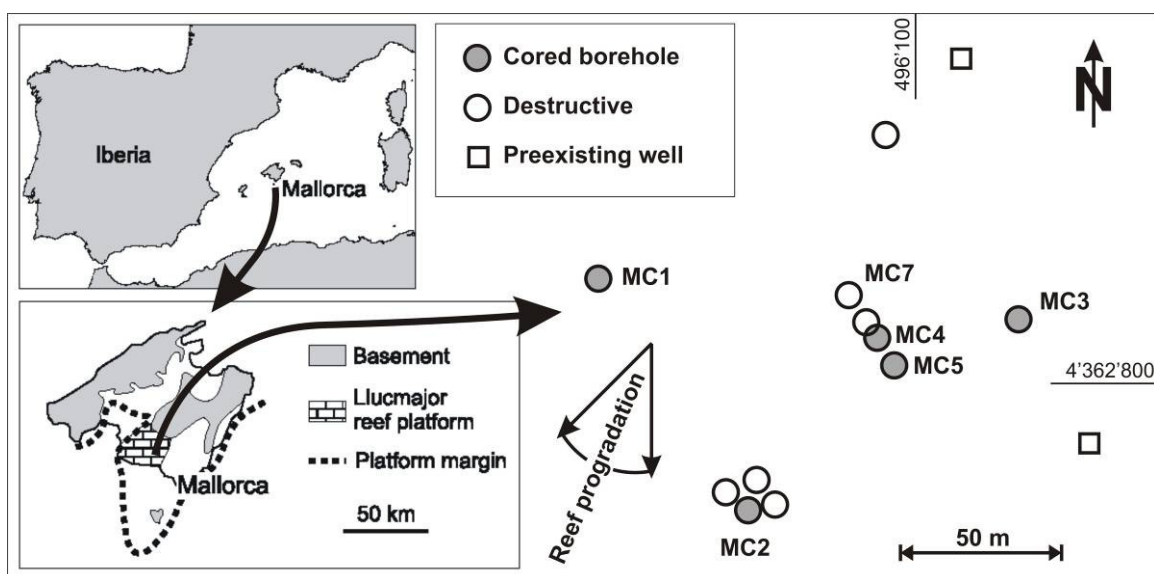
Figure 30:   The Campos site lies on the late Miocene reefal carbonate platform of Llucmajor about 6 km from the cliff coast and consists of 5 fully cored and 5 destructive 100 m long boreholes (modified after Pomar & Ward, 1995).

For the present study the five cored boreholes with excellent core recovery of 88-95% build the data basis together with some supplementary information from the destructive boreholes. The 5 cored boreholes revealed lithofacies types, which are comparable to those reported from the Cap Blanc section (Pomar et al., 1996). A detailed description of the geology at the rock-matrix-scale together with an analysis of the lithofacies types is given in chapter 2. The potential direction of reef-progradation was inferred from the reef tract-map of the platform (Pomar and Ward, 1995) and points towards the south or southwest. Pomar et al. (1999) illustrated that from borehole data only, without the information of outcrops about lateral continuity of the architectural elements, a correlation of lithologic units is difficult. Additionally paleobathymetric coral-morphology zonation within the reef core framework, which would allow a much better sequence stratigraphical understanding, is not feasible in boreholes. Using the sequence stratigraphical concepts derived at the well exposed cliff coast under consideration of scale and size of the depositional packages can significantly support the conceptual model of the present study. However, it is still hypothetical as long as no high-resolution data from cross-hole- or surface-geophysics is available, which could eventually trace the most important boundaries. Thus, geological sections together with a detailed analysis of sequence stratigraphy will be given in chapter 4, which is dedicated to the porosity structure at the crosshole-scale (chapter 4).
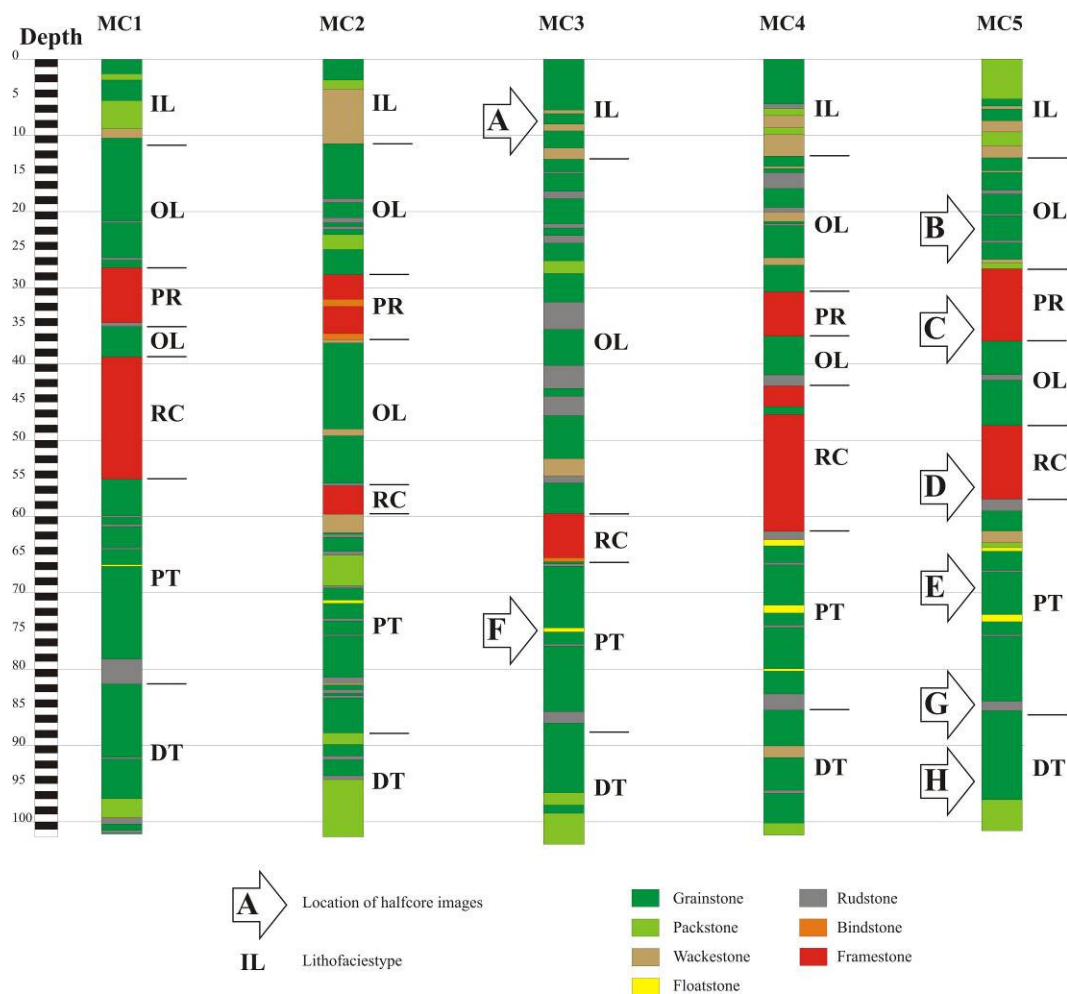
Figure 31:   The five fully cored boreholes of the test site with the main sedimentary textures and indicated boundaries of the lithofacies types inner lagoon (IL), outer lagoon (OL) including as well patch reefs (PR), reef core (RC), proximal talus (PT) and distal talus (DT). Furthermore, locations of extracted halfcore scans A-H (Figures 30 and 31) are given.

For the illustration of the lithofacies types and their position and extent along the boreholes observed at the test site near Campos, the observations made by visual core description are represented by seven simplified sedimentary textures (Figure 31). Furthermore, the five 100 m long boreholes are subdivided into lithofacies types, which from top to bottom are: Inner lagoon (IL), outer lagoon (OL), which as well includes patch reefs (PR), reef core (RC), proximal talus (PT) and distal talus (DT).

At the test site near Campos the reefal unit is capped directly by an alternating succession of grainstones to packstones (Figure 32A), with marly packstones to wackestones and layers of sandy clays. The latter are more abundant towards the bottom of this lithofacies type and mangrove roots with a restricted marine fauna as well as blackened grains and caliche hardpans are abundant. The dm- to m-thick layers are flatly bedded and a correlation is possible through all 5 boreholes. It is interpreted as inner lagoon with typical restricted biota and intermittent continental influence. The continuity and horizontal bedding infer that this succession is occurring over an area, much larger than the site-perimeter of the present study. The correlation with the inner lagoon facies described at the Cap Blanc section is quite evident, however stromatolites above the mangrove-root layer are lacking. A remarkable erosional surface builds the sharp boundary to the underlying outer lagoon, which builds the thickest and probably most heterogeneous lithofacies type of the reef complex.

Outer lagoon consists mainly of horizontal layers of intensively burrowed bioclastic or peloidal grainstones (Figure 32B) and rudstones with a non-restricted biota. Outer lagoon sediments are mostly deposited in a low energy and shallow water environment, which is protected from the open sea by the reefal barrier, however, channels cutting perpendicular through the reef allow sediment to be transported to the fore reef environment. Furthermore, bioclastic grainstones and rudstones from the outer lagoon act as internal sediment between the massive coral build-ups of the reef core. The predominant pore type is moldic porosity, which is fabric-selective and a type of non-touching vugs (Lucia, 1999). It originated from the dissolution of aragonitic constituents, like bivalves, gastropods, corals and coral-fragments. Due to cyclic sea level changes lots of erosional surfaces, which are marked either by bioclastic packstones to grainstones at the bottom and peloidal grainstones to rudstones at the top or red algal wackestones are abundant. These sequence boundaries mark high frequency regression- and transgression-cycles. The remarkable thickness of outer lagoon sediments together with the discontinuos patch reefs, observed in 4 of 5 boreholes (Figure 31), point to a lower order aggradational stack in the basinward direction.

The lateral geometry of patch reefs, which build an important sub-facies within the lagoonal deposits, is difficult to predict from borehole data only. Furthermore, vertically they are located above the present-day water level, which prevents the use of most logging tools. Observed thickness ranges from 6 m in MC4 to 9.5 m in MC5. Patch reefs, which are bounded by sequence boundaries, consist of coral framestones and are intensively bored by bivalves like *Lithophaga*, gastropods and boring sponges (Figure 32C). Encrusting biota and zones of red algal bindstones are typical. The predominant coral types *Porites* and *Tabellastraea*, originally built of the metastable aragonite, have been replaced by calcite or an important secondary moldic porosity developed through their complete dissolution. Furthermore, man size primary porosity can occur within the coral framework, which in combination with karst could lead to an interconnected channel system. Karst-related cavities are designated as tertiary porosity in this study. From the Cap Blanc area karst has been reported in the aggrading systems tract (AST) of the reefal complex, which developed presumably during lowstands of sea level at the water table in the reef front and the coral patches of the lagoonal beds (Ardila and Pomar, 2000).
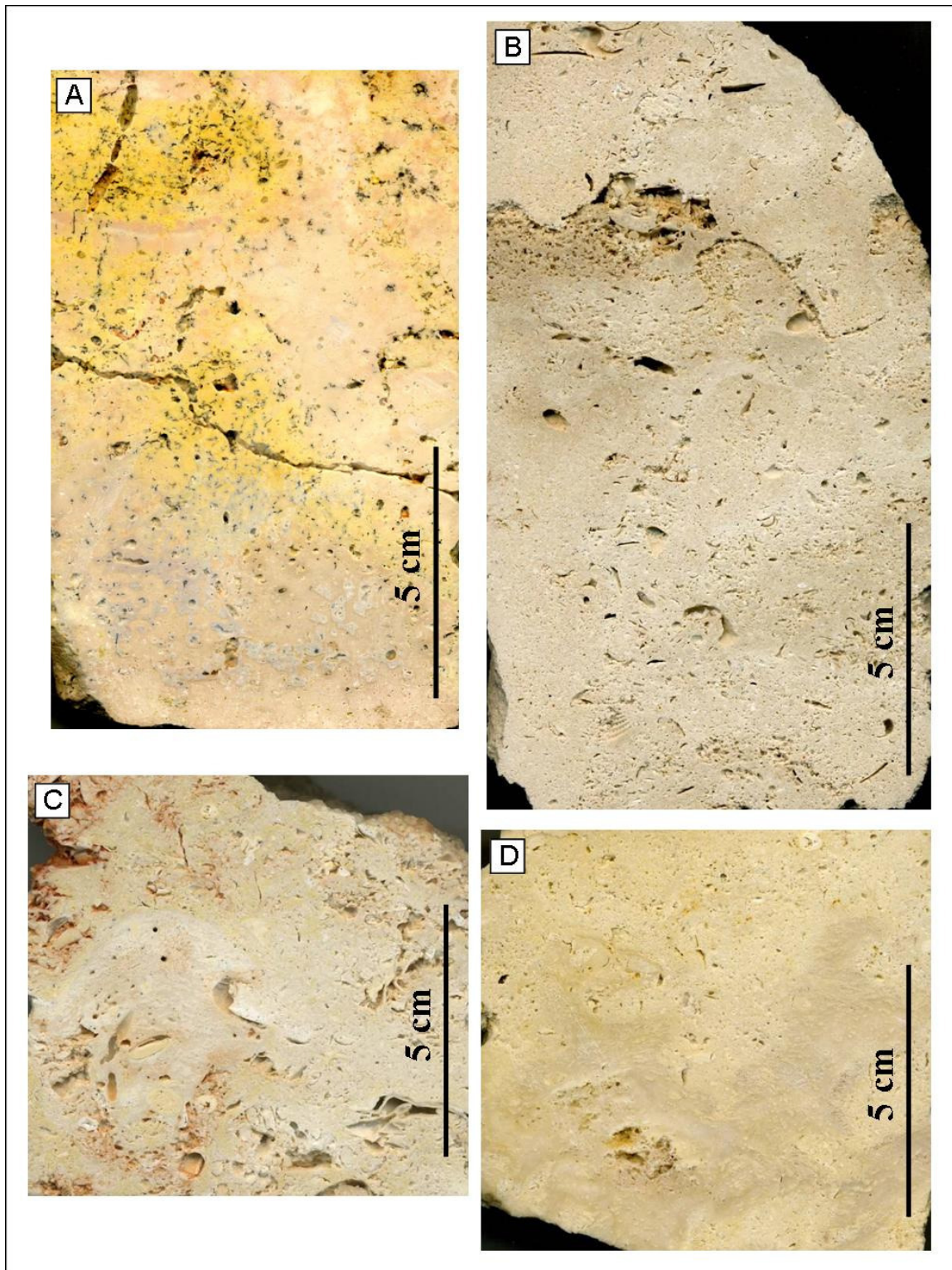
Figure 32:   Halfcore scans of inner lagoon recrystallized grain-dominated packstone with roots (A), outer lagoon bioturbated peloidal grainstone with moldic porosity (B), patch reef bored framestone with *Porites* and internal sediment (C), reef core framestone with branching *Porites* and internal sediment (D), (locations of halfcore images see Figure 31).
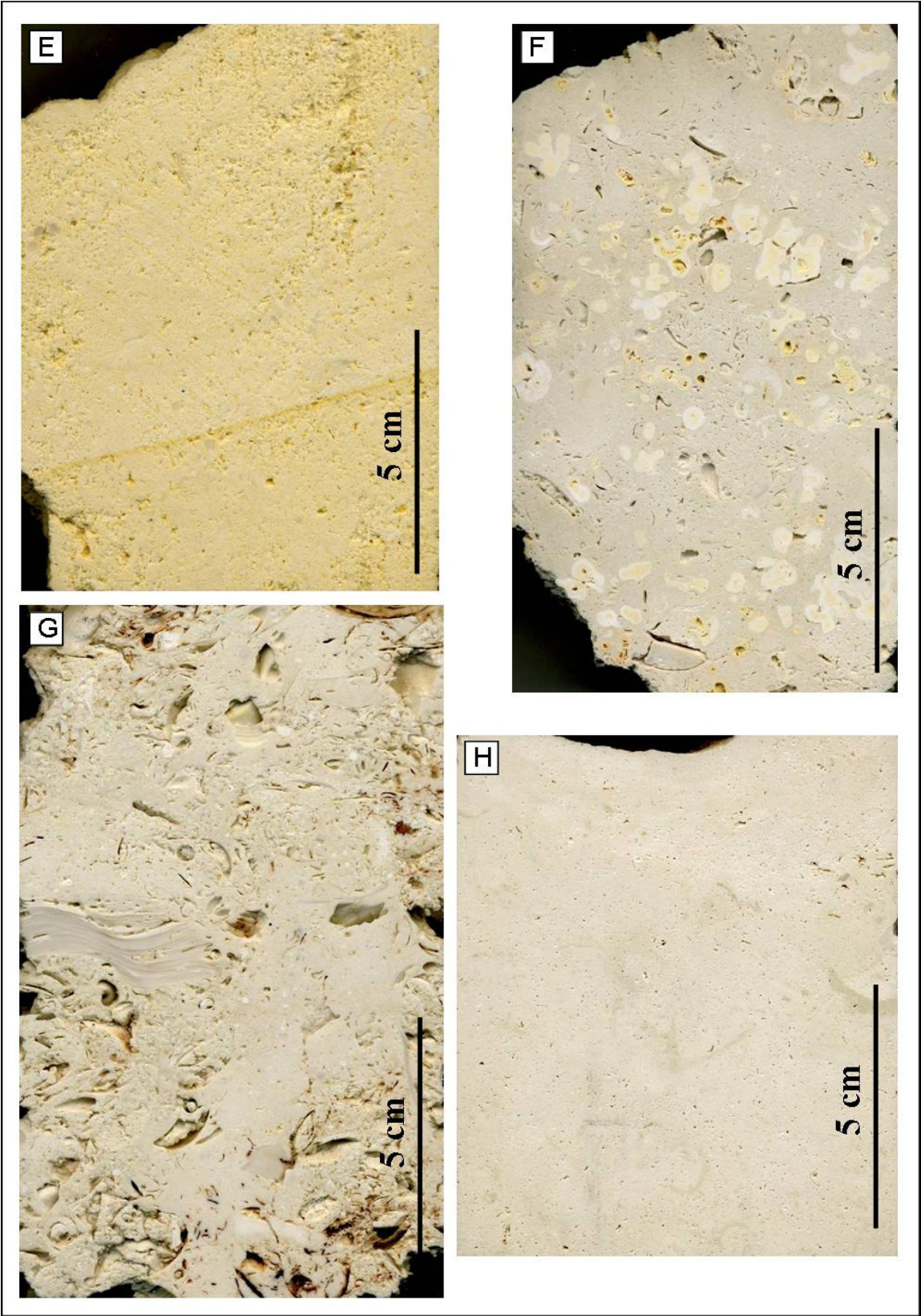
Figure 33: Proximal talus bioclastic grainstone with alteration fringes (E), proximal talus bored rhodolithic floatstone in a packstone-matrix (F), proximal talus bioclastic rudstone with oyster, molds of bivalves and gastropods and coral rubble (G), distal talus mud-dominated packstone (H), (locations of halfcore images see Figure 31).

Below outer lagoon the continuous and progradational reef core follows. It is characterized by framestones, which are locally filled in between by internal sediment, infiltrated from the lagoon (Figure 32D). In addition to the sea level driven morphology of the reef core, spurs and grooves, which provided a direct connection of the outer lagoon with the open sea are abundant. These channels, which are filled with internal sediment are part of the reef core and developed through tidal currents, which were present at the barrier reefs. At strike-section (boreholes MC1-4-5) the reef core is horizontal, continuous and thick (Figure 31). The latter points together with the fact that reef core at MC2 and MC3, with a thickness of 4 m respectively 6 m is thin and at a relatively low position in the borehole, to an aggrading stack at the strike-section. The upper boundary is built by erosional surfaces, where an unknown amount of the geological archive has been removed. The reef core observed at MC2, respectively MC3 formed during a sea level fall and is probably part of the offlapping systems tract (OST), whereas at MC5 a sea level maximum was reached and thus is part of the high stand systems tract (HST). The thickness of the reef core here is 10 m. MC1 and MC4 are part of the AST, which has developed during a fast sea level rise. At the AST the thick aggradational stack of individual sigmoids reaches a thickness of 16 m at MC1 and even 19 m at MC5. Especially the bottom of the reef core is karstified and dm-m-scale cavities are abundant. However, some of these cavities may belong to primary porosity (Figure 34B) rather than tertiary porosity. Karst can be identified by the presence of red-brown residual clays commonly occurring at the bottom of such cavities (Figure 34C). The framestones are well cemented and recrystallized. At certain levels, especially near karstified cavities, the coral framework-porosity can be almost totally occluded by blocky spar.

Basin-wards, the reef core interfingers with skeletal and intraclastic grainstones (Figure 33E) to rudstones of the proximal talus. The shedding off the reef crest and the outer lagoon during storm events leads to highly anisotropic and steeply bedded (10-30°) deposits, which consist of a succession of lenticular coarsening upwards layers. Coral rubble with boulders up to dm-size, sporadically occurring single corals in living position and thin layers of rhodolithic floatstones (Figure 33F) are typical for this lithofacies type. The rhodolithic floatstones commonly are condensed sections, which developed during sea level highstands and merge landwards into sequence boundaries. Talus sediments are not karstified any more and excursions of the gamma log are rare. The basis of the proximal talus consists of a prominent bioclastic rudstone, which has been observed in all 5 boreholes (Figure 33G). Below the sediments are much more fine-grained and lenticular rudstone layers become rare. Whereas the upper part of distal talus consists predominantly of grainstones, the lower part is more fine-grained and mud-dominated packstones are common (Figure 33H). This trend can also be seen in the gamma logs, which yield gradually higher values towards the bottom. The beds in general are dipping with less than 10°, however extensive burrowing blurred the fine-scale sedimentary textures and lead to an extremely homogenous lithofacies type. Large moldic pores are rare due to the lack of coarse grained coral rubble and macrofossils.

Fractures are rather seldom within this young reefal limestone. Sporadically some closed sub-vertical fractures are present, which most probably are related to the slight tectonic flexure and tilt of the carbonate platform, which took place during Pleistocene. MC3 is the only borehole of the present study, where small fracture sets have been recorded above and below the reef core. These open and sometimes solution enlarged fractures are mostly gently dipping with the upper fracture set oriented towards NE and the set below the reef core dipping towards SW, which is identical with the direction of reef-progradation. Thus, these fractures most probably are directly related to the reefal geometry and might be influenced by the local bedding.

A: MC2 (48.7-49.1 m)   B: MC2 (59.0-60.2 m)   C: MC3 (61.0-63.5 m)
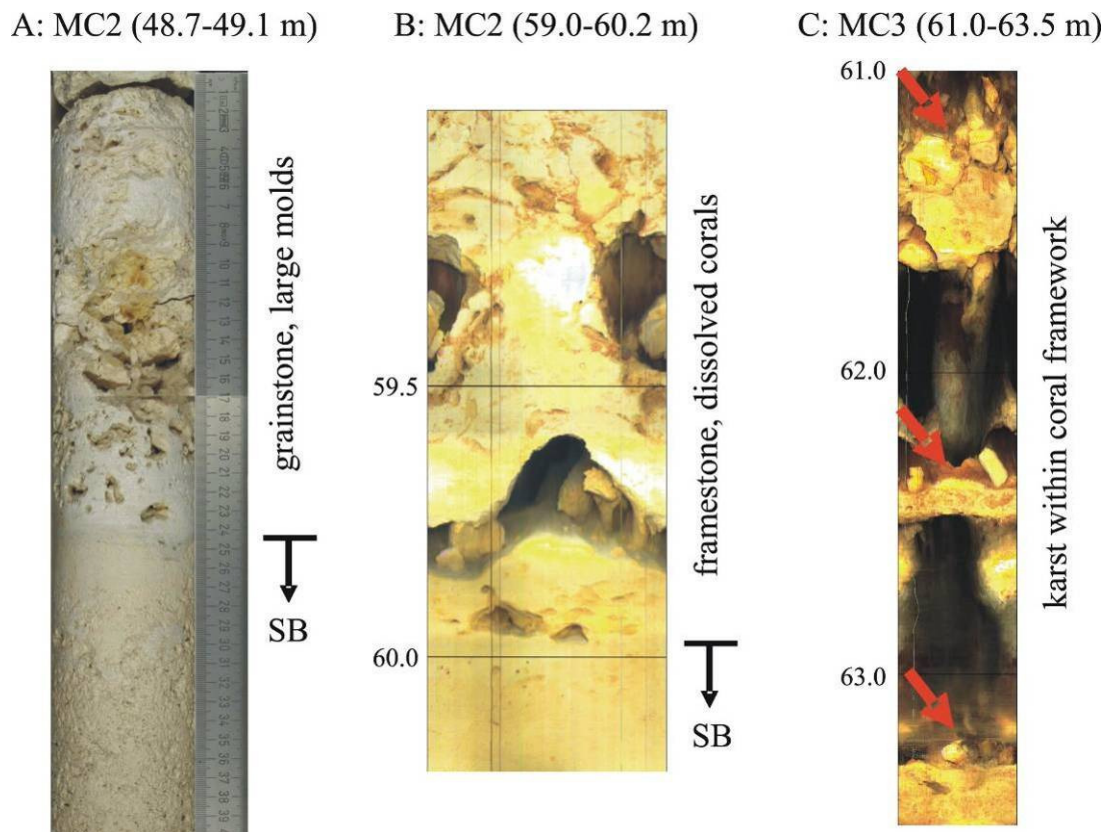
Figure 34:   Erosional surface (SB) in outer lagoon consisting of a wackestone with well cemented vuggy grainstone on top (A), erosional surface (SB) at the bottom of the reef core, where dissolved platty corals dominate (B), dm- to m-scale porosity of karstified reef core with basal layers of red-brown residual clays (C).

3.3. Methods

For the correct interpretation and emphasis of the individual investigation techniques it is indispensable to define first the terms resolution, accuracy, precision, scale and depth of investigation. Resolution concerns the minimum separation between two features such that the two features can be identified individually rather than as one combined feature. For borehole logs this relates to the physical separation of two features along the length of the well. Accuracy and precision define together with the bias the quality of a measurement. Precision refers to the closeness of agreement between the results obtained by applying the experimental procedure to a sample several times under prescribed conditions. Accuracy refers to the closeness of the measurement to the true value. As the actual or true values are unknown, the true value is an idealized concept and the accuracy is a qualitative concept (Lovell et al., 1998). The scale may be defined quantitatively with precise descriptions of the size and shape of the measurement. It is linked to the measurement technique and hence to the design of the tool. The different aspects of scale are especially important in anisotropic and heterogeneous media and will contribute to the measured data value. Depth of investigation is related to the volume of rock, contributing to the measurement. This volume is the amount of rock involved in the critical signal of the petrophysical parameter under investigation along the borehole. For many geophysical tools the source to receiver spacing is one of the major controls of depth of investigation. Depth of investigation and resolution are directly linked to each other. Further important controls are source energy, frequency and formation density.

Four main downhole investigation techniques have been used, which proved to be suitable in a highly heterogeneous reefal carbonate complex. The acoustic travel-time scan, which is a non-standard imaging technique for the assessment of the borehole wall heterogeneity, the impeller flowmeter (IFM) for the physical measurement of hydro-dynamically active zones, the induction log, which measures the electrical properties of the formation and the full-waveform sonic log (FWS) for the acoustic properties of the formation. All of these techniques cover different ranges of heterogeneity. Together with the geological control from visual core description and halfcore scans, they build a powerful and gapless approach for reservoir characterization at the borehole-scale of the Campos site (Figure 35). Each individual wire-line log has been corrected for the logging datum and for the winch-specific cable stretch, which proved to be essential for the correlation of petrophysical data to observations made on core.
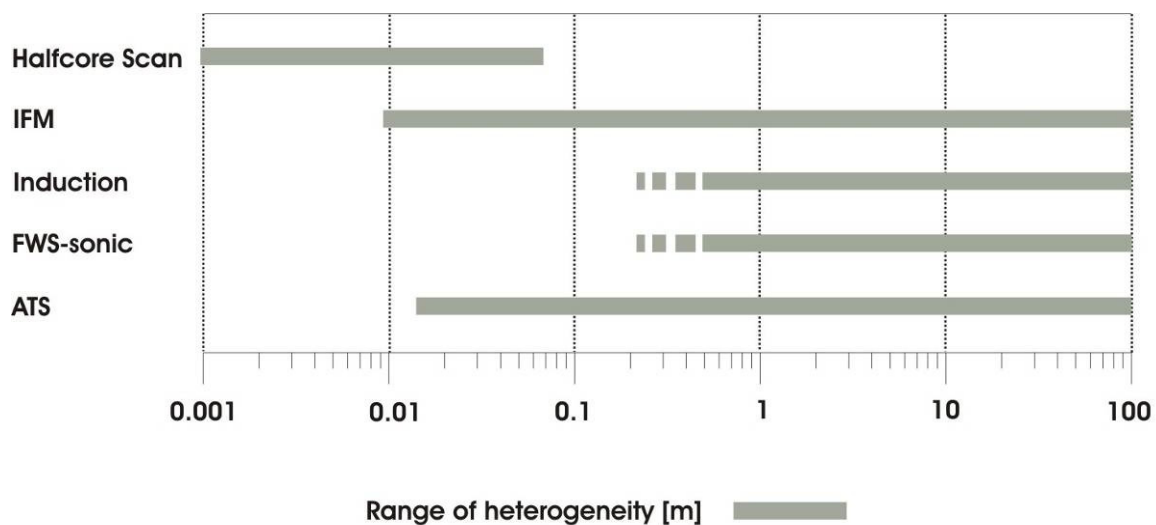
Figure 35:   The used data sources and investigation-techniques halfcore scan, impeller flowmeter (IFM), Induction log, full-waveform sonic, acoustic travel-time scan (ATS) and their range of heterogeneity, which can be recorded. An overlap of several techniques exists but the petrophysical attributes obtained are not directly comparable and need a sound geological understanding for appropriate interpretation.

3.3.1.   Optical assessment of the borehole-scale pore space (acoustic travel-time scan)

Reservoir characterization in highly complex carbonate reservoirs requires the use of high resolution tools, capable of resolving small-scale sedimentary structures (0.3-0.6 m), which are known to be important controls of reservoir behavior (Jackson et al., 1998; Russell et al., 2002). Reservoir rock types can be estimated by conventional wireline logs, but their low vertical resolution limits the utility for characterizing small-scale heterogeneity. Imaging tools capable of resolving such heterogeneities are FMI, FMS and optical- and acoustic borehole televiewer (BHTV). In the present study, the acoustic travel-time image has been used for the assessment of borehole-scale heterogeneity. Unlike for the other tools, the circumferential coverage of the acoustic image is 100%. Furthermore, it is not based on resistivity measurements, where pads have to touch the borehole wall and thus is much less sensitive to borehole roughness and large-scale cavities. The method described here will be called the acoustic travel-time scan (ATS). Data is recorded by a standard high-resolution acoustic probe, which yields an image covering 360° of the circumference and about 60 m of the saturated borehole length.

A comparison to core material and the optical BHTV reveals that the acoustic travel-time image exactly displays the borehole topography, which in most cases is controlled by karstic cavities, moldic pores, fractures and small-scale sedimentary structures (e.g. burrowing). Unlike the optical BHTV-images the acoustic image is not influenced by rock color or opaque borehole fluid. For the test site two acoustic images with excellent quality are available, namely MC2 from 37 to 100 m and MC3 from 38 to 100 m. The image of MC5 from 38 to 99 m is of less quality, however, the comparison to the optical BHTV-image provides a possibility to cross-check the obtained signals. A low image quality is mainly due to fast logging speed and badly centralized tool. Some image-equalization procedures have been tested, however they always resulted in a biased porosity image, which is not representative for heterogeneity observed on optical BHTV anymore. Some successful attempts of preprocessing the acoustic image in order to account for artifacts of de-centering and low contrast between vugs and background were made by Pézard et al. (2004). However, for the present study a preprocessing was not performed, since the investigation targets on pores with sizes larger than 1 cm. These larger heterogeneities in contrast to mm-size pores are much better defined by the acoustic image and much less affected by artificial effects.
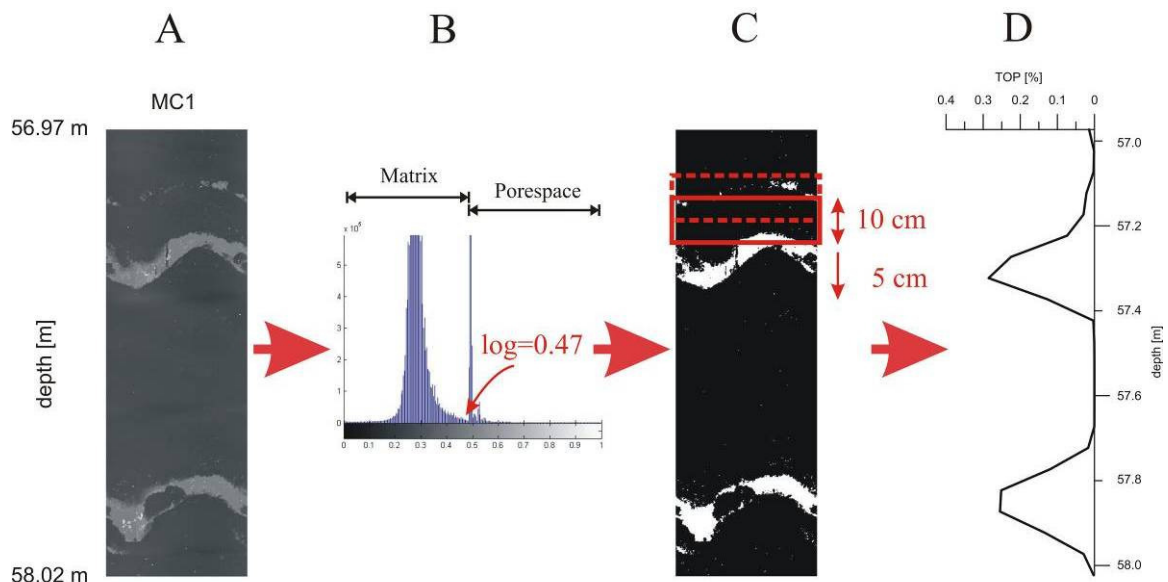
Figure 36:   Technique of the acoustic travel-time scan (ATS) with gray-level image of acoustic travel-times (A), histogram of travel-times with matrix- and pore space-peak and the indicated location of the threshold log=0.47 (B), the resulting binary image (C) and the representation of downhole heterogeneity (D).

For the analysis of the borehole-scale heterogeneity, a simple routine has been written with *Matlab*. The matrix of acoustic travel-time data is split into a depth-column and a matrix, where the travel-times are normalized. The values of the obtained gray-level matrix lie between 0 being black and 1 being white with 255 divisions (Figure 36A). In the next step the pores are detected by setting a threshold at an appropriate gray-level of the plotted histogram. The appropriate threshold is set manually by visually checking the histogram. Acoustic images with a high data quality allow for an easy determination of the individual threshold. A sufficient separation of a sharp porosity-peak is required for a precise recognition of the boundary between pore space and rock matrix (Figure 36B). For MC5 setting the threshold at the correct place was a compromise between capturing most of the pore space and precluding artifacts due to low data quality. At MC7 the rock matrix-peak was too flat and the porosity

peak too wide for a reliable separation of the two phases. The reliability of the threshold value has been checked visually at several key locations along the borehole. Applying the threshold on the gray-level image results in a binary image, where the rock matrix exhibits a value of 0 (black) and the pore space a value of 1 (white) (Figure 36C). The resolution of the tool is strongly dependent on the choice of the threshold, which in turn determines the critical caliper at which a travel-time is classified as a pore or as rock matrix. In *Matlab* the travel-times are normalized as follows:

$$\log = \frac{tt_{measured} - tt_{min}}{tt_{max} - tt_{min}}$$

With log being the threshold value and tt the measured, minimal and maximal travel-times of the acoustic image. The threshold is determined visually by comparing the thresholded sections with the optical BHTV-image and high resolution core images and it determines the threshold distance, which is the sum of the drilled borehole radius minus tool radius plus the smallest resolvable pore depth/size (Figure 37). Depending on the borehole-specific threshold, the resolution of the resulting binary image ranges between 1 and 2 cm, which is sufficient for the purpose of the present study (Table 3). With such a resolution no overlap to thin section porosity and no artifacts, which are due to artificial borehole roughness, such as scratches from the drill bit are present. This way, many artifacts are eliminated, which are related to out-washing, associated differences in the cementation of the rock and de-centralized tool. The high accuracy of this method can be checked quite easily by simply comparing optical BHTV-images with binary images from the ATS. The precision of the method depends on the correct assessment of the threshold value, consequently for the optical porosity a high precision of ±5% was observed.
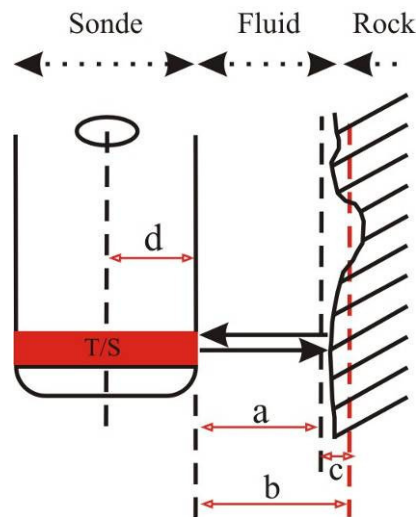
Figure 37:   Sketch illustrating the resolution of the ATS with the relevant distances for the threshold like tool-borehole spacing (a), tool-threshold distance (b), size resp. depth of critical pore (c) and half tool diameter (d).

One of the main advantages of the ATS is the full control on the scale of investigation by scanning the binary borehole image with a predefined window size and sampling interval (Figure 36C). For the ATS the scale of investigation commonly was chosen to be a rectangle (10x33 cm), which represents 10 cm of the unwrapped borehole surface. Recognition of the scale of investigation is crucial for a correct interpretation of the petrophysical signals. Jackson et al. (1998) used a spectral method for visualizing the scales of heterogeneity, which according to them is important for checking the mismatch between core and log data.

Furthermore, the sampling interval can be chosen individually, which allows for controlling the overlap of the scans. Two different concepts have been applied, a discrete scanning with no overlap between the individual scans and a moving-average scanning, where the sampling rate is smaller than the scan window. The discrete scanning is comparable to imaging logs, where no overlap between individual measurements occurs. However, unlike imaging logs each measurement is an average over a certain surface area of the borehole. The moving-average scan in contrast is rather comparable to standard wireline logs, where the sampling rate is smaller than the inherent scale of investigation. By looking into a larger volume, small scale heterogeneities are averaged out. In contrast to logging tools, where a larger investigation range increases the depth of investigation and the size of considered rock volume, for the ATS depth of investigation is zero and not affected by the window size. If there are heterogeneity changes not only in the vertical but also in the horizontal direction, window length and scan increment adapted to investigation scales and sampling interval of logging tools will not yield comparable data.

The ATS measures heterogeneity of the pore space but not anisotropy, since the method is directed and measures only one average value in the horizontal direction. The scans are represented as downhole log, which continuously records the total optical porosity (TOP) of the borehole wall in the predefined scan-window of 10 cm length and at a predefined sampling rate of 5 cm (Figure 36D).

3.3.2.   Preferential groundwater pathways within the formation (impeller flowmeter logs)

For characterizing hydraulic properties of talus and reef core and for identifying major permeable groundwater pathways, the IFM is a powerful tool. According to Muldoon et al. (2001) high permeability zones and matrix hydraulic conductivity in a fractured dolomite aquifer are controlled by the stratigraphy. In their integrated study they used gamma logs to identify the stratigraphic position of permeable features. In the present study in addition to data from core description, core images and gamma logs, also optical borehole televiewer logs (BHTV) are available for the correlation to stratigraphy and interpretation of the permeable features measured by the IFM. High quality IFM logs are available for boreholes MC2, 3 and 5. With this tool it is possible to identify preferential pathways by stimulating vertical upward flow within the borehole (Molz et al., 1989). The upward flow was created by a downhole pump placed above the flowmeter and pumping at a constant rate of about 1.5 l/s. Since transmissivities are too large, respectively measurable drawdown too small, only inflow rates were calculated (Van Meir et al., 2005). The IFM was run up and down the borehole at several cable speeds, however, in the present study it is sufficient to analyze logs, which were run at 6 m/min in the downward direction with both pumping and no pumping. The procedure of calibration for cross-sectional area and cable speeds are discussed in Van Meir et al. (2005). In short the no pumping log was subtracted from the pumping log, the results then multiplied with a calibration factor (which turns rpm into velocity) and finally with the cross-sectional area of the open borehole. The IFM logs are displayed in l/s and for the depth interval of 47.5-65 m, which is constraint by the water level and by the talus sediments, which did not yield any measurable flow with the IFM used in this study. The resolution of the method is approximately 1 cm and the depth of investigation, which is dependent on the ratio T/S lies in the dm-range (Table 3). The scale of investigation is spherical or cylindrical, depending on the hydraulic contrast between borehole and rock and lies as well in the dm-

range. Accuracy is rather intermediate and precision was determined to be ±12.5% for the calculated flow.

Method	Resolution	Depth of investigation	Scale	Accuracy	Precision
ATS	1-2 cm	0	10x33 cm, rectangular	high	$\Phi = \pm5\%$
IFM	~1 cm	dm's	several dm's, cylindrical or spherical	medium	$Q = \pm15\%$
Induction	50 cm	12-51 cm	dipol-field 50 cm high and 0.25-1 m in diameter	low	$\Phi = \pm10\%$
Sonic	40 cm	20-100 cm	~cylindrical, 40 cm high and 0.5-2 m in diameter	low	$v_p = \pm15\%$ for 1500m/s, ±55% for 6500m/s

Table 3:   Some tool-specific properties.

3.3.3. Electrical properties of the formation and boreholes (induction and conductivity logs)

The evaluation of formation properties by electrical logs has widely been used in subsurface characterization and can yield valuable information about the saturated porosity and changes of lithology. In the present study the double spaced induction tool DIL38 has been used, since for this tool no direct coupling with the formation is necessary, which is quite advantageous within the highly porous and badly cemented reefal carbonates of Llucmajor. Additionally to the induction logs, formation conductivity has been logged, which is indispensable for the determination of porosity. Induction logs are available for boreholes MC1, 3, 4, 5 and 7 for the depth interval between 40 and 100 m. Initially the signal of the induction log was calibrated by subtracting the mean offset value from the raw data set and dividing it by the tool specific calibration factor. At the test site no electrical installations or larger iron-bodies could affect the background value. After the initial calibration from cps to µS/cm the dataset has been corrected for the skin effect. The DIL38 works with an operating frequency of 39'063 Hz and the short spacing of the coils is 0.51 m. The values measured on the test site lie between 2000 and 8000 µS/cm, which yielded values for the correction of skin effect ranging from 6-12%. The criteria coil-spacing/skin depth<=0.65 is valid for the measured range of formation conductivities (Hearst et al., 2000). Since diameters do not exceed 100 mm significantly at the boreholes, where induction logs were run, no borehole correction was applied. The resulting signal of the induction tool is weighted through the geometrical factor. In the radial direction the major part of the electromagnetic field propagates within a radius L/4 to L, L being the coil spacing (Serra, 1984). Thus, depth of investigation ranges between 12 and 51 cm and out of 1 m from the sonde-axis the contribution is already very small. Consequently the field of the dipole, which is 0.5 m high and exhibits a diameter of 0.25-1 m, determines the scale of investigation. The vertical resolution is in the same order of magnitude as the coil spacing and thus 50 cm (Table 3).

Total porosity can be determined through Archie's equation (1942) in the water saturated part of the borehole, where induction log and fluid conductivity log both are available. Lab measurements performed by the ISTEM in Montpellier yielded an overall average cementation factor of 2.2. However, as results from 1inch mini-cores have shown, especially for the homogeneous lower part of the talus, a value of 1.8 is much more appropriate. Since the cementation factor is highly variable over the entire borehole length, an average can only lead to very approximate porosity values, thus accuracy is rather low and precision in the

order of ±10%. The formation conductivity is not only affected by the porosity and the fluid conductivity but also by the conductivity of the rock matrix, which varies with rock type and cementation.

The rock type does not vary within the reefal carbonate complex except for the sequence boundaries, which are clay-bearing. Since these sections are well constraint and build only a minor percentage of the logged formation, no clay correction has been performed. The finally derived porosity logs are compared to geology with a special emphasis of heterogeneity within individual lithofacies types. The results are discussed for relative porosity changes rather than for their absolute values, since scale disparity does not allow for a direct calibration with measurements from 1inch mini-cores and the cementation factor is highly variable.

3.3.4.   Acoustic properties of the formation (full-waveform sonic log)

Two sonic logs are available for the present study run with a full-waveform sonic probe from Robertson Geologging. The logs were run in the two boreholes MC4 and MC5 at a cable speed of 2 m/min. The tool was used in a non-compensated manner, since the transit-times did not yield any useful information. The p-wave first arrival picking was performed in two different ways. The manual picking on the full-waveform record allows for a fully controlled procedure with the possibility to visually compare the wave form of both transmitter-receiver pairs. However, the determination of a coherent transit-time for both waves is not always straight forward. Furthermore, an advanced threshold pickup algorithm within the software *WellCAD* has been used, which allowed for a comparison with the manual procedure. The two picking methods yielded comparable velocity profiles. Confidence for large amplitudes is not as high as in zones with moderate amplitudes, since manual picking in such zones is complicated by diffuse first arrivals and a high noise level, which results in cycle skipping and thus to too high porosity readings.

Regarding the size of the rock volume, which contributes to the measured signal, lab experiments showed that a thickness of at least 3λ is needed to propagate a pressure wave through several dm of formation (Serra, 1984). The sonic probe used here operates at a frequency of 23 kHz. Calcite-velocity at zero porosity is around 6500 m/s and changes to around 2000 m/s at porosities of 50% or higher (Anselmetti and Eberli, 1999). Thus, the sonic tool exhibits a depth of investigation, ranging from 20 to 100 cm and it is capable to resolve layers with a minimum thickness of 40 cm. The scale is defined by a cylinder, which is 0.4 m high and 0.5-2 m in diameter. Due to high variability in texture, porosity and pore types, carbonates show a wide range of V_P-values. The measured velocities allow for calculating the porosity through the empirical relationship of Wyllie, which is valid for the present study, since the requirements no overburden and low fluid pressures are accomplished. In order to get reasonable porosity values, two filters have been applied on the measured V_P, namely a low cut filter ($V_P < 1500$ m/s) and a high cut filter ($V_P > 6500$ m/s). Unrealistic values of V_P originate from inaccurate first arrival picking within *WellCAD*, which revealed to be a difficult task, especially within the reef core. Consequently the precision of the method is low and ranging from ±15% for low velocities up to ±55% for high velocities (Table 3).

Porosity calculated from sonic logs is not necessarily a total porosity, because it is strongly affected by pore shape and thus also controlled by the pore type (Anselmetti and Eberli, 1993; Brie et al., 1985; Kenter and Ivanov, 1995). Anselmetti & Eberli (1999) distinguished five

main pore types, namely moldic, intrafossil, interparticle, microporosity and low porosity carbonates (<10%). They calculated synthetic velocities using measured porosities on plugs and compared them to porosities derived from sonic logs. Largest deviations were observed in samples in which intrafossil- or moldic porosity dominates, thus porosity types, which build a framework-like fabric. In such fabrics sonic velocity and porosity are high and sonic logs tend to underestimate porosity (Anselmetti and Eberli, 1999; Lucia, 1999).

Sonic velocities in general have to be corrected for clay content and compaction of the clays, since clays lead to too low V_P or too high porosities (Fricke and Schön, 1999; Hearst et al., 2000). Stafleu et al. (1994) showed that a critical threshold of 5 to 8% clay inversely affects velocity. Within the saturated zone at the Campos site, no such clay contents occur, except at karstified zones and sequence boundaries. Clay content of karstified zones is not measurable due to extensive core losses at these zones and sequence boundaries are thin and well constraint through gamma logs and visual core description. Thus, a clay correction has not been performed for the present study. As a consequence velocity respectively calculated porosity values at karstified zones and sequence boundaries are inaccurate.

3.4. Results of the ATS

3.4.1. Acoustic travel-time scan for the characterization of optical heterogeneity

The ATS records optical porosity of the borehole wall, which depending on the chosen threshold is larger than 1 or 2 cm. This includes primary as well as secondary porosity, such as large elongated molds and dissolved corals or coral fragments. Furthermore, karst-related cavities are recorded, which is termed here as tertiary porosity. Several runs of different window sizes and scan increments were performed in order to check the behavior of the resulting curves. A larger window is in fact an average over a larger area, which results in attenuated peaks and generally smoother curves (Figure 38). A scan increment of 5 cm at a window length of 10 cm proved to be the best choice for an exact representation of heterogeneity along the boreholes of the present study. Except for some strongly karstified sections within reef core a TOP of 100% is barely reached with a 10 cm window. Thus, this setting enables us to access borehole-scale heterogeneity changes at a reasonable scale of investigation.

The comparison of ATS-data with optical BHTV and high-resolution core images revealed the nature of the recorded heterogeneities or pseudo-heterogeneities. Leached corals and coral fragments, distributed disperse in talus and outer lagoon (Figure 38a) or concentrated within the reef core framework or as lenticular accumulations of reef debris, together with large and elongated molds from bivalves and gastropods in outer lagoon and proximal talus (Figure 38d), are easily recognized by the ATS. Cavities due to leached corals exhibit sizes in the cm-dm-range, which is steadily recorded by this technique. Especially within reef core, where a dense framework of coral colonies is present, dm- to m-size primary pores, which have only partly been filled by internal sediment, can occur. Man size pores, which unequivocally have been recognized as primary pores, mainly by the occurrence of sedimentary cones consisting of bioclastic internal sediment, have been reported from the well exposed outcrops at the cliff coast (Pomar et al., 1996). On the landward test site near Campos, porosity in the dm-range is always associated with karst and thus a combination of primary or secondary porosity, transformed by karst-modification into tertiary porosity.
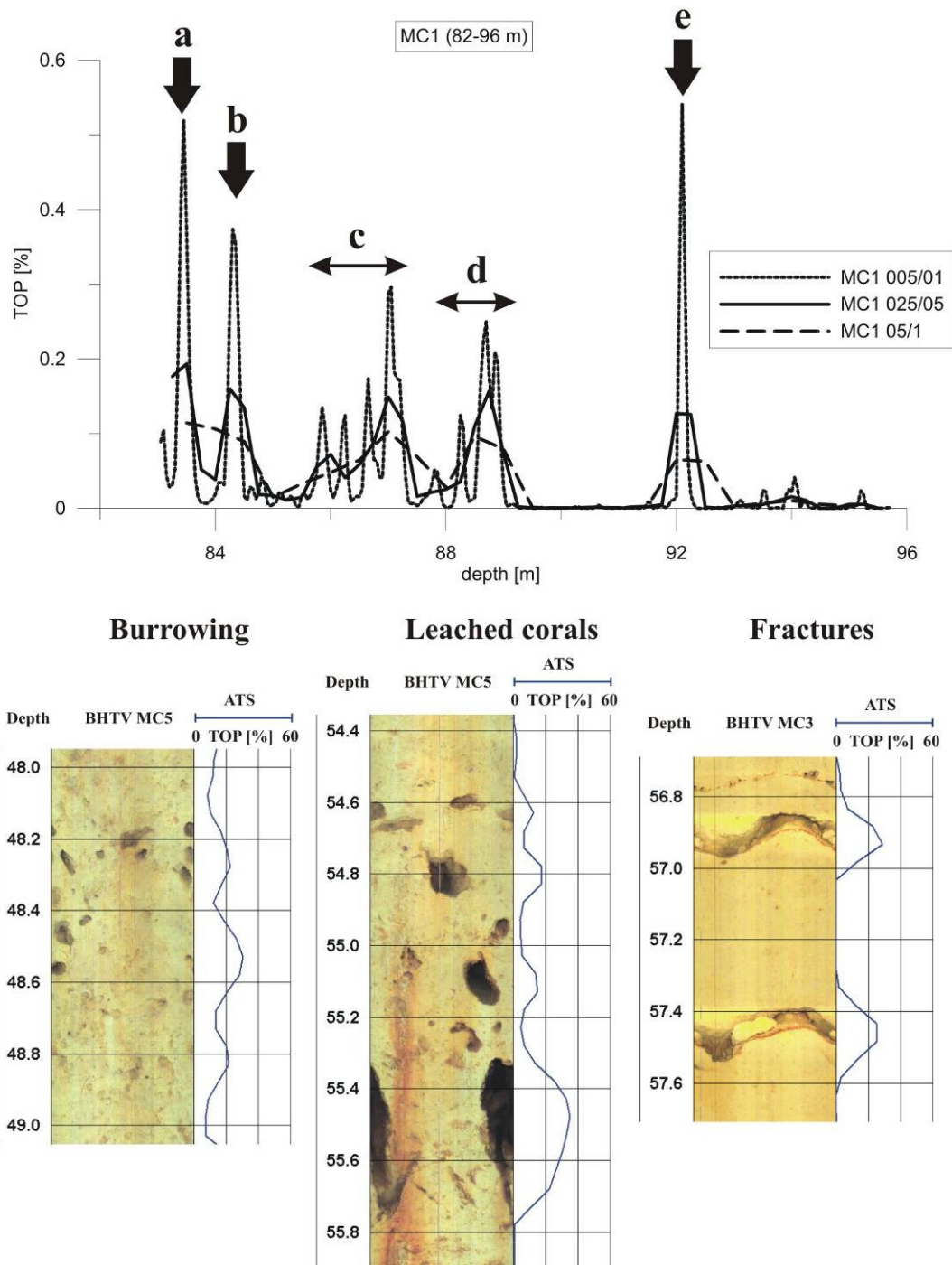
Figure 38:   ATS of MC1 (82-96 m) for different scan windows and scan increments. Best resolution is achieved for smallest scan window of 10 cm length. Comparison to optical BHTV enables to attribute geology to the observed peaks: leached out coral fragment (a), artifact due to de-centralized sonde (b), zone of intense burrowing (c), several small dissolved coral fragments (d), cavity due to weak cementation (e) – below BHTV-images and their corresponding signal on the ATS.

Further recorded heterogeneities are caused by burrowing (Figure 38c). Much of the reefal complex lacks well-defined stratification due to extensive burrowing. Burrows as observed on core material consist of small corridors, filled of fine grained, mostly non-cemented carbonate mud with maximal diameters up to a few centimeters, barely exceeding 5 cm. It is difficult to estimate the part of open burrows, which originate from out-washing through the drilling process. Nevertheless these burrows apart from whether originally they were open or closed

may not be neglected as heterogeneities, since the contrast in cementation and grain composition is remarkable and especially significant in homogeneous and fine grained parts of the reef complex. The importance of burrows as low- or high porosity heterogeneities is stressed in several papers (e.g., Anderson et al., 1994; Gingras et al., 2004). Depending on the borehole, burrowing can contribute up to 50% to the ATS. Zones with extensive burrowing yield similar signals, like for example leached corals or coral rubble (Figure 38c,d). However, the impact of the two heterogeneities at the borehole-scale porosity structure is different. Whereas leached corals are rather isolated, the traces of burrowing organisms, mostly crustacean, built a complex network of rarely interconnected corridors with lots of dead-end parts, which extends laterally.

Fractures, especially if open and solution enlarged, are accurately displayed on the ATS. Their signal is generally low amplitude, regular and among individual fractures of a comparable shape. Unlike observed for burrowing and molds of leached corals, the signal between single fractures, depending on the fracture density and the matrix in between, can drop back to zero (Figure 38). Fractures have been observed mainly in outer lagoon and proximal talus, in most cases in context with the reef core. The fracture-orientations might be correlated with the local bedding, since at MC3 fractures above the reef core dip landward and below it, they dip in the direction of reef-progradation, thus seaward. This phenomenon has also been observed to a minor extent in other boreholes of the test-cluster. Zones, which are barely cemented might be represented by an increase of the borehole caliper and therefore appear on the ATS. As observed on cores, especially within outer lagoon and talus sediments, cementation may be very low and the bioclastic components very loose. ATS-peaks from such zones can be pronounced, due to commonly rater large areas affected by out-washing. Even though not cemented, wackestones at sequence boundaries are not affected by out-washing, since the clay content causes sufficient cohesion. The only real type of artifact, which is not related to geology, is caused by a de-centered acoustic probe (Figure 38b). The shape of these artifacts cannot be distinguished from the other signals on the ATS and only a comparison to the optical BHTV can detect them unequivocally.

The results show, that in general geological heterogeneity does not yield bar codes, which can be recognized on the ATS. However, despite the fact that a calibration of the individual heterogeneity types seems impossible, all heterogeneities recognized with optical methods are recorded by the ATS. The few artifacts, which are mostly the result of a de-centered tool, can be controlled by cross-checks with optical methods. High quality acoustic images, which are obtained by low logging speed, properly centered tool and straight boreholes are mostly free of artifacts. Slight artifacts, e.g. caused by tool sticking to the wall, in most cases can be bypassed by simply choosing a less sensitive threshold. Recapitulating one can state, that the ATS reliably measures borehole-scale porosity but a cross-check with optical BHTV data or core material is needed in order to specify the origin of the signal, which is not always directly related to real porosity. In the next paragraph ATS-curves of boreholes MC2, 3 and 5 will be presented and main characteristics are discussed on borehole MC2.

3.4.2. Observations made on individual ATS-curves

At MC2 clear signal changes can be recorded at the boundaries RC/PT and PT/DT (Figure 39). Heterogeneity at the boundary OL/RC is rather transitional and without the knowledge from visual core description, a clear distinction would be difficult. In outer lagoon, leached corals (a) cause the main peaks of TOP. Background noise is due to burrowing and moldic porosity. RC at MC2 is moderately karstified and the lack of larger primary or karstified pores
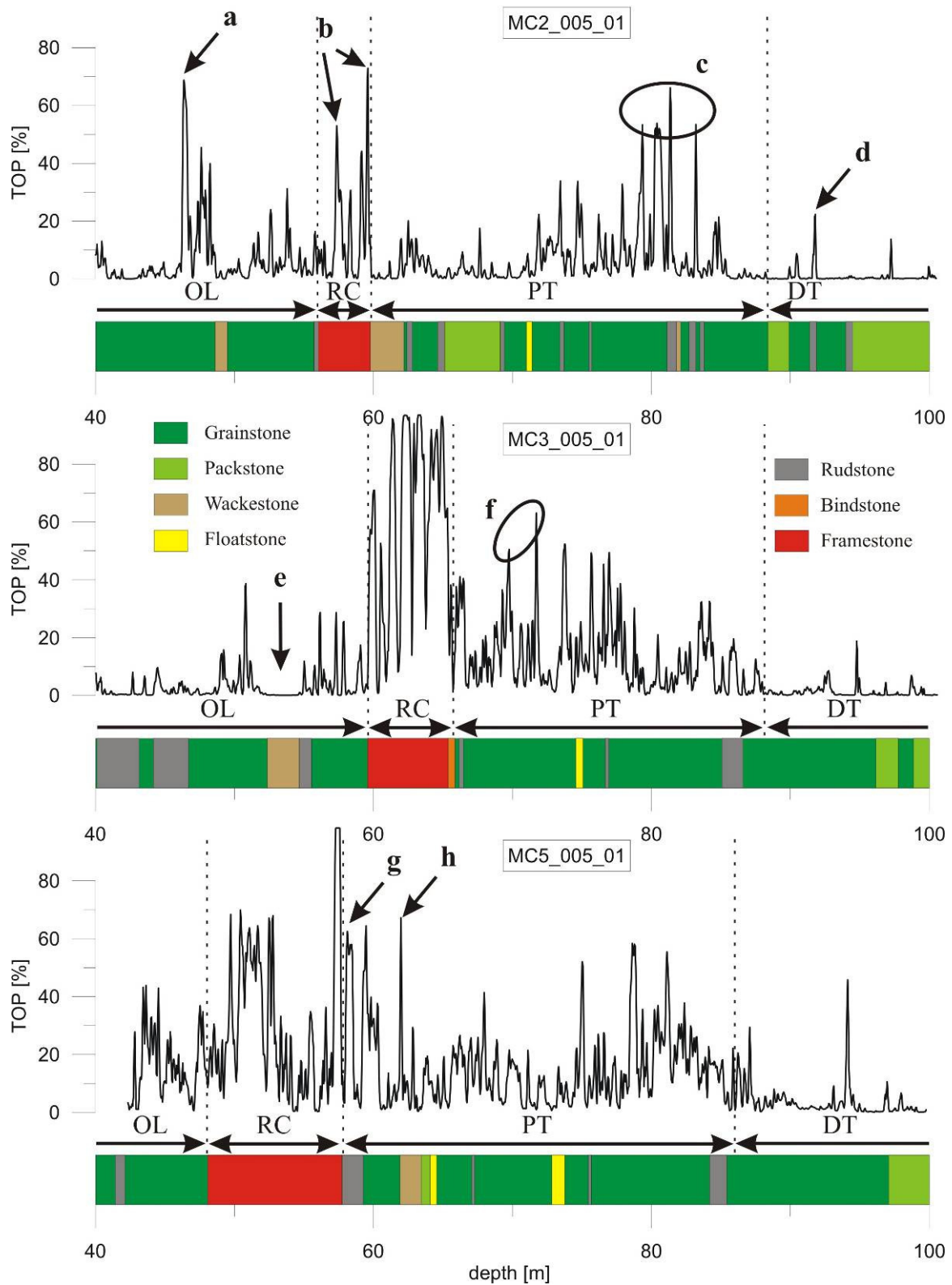
Figure 39:   ATS for boreholes MC2, MC3 and MC5 with a window length of 10 cm and a scan increment of 5 cm together with a correlation to geology observed on cores are given. Letters refer to heterogeneities, which are discussed in the text.

leads to moderate and rather narrow peaks on the ATS (b). The upper part of PT is dominated by burrowing, which leads to a certain background noise. A combination of extensive burrowing and moldic porosity in coarse grained sediment peaks in several single signals of more than 50% between 71 and 85 m (c). Below 85 m burrows are still present but they cause less contrast to the background sediment, concerning cementation and grain size distribution and thus are not recorded by the ATS. The lowermost lithofacies type DT is very homogeneous and only sporadically pronounced spikes are recorded, like for example at 91.2 m, where a dissolved coral is present (d). The results of MC2 show that distinguishing RC from OL or PT, if geology was unknown would be rather critical, since visually no characteristic behavior can be delineated. However, the lithofacies boundaries are easily recognized if the core description is correlated to the ATS. Especially the boundary RC/PT is sharp, since karstic cavities are missing in the upper part of PT and furthermore the boundary PT/DT, where the density and size of TOP-peaks reduces remarkably is unequivocally recognizable.

At borehole MC3 all boundaries between individual lithofacies types are pronounced. A plausible explanation for the low heterogeneity observed at OL of MC3 could be the absence of a patch reef (Figure 31), however lateral influence especially from the aggrading stack at MC5 should be present as well. For RC and PT, heterogeneity recorded by the ATS is quite different from the observations made on MC2 (Figure 39). In RC wider zones of high TOP exist. There especially within the middle and lower part of this lithofacies type, karst processes led to cavities with a vertical extent of up to 1 m, which can be correlated to TOP-spikes, which often reach 100%. The largest of these cavities are sealed at the bottom by red-brown residual clays. The dimension of the channels, the observed speleothemes and the degree of karstification are evoking to caves. A zone of zero TOP occurs between 52 and 54.2 m and is due to a sequence boundary, consisting of a wackestone (e). Pore structure in wackestones is characterized by intergranular porosity and small molds, which are below the resolution limit of the ATS. In the upper part of proximal talus, several peaks with TOP up to 60% are due to open fractures, which dip towards SW. Their density in combination with a low cementation leads to several small borehole-outbreaks (f).

In MC5 the upper boundary of RC is diffuse due to a much higher heterogeneity in OL, than observed in other boreholes. Outer lagoon here is thin and sandwiched between RC at the bottom and patch reef on top. The lower boundary of RC is much clearer due to the large channel at its bottom (Figure 39). One of the rare artifacts due to de-centered probe is present right below the RC (g). Above sequence boundaries in general coarser material with a rudstone-texture is sedimented. The sealing potential of the thick sequence boundary in proximal talus furthermore led to a vuggy zone on top (h). The boundary PT/DT is less straight forward, than in the other boreholes, since some single molds and larger burrows are blurring it. Consequently the heterogeneity boundary is not as sharp as the lithological difference would infer. Nevertheless a remarkable reduction in heterogeneity is present.

3.4.3.   Borehole-scale porosity distribution and relation to lithofacies types

Above we have looked at the origin of the heterogeneities, recorded by the ATS and the characteristics of individual lithofacies types. One main result of the observations made above is that no fingerprint signal can be attributed to a certain heterogeneity type, like burrowing, fracture sets or large moldic pores. However, optical heterogeneity along the borehole is reliably recorded by this technique and main lithofacies boundaries in most cases are

recognized. The distribution of borehole-scale heterogeneity to a certain extent is dependent on the distribution of lithofacies types, but secondary processes, like moldic porosity and diagenetic overprinting by post-depositional sea level fluctuations are important as well and might blur or even erase the original heterogeneity boundary. Nevertheless extent and strength of heterogeneity within individual lithofacies types seem to be comparable between different boreholes. In order to check the assumption that the lateral changes of heterogeneity within individual lithofacies types are of minor importance, histograms of measured TOP have been created for every single lithofacies type and borehole (Figure 40A).
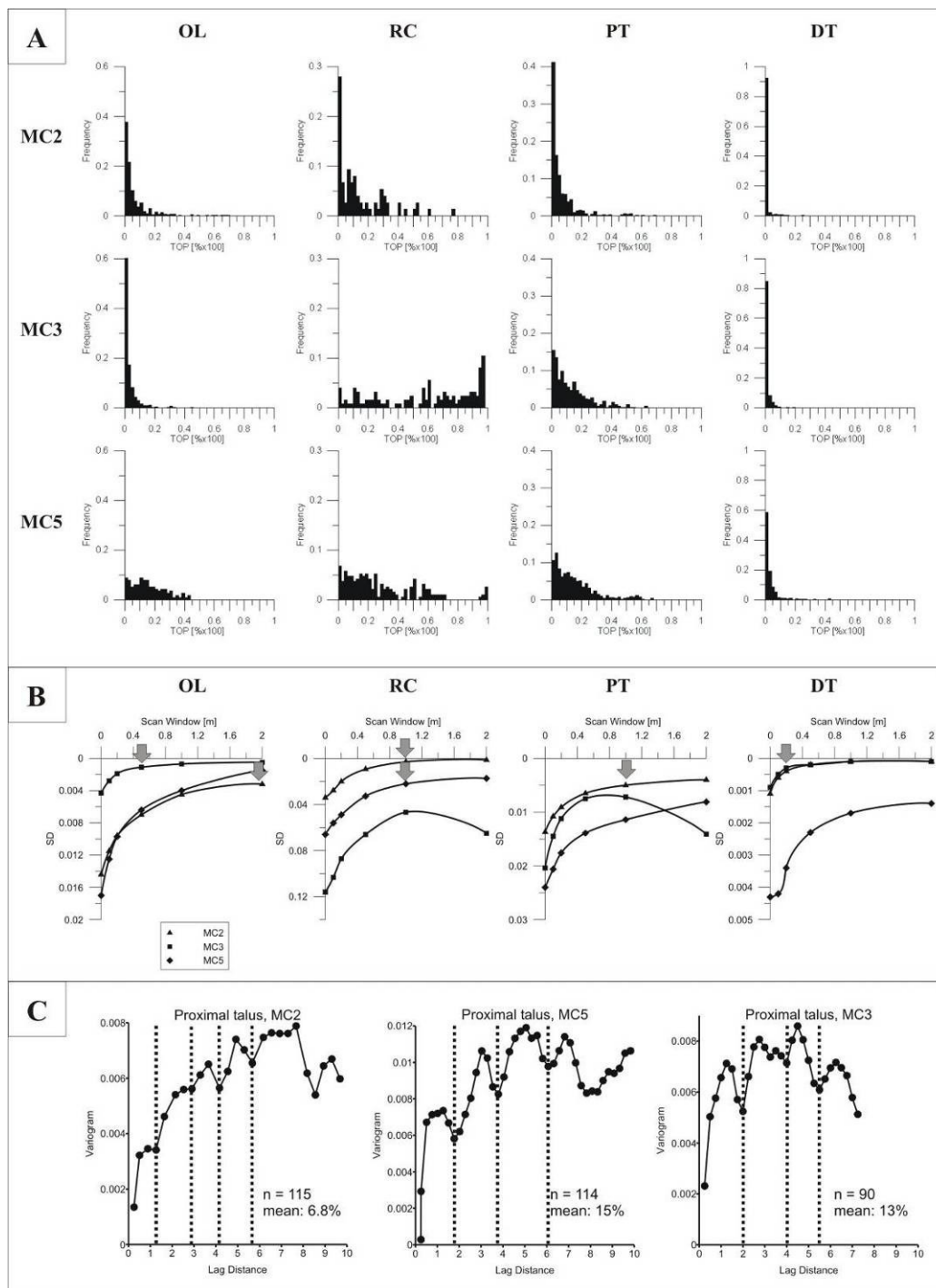
Figure 40:   Geostatistical parameters of ATS showing histograms of heterogeneity within individual lithofacies types for each borehole (A), the assessment of lithofacies-specific grid block size for modeling purposes (B), the evaluation of spatial correlation within proximal talus (C).

In the histograms, TOP from every 10 cm window, which has been recorded at a 5 cm step is plotted versus its frequency within an individual lithofacies type. The resulting distributions are mostly asymmetric and for OL and PT a lognormal distribution, which is widely used in literature for describing the distributions of porosity values (Isaaks and Srivastava, 1989), seems to come closest. Maximum TOP-values with 60-70% are higher in PT than in OL, where maximal values lie at 40-50% TOP. This difference could be due to the rudstones in PT, which contain high amounts of coral rubble and the single corals and coral fragments, present in the background grainstones, which mostly leached or karstified lead to high local TOP. If OL or PT is compared between individual boreholes, the shapes of the histograms are quite similar. The shapes of the histograms at RC resemble more a uniform distribution, where all TOP-values occur more or less at the same frequency. Frequencies recorded at low TOP are not so important any more and TOP up to 100% occurs. The irregularity and the high values of TOP are mainly due to the karst processes and the associated well cemented or recrystallized rock matrix. For this lithofacies type again the histograms of individual boreholes are comparable up to a certain degree and their shape is diagnostic for this lithofacies type.

The most characteristic distribution of TOP is beyond doubt recorded for DT, where in all boreholes at the smallest porosity-class a relative frequency between 60 and 95% is present. The lack of significant TOP-values larger than the smallest class, which includes all windows with TOP of 0-2%, expresses the homogeneity at low borehole-scale porosity. The main reason for the recorded spike at the lowest TOP-class is the fine grained sediment, consisting of mud-dominated packstones and grainstones, lacking larger accumulations of leached fossil-debris and single coral heads. The comparison of DT between the three boreholes reveals that lateral heterogeneity changes are almost non-existent. The results obtained from plotting TOP of ATS in histograms prove the division of the reefal complex into 5 main lithofacies types to be valid. They can be traced laterally among all 3 boreholes, since within individual lithofacies types the distribution of TOP between boreholes is comparable and the shape of their histograms diagnostic.

3.4.4.   Assessment of scale-dependency and periodicity by using ATS

One of the main advantages of the ATS is its ability to change the scale of investigation by choosing a larger or smaller scan window. After Bear (1979) the REV is defined as the scale of investigation at which the porosity does not change significantly any more, if the elementary volume is being changed between a minimal and a maximal value. Thus, at the REV, heterogeneity variations and the standard deviation of the porosity distribution are close to zero. Standard deviation (SD) from the porosity data has been plotted versus window size for six different window sizes, ranging from 0.001-2 m (Figure 40B. The window size, at which the standard deviation does not reduce anymore significantly, marks a minimum for the REV. There where a REV has been found, values are around 1 m in RC and PT and between 0.5 and 2 m in OL. Homogeneity is thus only reached at the m-scale or in most cases even above. Overall trends, like the constant decrease of heterogeneity recorded in PT of MC3, do not allow for a determination of the REV. As observed in the histograms already, DT by far is the most homogeneous lithofacies type. For boreholes MC2 and MC3, very small REV's of 0.2 m window length have been found. At MC5 the relative standard deviation is much larger and no plateau is reached at smaller windows. This is mainly due to the pronounced spike on the ATS-curve within DT, where a leached coral leads to a single peak of 50% TOP (Figure 39).

Nearly all geology-related data exhibit spatial correlation, which means, that the data are not totally random and neighboring values bear some relation to each other (Lucia, 1999). Variography can be used to quantify the spatial continuity that is either explicitly exhibited in the data or inferred from the data through geological interpretation. The variogram calculation provides the ability to extract the size of geological modeling cells. Furthermore, cyclicity in a vertical variogram may be linked to underlying geological periodicity. In this study the variogram has been used in order to check for periodicity within individual lithofacies types, which provides us with more information about heterogeneitiy and possible anisotropies of the borehole-scale porosity structure. Variography has been applied on all boreholes and all individual lithofacies types but only for proximal talus the dataset was long enough for a reliable analysis (Figure 40C). For PT a sill seems to be reached, however at larger lag distances. The most suspicious feature of these variograms is the periodicity, which has been recorded in all boreholes and exclusively in PT. Unlike in other lithofacies types, several local minima are present, which can be interpreted as cycles. Periodicity in variograms is only achieved if the cycles are regular and of equal thickness, otherwise the local minima would be equalized. The distribution of minima indicates a cycle thickness of 1.2-1.4 m at MC2, 1.8-1.9 m at MC5 and 2 m at MC3. If we think about a geological dip-section MC2-5-3, which dips more or less in the direction of reef-progradation, MC2 lies at a distal, MC5 at an intermediate and MC3 at a proximal location of a virtual carbonate factory in the background. This phenomenon of cycles in the PT has also been observed on outcrops at the well exposed cliff coast of Cap Blanc, where clinobeds, which coarsen upwards, are present. According to Pomar et al. (1996) these clinobeds may be high-amplitude or low-amplitude, reflecting the depth of the fore-reef platform adjacent to the reef.

3.5.   Results of standard logs

3.5.1.   Permeable features by flowmeter logs

The IFM used in the described configuration logs permeable features along the borehole. Permeable features are mostly of secondary or tertiary origin, such as open fractures, leached corals within the reefal framework or cavities, interconnected by karst. The large hydraulic contrast, which is built by the karstified reef core, is the main reason for the relatively low flow resolution of the method. If a permeable feature yields flow at a distinct depth, which results in a step on the log, it is called discrete. If the flow occurs continuously over a certain distance, the permeable feature is called diffuse.

In MC2 about 90% of the total flow has been recorded within 2.5 m of the karstified reef core (Figure 41A). Here three discrete permeable features A-C occur at leached corals, with sizes at the dm-scale. These corals are affected by karst, since thin red-brown residual clays, as well as red stained calcite precipitations are present. Thus, the hydraulic productivity of this zone is most probably due to an interconnected channel network. The sequence boundary beneath the reef core, which consists of a redalgal wackestone with high clay content, seems to act as a low permeability-zone and might have supported the karst development at the bottom of the reef core during post-depositional sea level lowstands. The discrete permeable feature D cannot be characterized very clearly from core analysis and optical BHTV, but might be related to extensive burrowing and the overlying sequence boundary.
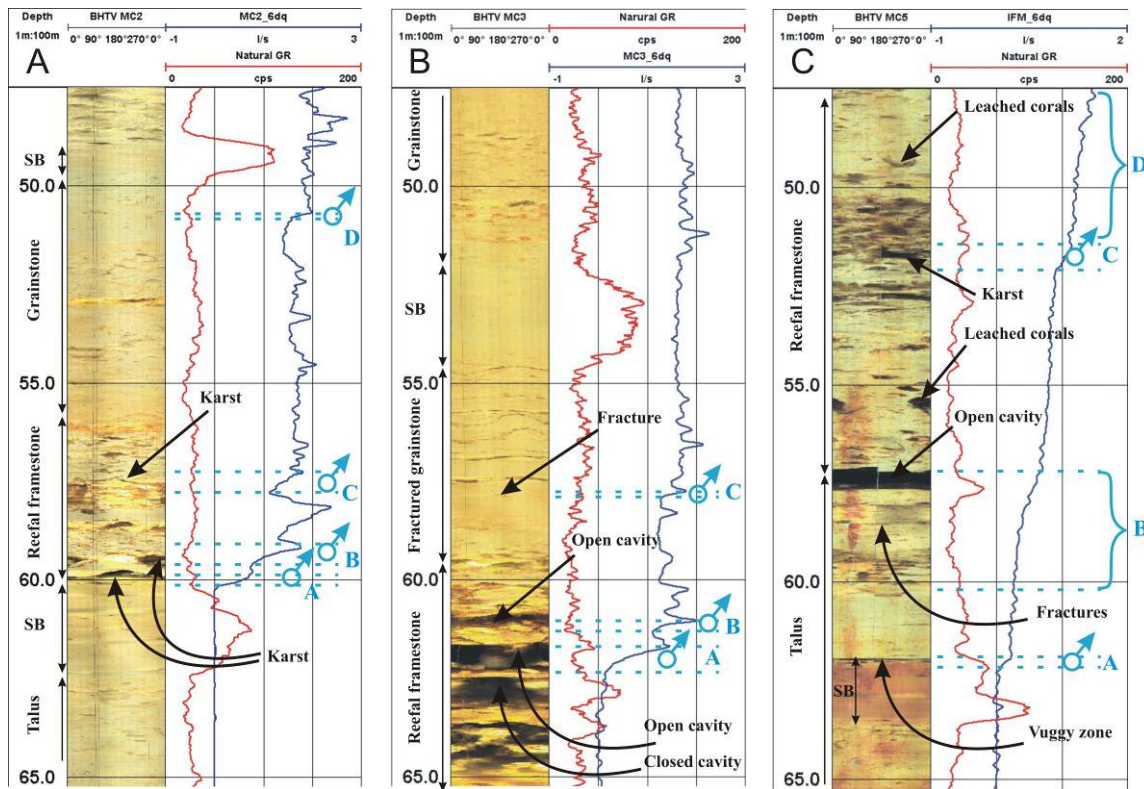
Figure 41:   Correlation of discrete and diffuse permeable zones recorded by IFM, to gamma log and BHTV-image for boreholes MC2 (A), MC3 (B) and MC5 (C). Geology, including sequence boundaries (SB), is given as well.

MC3 is the borehole, where karst is developed best, with cavities of up to 1 m height. The two major permeable features A and B, which yield together about 80% of the total flow, are located in the upper half of the reef core (Figure 41B). Pronounced excursions of the gamma log at large scale cavities in the lower part of the reef core prove their karstic origin and furthermore point to a complete occlusion with residual clays. The cavity at the discrete permeable feature A has about the same size like the one beneath, but a low gamma signal indicates an open system, which yields about 70% of the total inflow in this borehole. The small discrete feature C lies within a fractured zone, which is sandwiched between a sequence boundary on top and the reef core below. Here lots of small open fractures occur with red-stained calcite covers, of which the least prominent and lowermost one is hydraulically active. This example illustrates, that core description and porosity logs alone are not sufficient for a reliable characterization of the borehole-scale porosity structure.

In borehole MC5 major inflows are not exclusively concentrated on small and easily detectable flow features, but as well zones of diffuse inflow along larger intervals, without remarkable single contributors occur (Figure 41C). A discrete permeable feature A is located in grainstones to rudstones of the proximal talus and directly underlain by a sequence boundary. The sequence boundary, which acts at least partially as a seal, allowed the development of a vuggy zone. Within reef core, some larger cavities, most likely originating from dissolved corals, do not affect the IFM. Two prominent larger permeable features of diffuse flow B and D have been recorded, of which the first one will be presented. Zone B is located within a fractured zone, right below the reef core. Within this zone some fractures with reddish calcite precipitations are present. An out-washed cavity, which marks the bottom of the reef core as well, contributes to the flow. Unlike in other boreholes, this portion of proximal talus is sandwiched between the hydraulically active reef core and the mentioned

sequence boundary, about 3 m beneath. Presumably the fractures are rather well connected and yield minor contributions, with increasing intensity from the first fracture above the low permeable sequence boundary, towards the high permeable karstic cavity at the top. Thus, besides the karst, as well fractures seem to be interconnected here and probably even cut the karstic channels at the bottom of the reef core.

The IFM logs are indispensable for the hydraulic characterization of the reef core and show clearly, which at the large-scale cavities are hydraulically relevant. Main inflows within reef core occurred in karstified sections and zones of leached corals, which presumably both build a well interconnected channel system through the whole reef complex. Furthermore, fractured sections and intensively burrowed grainstones, which especially occur in outer lagoon, can lead to a diffuse inflow over larger borehole intervals, without the occurrence of distinct inflow points. Most permeable features outside the reef core are associated to sequence boundaries, which obviously exhibit a certain sealing potential.

3.5.2.   Porosity from induction/conductivity logs

The combination of induction- and conductivity log yields a saturated total porosity, which includes the primary, secondary and tertiary fraction of porosity, within the investigation-scale of the induction probe. Since the exact cementation factor is highly variable and unknown, porosity values are rather relative than absolute. In all boreholes, the remarkable zone of a rapid porosity increase, which is followed by a subsequent decrease, lies within the mixing-zone, where Archie's equation is not valid anymore (chapter 3.6.4). Thus, this section of the induction log will be skipped for the interpretation of porosity.

In the upper part of MC1, data is biased by 3 lost drill bits at depths of 48 m, 56 m and 59 m (Figure 42). Below the mixing-zone within the grainstones of proximal talus, porosity oscillates only very little. The rudstone at the bottom of proximal talus is expressed by slightly lower porosity. The amount of total porosity does not change in the distal talus below, but less high-frequency oscillations are present, than in the upper proximal part, which might be a result of the homogeneity. The upper part of the talus consists of much more rudstones and layers with large moldic pores, which cause heterogeneity at the borehole-scale. A comparison to the observed geology on core material reveals, that small layers of rudstones, with thickness <0.5 m, are not recognized by the induction tool, which is consistent with its vertical resolution.

At MC3 in which the reef core is thin and lies at a lowstand position, capped by thick outer lagoon deposits, induction porosity behaves differently. In outer lagoon porosity varies quite uniformly between 25 and 35%. The oscillation here is the result of an alternation of coarse and fine grained deposits. In general at the bottom part of rudstones, which consist of large and elongated molds in a well cemented matrix, porosity reaches a minimum. The boundaries OL/RC and RC/PT are sharp and easily recognizable on the induction porosity curve. Within reef core, induction porosity is highly variable, expressing the dense and recrystallized zones, with large karstic cavities in between, partly filled with residual clays. The part between mixing-zone and basal rudstone, which marks the transition to distal talus, is not as uniform as observed in other boreholes. Oscillations of low frequency, overlain by those of high-frequency dominate here. Sporadic accumulations of fractures, which are better cemented and recrystallized at low porosity zones and less cemented at high porosity zones, seem to correlate to the observed low-frequency signal. Below the basal rudstone, high-frequency

oscillations are not present anymore, indicating the much more homogeneous distal talus. The high-frequency oscillations are due to leached coral rubble and molds of other large fossils.
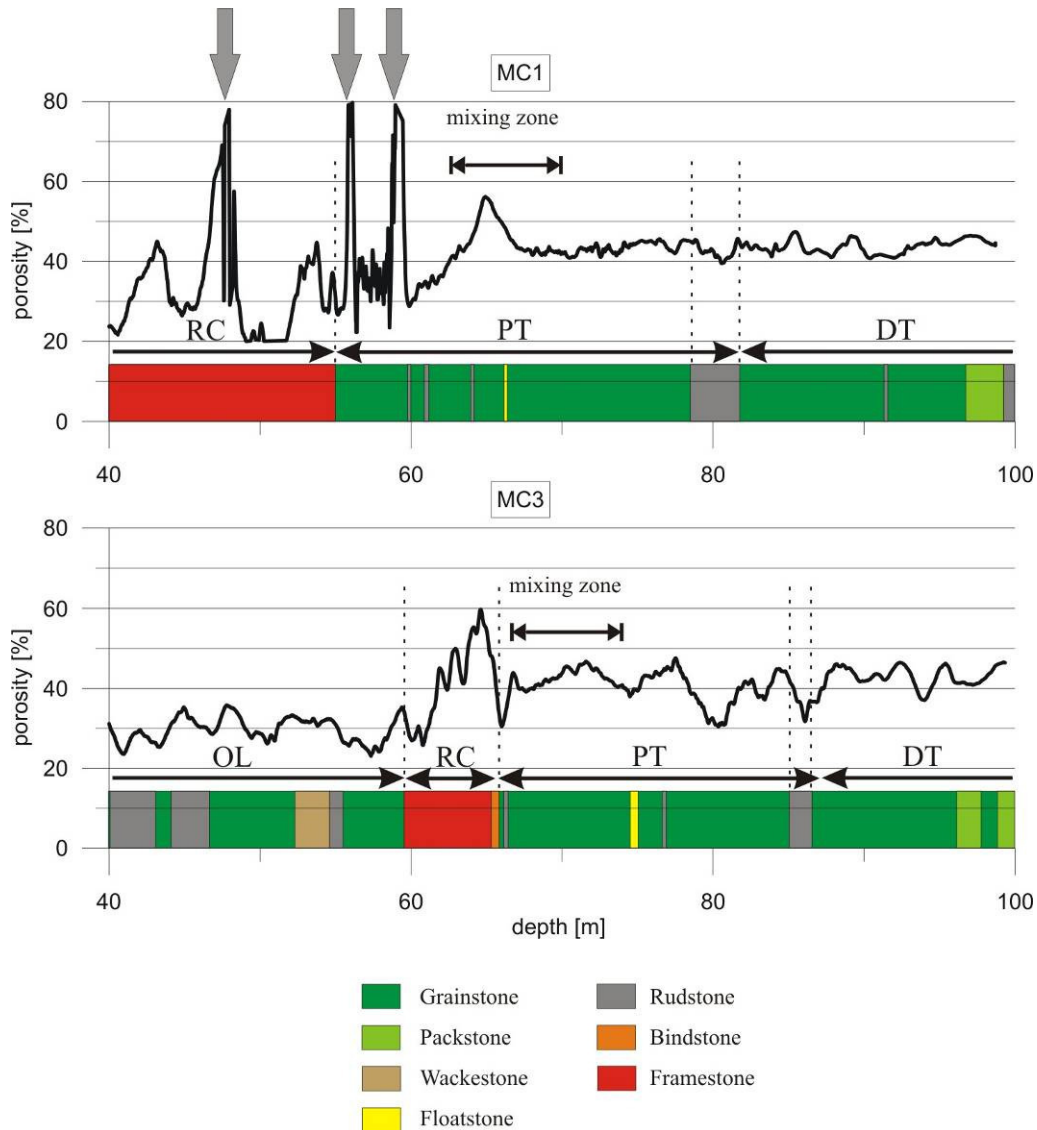
Figure 42:   Porosity from induction logs for boreholes MC1 and MC3 with a correlation to geology observed on cores. Artifacts are indicated by vertical arrows. The approximate range of the mixing-zone is given as well.

Boreholes MC4, MC5 and MC7 show comparable characteristics on the induction-porosity log, especially in the talus (Figure 43). In MC4 the porosity contrasts seem to reduce towards the bottom of the reef core. A comparison to core material shows, that the high porosity peaks on the induction log exactly correlate to karst cavities, which are getting smaller towards the bottom of the reef core. The bottom of these cavities commonly is covered by residual clays. In MC5 below the reef core, a gradual increase of porosity was recorded, starting at low porosity of approximately 25%. This increase is real, since located above the mixing-zone and proven by measurements on 1inch mini-cores (chapter 3.6.4). At 63 m the gradual increase is interrupted by the influence of a sequence boundary, showing slightly enhanced porosity, which is due to the clay effect. The lower part of proximal talus, with porosity of 45%, is quite uniform and mainly controlled by high-frequency oscillations, originating from thin lenticular layers of reef rubble or resulting from larger molds, which are abundant in the more

fine grained background sediment. The basal rudstone exhibits reduced porosity of slightly less than 40 %, which is due to a better cementation of the bioclastic material.
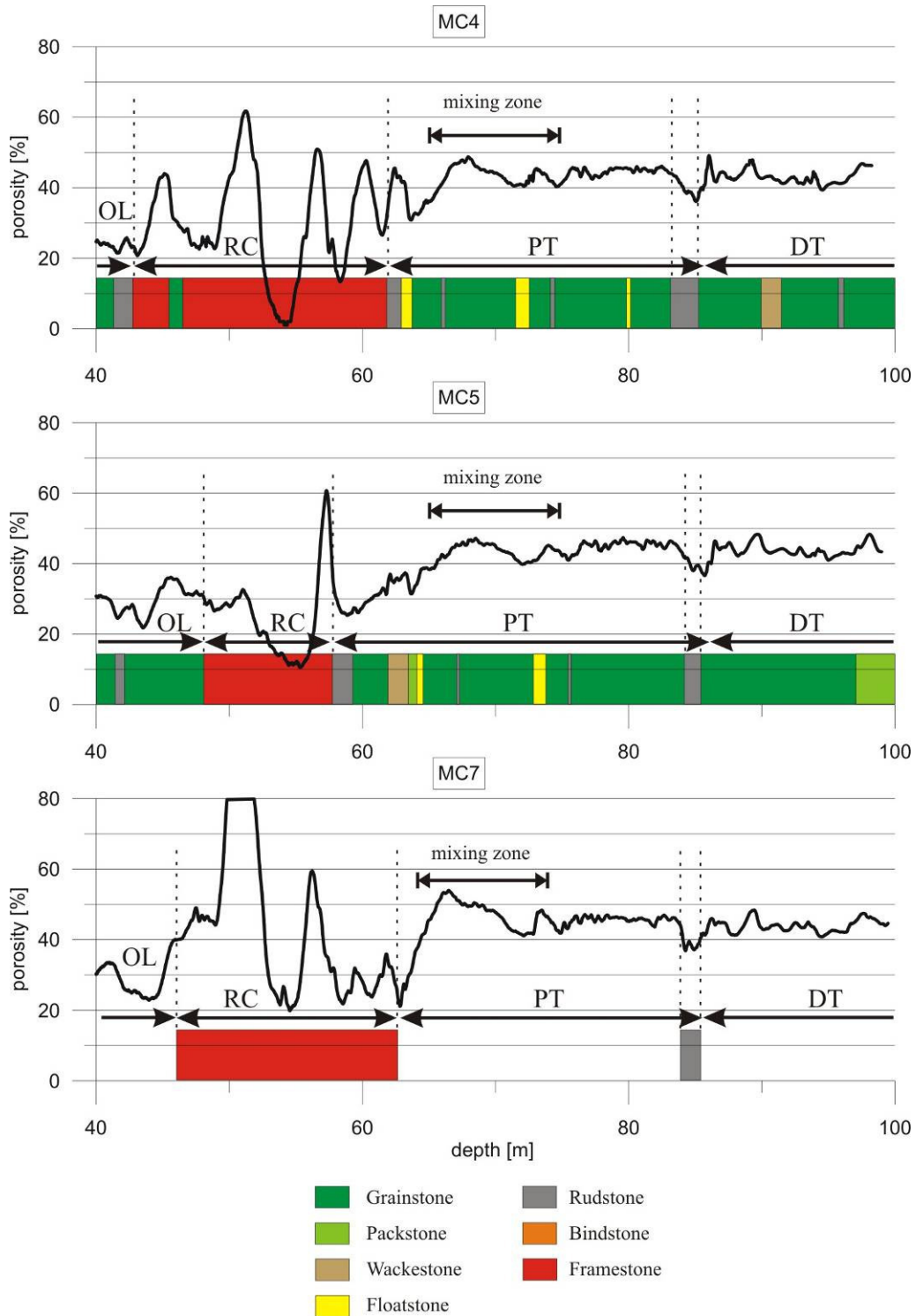
Figure 43:   Porosity from induction logs for boreholes MC4, MC5 and MC7 with a correlation to geology observed on cores. For MC7 no core material was available - geology is based on BHTV-image. The approximate range of the mixing-zone is given as well.

3.5.3. Porosity from full-waveform sonic logs

The sonic log is strongly affected by the pore type and secondary porosity with a framework-like fabric is generally underestimated. Consequently the sonic log is rather a method for capturing the primary porosity (Hearst et al., 2000). Since within the Miocene reefal carbonate of the present study the largest porosity-fraction consists of secondary porosity, porosity calculated from V_P is biased and thus care has to be taken with absolute values. Data quality of MC4 is much better than of MC5, however, as well the latter yielded some important information about the borehole-scale porosity structure.

At MC4 three domains of different characteristics in sonic porosity can be delineated (Figure 44). In general one observes a high variability of sonic porosity, oscillating between 3 and 100% in the upper part, followed by an intermediate part of low variability at an average porosity of 50-55% and a bottom part, which additionally exhibits reduced average porosity of 40-45%. The sonic log in MC5 as well revealed the three domains with different sonic porosity. Due to the lower data quality and the related cycle skipping, here much more individual and narrow spikes are present, but the general trends are the same. The upper part is characterized by high variability and several readings of 100% porosity. Recapitulating the depth of investigation, which is 20 cm for the lowest recorded velocity, such recordings are typical for larger cavities, with a size of at least a few dm. A comparison to the core and BHTV-images confirms this statement. In between and associated with karst lie high velocity zones, where the porosity readings are 10% or even less (a-d). These high velocity zones, as seen on core material are dense, recrystallized rock with low porosity. Lowest matrix porosities measured on 1inch mini-cores are of a few percent and originate from exactly these locations on top or below large open karstic cavities. In MC5 a further high velocity zone is present at a vuggy zone, above a sealing sequence boundary, which built the basis for enhanced recrystallization processes.

The second domain starts at the boundary RC/PT, where a remarkable transitional decrease in variability to moderate average values of 50-55% can be recorded. Here sonic porosity, which in contrast to induction porosity is not influenced by the mixing-zone, clearly shows the transitional behavior of the uppermost talus, where recrystallized and leached reef rubble is getting more abundant towards the reef core. Below, untill a depth of 86.1 m, at least 5 distinct porosity-plateaus can be delineated. Some of these plateaus can be correlated to fossil-bearing rudstones, like for example the rudstone at the basis of proximal talus, where sonic porosity is significantly increased. These rudstones are characterized by an increased amount of large molds and the rock is partly well cemented. Some narrow spikes of sonic porosity like observed at 75.8 m do not have geological significance and are artifacts of erroneous p-wave picking.

Slightly below the basal rudstone, which correlated with the derived sonic porosity, in both boreholes a remarkable step down to about 10% lower porosity of 40-45% is recorded. This step exactly fits with the boundary PT/DT, which has been described on core material. The slight rise of sonic velocity occurs right at the transition to a lithofacies type, which is more fine grained and much more homogeneous, but which according to data from 1inch mini-cores and induction logs exhibits a comparable total porosity. It lacks large, elongated moldic pores and the pore structure is mainly built of round shaped, small molds, which are embedded in a micritic or microsparitic matrix, leading to microporosity of 30-40%. Furthermore, matrix permeability is relatively low (chapter 2). The dominating small, round shaped moldic pores are supposed to build a rigid framework-like pore structure, which despite the high amount of total porosity, leads to relatively high sonic velocity. Thus, the

sonic tool tends to overlook these small secondary pores, a phenomenon, which is well documented in literature (e.g., Anselmetti and Eberli, 1999; 2001; Hearst et al., 2000).
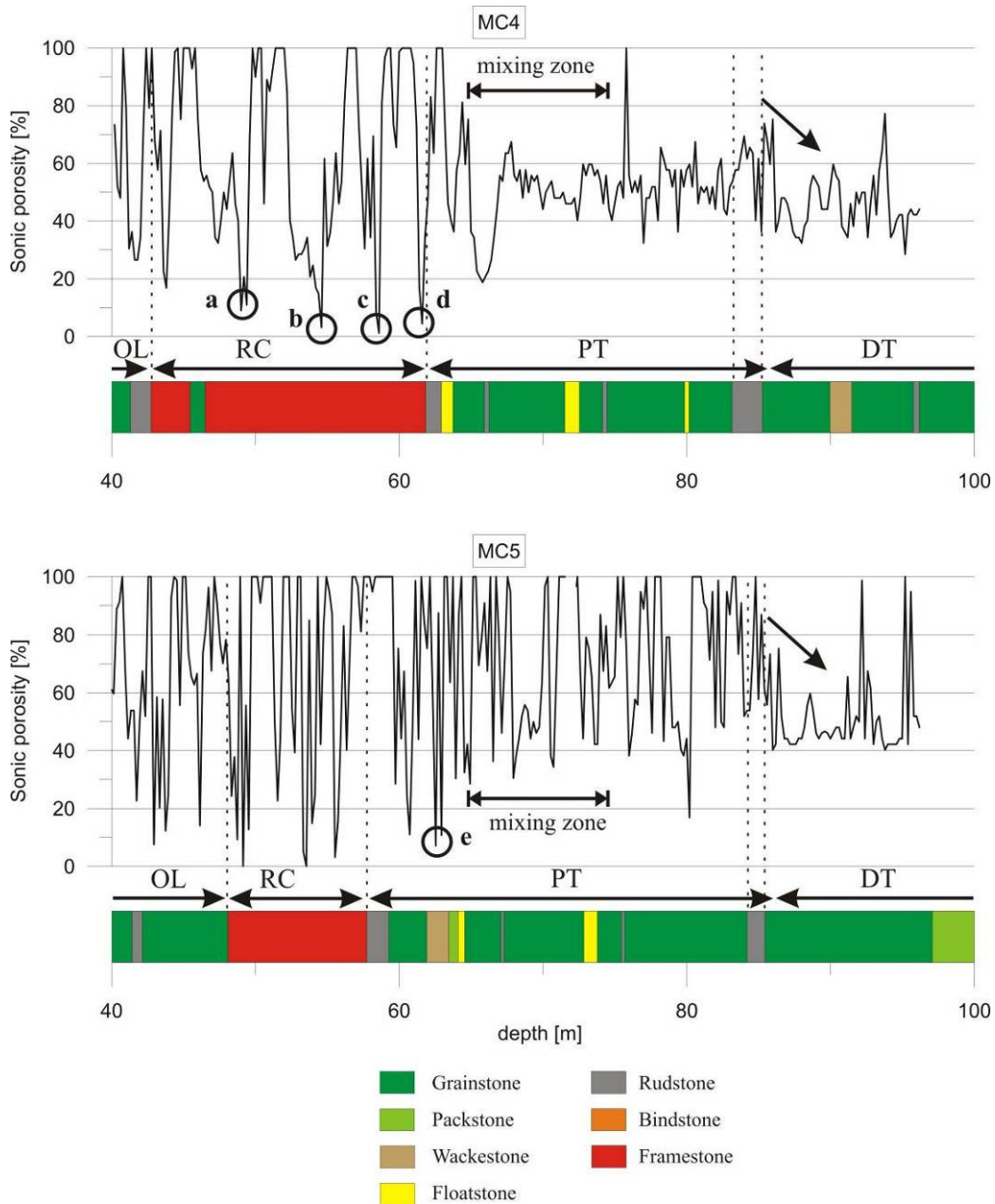
Figure 44:   Porosity from full-waveform sonic logs for boreholes MC4 and MC5 with a correlation to geology observed on cores. The most pronounced low porosity zones, which correspond to intensively recrystallized rock (a-e) are indicated – furthermore the mixing-zone is indicated and the prominent step in porosity at the transition PT/DT is marked by an inclined arrow.

3.6.   Data integration and genetic interpretation

In the following section the log responses from all applied investigation techniques will be interpreted and integrated into a qualitative porosity model under consideration of their inherent scale of investigation for each lithofacies type individually. The results in chapters 3.4 and 3.5 have undoubtedly shown, that visual core description, electrical, acoustic and optical properties yield different insights into the 3D-pore space, which can combined together enhance the understanding of borehole-scale heterogeneity within the reefal unit significantly. From the integration of the available information, below for each lithofacies type the primary pore structure and the related depositional processes will be given. Additionally post-depositional processes, which led to the important secondary porosity, will be considered and finally if significant, the impact of karst and mixing-zone on the pore structure is interpreted.

3.6.1.   Sequence boundaries

Prominent sequence boundaries (SB's) are present in MC2 at 49-50 m (Figure 34A) and 60-62 m (Figure 34B) at MC3 52-55 m (Figure 41B) and at MC5 62-63.5 m (Figure 41C). SB's within this reefal carbonate developed during sea level lowstands through subaerial exposure of the reefal complex. This process took place during the evolution of the reef and led to altered rock and the formation of fine grained wackestones with an intergranular porosity. As IFM logs have shown indirectly, the pore space within these wackestones is not connected and for the rock matrix a total porosity, which includes as well moldic pores of 10-20% could be found (chapter 2). Since electric and acoustic logs yield a biased signal in the zones of increased clay content like at SB's, only the ATS was capable of recording borehole-scale porosity, which is mostly zero. An exception builds MC5, where at the SB below reef core with 6% highest values have been recorded. The predominant pore type, which causes this porosity is moldic and thus already a secondary porosity. Moldic porosity formed through the dissolution of aragonitic constituents.

The vuggy zones, which have been recorded above SB's, undoubtedly formed through secondary processes. As observations on core material have shown, the vugs are mostly solution enlarged molds, which tend to be enlarged rather in the horizontal, than the vertical direction. These zones most probably formed during former sea level lowstands, when fluid activity was concentrated above the partly sealing SB's, leading to massive dissolution along these heterogeneities. Manfrino & Ginsburg (2001) as well observed vuggy zones, which were associated with sequence boundaries, however, mostly below them. As could be demonstrated by IFM logs, the vugs are interconnected and contribute significantly to total flow. Since the size of most vugs is at the cm-scale, here borehole-scale porosity of up to 65% has been recorded within the scale of investigation of the ATS (Figure 39, MC5h).

3.6.2.   Outer lagoon

Borehole-scale heterogeneity in outer lagoon lithofacies is dominated by the presence of patch reefs, rudstones of reef rubble and accumulated shell fragments and small single corals in the background sediment. Patch reefs with their recrystallized and well cemented rock matrix exhibit low porosities of 10-30% (chapter 2). The recrystallization of the originally aragonitic coral framestones through neomorphism, together with the occlusion of the framework porosity by blocky spar is a post-depositional process, which led to a very dense rock matrix.

However, some of the corals were leached out and thus the pore structure is different from the bioclastic sediment of outer lagoon. Pores are in general larger, vuggy and surrounded by a recrystallized matrix. At the test site unfortunately all patch reefs lie above water level and thus were not recorded by the logs.

For the bioclastic sediment of outer lagoon the induction tool recorded porosity in the order of 30%, however, with a cementation factor, which is mostly representative for the lower talus and thus the value might not be representative. At the rock-matrix-scale for the packstones to rudstones of outer lagoon with 1inch mini-cores and digital image analysis on thin sections, much higher porosities were found, which generally range from 20-55% (chapter 2). Additionally the ATS yielded optical porosity of 3-8% for pores larger than 1 cm. The pore structure consists of large elongated molds, which are interconnected through the primary intergranular pore space and total borehole-scale porosity consists of 20-55% porosity at the rock-matrix-scale and 3-8% porosity of pores larger than 1cm.

Originally the primary pore space consisted of intergranular pores, whose shape, anisotropy and total porosity was controlled by the distribution and composition of the bioclastic packstones to rudstones. Subsequent diagenesis led to the formation of moldic porosity as the dominant pore type, which is interconnected through the remaining intergranular pores. Within outer lagoon about 70-95% of the pores are of moldic origin (chapter 2). Pores, which are beyond the rock-matrix-scale, have been recorded by the ATS. It could be shown, that pores within outer lagoon, which contribute to the ATS are either larger molds, like leached corals and coral fragments or fractures. These are both part of the secondary porosity. The fractures are mostly open, sometimes solution enlarged and seem to be oriented along the local bedding. From the present dataset the origin of these fractures cannot be decided, however, they are definitely not due to karstic collapse, as postulated from the coast (Ardila and Pomar, 2000) and thus must be the result of a larger tectonic event. In this study their importance for the borehole-scale pore structure has been demonstrated by IFM logs. The permeable features C in MC3 respectively B in MC5 (Figure 41) are unambiguously due to such open fractures. At the borehole-scale these fractures are not significantly contributing to total porosity but they are the only structure with a high potential of lateral interconnection. Furthermore, some of these fractures are solution enlarged and contain red-brown residual clays or sinter and thus show initial stages of karst. Karst, which is much more important within the underlying reef core, will be discussed in more detail below.

3.6.3.   Reef core

The reefal framestones, which consist of dense recrystallized coral colonies with low matrix porosity of 0-30% are interrupted by internal sediment, which mostly originates from the outer lagoon. Matrix porosity of the internal sediment with 20-40% is much higher and the predominant pore type is intergranular (chapter 2). Within the well recrystallized patches of reefal framestone, porosity is mostly vuggy and occluded by blocky spar. High variability in log responses for reefal limestones has been reported by many authors (e.g., Warzeski et al., 2001). At the test site near Campos at borehole-scale, porosity variations are highest within reef core. This result has been proved by all logging techniques. ATS recordings, ranging from 50 to 100% for the 10 cm window, are typical for the reef core. However, large differences have been recorded between individual boreholes. On core material and optical televiewer, large karstic cavities have been observed at MC3, which lead to an overall ATS-porosity of 62%, of 28% at MC5 and of 15% at MC2. These percentages are accurately

representing the degree of karstification. Karst is the most important control of heterogeneity on this lithofacies type.

Large dissolution cavities and karstic channels are associated with dense and recrystallized rock through increased recrystallization and cementation processes. Some of the lowest matrix porosities measured on 1inch mini-cores are exactly from these locations and range between 5 and 10%. Consequently within the karstified reef core at this scale, high porosity contrasts are present. These porosity contrasts lead to strong oscillations in the recorded signals of the standard logs. The comparison of the sonic and the induction log at borehole MC4 reveals excellent correlation at the most variable zone (Figure 45). High velocity respectively low sonic porosity between the karstic cavities a-d is related to their well recrystallized and cemented bottoms or roofs. Similar observations were made with induction-porosity, however, unlike sonic recordings, the amplitudes of the porosity variations are getting smaller towards the bottom of the reef core. On core material a gradual decrease in thickness of the karstic cavities and the well cemented rock in between has been observed. When the thickness of the beds or cavities falls below a certain threshold, the resolution of the induction tool is not sufficient anymore and yields an apparent value. The inherent scale of investigation of standard wireline logs thus within reef core records the high degree of heterogeneity, but is too inaccurate to handle the pronounced petrophysical contrasts.
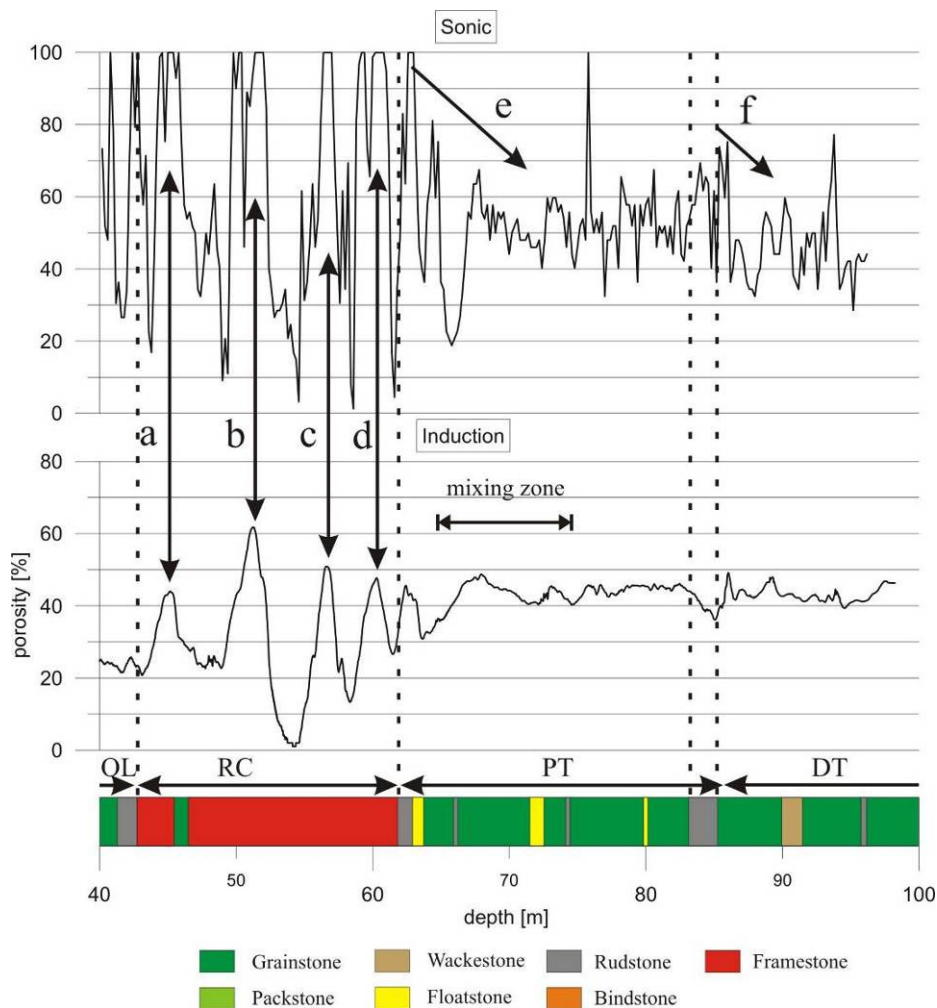
Figure 45: Integrated interpretation of borehole MC4, using sonic log and induction log, illustrating the good relative correlation of high sonic porosity with high induction porosity within the reef core (a-d). Furthermore, the transition within proximal talus is indicated (e) and the step at proximal/distal talus (f).

In contrast to the induction porosity, compared to measurements on 1inch mini-cores, the sonic tool seems to yield reasonable values within the karstified part of the reef core, with matrix porosities of 5-30%. As could be shown, the roofs of karstic cavities are mostly well recrystallized and at the bottom thick residual clays are biasing the signal. With the IFM most permeable features could be recorded within reef core, which hydraulically is the most permeable zone of the reefal complex. The permeable features are predominantly found on karstified horizons, towards the bottom of the reef core and at leached corals, which obviously are part of an interconnected network. The development of residual clays at more mature zones even led to the occlusion of some karstic porosity as observed in borehole MC3 at around 63 m. Karst controlled reservoir heterogeneity, like it is observed in this lithofacies type, is a well known phenomena in carbonate reservoirs (e.g., Kerans, 1988). Most inflows are located on discrete horizons, which illustrate the high contrast in the connection of the pore space between rock matrix and porosity at larger scales (Figure 41). However, especially in borehole MC5, some diffuse zones could be detected with the IFM. In these zones smaller and well interconnected permeable features could be the cause but observations on core material and optical BHTV did not lead to a satisfying conclusion.

The reef core is the lithofacies type, where scale-dependency of porosity is best developed. At the rock-matrix-scale lowest porosity has been measured, since the rock is mostly recrystallized and the original porespace occluded by blocky spar. AT the borehole-scale the cm- to dm-scale cavities, which are mostly related to karst and large molds, are affecting the signal of wireline logs and as the ATS has shown, contribute significantly to the porosity of this lithofacies type. Due to scale disparity calibration of induction- and sonic logs with lab-measurements for this specific lithofaciestype is not possible. Thus, in such an environment, the scale at which porosity has been recorded is of eminent importance.

The complex porosity evolution within reef core started with the growth of the coral colonies, which overgrew each other and led to large primary pores, which were preserved, if not filled with internal sediment. Recognition of such primary pores from boreholes only is difficult, however, these megapores, which can reach up to man size have been reported from the cliff coast (Pomar et al., 1996). The internal sediment consists to a large extent of intergranular porosity, which partly was preserved. In contrast growth-framework porosity disappeared mostly, since corals neomorphosed to calcite or they were totally leached out after deposition. Further secondary processes were the occlusion of most porespace within the corals by blocky spar, which most probably took place during numerous cycles of exposure and flooding of the platform. The freshwater lenses, which moved up and down the whole reefal complex several times, are the most important control on diagenesis. According to Melim et al. (2001b) besides original lithology and depositional environment, the sea level history is a major control on diagenesis in carbonates. During these oscillations several sea level stillstands must have occurred, which led to an important tertiary porosity, the karst (chapter 4). The high degree of heterogeneity was important for the initiation of karstified horizons. Preexisting primary and secondary pores with sizes at the dm-m-scale acted as important nucleus for karst processes, which mostly took place at the vadose/phreatic transition. In these large primary and secondary pores dissolution was more efficient, since saturated fluids could be replaced quickly by non-saturated ones. Consequently the sea level stillstands led to an interconnected channel network, which is oriented rather in the lateral than in the vertical direction.

The statistical analysis of the ATS-data yielded rather uniform than lognormal distributions for the reef core (Figure 40). Especially the high TOP-values of the distribution are mainly controlled by the karst processes. Despite the fact that the degree of karstification within reef core can be developed very differently between individual boreholes, the uniform distribution

seems to be the best model for all boreholes, which is a prove for the lithofacies-approach in order to describe heterogeneity of the reefal complex. The ATS as well as other logs show that the boundary to outer lagoon is not always straight forward, since internal sediment from the lagoon was swept into the reef core, which generally at the top is less karstified. Furthermore, erosional surfaces, which occur at the boundary OL/RC are mostly not recognized on logs. Thus, lithologically the boundary of these two lithofacies types is rather transitional. The lower boundary to proximal talus is much more pronounced, since karst is more important at the bottom of the reef core and internal sediment seems to be less abundant or was totally changed by the subsequent recrystallization and cementation processes. Consequently the transition of the reefal coral framework to the underlying, mostly coarse grained grainstones to rudstones, which are built of reef rubble and sediment shed off the lagoon on cores, can be recognized with ease (Figure 46a).

3.6.4. The transition reef core/proximal talus

Proximal talus starts with a transitional zone, which extends depending on the borehole about 8-13 m downwards. Within this transitional zone the freshwater/saltwater mixing-zone occurs, however, in most boreholes it starts a few meters below the boundary reef core/proximal talus. The conductivity gradients within the mixing-zone of both formation- and fluid-conductivity cannot be simply related to porosity by Archie's equation anymore, since there responses suffer from a non-linear behavior. The non-linear behavior could be evaluated by comparing the induction log with the corresponding synthetic resistivity log, which was extracted at 0.64 m of the electrical resisitivity single-hole tomogram (chapter 4). Especially at the mixing-zone, the extracted resistivity log does not exactly fit with the induction log. Thus, the rise of induction-porosity from low values of 20-30% up to 45-55% 5 to 10 m below, which then again slightly decreases downhole to the average value of lower proximal talus, is biased. However, several indications could be found, which point towards similar porosity trends within this zone. First in boreholes MC1, 4 and 5 small intervals of proximal talus above the mixing-zone are present, showing a clear increase of induction porosity from low values of 20-30% to over 40% (Figure 42 and Figure 43). Second the trend that porosity below the reef core increases up to a maximum and then falls to the average value of proximal talus, has also been observed on 1inch mini-cores of borehole MC5 (Figure 46, part b). Consequently at least part of the trend from low porosity at the top to high porosity below is real and not an artifact of the mixing-zone.

Towards the top of proximal talus an overall trend of coarsening upwards can be recorded, since the prograding reef core, which interfingers with the talus at its toe, deposits coarse grained reef rubble. As one gets to more distal parts, the amount of reef rubble decreases and mud, which leads to much higher microporosity, is more abundant. The original pore space thus was dominated by intergranular and intrafossil pores. As has been shown in chapter 2, at least parts of this primary porosity have been preserved and intergranular porosity is even bit more abundant than moldic porosity. Furthermore, with the ATS primary porosity, caused by extensive burrowing could be recorded (Figure 39, MC2c), which can lead to local ATS-porosity of up to 50%.

Secondary processes, which affected the pore structure of the uppermost proximal talus, were the formation of important moldic porosity by leaching out corals, coral fragments and debris from bivalves and gastropods and the recrystallization of the metastable aragonite to calcite. Whereas at the top close to reef core, rather large aragonitic components were abundant, the size of these components decreased towards the bottom and the mud content became more

important. Molds are rather large and elongated and their interconnection through the intergranular pore space, like observed in outer lagoon, much less pronounced. Leaching worked for total porosity and recrystallization against it. As observations on core material have shown, recrystallization, which occurred through neomorphism, is highest at the top of the transitional zone and gradually decreases towards its bottom. Increased recrystallization in the transition zone below the reef core is most probably a combination of effects from fluid circulation within the adjacent hydraulically active reef core, which affects the zone below and the grain size distribution and composition of the grains, which originally were mostly built of aragonite.
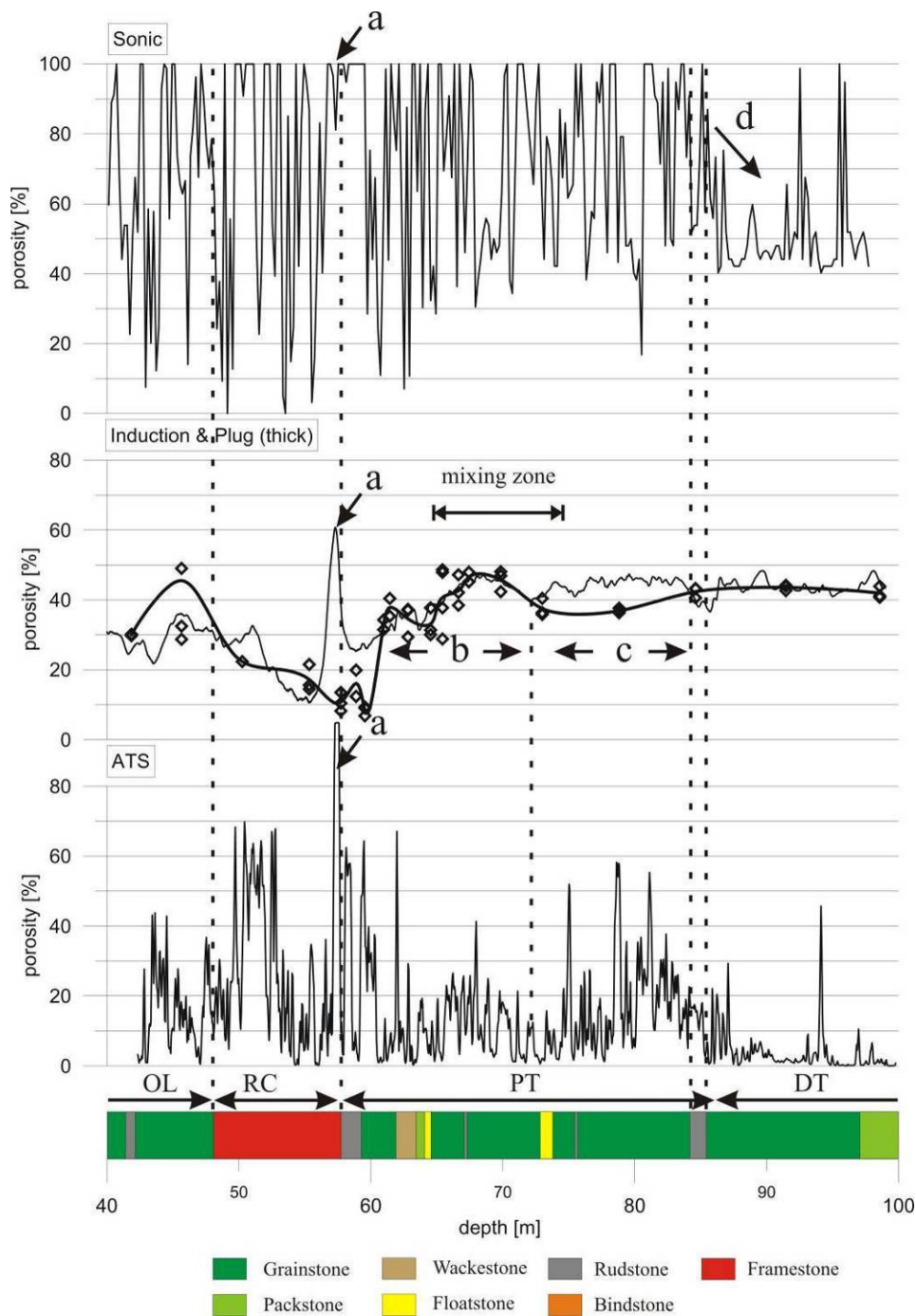
Figure 46:   Integrated interpretation of borehole MC5, using sonic log, induction log, porosity from 1inch mini-cores and ATS-data. Bottom of reef core is marked by karstic cavity (a), which can be seen in all logs. For zones (b), (c) and (d) see text.

Proximal talus is known to be a zone of increased diagenesis, which can complicate the correct geological interpretation of logs (pers. comm. G. Eberli). The recorded log-responses support the interpretation above. Induction-porosity, however biased, increases from top (20-30%) to bottom (45-55%). More reliable than data from electrical logs at the mixing-zone, is data from the FWS-probe, which recorded a transitional zone, where the high sonic-porosity-variations from the reef core above gradually decrease to moderate variations at average values of about 50-55% (Figure 45e). Sonic porosity, which is rather affected by primary porosity and pore structure than total porosity, is most variable in the zone of patchy recrystallization and stabilizes at a high value in the zone of moderate cementation and high amount of moldic, respectively low intergranular porosity. With the ATS secondary porosity, like leached corals, vuggy zones and sporadically fractures have been recorded (Figure 39, MC2a), leading in some boreholes to local porosity (>1 cm) of 60% within the applied investigation scale of the tool. The vuggy zones, which especially occur above sequence boundaries, have already been mentioned as important permeable features, which have been recorded by the IFM. Furthermore, in MC5 fractures below the reef core are causing diffuse permeable features (Figure 41B), thus building an important interconnection of the pore space at the borehole-scale.

The data set of the present study allowed for the characterization of additional processes, which occurred at intermittent sea level changes throughout Pleistocene and Holocene times and which have affected the pore structure of the reefal complex. Observations at the rock-matrix-scale revealed exclusively for MC5 right below the reef core very low porosities of 5-30% (Figure 46). In other boreholes at similar locations, matrix porosities are 20-30%. Additionally in chapter 2 for this part of MC5 an anomalous secondary anisotropy has been reported, where smaller pore-classes exhibit larger anisotropy than larger ones. It was found that the phenomena at MC5 cannot be linked directly to the presence of the reef core. In chapter 4 it will be demonstrated, that the upper proximal talus at MC5 is part of a high velocity zone, which can be correlated to the sea level stillstand of the Younger Dryas event. This sea level stillstand lasted for more than 1000 years and led to significant occlusion of the pore space by cementation with blocky spar.

In addition to the sedimentological reason for a different pore structure, the mixing-zone can affect the formation significantly. Recently Melim et al. (2004) reported from the Great Bahama Bank the alteration of aragonite-rich rock to calcite, which is supposed to be the result of mixing-zone processes. The affected limestone is characterized by enhanced moldic porosity, blocky calcite cementation and recrystallization of lime mud to micrite and microspar. However, data from the present-day mixing-zone on Mallorca shows that porosity and permeability are not significantly enhanced within the transitory location (Price and Herman, 1991). According to them in the phreatic zone the molluscs that were once aragonite are mostly molds, but some have been neomorphosed to calcite. They furthermore conclude that the water table is much more important for the local porosity structure, since below the water table in general a zone of increased vuggy porosity is observed. These observations have been made on Pleistocene beach calcarenites at the margin of the Llucmajor platform and the same is likely to be true for the inner parts of the reefal platform. Doubtless moldic porosity is important at the present-day mixing-zone near the test site but not significantly different from the other parts of proximal talus. Additionally at MC5 for example, the increase of porosity starts already significantly above the mixing-zone (Figure 43). The increase in secondary porosity below the reef core as demonstrated can be explained by depositional and post-depositional processes, which do not require the impact of a mixing-zone. Furthermore, as hydrologic investigations have shown, thickness and position of the mixing-zone has changed considerably throughout the last 100 years, due to excess

abstraction of freshwater (Baron and Gonzalez, 1987). Thus, at the test site, measured signals and observed porosity are most probably not or only marginally affected by the present-day mixing-zone.

3.6.5. Lower part of proximal talus

Proximal talus is a heterogeneous lithofacies, where porosity distribution at the borehole-scale is close to lognormal and comparable between individual boreholes (Figure 40A). Important depositional processes, which had significant impact on the pore structure, are extensive burrowing and cyclic deposition of coarsening upwards clinobeds. Burrowing is significant within the grainstones and lenticular rudstones, causing high porosity heterogeneities in this part of the reef. As observations on core material have shown, the traces are generally less cemented and better sorted than the surrounding sediment and thus porosity and interconnection are enhanced both. In the lower part of proximal talus, about 50% of the borehole-scale porosity recorded by ATS originates from burrows.

ATS-data furthermore revealed the existence of a periodicity, which is most probably due to clinobeds, which coarsen upwards and whose thickness is reflecting the depth of the fore-reef platform adjacent to the reef, since clinobeds commonly are thinning out towards distal parts (Figure 40C). According to this interpretation during deposition, water depth at MC3, where the cycles showed an average thickness of 2 m, was shallow and deep at MC2, with and average thickness of 1.2-1.4 m. These are characteristic features of a reefal platform in the direction of reef-progradation (Figure 30). At the outcrop analogue near Cap Blanc these clinobeds have been found to be well cemented at their upper coarse grained boundary, below cementation in general was very weak. The proximal beds in general dip at angles of 20-30° in the direction of reef-progradation. Especially the upper coarse grained boundaries of individual clinobeds with lots of secondary porosity, such as dissolved shells of molluscs and leached coral rubble, have been detected by the ATS-technique at the test site near Campos. An important depositional process has been recognized here indirectly by recording secondary porosity, which is concentrated along borehole-scale sedimentary structure. Whereas clinobeds are due to syndepositional high-frequency cycles, lenticular rudstone layers, which additionally are common within proximal talus, originate from intermittent storm events.

After deposition of the talus sediments, secondary porosity developed through the dissolution of mostly large and elongated fossil debris. In addition to these, at the rock-matrix-scale as well small and round shaped molds occur here, which originate from the dissolution of peloids and rounded bioclasts. Below the mixing-zone, induction data is again reliable and shows a porosity of 45%, whereas sonic porosity is about 50-55%. Furthermore, sonic- and induction logs both exhibit high-frequency/low amplitude variations, which have not been observed at other lithofacies types. These variations are due to an increased amount of large and elongated moldic pores, which are either part of lenticular rudstone layers or which occur scattered in the bioclastic grainstones of the background sediment. Porosity measured on plugs ranges between 30-50%, which is remarkably lower than recorded by the logs. Since the induction log is rather stable and the cementation factor appropriate for this part of the reef, here a comparison to porosity from plugs and porosity recorded by the ATS can be made (Figure 46). For zone c at borehole MC5 plug porosity is about 10% lower than induction porosity. For this zone with the ATS an average borehole-scale porosity (>1 cm) of 16% has been measured, which can explain most of the discrepancy between these methods. Thus, the

values of the induction log for proximal talus are at a reasonable range. Generally average ATS-values for the lower part of proximal talus range between 11% and 16%.

The higher variability of sonic porosity is due to a better cementation of rudstones and larger corals or coral fragments in the background sediment, which compared to the moderately cemented grainstones in between lead to certain velocity contrasts. Sonic velocity is known to be affected by the pore type and according to several authors is rather recording primary than secondary porosity (e.g., Hearst et al., 2000). However this statement has to be qualified by the fact that about 60-80% of the porosity at the rock-matrix-scale is of moldic origin (chapter 2). At the borehole-scale the fraction of secondary porosity is even higher, since a significant additional amount of large and elongated molds (>1 cm) has to be added, which finally yields a total secondary porosity-fraction of about 70-90%. Despite these high amounts of secondary porosity, recorded sonic porosity is rather higher than induction porosity. According to Anselmetti & Eberli (1999) moldic pores, which build a framework-like fabric are not detected by the sonic tool, since too high velocities are recorded there. From the present study and earlier work done about the matrix of this rock it can be stated, that large and elongated moldic pores are the predominant pore type in proximal talus, which do not seem to build a framework-like fabric, since porosity derived from sonic logs is high and permeability measurements on 1inch mini-cores yielded as well rather high values.

The basal rudstone, which in all boreholes builds the boundary towards distal talus, is well recrystallized or cemented, contains lots of large moldic pores and lacks a high amount of microporosity. Due to the low matrix-porosity, total porosity of these rocks is reduced. In all boreholes the induction-porosity is reduced by about 10%. In general for rudstones with thickness larger than 1 m, a low induction-porosity is recorded but sonic-porosity on the other hand is increased (Figure 45). Whereas single fossils, like coral fragments, bivalves or rhodoliths tend to cause high velocity anomalies on the sonic log, large and elongated molds within well recrystallized rudstones rather seem to attenuate the elastic waves and thus too high sonic-porosities are calculated.

3.6.6. Distal talus

Distal talus is the most homogeneous lithofacies of the reefal complex. In the distal part towards the basin, mud-dominated packstones to grainstones were deposited, which mostly lack coarse grained components. Originally most of the pore space was intergranular, with a considerable amount of mud. The deposited sediment was intensively burrowed and slightly compacted. The most important secondary process was the formation of moldic porosity, which due to the grain size and shape mostly consists of small and round shaped forms. The original mud recrystallized to micrite or microspar and micritic crusts were formed. The resulting rock is homogeneous, few cemented and exhibits matrix porosity in the order of 40-45%, which is dominated by molds and microporosity (chapter 2).

Within distal talus average pore size is significantly smaller, than in the other lithofacies types. The predominant pore type is moldic, however, in contrast to outer lagoon and proximal talus, molds here are much smaller and round shaped. In the proximal talus large and elongated pores with sizes >0.5 mm are much more abundant than in distal talus, where molds <0.5 mm dominate. In addition to the increased moldic porosity, the micrite to microspar in between exhibits a high amount of microporosity. Image analysis on ESEM-images yielded intrinsic microporosity of 30% or even higher (chapter 2). The resulting pore structure is building a rigid framework of isolated moldic pores, which lacks a significant

amount of intergranular porosity, which could act as efficient connector between the molds. This pore configuration results in constantly small pore throats of 1-2 µm size only.

At the borehole-scale the recorded signals are correspondingly different from the proximal talus. Whereas the induction tool yields more or less similar values for proximal and distal talus, sonic porosity as well as total optical porosity (TOP) from the ATS is significantly lower within distal talus. Induction porosity is in the order of 45% and comparable to porosity measured on 1inch mini-cores (Figure 46). In such homogeneous sediments, which mostly lack larger pores and exhibit a small REV in the order of 20 cm at the borehole-scale (Figure 40B), one would suppose only a minor increase in TOP from the rock-matrix-scale to borehole-scale. The ATS-technique yielded average borehole-scale porosity (>1 cm) ranging from 1-3% only. Consequently whereas in proximal talus pores >1cm contribute significantly to total porosity recorded by the induction tool, in distal talus matrix porosity is much more important. Sporadic peaks, which occur on the ATS of distal talus, are caused by leached single corals or coral fragments. As mentioned, the induction porosity does not change at the boundary PT/DT but the character of the curve changes. Whereas within proximal talus high-frequency porosity variations are overlain to the main signal, the lower part lacks these oscillations. It could be shown that this is due to the lack of macropores, rudstones and isolated recrystallized reef rubble, which would turn the signal anxious.

In addition to the prominent reduction of the ATS-signal, at the boundary PT/DT as well sonic porosity is reduced by about 10% to values of 40-45% (Figure 45f and Figure 46d). As has been shown, this remarkable reduction can be explained by the framework-like pore structure observed at the rock-matrix-scale. It is well known that such a pore structure tends to yield too low sonic porosity (Anselmetti and Eberli, 1999; 2001). The small, round shaped molds are surrounded by micritic crusts, micrite and microspar and thus barely interconnected. The low connection of the pore space furthermore has been demonstrated in chapter 2 by permeability measurements on 1inch mini-cores.

Clear signal changes have been found at the transition from proximal to distal talus, indicating changes of porosity structure, including pore size, shape, distribution and interconnection. Histograms and variograms of porosity, recorded by the ATS revealed diagnostic properties, which are distinct from observations made at other lithofacies types (Figure 40A, B). Distal talus is homogeneous, mostly lacks larger pores and exhibits the smallest REV of the whole reef complex. Lateral variation of the petrophysical properties is minor, since no significant differences could be recorded between individual boreholes.

3.7. Discussion – impact on reservoir hydraulic properties

The reefal rock with its porosity structure encountered at the test site is doubtless a high quality reservoir. It has been shown, that borehole-scale pore structure is developed very differently for individual lithofacies types and that post-depositional processes were of eminent importance for the evolution of the pore structure in time and space. It could as well be shown, that up to certain degree secondary and tertiary heterogeneity follows the sedimentary structures. Below possible hydraulic impacts of the most important heterogeneities will be discussed, starting with those caused by primary processes.

Burrowing is a primary process, which took place right after deposition and which occurs in all lithofacies types. The importance of burrows as low- or high porosity heterogeneities is

stressed in Gingras et al. (2004). At the test site, enhanced porosity caused by burrowing was mainly recorded by the ATS within proximal talus. Here non-cemented burrows with increased grain size and sorting build a zone of less hydraulic resistance, which results in increased permeability. Burrowed horizons thus might be important reservoir heterogeneities, controlling permeability if further conductive features are missing. In contrast to burrows, leached and dissolved corals and coral fragments are open and surrounded by a well recrystallized or at least well cemented rock matrix. Thus, at a larger scale, single corals do not necessarily lead to a higher permeability, since often the pore space in the surrounding rock matrix is occluded by blocky spar. Unfortunately the applied flowmeter did not allow for measuring permeable features within burrowed zones, since the hydraulic contrast to the reef core is too large. Nevertheless it can be supposed, that the flow out of such a zone is rather diffuse than discrete.

It was shown, that along clinobeds borehole-scale porosity developed, which could be recorded by the ATS. Here the depositional structure significantly controls the distribution of secondary porosity. The periodicity of the discrete layers with concentrations of large and elongated molds in combination with the basinward dip of 10-30° and thinning out, leads to anisotropy at the crosshole-scale. Most probably this anisotropy is important for the hydraulic behavior of the talus. Depositional- and post-depositional anisotropy, which is important for the hydraulic behavior of the rock, has been found in many sedimentary environments, a comprehensive summary is given in Anderson et al. (1994). These authors furthermore stress the importance of sequence boundaries as controls on reservoir anisotropy.

Sequence boundaries as well as clinobeds are relatively continuous heterogeneities, which dip basinwards. Whereas accumulations of large molds related to clinobeds are of less hydraulic resistance, wackestones and mud-dominated packstones of sequence boundaries exhibit a sealing effect. The important role of sequence boundaries as hydraulic barriers in Miocene carbonates has been mentioned in recent papers (e.g., Melim et al., 2001a). They state that based on their data set, sequence boundaries may be coincident with large changes in permeability but in other cases, permeability changes across sequence boundaries are less, than variations within sequences. At the test site near Campos, sequence boundaries, which are located within outer lagoon and proximal talus, might have a great impact on the hydraulic anisotropy of the system. As shown, porosity within wackestones is low, mostly intergranular and not connected. It is supposed, that within these bioclastic grainstones to rudstones, the occurrence of wackestones, which laterally extend over tens of meters causes effective hydraulic barriers, forcing the flow field to certain anisotropy. Sequence boundaries are less effective within reef core, where between karst cavities, associated residual clays, recrystallized coral colonies and internal sediment, pronounced hydraulic contrasts are present. Indirectly the importance of sequence boundaries as hydraulic barriers could be shown by IFM logs. In outer lagoon and proximal talus several inflow zones, recorded by the IFM, are related to sequence boundaries, which can act directly as a seal (Figure 41A) or which facilitate secondary permeable features like vuggy zones in the overlying rock (Figure 41C). Secondary heterogeneity, which affects the hydraulic properties of the reefal complex, such as moldic porosity and local fracture sets, are discussed below.

Moldic porosity is the most abundant porosity type of the reefal complex. Moldic pores are generally considered not to contribute to permeability, since they are often isolated from other pores (Lucia, 1999). However, other authors found that moldic pores can be well connected in a continuous pore network (Melim et al., 2001a). In chapter 2 it has been shown, that both possibilities occur within the reefal complex of Llucmajor. Large and elongated moldic pores are interconnected through the intergranular pore space in outer lagoon and proximal talus. In

distal talus small, round shaped molds in combination with micritic crusts and microsparite lead to a highly porous rock, with a framework-like porosity structure. Here the molds are barely interconnected and the microsparite contains large amounts of microporosity, which as well is hardly accessible. This porosity structure is the main reason for the prominent reduction in sonic porosity at the boundary PT/DT, indicating a low permeable environment at a high total porosity (Figure 45f). With the ATS, only very minor amounts of porosity >1 cm could be recorded, which as demonstrated exclusively consist of sporadic molds. Furthermore, induction-porosity is in the same range as porosity from 1inch mini-cores. Consequently permeability of this lithofacies is mainly controlled by the pore structure observed at the rock-matrix-scale. As a result despite the high total porosity, permeability measured on 1inch mini-cores is rather small, with a measured geometrical mean of 50 md and values ranging from 15 to 190 md only (chapter 2).

Fractures within the young unburied reef complex of the present study are rather seldom. Sporadic closed sub-vertical fractures could be related to the slight tectonic flexure and tilting of the carbonate platform, which took place during Pleistocene (Pomar et al., 1996). Furthermore, in outer lagoon and proximal talus locally gently dipping open fractures are present, which seem to be parallel to the local bedding and thus most probably, are directly related to the reefal geometry. Some indications about their hydraulic relevance was provided by the IFM logs, which recorded permeable features at some but not all of the latter fractures. The comparison to core material and optical BHTV did not yield characteristics, which would allow for a prediction of whether a fracture yields no flow (most fractures on Figure 41B), discrete flow (Figure 41B feature C) or diffuse flow as part of a fracture set (Figure 41C feature B). At the borehole-scale these fractures are not significantly contributing to total porosity but within outer lagoon and proximal talus they build permeable heterogeneities, with a high potential of lateral interconnection. Some fractures are solution enlarged and the walls covered with red stained calcite precipitations or thin layers of residual clays, which are further arguments for their contribution to reservoir quality.

The tertiary process karst builds the dominating heterogeneity of the reef core lithofacies from which the highest percentage of flow could be recorded by IFM logs. Large primary pores and leached corals led already to a highly heterogeneous pore structure, which was intensified by the subsequent karst. Karst bridged the preexisting dm-scale pores and as the recorded signals on the IFM suggest, developed an interconnected channel-system, which is mainly concentrated at the bottom of the reef core. This statement is supported by electric and seismic crosshole investigations, which have been carried out on the test site (Friedel et al., 2004; Maurer et al., 2004). The karst controlled heterogeneity within reef core is doubtless the most productive zone of the whole reef complex. It has been shown, that the bottom of larger cavities is often covered by red-brown residual clays. These clays can seal parts of the karstic system. Clays, which build cave fills have been recognized by several authors as effective seals for vertical fluid exchange (e.g., Kerans, 1988). Considering the size and maturity of the karst system observed in the present study, their lateral continuity might be in the order of several meters and thus limited.

Several authors stress, that permeability in karstic aquifers is often scale-dependent (Mace and Hovorka, 2000; Teutsch, 1991), which implies, that measurements at smaller scales may not apply at larger scales. This is especially true for the reef core lithofacies type, where it appears, that besides porosity also permeability increases with scale. For the recrystallized rock matrix of the reef core, lowest permeabilities of the whole reef complex were recorded on 1inch mini-cores, yielding a geometric average of only 9 md (chapter 2). At the borehole-scale in contrast, depending on the borehole, between 60 and 90% of the flow recorded by

IFM logs originates from reef core, which doubtless is the most transmissive lithofacies type of the reefal complex.

3.8.   Summary

The whole reefal complex is dominated by moldic porosity, which in the upper part like outer lagoon and upper talus is characterized by large and elongated molds, which mainly are detected by the ATS and in the lower part of talus is characterized by small and round shaped pores. At the borehole-scale besides moldic or vuggy secondary pores, tertiary porosity is present exclusively within reef core. Karst associated with post-depositional sea level changes led here to the most efficient large scale effective porosity of the whole reef complex. Below a short summary of the most important features of the pore structure will be given (Table 4):

Lithofacies type/subtype	Rock-matrix-scale porosity (Chapter 2)	Borehole-scale porosity (this study)	Dominant processes
SB	Total porosity: 10-20% moldic and intergranular	ATS: generally 0%, MC5 6% sealing, vuggy zones above with single ATS up to 65%	**primary** subaerial exposure
OL	Total porosity: 20-55% consisting of 5-30% primary (intergranular) 70-95% secondary (moldic)	ATS: 3-8%, mostly molds Induction and sonic not representative	**secondary** few solution enlarged fractures with initial karst, molds
RC	Total porosity: 5-30% of corals, 20-40% internal sediment intergranular and framework	ATS: 15-62% Induction+sonic highly variable karst, Vuggy porosity and primary macropores (dm-scale)	**tertiary** initial macropores, karst, well connected residual clays
RC/PT	Total porosity: (5), 25-50% intergranular high on top and lower towards bottom, moldic vice versa, burrows	ATS: variable, locally 60% Induction: 20-30 up to 45-55% Sonic: 50-55% molds large/elongated	**secondary** anisotropy, blocky spar cementation by sea level stillstand mixing-zone no impact
lower PT	Total porosity: 30-50% moldic high, intergranular low molds large/elongated, small/round, burrows	ATS: 11-16% (burrowing=50%) detection of clinobeds and rudstone lenses Induction: 45%, 70-90% is moldic, interconnected	**primary/secondary** sonic porosity is too high despite dominant moldic
DT	Total porosity: 40-45% moldic and microporosity	ATS: 1-3% Induction: 45% Sonic: remarkable fall to 40-45% molds small/round, microporosity	**secondary** molds within micrite building a framework, homogeneous

Table 4:   Summary of the observed porosity structure at different scales, with typical recorded values and the dominant processes.

Sequence boundaries could potentially seal parts of the reservoir, since the pore structure consisting of intergranular and moldic pores is not interconnected. Vuggy zones, which have been recorded above some sequence boundaries, have formed through secondary processes. They consist of solution enlarged molds, which are well interconnected. Sequence boundaries are important in outer lagoon and proximal talus, where their low permeable pore structure causes important heterogeneities. In outer lagoon secondary processes are dominant and about 70-95% of the pores are of moldic origin. The molds are well interconnected through the intergranular pore space. It could be shown, that pores within outer lagoon, which contribute to the ATS are either large molds, like leached corals and coral fragments or fractures. The

few fractures, which occur, are parallel to the local bedding and sometimes solution enlarged. They do not significantly contribute to borehole-scale porosity, but within outer lagoon and proximal talus they build structures with a high potential of lateral interconnection, as has been shown by IFM logs.

Reef core is undoubtedly the most heterogeneous lithofacies type. Here within recrystallized coral colonies, the primary pore space is mostly occluded by blocky spar and thus porosity at the rock-matrix-scale is in the order of 5-30% only. Karst is the most important control of heterogeneity on this lithofacies type. At the dm-scale karstic channels are present, which interconnect large primary and secondary pores. The existence of channels can be suggested from optical BHTV and the discrete permeable features, detected by the IFM. Large dissolution cavities and the interconnecting channels are associated with dense and recrystallized rock. Consequently within the karstified reef core at this scale, high porosity contrasts are present, which led to strong oscillations in the recorded signals. The reef core is the lithofacies type, where scale-dependency is best developed. Depending on the degree of karstification, for reef core average ATS-values ranging from 15-62% have been recorded. Calcite precipitations and residual clays, which can even lead to total occlusion of the cavities, are important concomitant phenomenon. The residual clays locally might act as seals. However, their lateral continuity is not greater than a few meters in a karstic environment of such a low maturity.

The most remarkable zone of the reefal complex is doubtless the upper part of proximal talus, where with all to porosity related investigation techniques suspicious anomalies have been recorded and could be correlated to a great extent to observations made at the rock-matrix-scale. Porosity from induction/conductivity logs points to low porosity of 20-30% at the top, which gradually increases towards lower parts to 45-55% and sonic porosity changes from highly variable to average values of 50-55% (Table 4). Increased recrystallization in the transition zone below the reef core is most probably a combination of effects from fluid circulation within the adjacent hydraulically active reef core, which affects the zone below and the grain size distribution and composition of the grains, which originally were mostly built of aragonite. Most probably the impact of the present-day mixing-zone is much less important, than former sea level stillstands, which led to a directed occlusion of the pore space, like observed in borehole MC5.

In the lower part of proximal talus depositional processes, which had a significant impact at the borehole-scale pore structure are extensive burrowing and cyclic deposition of coarsening upwards clinobeds. It was found, that burrowing within the grainstones and lenticular rudstones causes high porosity heterogeneities. In this part of the reef, burrowing contributes approximately 50% to the borehole-scale porosity, recorded by the ATS. Porosity from induction logs is 45%, to which porosity >1 cm, depending on the borehole, accounts between 11 and 16%. From the present study and earlier work done about the matrix of this rock it can be stated, that large elongated moldic pores are the predominant pore type in proximal talus, which do not seem to build a framework-like fabric, since porosity derived from sonic logs is too high, compared to induction-porosity and permeability measurements on 1inch mini-cores point to a rather well interconnected pore space at the rock-matrix-scale.

Within distal talus, the most important secondary process was the formation of moldic porosity, which due to the grain size and shape mostly consists of small and round shaped forms. The original mud recrystallized to micrite or microspar and micritic crusts were formed. The resulting rock is homogeneous and exhibits matrix porosity in the order of 40-45%, which is dominated by molds and microporosity. Induction porosity yields similar

values for proximal and distal talus, but total optical porosity from the ATS as well as sonic porosity is significantly lower within distal talus. The ATS yielded average porosity ranging from 1-3% only (Table 4). The REV calculated from this dataset is in the order of 20 cm, illustrating the high homogeneity at the borehole-scale. The remarkable reduction of sonic porosity by about 10% can be explained by the change of the porosity structure, which occurs at the boundary PT/DT. In distal talus the small and round shaped molds are surrounded by micritic crusts, micrite and microspar and thus barely interconnected.

As has been demonstrated, lithofacies types as larger genetic units are important for the distribution of porosity within the reefal complex. Secondary and tertiary porosity to a certain degree followed the primary sedimentary patterns and structure. In zones of extensive diagenetic alteration, such as at the transition reef core/proximal talus, where blocky spar cementation of former sea level stillstands led to significant occlusion of the pore space, lithofacies boundaries are blurred and not sharp any more.

The used standard investigation techniques together with the non-standard ATS proved to be a powerful combination for the assessment of scale-dependent heterogeneity. With the ATS-technique lithofacies boundaries, detected by sonic- or induction-tools, could be confirmed and its ability to assess TOP at different scales of investigation provided important insights into REV's and cyclicity, which are both important for the porosity structure at the borehole-scale.

4. Crosshole-Scale Porosity Structure of a Miocene Reefal Carbonate, Mallorca (Spain)

D. Jaeggi, H. Maurer, S. Friedel, M. Herfort, S. Löw

Abstract

This chapter is about the crosshole-scale (meters to site scale) 3D-porosity structure of a Miocene reefal carbonate on Mallorca, which includes reef geometry and spatial distribution of lithofacies types and petrophysical parmeters. Besides the discussion of the results from the geological and geophysical investigation, a comparison of the petrophysical signals with the geological model, derived from sequence stratigraphy and core analysis is provided. The main focus is set on the crosshole lateral and vertical distribution of large scale heterogeneity, such as karst, high resistivity- and high velocity zones, their evolution and internal pore structure.

In order to correctly interpret the lithofacies distribution observed on the 5 fully cored boreholes within the cube of 100 m side-length, outcrop analogues of the cliff coast have been studied, which are located 6 km off the test site. These studies together with sequence stratigraphical concepts applied on the borehole data, lead to a reliable geological model. The techniques, which are capable of resolving structures between boreholes, such as karstic channels and solution enlarged primary megapores, are mainly provided by geophysics. The crosshole-scale pore structure on the test site includes vertical and lateral heterogeneity, resulting from the complex lithofacies distribution and karstification at certain levels.

Such heterogeneity can be captured by using geoelectric single-hole tomography as well as seismic crosshole tomography, two methods, which are not standard in reservoir characterization. These techniques provide information about the petrophysical structure of the reservoir at the m- to 10 m- scale in the vicinity of and between boreholes, in addition to wireline logs. The high resistivity contrasts observed at several levels in the reef core display the complexity of the distribution of large scale primary and secondary porosity, which acted as a nucleus for karstic processes at certain levels. The method even allows for correlating permeable features between boreholes, which have been recorded by the impeller flowmeter. The results have shown that a complex and lateral continuous network of karstic channels is present within reef core, which leads to permeable features at several distinct horizons.

Seismic tomography is capable of resolving p-wave velocity within the formation, even for larger borehole spacing. It revealed the existence of a high velocity zone, which only partly is controlled by the extension of the reef core, but which as well correlates with the high resistivities, recorded by electrical resistivity tomography. In most parts of the reefal complex, post-depositional processes changed the primary pore structure of sedimentary textures. Among these processes the sea level history revealed to be the most important control for diagenesis. With the sea level stillstand of the Younger Dryas, especially the lower parts of the high velocity zone could be explained, where increased cementation with blocky spar was observed. The upper parts of the high velocity zone seem to be caused by the neomorphosed coral framework and diagenetically altered rock in the vicinity of karstified horizons.

4.1. Introduction
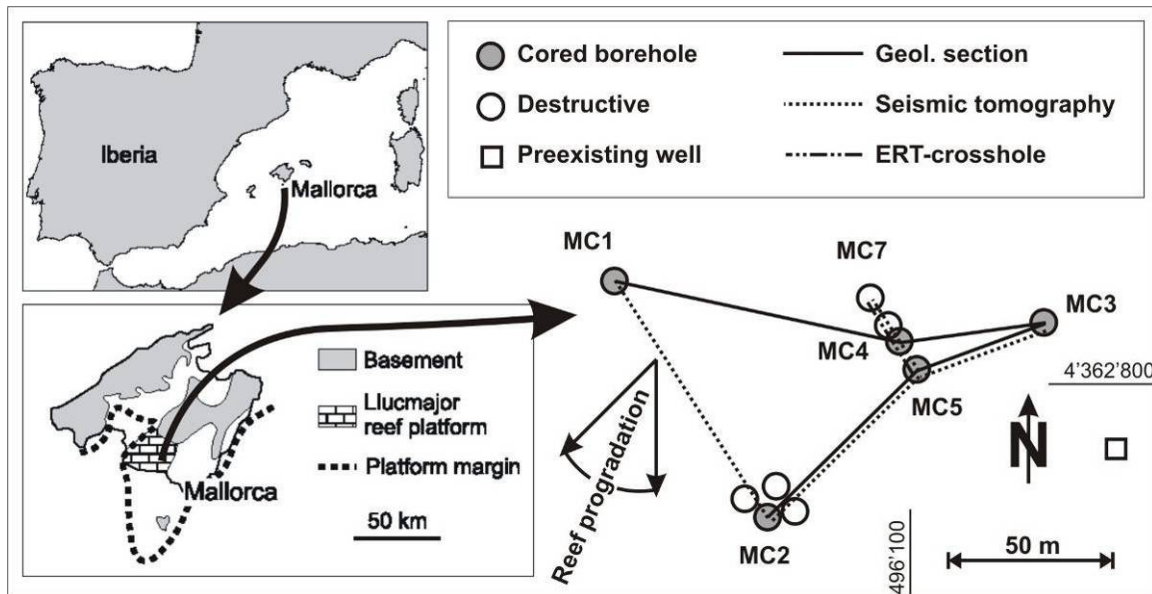
Figure 47:   The Ses Sitjoles site on the late Miocene reefal carbonate platform of Llucmajor (modified after Pomar & Ward, 1995).

In 2002, a project was initiated with EU funding, to develop diagnostic technologies for use in characterizing aquifers, suffering from salt water intrusion. The test site is situated on the Miocene Llucmajor reefal carbonate platform on the island of Mallorca (Spain). At Ses Sitjoles, near the town of Campos, on a cultivated field of 100x100 m, 5 fully cored 100 m deep boreholes (MC1-MC5) and 1 destructive borehole (MC7) were drilled, which build the main access to the subsurface for the present study (Figure 47). Matrix-scale and borehole-scale porosity structure have been described in chapters 2 and 3, which both yielded information about heterogeneity in the vertical direction. In the lateral direction some indications could be given, comparing the observations among different boreholes, however, the real geometry and lateral extension of observed features could only be assumed and was still quite speculative. Permeable features could be detected on certain horizons by impeller flowmeter logs (IFM) and a strong correlation with karstic channeling was supposed, but no information was available about their lateral extension and a correlation between boreholes, which would prove the karst system.

The present study tries to fill up this gap and thus concentrates on the crosshole- or site-scale porosity or heterogeneity, which besides cored boreholes has been accessed by single-hole and crosshole geophysics, namely electrical resisitivity tomography (ERT) and seismic tomography. The main focus is set on the distribution and interconnection of large primary or secondary pores and karst, which is termed here as tertiary porosity. Furthermore, in this chapter we want to investigate the high resistivity- and high velocity zones within the reefal complex, their evolution, lateral and vertical distribution and internal pore structure. Finally the impact of this large scale heterogeneity on the reservoir behavior will be discussed. Methods, which are capable of resolving structures between boreholes and especially structures, such as karstic channels and solution enlarged primary pores of dm-m-scale are mainly provided by crosshole geophysics. Furthermore, the multi-scalar pore structure of carbonate reservoirs is strongly controlled by depositional and post-depositional processes. The primary or depositional patterns can be studied on outcrop analogues and high resolution

sequence stratigraphy can act as a model for the site under investigation (e.g., Kerans et al., 1994).

Extensive outcrop studies have been carried out by Pomar et al. (1995; 1999; 1996) especially at the well exposed cliff coast near Cap Blanc. The studies provided detailed insight into the architectural patterns and their lateral distribution and continuity on the regional scale (km-scale). Additionally the different lithofacies types were characterized and a diagenetic history based on observations at the cliff coast and numerous boreholes widespread over the entire platform was derived. Part of the present study is based on the outcomes of the subsequent publications, with their geometrical and stratigraphical models. In order to set up a reliable geologic and genetic model of the test site, additional outcrop studies were performed with a special emphasis on the lithofacies boundaries and parameter variations within individual lithofacies types, such as cementation and porosity. Outcrop studies are powerful in tracing the lateral continuity of lithofacies boundaries and studying the architecture of the reef, with its controlling sequence boundaries. Furthermore, they are crucial for getting an understanding for the different scales of heterogeneity, which under the assumption of comparable reef genesis at the landward test site is of major importance for the interpretation of local geology.

However, the use of outcrop analogues has certain limitations, especially for predicting karst and facies variations at meter- and decameter-scale. Reefs due to their inherent architectural complexity cannot be characterized by 1D-investigation methods only (Montgomery, 1996; Montgomery et al., 1999). Furthermore, for reliable reservoir models the integration of concepts of lateral and vertical heterogeneity predicted by the karst concept is important (Mace and Hovorka, 2000; White, 2003; Worthington, 2003). In addition cave-fill seals are known to be important controls on reservoir heterogeneity, which together with the open karstic porosity can lead to significant compartmentalization of a reservoir (Kerans, 1988; Lucia, 1999). From the Llucmajor reefal platform, several intensively karstified zones have been reported in the aggrading systems tracts of the reefal complex, which developed presumably during lowstands of sea level at the water table in the reef front and in the coral patches of the lagoonal beds (Ardila and Pomar, 2000). Recent studies on the boreholes near Campos revealed certain karstified horizons at the basis of the reef core, which might be of eminent hydraulic significance for the entire reefal complex (chapter 3). In order to account for these important reservoir controls with unknown lateral extension, additional on-site investigation techniques have been applied.

Porosity models, which are based on the distribution of lithofacies types, result in a better definition of porosity, both vertically and laterally (Khalifah and Makkawi, 2002). These authors furthermore state that the seismic controlled model was the most precise, since seismic data has a much greater sample density than well data. Seismic data are routinely and effectively used to delineate the structure of a reservoir. However, there has been limited application of seismic data in the direct mapping of reservoir properties, such as porosity. Furthermore, seismic lines do not provide sufficient resolution for accurate facies interpretations on the Llucmajor platform (Pomar, 1993). One main restriction for high resolution surface seismics is the special geological configuration of the Llucmajor platform, where the shallow inner lagoon with several clay-dominated horizontal beds absorbs most of the seismic energy imposed. Thus, imaging the complex reefal structure below the capping lagoonal beds is a difficult task. On a small test site, with closely spaced 100 m deep boreholes like Ses Sitjoles, other techniques are more suitable. The crosshole-scale pore structure at Ses Sitjoles includes vertical and lateral heterogeneity due to the complex lithofacies distribution and karstification at certain levels. Such heterogeneity can be captured

by using borehole-based seismic- and geoelectric tomography. These techniques, which are not standard in reservoir characterization, provide information about the lateral heterogeneitiy in addition to wire-line logs (Friedel et al., 2004; Maurer et al., 2004). However, for the correct interpretation of the tomograms, data acquired at the rock-matrix-scale (chapter 2) and the borehole-scale (chapter 3) is indispensable.

In the present study single-hole electrical resistivity tomography proved to be very useful for delineating the zones with significant karstic channeling. Due to the axial-symmetric scale of investigation, which is 5-10 m, the lateral continuity of features observed at the borehole wall can be studied and additional heterogeneity in the vicinity of the borehole, which is not evident from the wire-line techniques only, can be detected (Friedel et al., 2004). Furthermore, for closely spaced boreholes electrical crosshole tomography provides the possibility to trace karstic horizons between boreholes. In addition to electrical resistivity tomography, seismic crosshole tomography has been applied for cross-checking data obtained by the two methods as well as for getting reliable results for larger borehole spacing (Maurer et al., 2004). Although the resolution of seismic tomography is not as high, heterogeneity, which is imaged by the resistivity tomography, can be confirmed and additional information about the relationship between the petrophysical and the geological models is provided. Seismic tomography furthermore supports the interpretation of the geological history at the test site and links the post-depositional sea level history to some anomalous findings made at the rock-matrix- and borehole-scale, which are discussed in chapters 2 and 3. The applied approach of a stepwise change from small to large scale, with the permanent cross-check through different investigation techniques, proved to be a successful approach for characterizing a complex reefal structure like the upper Miocene Llucmajor reefal platform.

4.2.   Geological setting and parameters controlling crosshole-scale heterogeneity

The investigation area lies on the upper Miocene prograding reefal platform of Llucmajor in the south-western part of the island Mallorca about 6 km landward from the well exposed cliff-coast, the so-called Cap Blanc section (Figure 47). The steep sea cliffs, which display in exquisite detail the facies architecture and the high frequency depositional sequences of the reefal unit build the western and southern margins of the platform and have been extensively described during the last 15 years (e.g., Pomar, 1993; Pomar and Ward, 1999; Pomar et al., 1996). To the east the Campos basin, which seems to have subsided only during Pleistocene time (Jenkyns et al., 1990) and to the north the Mesozoic basement of the Serra de Levante to which the platform onlaps build the boundaries. During late Tortonian and early Messinian time the platform prograded on a gentle depositional profile about 20 km towards south and south-west and shows a highly complex architecture, driven by eustatic sea level changes. Pomar & Ward (1995; 1999) described the stratigraphic and diagenetic heterogeneities of the reefal complex, mainly based on the outcrops at the cliff coast. They found the sigmoid to be the basic building block of this prograding platform, which stacks into progressively larger accretional units, reflecting hierarchical orders of glacioeustatic sea level cycles of 7th to 4th order (Pomar, 1993). Up to four systems tracts, which are related to specific parts of the sea level cycle, are described by Pomar & Ward (1999). A characteristic of the Llucmajor reefal platform is that in the aggrading systems tract (AST) no backstepping occurs. These authors defined as well a diagenetic heterogeneity, which is characterized by secondary, mostly moldic porosity and pervasive dolomitization.
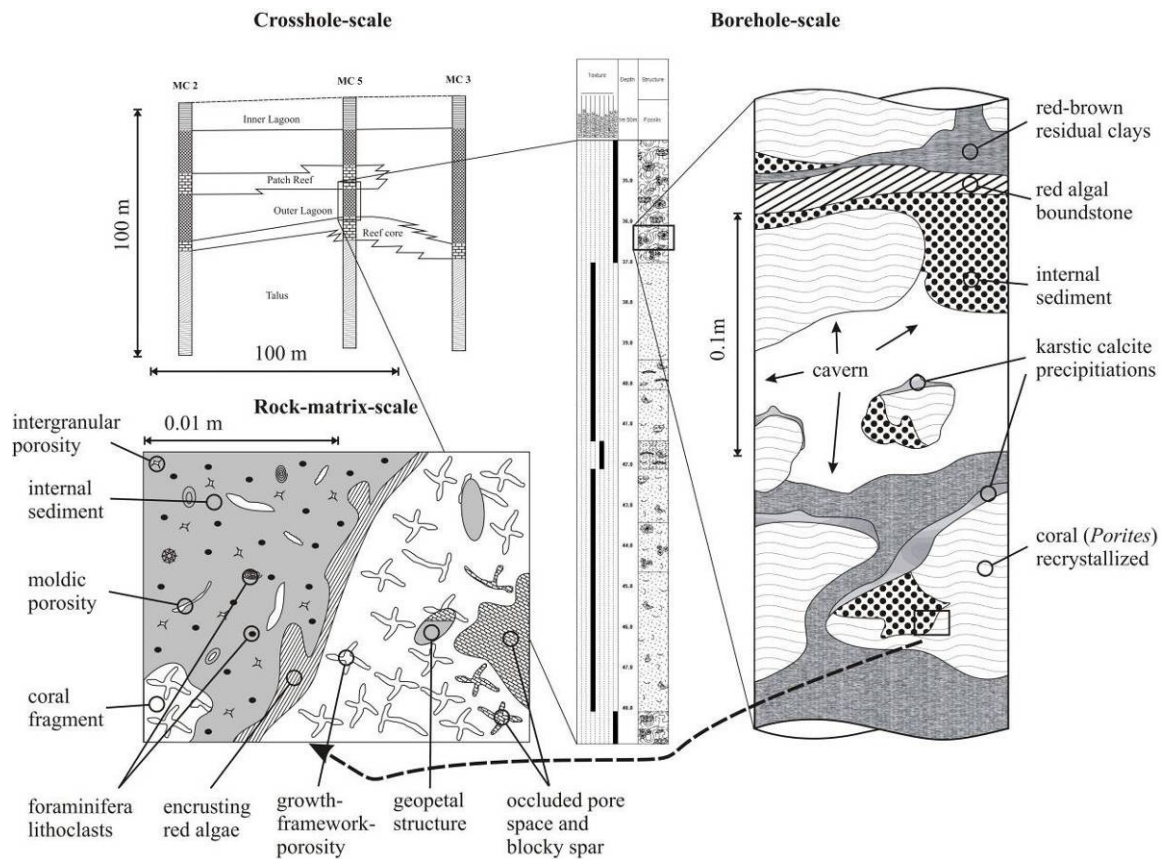
Figure 48:   Illustration of the multiscalar approach used in this study. Rock-matrix-scale and borehole-scale have been described in chapters 2 and 3.

The architectural patterns together with the five main lithofacies types inner lagoon, outer lagoon, reef core, proximal- and distal talus have been recognized as well at the landward Ses Sitjoles test site and are extensively described in chapters 2 and 3 (Figure 48). In contrast to the outcrop area, dolomitization is non-existent at the test site of the present study. The 5 fully cored boreholes with excellent core recovery allowed for a precise characterization of the rock-matrix- and borehole-scale heterogeneity. The importance of secondary porosity, mostly moldic porosity, could be confirmed and its downhole evolution and distribution was discussed. The whole reefal complex is dominated by moldic porosity, which in the upper part of the boreholes, like outer lagoon and upper talus, is characterized by large and elongated molds, which mainly are detected by the acoustic travel-time scan (ATS) (chapter 3). In the lower part of talus, moldic porosity is characterized by small and round shaped molds. The latter are the main reason for the prominent reduction in sonic porosity at the boundary proximal/distal talus, indicating a low permeability environment at high total porosity. It was found that the distribution of pore types is strongly controlled by the distribution of lithofacies types and the subsequent diagenesis. Post-depositional sea level changes with moving freshwater lenses affected the pore space of the formation significantly, leading to extensive cementation with the resulting occlusion of the pore space.

In addition to primary and secondary porosity karst, termed here as tertiary porosity, could develop and predominantly affected the lower parts of the reef core (chapter 3). Karst associated with post-depositional sea level changes led here to the most efficient large scale effective porosity of the whole reef complex. Logs run with the impeller flowmeter (IFM) have shown that not all karstic cavities are productive, since residual clays mostly occurring at the bottom of karstic cavities can act as effective seals. The adjacent parts of these openings

are strongly recrystallized, building extreme porosity contrasts in the sonic and the induction log. Unlike reported by Pomar and Ward (1999) from the cliff coast, karst-controlled reservoir heterogeneity near the test site is conspicuous and its hydraulic significance has been proven by IFM logs (chapter 3) (Van Meir et al., 2005). The investigations on the boreholes showed that post-depositional processes, which to a certain extent are controlled by the distribution of primary architectural patterns, blur the lithofacies boundaries.

At the transition reef core/proximal talus depositional- and post-depositional processes are complex. Furthermore, the present-day mixing-zone is biasing data from electrical investigation methods. In this study the mixing-zone at Ses Sitjoles is defined as the part, in which electrical conductivity of the fluid ranges from 5'000 µS/cm at 60 m to 35'000 µS/cm at about 80 m borehole depth. Based on data of the rock-matrix- and borehole-scale, a general downhole increase in porosity from 20 to about 45% was postulated at the top of proximal talus. This increase is most probably related to the special depositional and diagenetic environment at the zone, where reef core interfingers with proximal talus and has nothing to do with the present-day mixing-zone. Furthermore, exclusively at borehole MC5 most probably the diagenetic overprint of a paleo-water-level has blurred the lithofacies boundary additionally (chapter3). Thus, not all lithofacies types are sharply bound and the geological and the petrophysical model do not overlap at every location within the reefal complex.

In chapter 3 the importance of sequence boundaries as hydraulic barriers was demonstrated indirectly. In outer lagoon and proximal talus several inflow zones recorded by the IFM are related to sequence boundaries, which can act directly as a seal or which facilitate vuggy zones in the adjacent host rock. Thus, in addition to the constraining of the lateral facies distribution and defining systems tracts, the sequence stratigraphical model is directly of importance for inter-well heterogeneity and the hydraulic behavior of the reservoir.

4.3.   Methods

4.3.1.   Sequence stratigraphy based on outcrop analogues and cored boreholes

Core description of the five fully cored boreholes (chapter 3) led to the construction of two geological cross-sections, a dip-section MC2-5-3, which is parallel to the direction of reef-progradation and a strike-section MC1-4-3, which is parallel to the reef tracts (Figure 47). Sequence stratigraphical concepts were derived from the outcrops at the well exposed cliff-coast near Cap Blanc and yielded the main understanding concerning size-relations among individual architectural elements, shape and development of the architectural elements and the lateral continuity of sequence boundaries and systems tracts. In Pomar & Ward (1995) diagnostic criteria are discussed for the construction of a sequence stratigraphical model from boreholes only. Diagnostic features for aggradation, progradation or offlap patterns are the elevation of the facies tops, the reef core thickness, the upward or downward shifts of reef cores and if possible the reef core internal succession and the thickness of the existing coral-morphology zones. This coral zonation theoretically would allow for the reconstruction of paleo-water-depths. However, coral bathymetry based on core material without lateral control is problematic and thus has not been performed in the present study. Pomar & Ward (1999) have shown that outcrop analogues provide important geometrical information for the interpretation of sequence stratigraphy and lithofacies distribution and help in tracing chronostratigraphic boundaries between individual boreholes.

For the exact identification of lithofacies- and sequence boundaries, several wireline logs have been used (chapter 3). The most important log was the natural gamma log, which marked erosional horizons by pronounced excursions. However, correlation of gamma log signals between individual boreholes was difficult, since the signals did not preserve the shape of their amplitude over larger distance, except for the clayey and marly beds of the inner lagoon. Furthermore, optical televiewer, induction- and sonic log provided information about lithological or petrophysical boundaries. On core material some of the most important diagnostic features are wackestones to mudstones, color changes to grey or red stained rock, abrupt changes in cementation, distinct horizons of vuggy porosity and total lack of macroscopic biota. Further diagnostic features are given in Manfrino & Ginsberg (2001) and to a large extent could be used for the identification of sequence boundaries at the test site near Campos. Furthermore, distinct sea level changes could be identified in the sedimentary record by changes of the textural composition. Kenter et al. (2001) reported from the fore reef slope bioclastic packstones and grainstones as indicative for sea level lowstands and exposed platform top. Peloidal, bioclastic packstones and grainstones on the other hand are indicative for sea level highstands and flooded platform top. Nevertheless, especially erosional surfaces on top of the reef core lithofacies as well as downlap surfaces are difficult to recognize on core material only.

4.3.2.   Single- and crosshole electrical resistivity tomography

Data acquisition and processing are discussed in Friedel et al. (2004) and thus will be introduced here only briefly. Data were acquired with a string of 50x1 m spaced electrodes, whereby the uppermost electrode was placed roughly at the sea level 40 m below surface. Measurements with 0.5 m spaced electrodes yielded similar results. Data were recorded with Wenner, Schlumberger and dipole-dipole configurations. The standard resistivity inversion software *RES2DINV* was used for delineating the resistivity structure around the boreholes. Tsourlos et al. (2003) state that compared to traditional borehole logging tools, such geoelectrical single-hole tomography may offer several advantages: The resistivities obtained are more reliable, since they are constraint by more data and furthermore by considering electrode configurations with large separations, greater lateral penetration is obtained. For the single-hole tomography axial symmetry around the borehole is assumed, in which only two spatial coordinates are involved for both the resistivity model and the source. Crosshole tomogram data presented in this study has been recorded using crosshole configurations with potential- and current-electrode in one borehole, which yield larger amplitudes.

With ERT voltages are measured under a well defined geometrical setup. The recorded values are a function of formation resistivity and geometry. Formation resistivity is dependent on fluid resistivity, total porosity and its connectivity, mineralogy, cementation and the texture of the rock. The numerical inversion algorithm calculates one possible true resistivity distribution of the subsurface. In order not to fit any noise, the iterations go on, till the misfit is equal to the RMS. With a fluid conductivity log and a rough estimate of the cementation factor m, porosity trends can be calculated by using Archie's equation. In this study a constant cementation factor m=2.0 was used, which is a sufficiently accurate estimate, for evaluating relative porosity distribution.

The resolution of the method is dependent on the chosen cell size, which is either 0.5 m or 1 m. For single-hole as well as for crosshole ERT the two cell sizes yielded similar results. However, the accuracy of images with larger cells is higher, due to averages over a larger

volume. Furthermore, close to the electrodes accuracy is higher, than further away. Generally for cases, where the borehole spacing is larger than half of the borehole length, the subsurface cannot be imaged accurately anymore by crosshole ERT. In zones where the mesh was chosen too fine or data was incompatible, comb-like artifacts may be present. Further artifacts, which are due to the tube, may occur in the vicinity of the borehole, however, else the data quality is excellent and the mismatch of the inversion with 6-15% low. Within proximal talus high resistivity-gradients of the mixing-zone dominate, which has to be considered when interpreting the resistivity distribution there.

With single-hole ERT the cavities, which are recognizable along the borehole can be traced into the formation. The main aim is to prove the karstic origin of features observed at the borehole, by tracing them laterally into the formation and to separate elongated and interconnected large scale tertiary porosity from isolated secondary or primary features, such as leached out corals and dm-m-scale primary pores. A further target is to check the lateral continuity of resistivity anomalies, such as low resistivity zones (LRZ) and high resistivity zones (HRZ). For single-hole data, displayed heterogeneity ranges from several dm to about 5-10 m (Figure 49). The recorded heterogeneity comprises dm-m-scale pores of primary, secondary and tertiary origin and contrasts in matrix-porosity and differences in cementation, e.g., between individual lithofacies types.

Crosshole ERT in addition to single-hole ERT provides the possibility to trace karst laterally between closely spaced boreholes. In the present study the main aim of crosshole ERT is the correlation of LRZ's, such as karstic features and HRZ's, such as recrystallized rock of low porosity between boreholes in order to verify, whether there is an interconnected channel network or not. With the crosshole data, heterogeneities ranging from meters to several tens of meters can be investigated (Figure 49). These heterogeneities comprise predominantly the distribution of HRZ's and LRZ's.
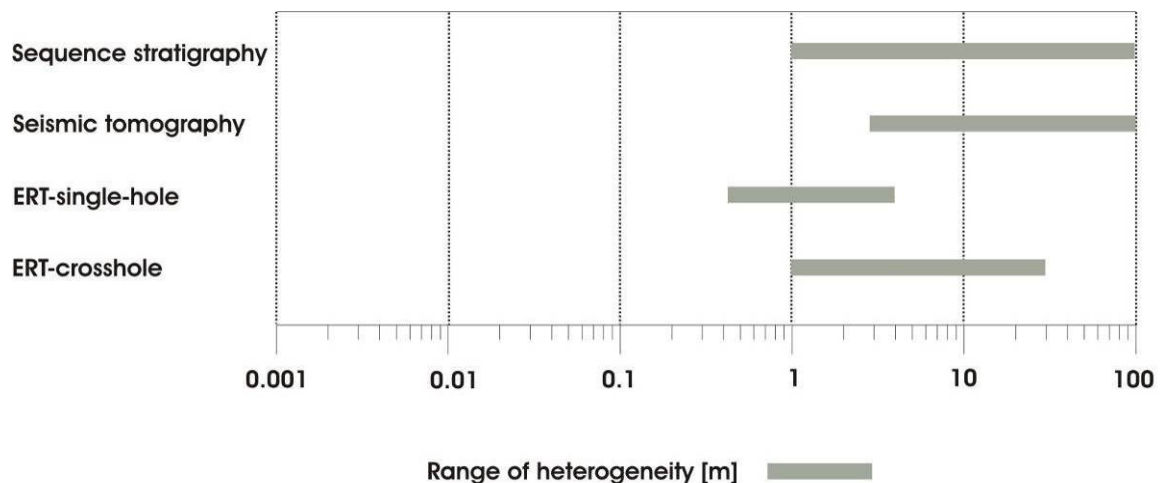
Figure 49:   Investigation techniques and their range of heterogeneity, which can be recorded.

4.3.3.   Seimic crosshole tomography

The tomographic planes were recorded with a high-frequency sparker source and a hydrophone streamer. The upper source and receiver positions were placed at sea level and the lower positions were located at about 90 m with a constant spacing of 1 m. The exact position of each transmitter and receiver has been calculated by using borehole geometry data.

The elastic waves travel through the medium and receivers record the whole waveforms from which the first arrival of the p-wave is picked in a semiautomatic manner. The tomographic planes were subdivided into quadratic cells of 1.5 m side length. Tomographic inversions of the travel-times were performed using a non-linear inversion algorithm, with initial values of 2500 m/s. The colormaps of the tomograms have been set in such a manner, that the range between 2400 m/s and 3000 m/s is finely graded, since there obviously the most remarkable structural elements are present. For more information about data acquisition, processing and preliminary results, the reader is referred to Maurer et al. (2004).

P-wave velocity is a function of the elastic rock properties and the density. Important geological factors, which affect the velocity are cementation, recrystallization, primary porosity and pore structure. From sonic logs it is known, that V_P is strongly affected by the pore type and secondary porosity with a framework-like fabric is generally underestimated (Anselmetti and Eberli, 1999; Hearst et al., 2000). The empirical equation of Wyllie, which relates porosity to measured V_P, velocity of rock and fluid, thus is of limited use, if variations of rock properties are considerable. With seismic tomography high- and low velocity heterogeneities ranging from a few meters up to 100 m can be investigated (Figure 49).

The resolution of the method is dependent on the maximal frequency and the geometry of the setup. The resulting resolution is in the order of 2-3 m. Crosshole seismic tomography allows for the detection of high- or low velocity heterogeneities between largely spaced boreholes, however, due to the dominant seismic wavelengths of 4-6 m, the seismic velocity-depth functions are relatively smooth, representing average values over quite large volumes around the boreholes. In general high-velocity heterogeneity is recorded more accurately than low-velocity heterogeneity, which is rather overestimated. For a reliable interpretation of the data as well the restrictions of this method have to be addressed. Due to poor ray coverage at the edges of the tomograms, the resolution is lower than for the rest of the images. In zones of high absorption, the signal is attenuated and the resulting loss in data leads to a lower resolution. Hyperbolic stripes are multiples due to attenuation and persist, if the smoothing of the tomograms is not chosen too high.

The main aim of seismic crosshole tomography is to highlight and to study the distribution of high velocity and low velocity heterogeneity between boreholes with considerable spacing. Due to the large scale of investigation and a resolution, which is lower than for ERT, karstic cavities in most cases cannot be imaged directly. High velocity zones (HVZ) are mostly highly cemented, recrystallized and of low porosity at the rock-matrix-scale. A further target is the detection of changes in the porosity structure, within and between individual lithofacies types.
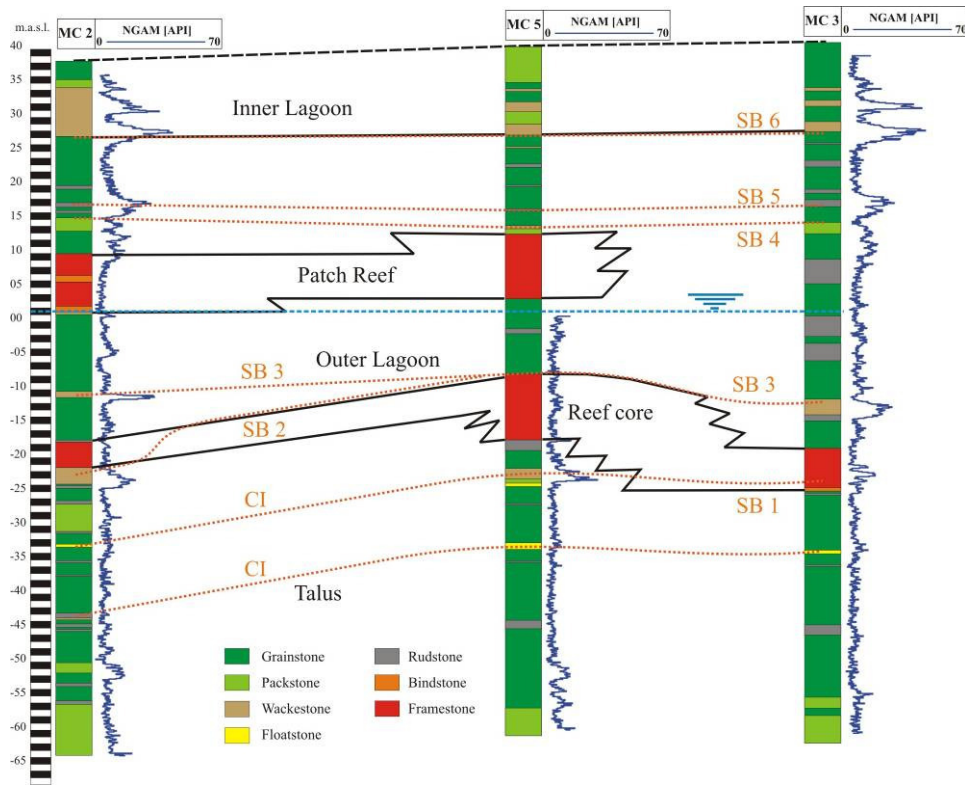
Figure 50:   Dip-section of the geological situation at the test site, constraint by sequence stratigraphy, which is based on geological description, natural gamma and other wireline logs. CI=condensed interval, SB=sequence boundary (trace of section see Figure 47)
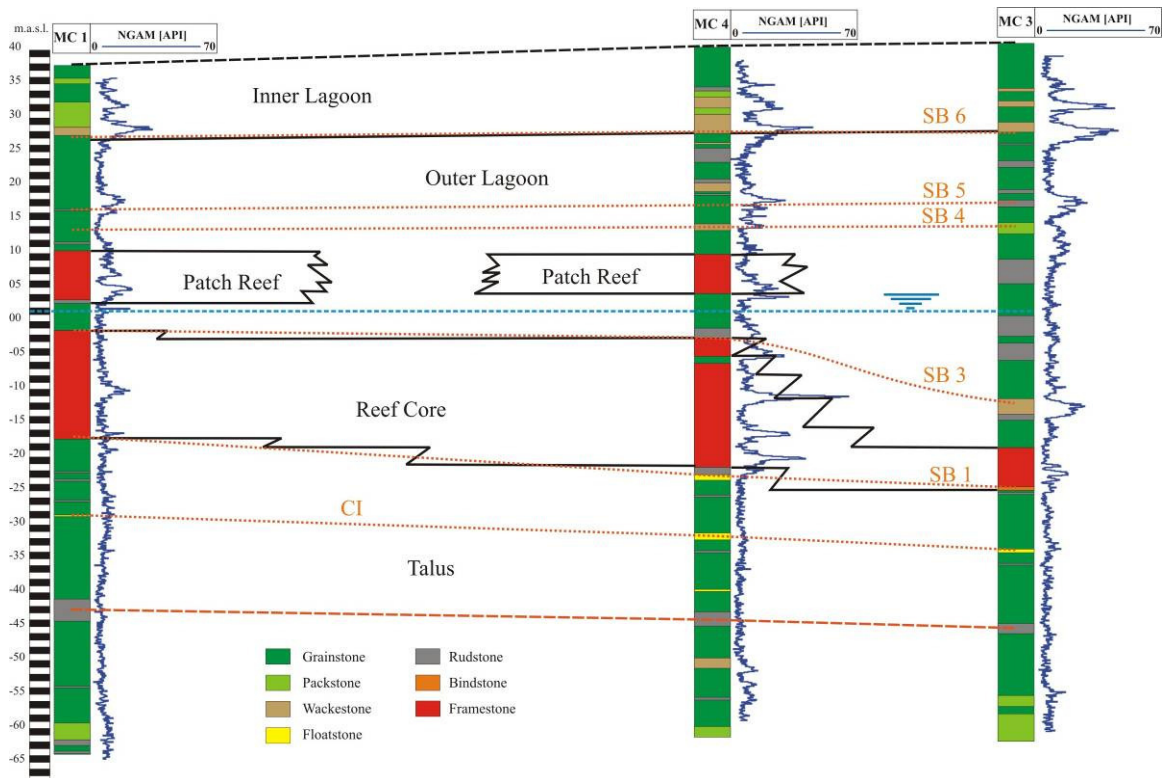
Figure 51:   Strike-section of the geological situation at the test site constraint by sequence stratigraphy, which is based on geological description, natural gamma and other wireline logs. CI=condensed interval, SB=sequence boundary (trace of section see Figure 47)

4.4. Results and interpretation

4.4.1. Geology and sequence stratigraphy of the test site

The potential direction of reef-progradation was inferred from the reef tract progradation-map of the platform (Pomar and Ward, 1995) and points towards the south or southwest. The observations made on core material and wireline logs will be presented below, together with a brief interpretation of the depositional history of the reefal complex at the test site near Campos (see Figure 50 and Figure 51):

In the lowermost part of the reefal complex very fine grained sediments of distal talus are present, which mark the basin-ward continuation of a prograding talus. Within distal talus mud-dominated packstones to grainstones are present, illustrated by the natural gamma log, which towards the bottom yields gradually higher recordings. In distal talus beds normally are dipping with less than 10°, however, the bedding barely is recognizable due to extensive burrowing. It is known, that burrowing can destroy depositional anisotropy, however, new secondary anisotropy can be built, since burrowing is enhancing both grain size and sorting (e.g., Anderson et al., 1994). On top of distal talus a prominent recrystallized rudstone is present, which due to the large and elongated moldic pores is much more permeable than the underlying sediments. It builds already the bottom of the proximal talus, which is steeply bedded, more heterogeneous than distal talus and containing large and elongated moldic pores. The basal rudstone is present in all 5 cored boreholes and thus builds a well constraint boundary. It is the first coarse grained storm-induced deposit of the prograding reef onto the deeper platform.

Furthermore, rhodolithic floatstones occur, marking basin-ward condensed intervals (CI). The condensed interval corresponds to high stand systems tract (HST), offlapping systems tract (OST) and low-stand systems tract (LST) and the landward equivalent of the top of the distally condensed interval is an erosional surface (Pomar and Ward, 1995). Two main condensed intervals could be found of which the lower one is not merging into a landward sequence boundary within the perimeter of the present study, indicating that it belongs to an older off-lapping part of the reef, which is located more landwards. Along the strike-section MC1-4-3 (Figure 51) it can be correlated more or less horizontally between the boreholes and at the dip-section MC2-5-3 (Figure 50) it plunges towards the basin at MC2. The rhodolithic floatstones are composed of red-algal concretions in a wackestone-matrix. The upper condensed interval merges at MC5 into a sequence boundary SB1, which can be traced as well in the strike-section, right at the bottom of the reef. Near MC3 the corresponding LST is present and marks the first reefal entry within the perimeter of the present study. Reef core here is lying at a low relative position and with only 6 m thickness it is rather thin.

After the erosional event of SB1 the reef core aggraded at least 15 to 20 m, building thick outer lagoon deposits at MC3 and as well thick talus deposits between MC5 and MC2. The talus is composed of several clinobeds, which coarsen upwards, are getting less steep towards the basin and which are thinning-out towards distal parts. Variography at borehole-scale porosity (>1 cm) was assessed by the ATS-technique and revealed changing thickness of the clinobeds from MC3 with 2 m over MC5 with 1.8-1.9 m to MC2 with 1.2-1.4 m, indicating the progradation of the reef towards MC2 (chapter 3). The evaluated thickness of the clinobeds could be confirmed by outcrop-observations at the strike-section of Cap Blanc. Thick reef core is present in boreholes MC1 with 16 m, MC4 with 19 m and MC5 with 11 m, which are all part of the AST, marking here a high-order sea level maximum. The

predominant coral genera *Porites* and *Tarbellastraea*, originally built of the metastable aragonite, have been replaced by calcite or secondary moldic porosity developed by their complete dissolution. Internal sediment originating from outer lagoon, locally filled up the space between individual coral colonies. In addition to the sea level driven morphology of the reef core, spurs and grooves are abundant. These channels provided a direct connection of the outer lagoon with the open sea. They are filled with internal sediment, part of the reef core and developed through tidal currents, which were present behind the barrier reefs.

Especially the bottom of the reef core is karstified and dm-m-scale cavities are abundant. However, at least some of these cavities may belong to primary porosity, rather than tertiary porosity. The framestones are commonly well cemented and recrystallized. In certain zones, especially near karst-cavities, the coral framework-porosity can be almost totally occluded by blocky spar. Good hints for karstification are red-brown residual clays, commonly occurring at the bottom of such cavities (chapter 3). From the Cap Blanc area karst has been reported in the AST of the reefal complex, which developed presumably during lowstands of sea level at the water table in the reef front and the coral patches of the lagoonal beds (Ardila and Pomar, 2000). Basin-wards the reef core interfingers with skeletal and intraclastic grainstones to rudstones of the proximal talus. During storm events non-cemented sediment was shed off the reef crest and the outer lagoon, which led to highly anisotropic and steeply bedded (10-30°) deposits in the proximal talus. These deposits consist of a succession of lenticular rudstone layers within a grainstone background. At a sea level lowstand main sediment influx was skeletal material, which was scoured by contour currents. At a sea level high stand, peloidal sands from the platform interior were shed downslope, as observed as well on the Great Bahama Bank (Kenter et al., 2001). Coral rubble with boulders up to dm-size, sporadically occurring single corals in living position and thin layers of rhodolithic floatstones are typical for this lithofacies type.

After a sea level highstand, which again initiated the development of a condensed interval, located basin-wards outside the perimeter of the present study, the sea level dropped and the reef core off-lapped towards MC2. The OST is characterized by thin prograding and downstepping reef core and only minor deposition in the talus. The corresponding erosional surface SB2 removed some parts of the reef core and the outer lagoon behind the stack. This erosional surface can only be traced till borehole MC5 since behind, it later on was removed by a younger erosional event. The reef core at MC2 is most probably still part of the OST, which is indicated by the low relative position of the reef core and the small thickness of only 4 m. Outside of the perimeter, another sea level rise led to aggradation and a transgression of lagoonal sediments onto the eroded reef core and outer lagoon. The subsequent sea level fall led to a further sequence boundary SB3, which at MC2 and MC3 is marked by a prominent excursion on the gamma log, however, not at MC5 where it coincides with the lithofacies boundary outer lagoon/reef core. This erosional event again removed big parts of the geological archive and minor remnants of the former AST are only present in the outer lagoon between MC2 and MC5 on top of the reef core.

Afterwards most probably a lower order sea level rise led to extensive aggradation in all depositional systems, which is expressed on the test site by thick lagoonal deposits. Unlike observed at the outcrop-analogues near Cap Blanc, here a patch reef configuration is postulated for the outer lagoon, deduced mainly from the distribution and thickness of coral framestones and the occurrence of erosional horizons. In four of five cored drillings two main zones of coral framestones have been found on top of each other, separated by bioclastic grainstones to rudstones of the outer lagoon (chapters 2 and 3). At borehole MC3 no patch reef was found, however, the presence of coarse grained material, such as rudstones full of

reef rubble and fragmented bivalves and gastropods is as well a hint for coral build-ups located nearby, which were able to grow above wave base level and thus produced large amounts of coarse grained reef-rubble. Patch reefs, which build a subfacies within the lagoonal deposits, are difficult to recognize from borehole data only, since they exhibit a complex topography and lateral distribution. Like observed for reef core, coral colonies are separated from each other by internal sediment. Furthermore, at Ses Sitjoles they are located above the present-day water level, which prevents the use of most logging tools. Observed thickness ranges from 6 m in MC4 to 9.5 m in MC5. Patch reefs consist of coral framestones, are intensively bored by bivalves like *Lithophaga*, gastropods, boring sponges like *Cliona* and encrusting biota like red-algal bindstones are typical (Figure 48). Comparable to reef core, some of the corals are leached and large primary pores are present, which both can be karstified. However, karst is much less pronounced than in the underlying reef core.

Outer lagoon consists mainly of horizontal layers of intensively burrowed bioclastic or peloidal grainstones and rudstones with a non-restricted biota. Outer lagoon sediments are mostly deposited in a low energy and shallow water environment, which is protected from the open sea by the reefal barrier, but channels cutting through the reef allow sediment to be transported to the fore reef environment. Furthermore, bioclastic grainstones and rudstones from the outer lagoon act as internal sediment between the massive coral build-ups of the reef core. The predominant pore type is moldic porosity, which is fabric-selective and a type of separate vugs, which is only interconnected through the intergranular pore space (Lucia, 1999). It originated from the dissolution of aragonitic constituents like bivalves, gastropods, and coral-fragments. Due to cyclic sea level changes, lots of erosional surfaces are abundant, marked either by bioclastic packstones to grainstones at the bottom and peloidal grainstones to rudstones at the top or red algal wackestones. These sequence boundaries mark high frequency regression- and transgression-cycles. On top of the patch reef, which is highest at MC5, two erosional surfaces SB4 and SB5 are present. The grainstones to rudstones above could be due to a 5th order sea level cycle, however, many sequence boundaries are present above the patch reef and only a minor number can be correlated between the 5 boreholes.

A remarkable erosional surface SB6 builds the sharp and very planar upper boundary of the reefal unit. Above SB6 large excursions of the gamma logs mark a completely different depositional environment. The reefal unit is capped directly by an alternating succession of grainstones to packstones with marly packstones to wackestones and layers of sandy clays. The latter are more abundant towards the bottom of this lithofacies type, where sporadically as well bentonites of volcanic ashes are present. In the middle and upper part mangrove roots with a restricted marine fauna as well as blackened grains and caliche hardpans are abundant. The dm- to m-thick layers are flatly bedded and a correlation is possible through all 5 boreholes. This lithofacies type is interpreted as inner lagoon with typical restricted biota and intermittent continental influence. The continuity and horizontal bedding infer that this succession is occurring over an area, much larger than the site-perimeter of the present study. The correlation with the inner lagoon-facies described at the Cap Blanc section is plausible, however, stromatolites above the mangrove-root layer could not be found at Ses Sitjoles.

4.4.2.   Single-hole ERT

ERT is available as single-hole data for boreholes MC3, MC4 and MC5. Data are displayed from the water level at 40 m depth down to 75 m (Figure 52). Additionally for boreholes MC3 and MC5, ERT-tomograms have been recalculated into images of the porosity distribution. The dm-m-scale pores in the saturated zone exhibit low resistivitiy of 1-10 Ohm m and thus

they build pronounced contrasts to the 100-300 Ohm m of recrystallized rock, with low matrix-porosity (Table 5). Grainstones of outer lagoon and the internal sediment of the reef core both yield values in the intermediate range of 10-100 Ohm m.

On the single-hole tomograms planar resistivity boundaries, which extend laterally into the formation are mainly recognized within reef core lithofacies, however, as well isolated low resistivity anomalies occur there. Karst preferably developed within reef core, where a high internal heterogeneity, such as dm-m-scale primary and secondary pores within recrystallized coral framestones and moderately cemented internal sediment built the basis for extensive dissolution. As the single-hole tomograms show, major cavities in most cases extend laterally into the formation. Furthermore, in chapter 3 measurements with IFM yielded permeable features at most of these karstic cavities, like observed in borehole MC4 for all 3 LRZ's within reef core or LRZ D at MC5 (Figure 52). Here resistivity ranges between 1 and 10 Ohm m and an excellent lateral continuity was recorded. Since the single-hole tomogram exhibits cylindrical symmetry, the heterogeneity of low resistivity can only be localized in the vertical but not radial direction. The sharp boundaries and the uniform resistivity, which is not interrupted by higher values, suggest the existence of an interconnected channel network on these horizons. A further indication about the existence of interconnected channel networks, which are located within several horizontal planes, is given by the fact that not for all continuous low resistivity zones at the boreholes large karstic cavities could be observed. Zone D at MC5 for instance is not marked by a pronounced karstic cavity but leached corals occur there and as the IFM-data suggests seem to be connected to the channels, which are close nearby.
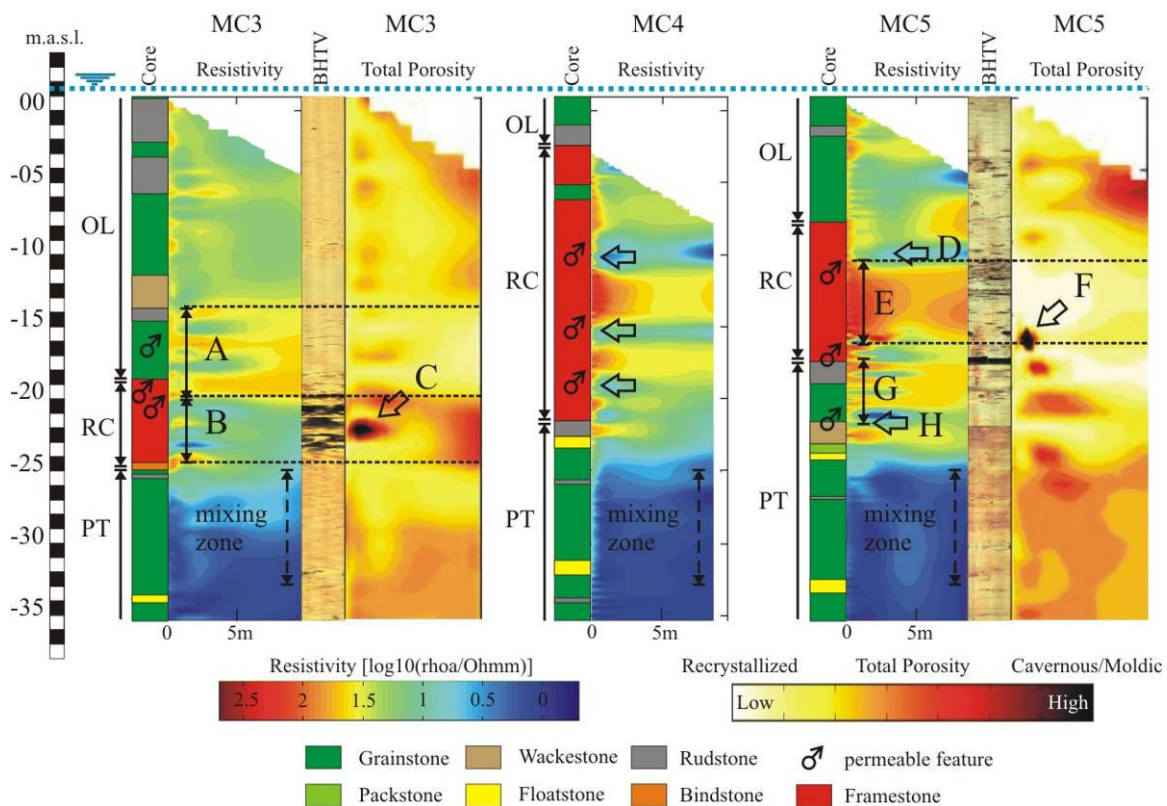
Figure 52:   Single-hole ERT of boreholes MC3, MC4 and MC5 with comparison to optical BHTV and permeable features from impeller flowmeter. ERT-images are axial-symmetric and the origin is on the left side. For discussion of zones (A-H) see text.

	Cavities dm-m-scale	Grainstones of OL/internal sediment	Rock of low matrix porosity
Geological characterization	Open cavities, interconnected, locally occluded with residual clays	Intergranular and moldic porosity, cementation rather low	Recrystallization by neomorphism, blocky spar cementation
Processes	Karst development (tertiary porosity)	Primary and secondary porosity	Secondary reduction of porosity
ERT [Ohm m]	1-10	10-100	100-300
Seismic tomography [m/s]	-	2600	>3000

Table 5:   Typical values for resistivity and velocity, recorded at Ses Sitjoles and their geological characterization and the controlling processes.

Residual clays can be important controls on the hydraulics of tertiary porosity (Kerans, 1988). Zone B at MC3 lies within intensively karstified reef core with cavities up to 1 m height. In chapter 3 it could be shown that permeable features occur only in the upper part of this zone, since below thick residual clays occlude most of the pore space. Here the calculation of porosity from formation and fluid resistivity yields additional information about large scale heterogeneity. The lower part of the karstified zone B is occluded by clays but here isolated cavities (C), which could not be detected at the borehole occur. The porosity-image shows a continuous zone of high porosity at the top of zone B, which is consistent with two permeable features detected with IFM there.

We use lateral continuity of LRZ's for proving interconnected karstic pore networks and have seen that as well isolated high porosity anomalies can be associated with karst, if residual clays are abundant. Further isolated high porosity anomalies are recorded in MC5, among which heterogeneity F at the bottom of the highly resistive zone E is the most prominent one. Here no lateral continuity is present and F although located quite close to the boreholes is not recognized by the IFM as a permeable feature. At the bottom of zone E leached corals have been detected as part of a recrystallized coral framework, which furthermore was affected by blocky spar cements. From the coast near Cap Blanc dm-m-scale primary pores have been reported (Pomar et al., 1996) and are likely to occur as well at Ses Sitjoles, however, are difficult to recognize on boreholes. Thus, within reef core, isolated features on the tomograms or the recalculated porosity image in most cases might be of primary or secondary origin but as feature C at MC3 has shown, tertiary processes, such as occlusion with clays can lead as well to isolated anomalies. Despite the various possibilities for their genetic origin, isolated low resistivity anomalies in contrast to horizontal and continuous ones never could be detected by the IFM.

HRZ's are mainly located within reef core and usually close to the low resistivity heterogeneities. Especially if bound by karstic horizons, they extend continuously in the horizontal direction. As observations on core material have shown, high resistivities of 100-300 Ohm m are typically caused by a recrystallized, well cemented rock matrix, in which a significant amount of the primary pore space is occluded by blocky spar. The occurrence of karstic horizons, together with their bounding HRZ's suggests a correlation. As mentioned, karst developed preferably within the highly heterogeneous reef core, which is mostly recrystallized and well cemented. Karstic systems are characterized not only by massive dissolution but also precipitation processes occur, which in highly porous young unburied rock, like on the Llucmajor platform, have major impact on the primary and secondary pore structure. At the rock-matrix-scale occlusion of the intergranular pore space with blocky spar was observed mainly within internal sediment, located close to karstic cavities (chapter 2).

Within the karstified reef core of MC3 recrystallized horizons have been observed on core material and wireline logs (chapter 3), but no pronounced HRZ is recorded by ERT. The reason for this discrepancy is caused by the low resolution of the method, which is not capable to resolve layers with a thickness of a few dm only. Furthermore, clays with their low resistivity have a significant impact on the resistivity-signal of the formation.

Sequence boundaries are important low porosity zones within the reefal unit. Their impact on the resistivity structure of the reefal complex is proven by intermediate resistivities of 10-100 Ohm m within grainstones of outer lagoon at zone A in MC3 and proximal talus at zone G in MC5. These zones are sandwiched in both cases between sequence boundary and reef core. The rock at these locations is well cemented and parts of the pore space are occluded with blocky spar. Permeable features have been recorded either at open fractures (A) or within vuggy zones on top of the sequence boundary (H). Vuggy zone and sequence boundary both are laterally continuous as shown on the porosity image. Higher fluid activity, which led to the occlusion of the rock-matrix-scale pore space and permeable features like solution enlarged fractures and vuggy zones, are indirect hints for the sealing potential of the sequence boundaries.

4.4.3.   Crosshole ERT

Crosshole ERT is available for the composite section MC5-4-7. The electrode-string extends from sea level at 40 m depth till 90 m for boreholes MC4 and MC5 and from 40-65 m for borehole MC7 (Figure 53).

Close to the borehole the same resistivity distribution as observed on single-hole ERT is recorded, but further away crosshole ERT provides a much better image about the distribution of low and high resistivity heterogeneity. Crosshole ERT unambiguous shows the lateral continuity of low and high resistivity zones, which can be correlated between the boreholes. Obviously processes, which control the distribution of resistivity, occurred rather in the horizontal direction than in the vertical one.

On the crosshole tomogram with 0.5 m cell-width, zones of high resisitvity can be identified especially within reef core between A and B and below the reef core between B and C. A, B and C mark zones of low resistivity, which at the intersection with the boreholes excellently correspond to inflows recorded by the IFM log (chapter 3). If the cell size is increased to 1 m side-length, the layered character of the zone between MC5 and MC4 is seen even better. Out of the three main permeable layers at least the two upper ones A and B suggest karst horizons, with a good lateral continuity of the LRZ. The karstic character is proven by observations on core material, which revealed dm-scale cavities, partly filled with residual clays and the development of speleothems. The lateral resistivity changes within the LRZ's could be artifacts due to low accuracy further away from the borehole or illustrate the channeling within the karstified horizon, which does not follow the shortest distance between two boreholes. It has to be mentioned that the displayed 2D-representation comprises data from the 3D-space consequently as well certain side effects have to be considered. However, despite these uncertainties, at both levels A and B, permeable features of individual boreholes are located within the same horizontal plane and the channeling character can be observed directly on optical BHTV-images. A channeling thus is present, which interconnects larger primary and secondary pores. These pores are unevenly distributed on the karstified horizon and consequently the real traces of the channels in the horizontal plane are unknown.

The comparison to single-hole ERT and BHTV-images at MC5 reveals that A corresponds to inconspicuous leached corals within a slightly karstified part of the reefal framestone, B builds a larger open cavity with significant lateral extent and C is a vuggy zone above a less permeable sequence boundary. At borehole MC4 the corresponding permeable features on core material are recognized as karstic horizons. Thus, the character of corresponding permeable features can change significantly. It has been mentioned, that at these levels dm-m-scale primary pores are interconnected through tertiary porosity. Thus, depending on where the borehole hits such a horizon, primary, secondary or tertiary porosity is present, being part of the same interconnected network. The vuggy zone above the sequence boundary grades into a karstic cavity at the reef core in MC4. Within the heterogeneous reef core the sequence boundary cannot be traced anymore but in the grainstones to rudstones below, it proves its sealing potential, which lead to the permeable zone C. The development of vuggy zones, which are related to the sealing potential of sequence boundaries, is a well documented phenomenon (Manfrino and Ginsberg, 2001).
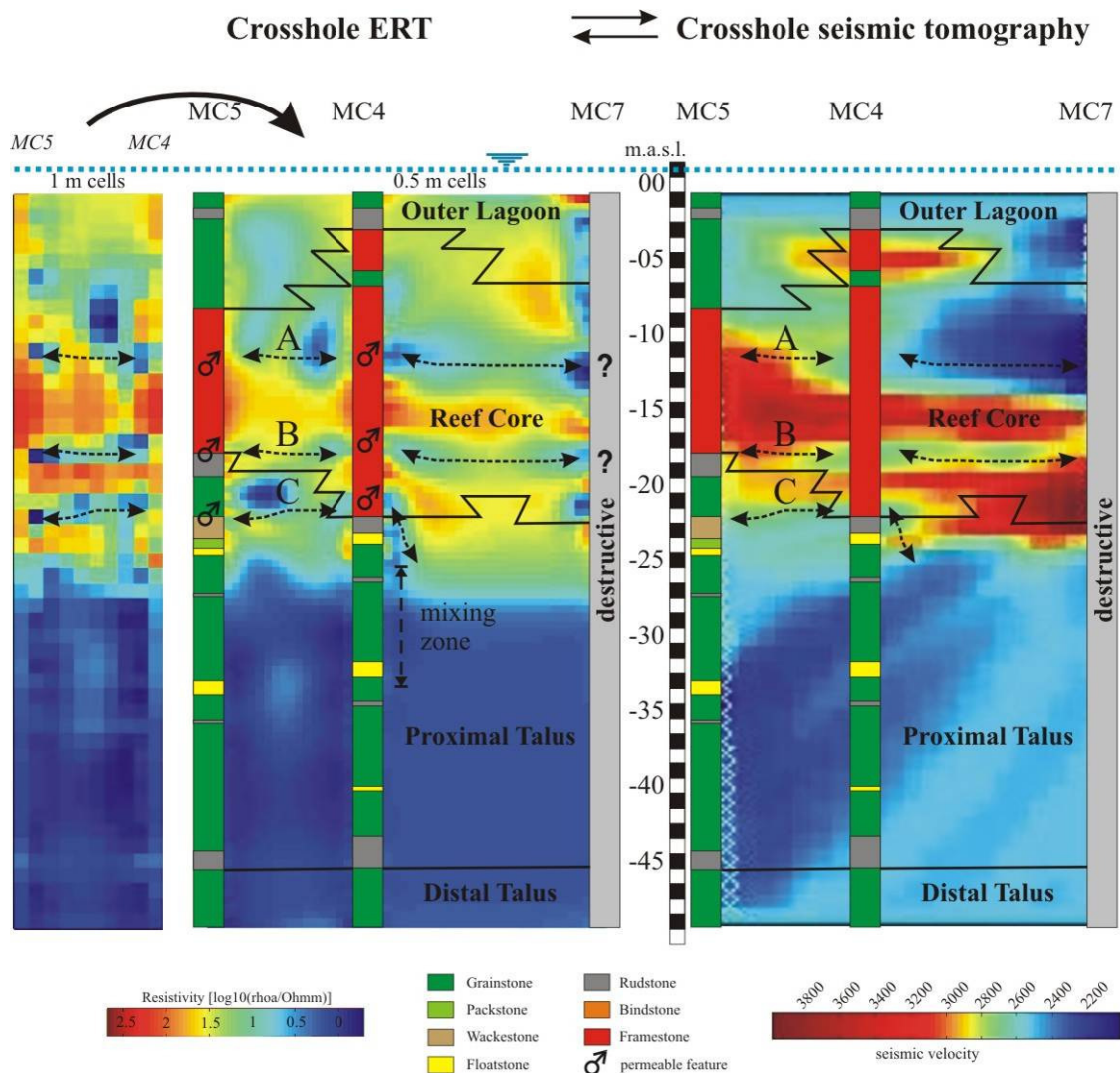
Figure 53:   Crosshole ERT for section MC5-4-7 with 0.5 m cell size and section MC5-4 with 1 m cell size on the left side. Dashed arrows are indicating possible flow paths. On the right side the crosshole seismic tomogram of the same section is given.

The crosshole tomograms show, that karst is developed along horizontal planes and thus as well the modification of porosity in the adjacent rock took place rather in a lateral than in a vertical sense. The shape and extension of highly resistive zones are thus only to a limited extent controlled by the original distribution of primary sedimentary fabrics. This statement is furthermore supported by the mismatch between lithofacies boundaries and resistivity boundaries. Highest resistivities are mainly limited to reef core but not exclusively and low values occur as well, without evidence for karst-influence. The similarity of internal sediment with grainstones of outer lagoon is the main reason for the mismatch in the upper reef core. Enhanced cementation and occlusion of the rock-matrix-scale pore space, which as well affects the upper talus, causes fuzzy transitions in the lower part of the reef core. Consequently lithofacies boundaries cannot be recognized on ERT's.

The layering, which could be detected by the crosshole tomograms, is real as has been proven by core material and wireline logs. The high resistivity contrasts observed at several levels in the reef core display the complexity of the distribution of large scale primary and secondary porosity, which acted as a nucleus for karstic processes at certain levels. The finding from single-hole ERT, that especially within reef core several distinct layers are present, which mostly are closely related to karst can be confirmed with the crosshole data. Crosshole data furthermore proved that permeable features observed with IFM logs on three different levels at individual boreholes can be correlated horizontally and thus are connected to each other.

4.4.4. Seismic tomography

Seismic crosshole tomograms are presented for sections MC2-5-3, MC5-4-7 and MC2-1 (Figure 47). The hydrophone streamer extends from sea level at 40 m depth till 90 m for all boreholes except MC7, where hydrophones were placed between 40 and 65 m. Typical V_P for recrystallized and cemented rock of low rock-matrix-scale porosity are >3000 m/s (Table 5). Grainstones of outer lagoon and the internal sediment of the reef core both exhibit values around 2600 m/s. Within talus depending on the pore structure, values between 2400 and 2600 m/s are present. Velocities from seismic tomography are in good agreement with velocity recorded by sonic logs at Ses Sitjoles (chapter 3) (Figure 54). In order to get comparable data, the seismic pseudolog has been extracted from the tomogram within the depth of investigation of the sonic tool.
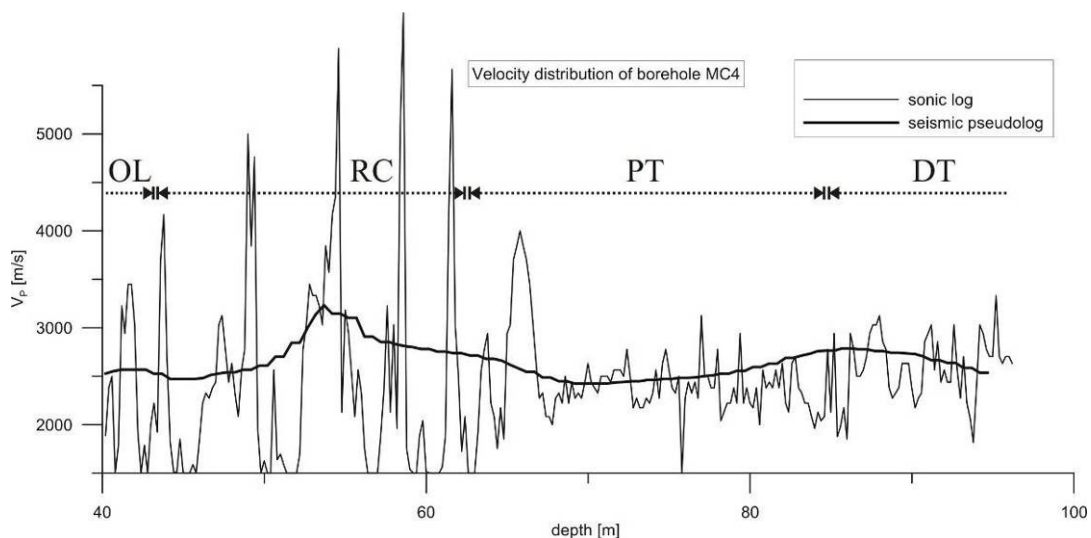
Figure 54:   Velocity distribution of borehole MC4 for sonic log and seismic pseudolog.

With seismic tomography due to the low resolution of 2-3 m, only larger structures and overall trends are accurately displayed. The sonic log in contrast exhibits a resolution in the order of 40 cm, which allows for more accurate values in highly heterogeneous lithofacies types, like the reef core. Consequently the seismic pseudolog represents an averaged sonic log, in which the local extremes of recrystallized corals and dm-scale karstic cavities are suppressed. The overall trends, like enhanced V_P within parts of the reef core, low values of about 2400 m/s in proximal talus and the prominent step to higher velocity at the boundary PT/DT are recorded with both methods, which illustrates that seismic tomograms display reasonably well V_P-heterogeneity.

Within the young reefal carbonate of the present study, high seismic velocity can be due to several reasons. Cementation and recrystallization, which have been observed within reef core at karstified sections and neomorphosed coral colonies lead to enhanced V_P. Furthermore, the occlusion of primary and secondary pore space with blocky spar, which has not only been observed within reef core, but as well in grainstones to rudstones of the upper proximal talus, affects the elastic properties of the rock and results in enhanced V_P. Measurements at the rock-matrix-scale yielded porosities of 5-30% and permeabilities ranging from 0.01-500 md with a mean of only 9 md for rock samples out of the HVZ (chapter 2). Thus, at the HVZ the rock is characterized by low porosity and low permeability at the rock-matrix-scale, which results from enhanced secondary processes like dissolution, neomorphism and cementation. Furthermore, it has been shown for ERT, that within reef core as well tertiary processes affect the rock matrix. On the seismic tomograms karstic cavities are mostly not displayed as low velocity zones, as could be presumed. Observations at the karstified sections have shown that on the contrary they mostly are located within the HVZ (Figure 54). This is due to the low resolution of the method, which mainly records the dense rock in the vicinity of karstic cavities. Additionally low-velocity heterogeneity is rather overestimated. Consequently from mapping the HVZ only, karstic features cannot be predicted, since dense rock as well occurs at non-karstified zones within the reef. In contrast to the electrical properties, elastic rock properties are affected by the pore structure. At the rock-matrix-scale a prominent change of the pore structure has been detected at the boundary PT/DT (chapter 2). In proximal talus large and elongated moldic pores within a grain-dominated matrix are present, which changes to small and round-shaped molds in a mud-dominated matrix within distal talus below. The change to a framework-like pore structure results in slightly enhanced V_P of 200 m/s up to values of 2600 m/s at similar total matrix-porosity (Figure 55A).

The lateral continuity of the HVZ is excellent and V_P-values larger than 2800 m/s are limited to the reef core or the uppermost part of proximal talus (Figure 55). The thickness of the HVZ is about 5 m at MC2 and MC3 and 10-17 m at MC1, 4, 5 and 7. Thus, at locations, where the reef core is part of LST or OST, like at MC2 or MC3, the HVZ is rather thin and where the reef core is part of the AST or HST, like observed at MC1, 4, 5 and 7, the HVZ is thick (Figure 56). Despite significant changes in thickness, the basis of the HVZ is usually located at about 23 m below present-day sea level. This fact together with the observed lateral continuity, which is partly influenced by the primary reefal structure, suggests an evolution through post-depositional events, which are related to sea level changes. The combination of occluded pore space in grainstones to rudstones of proximal talus, recrystallized corals and rock affected by karst within reef core together leads to a complex shape of the HVZ in the strike-section MC5-4-7 (Figure 53). The HVZ here lies within a thick AST and is split into several subhorizontal layers, which are separated by zones of low to moderate V_P. Whereas the lower part below reef core (Figure 55B), as observed on 1inch mini-cores, was affected by directed cementation and occlusion of the intergranular pore space (chapter 2), the middle and

upper part is characterized by neomorposed coral framework and karstic levels with their speleothems and accompanying cementation of the adjacent rock (Figure 53A, B).
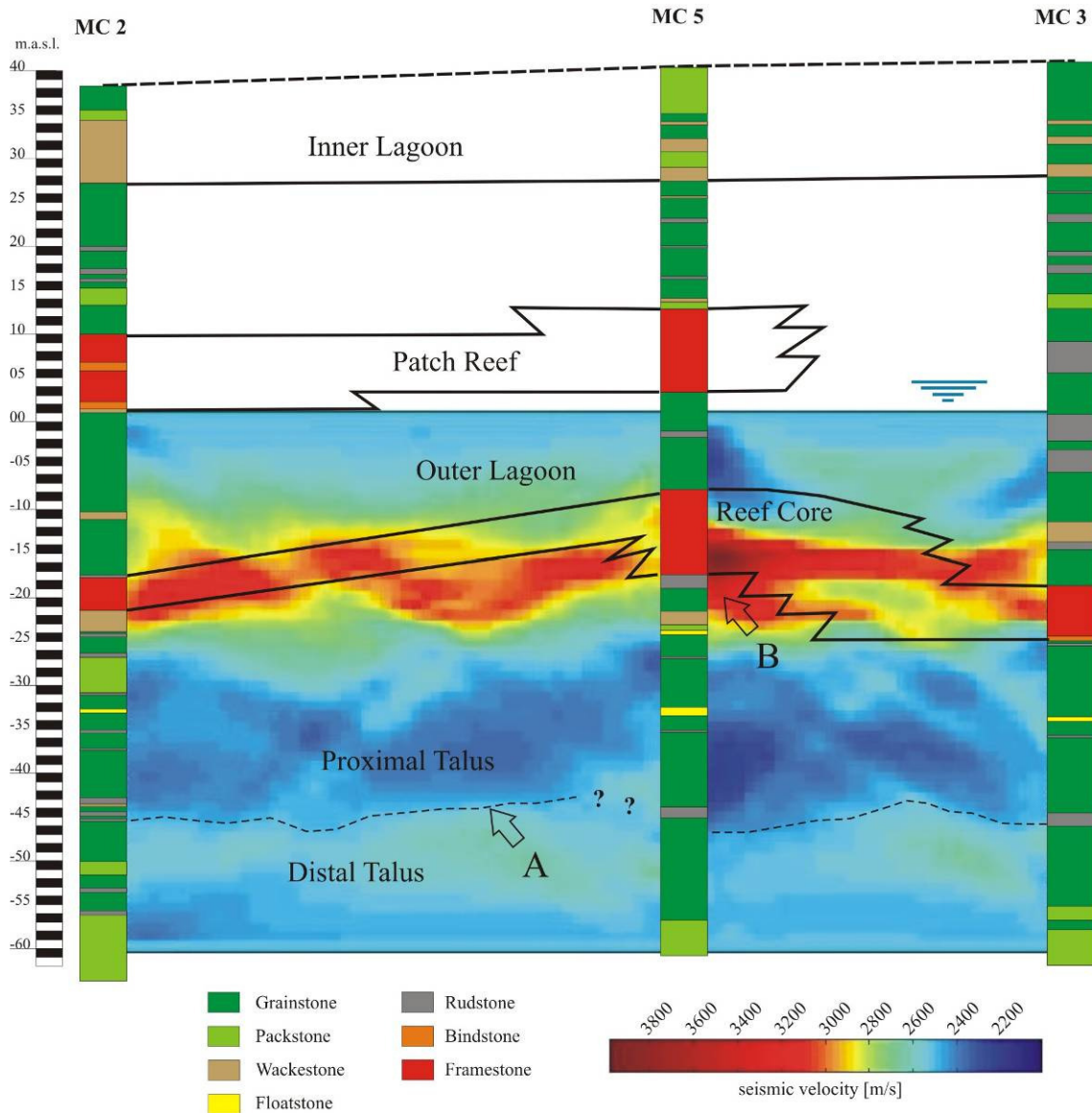
Figure 55:   Dip-section MC2-5-3 with seismic crosshole tomogram. Note that the high velocity zone does not correlate with the reefal geometry. Main discrepancies are observed at MC5, which is part of the AST. For the discussion of the individual zones see text.

Section MC5-4-7 illustrates, that seismic- and electrical tomograms are comparable. Dense recrystallized rock, where the pore space is occluded, exhibits both high resistivity and high V_P. On this tomogram due to the small borehole spacing, as well low velocity anomalies, such as karstic cavities are imaged reasonably well. The karstified horizon B is imaged by both methods and as well the two recrystallized and cemented zones above between A/B, respectively below between B/C are represented by both methods. With seismic tomography the lateral changes and the correlation between boreholes is much clearer for largely spaced boreholes. Furthermore, the elastic waves are not influenced by the present-day mixing-zone and thus help in distinguishing signals, which are not displaying petrophysical properties of the formation. On the other hand for closely spaced boreholes ERT shows more details, especially in karstified zones, where V_P is commonly overestimated. In many cases high

resistivity correlates to high velocity and vice versa. It appears that in the upper part of the reef core ERT and seismic tomography do not correlate anymore, which is due to less pronounced differences in cementation, recrystallization and the missing karst there.

P-wave tomography in general does not display lithofacies boundaries, since secondary and tertiary processes changed the primary pore structure and blurred the original sedimentary fabrics. Secondary and tertiary processes must be related to former sea level fluctuations, which affected the rock rather in the horizontal than in the vertical direction. At locations, where the rock exhibited a high initial heterogeneity, especially tertiary processes had a large impact on the pore structure and built high-velocity heterogeneities. At Ses Sitjoles the transition PT/DT, where a significant change of the pore structure from intergranular/moldic to framework-like/moldic is present, was out of reach for the water level of post-depositional sea level changes. Consequently this lithofacies boundary was preserved (Figure 55).
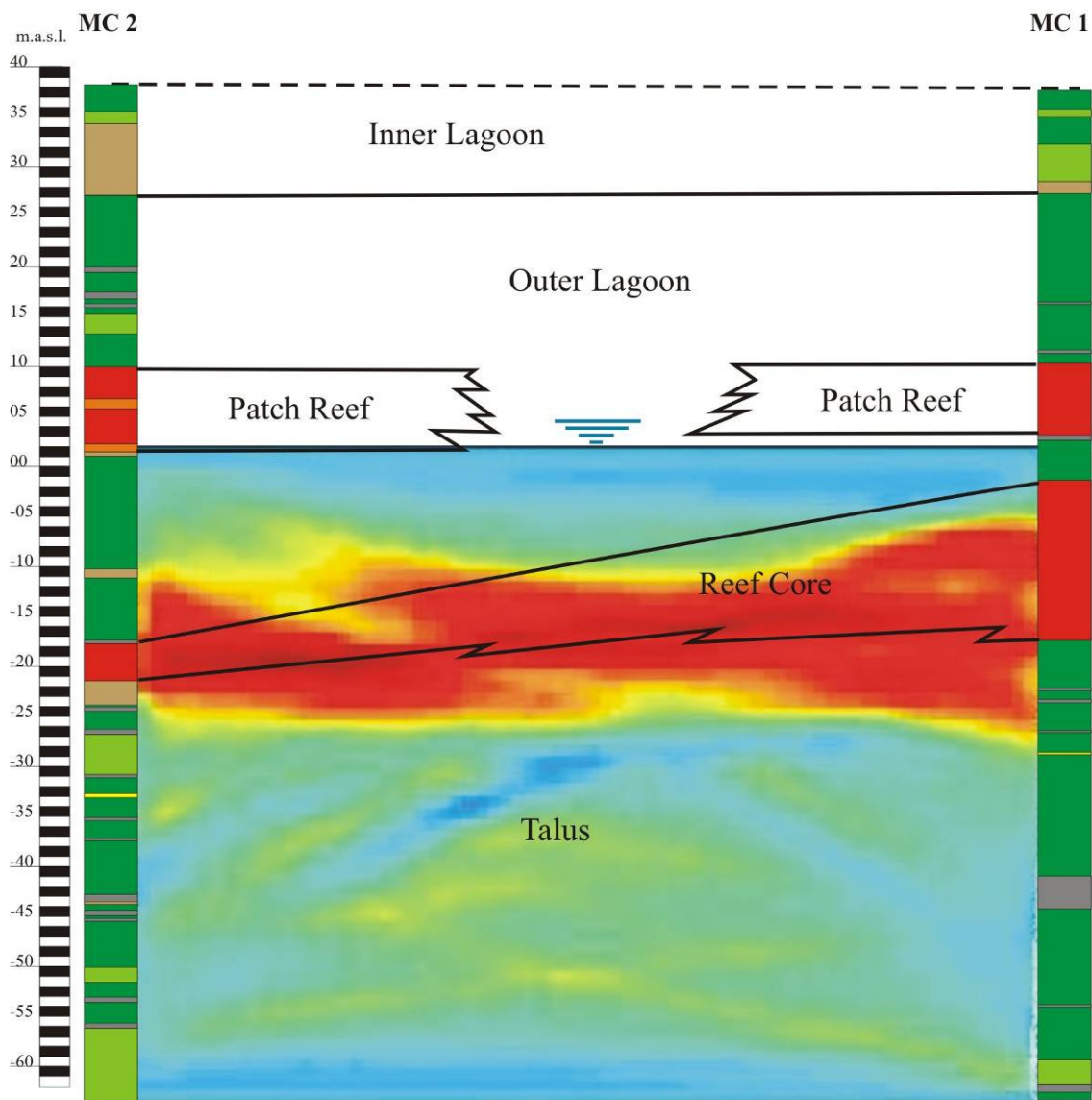
Figure 56:   Strike-section MC2-1 with seismic crosshole tomogram. For the discussion see text.

4.5. Discussion

The results have shown that with electrical and seismic tomograms only, the geological 3D-structure of the reef complex, especially top and bottom of RC cannot be displayed adequately. However, both methods are indispensable for large scale porosity prediction. Thus, it makes no sense to adapt the geological model (Figure 50) to the features observed on the seismic crosshole tomograms. We found a highly complex reefal architecture, which controls the distribution of lithofacies types and primary porosity. However, secondary porosity, mostly moldic, is much more important within this young and unburied reefal carbonate. The distribution of secondary porosity is controlled by the lithofacies distribution but as well by further processes as has been evaluated with ERT and seismic tomography. There are certain distinct zones, where the depositional patterns of the lithofacies types do not anymore directly control the petrophysical properties. With both methods ERT and seismic tomography, a laterally continuous zone of increased resistivity and seismic velocity could be found between -10 and -23 m below present-day sea level. The complex geometry of the zone is only partly controlled by the primary reef geometry and original sedimentary textures. Resistivity and p-wave velocity both are increased for dense, recrystallized rock of low matrix porosity and zones, where significant parts of the pore space are occluded with blocky spar. Coral colonies of the reef core mostly neomorphosed to calcite and build dense, recrystallized rock of low matrix porosity. Furthermore, karst is accompanied with well cemented and dense rock, which is the result of enhanced dissolution- and precipitation processes around karstic cavities. And finally as well below the reef core, within grainstones and rudstones of proximal talus, resistivity and V_P can be increased. In chapter 2 we have shown on 1inch mini-cores of MC5 that this zone exhibits increased cementation with blocky spar and a secondary anisotropy, which was found in small pore classes and suggested a paleo-water level as possible mechanism.

Karst plays an important role for recrystallization and cementation processes within the reefal unit. Most of the karstic horizons lie within the HVZ. Karst can be indicated by both HVZ and low velocity anomalies. In most cases they both occur together within the reef core, what is consistent with the theory. However, karst prediction from seismic tomograms only is very problematic within this young unburied reefal carbonate. Especially ERT as well as core analysis and IFM logs have shown that karst is concentrated on distinct levels within the reef core, which can be correlated horizontally between individual boreholes (Figure 53A, B). Karst is developed within certain planar horizons as an interconnected branching channel-network. The network was not hit by all boreholes, however although visually not evident on core material, IFM logs revealed permeable features at leached corals and fractures at these levels. All these facts imply the influence of a post-depositional process, which controls karst within reef core and the cementation of rocks that are not influenced by karst.

4.5.1. Sea level changes in the geological record of the reefal complex with a special emphasis on the Younger Dryas event

The geometry of the Llucmajor reefal unit is controlled by a complex sea level history, driven by glacioeustatic processes (Pomar, 1991). Estimated amplitudes of these cycles are less than 15 m, 20-30 m, 60-70 m and about 100 m (Pomar and Ward, 1999). The hierarchy of the cyclicity is interpreted as four orders below that of the 3rd order global cycles of Haq et al. (1987). During Upper Tortonian and Lower Messinan, the reefal carbonate complex

prograded about 20 km over the Tortonian ramp until the Late Messinian salinity crisis, where the carbonate production was abruptly shut down and the reefal complex exposed (Pomar, 2001a; 2001b; Pomar et al., 2004a). From the coast channels and caves, which are related to Tertiary and Quaternary karstification are known. Ardilla & Pomar (2000) reported V-incasion structures, structures of karstic collapse, which have formed at sea level lowstands during progradation of the reef complex. Such structures could not be observed on the test site at Ses Sitjoles, since the karstic system within the reef core is not mature enough for building large collapse structures and thus karst at our test site most probably initiated at a later stage of the post-depositional reef history.

From the coast it is known, that Lower Pleistocene base levels determine the presence of large caves, nowadays flooded by sea water (Baron et al., 1995). Post-depositional sea level changes affected the pore structure and mineralogy of the reefal complex as well. This is indicated by various stages of phreatic calcite cement unevenly distributed through the whole complex (Pomar et al., 1996). The transgressive Late Messinian Santanyi Limestone and marly Pliocene deposits, which onlap or overly the older Miocene rocks indicate that after deposition the reefal complex was flooded several times (Pomar and Ward, 1995). During Pleistocene several major sea level fluctuations took place, which built terraces at the exposed Miocene rocks near the south-eastern coast of Mallorca. From these terraces at least six glacio-eustatic littoral-sedimentary cycles were recognized (Jenkyns et al., 1990). The younger record of Upper Pleistocene to Holocene sea level changes is documented by infralittoral sedimentary prisms, which have been recorded on the continental shelf (Hernandez-Molina et al., 1994). Gines & Gines (1995) reported within caves up to 40 m above present-day sea level a great number of epiphreatic calcite crystallizations, which mark paleo water levels. These horizons developed during middle to upper Pleistocene and can be correlated even between different caves. Non published investigations in submarine caves on Mallorca yielded additional epiphreatic cements at levels, which are comparable to the observations made at the test site near Campos. Since in the submarine caves these levels could be related to Pleistocene-Holocene sea level stillstands, in the following discussion we will concentrate on these youngest sea level events.

During the late Pleistocene-Holocene, sedimentation on the continental shelf around the Balearic Islands was mainly skeletal carbonate sand with some lithoclasts, which built sedimentary prisms at different depths (Hernandez-Molina et al., 1994). The top of the sedimentary prisms is controlled by the wave base level of the actual sea level, however, the prisms could only prograde during periods of stillstand or low rates of sea level change. One of these prisms can be correlated with the Younger Dryas cooling event, which lasted from 13'000-11'500 years B.P. (e.g., Renssen and Isarin, 2001). The top of the modern prism on the continental shelf of Mallorca defines the recent base level, which is located at -22 m below present-day sea level, whereas the one of the Younger Dryas is located at -40/-45 m (Figure 57). Main subsidence within the fault scarp system between Mallorca and Cabrera took place from Lower till Middle Pleistocene. Since Middle Pleistocene tectonic activity was not significant anymore. Thus, if it is assumed that the wave base level remained at the same depth, for Mallorca the resulting paleo-water level is located about -18 to -23 m below present-day sea level.
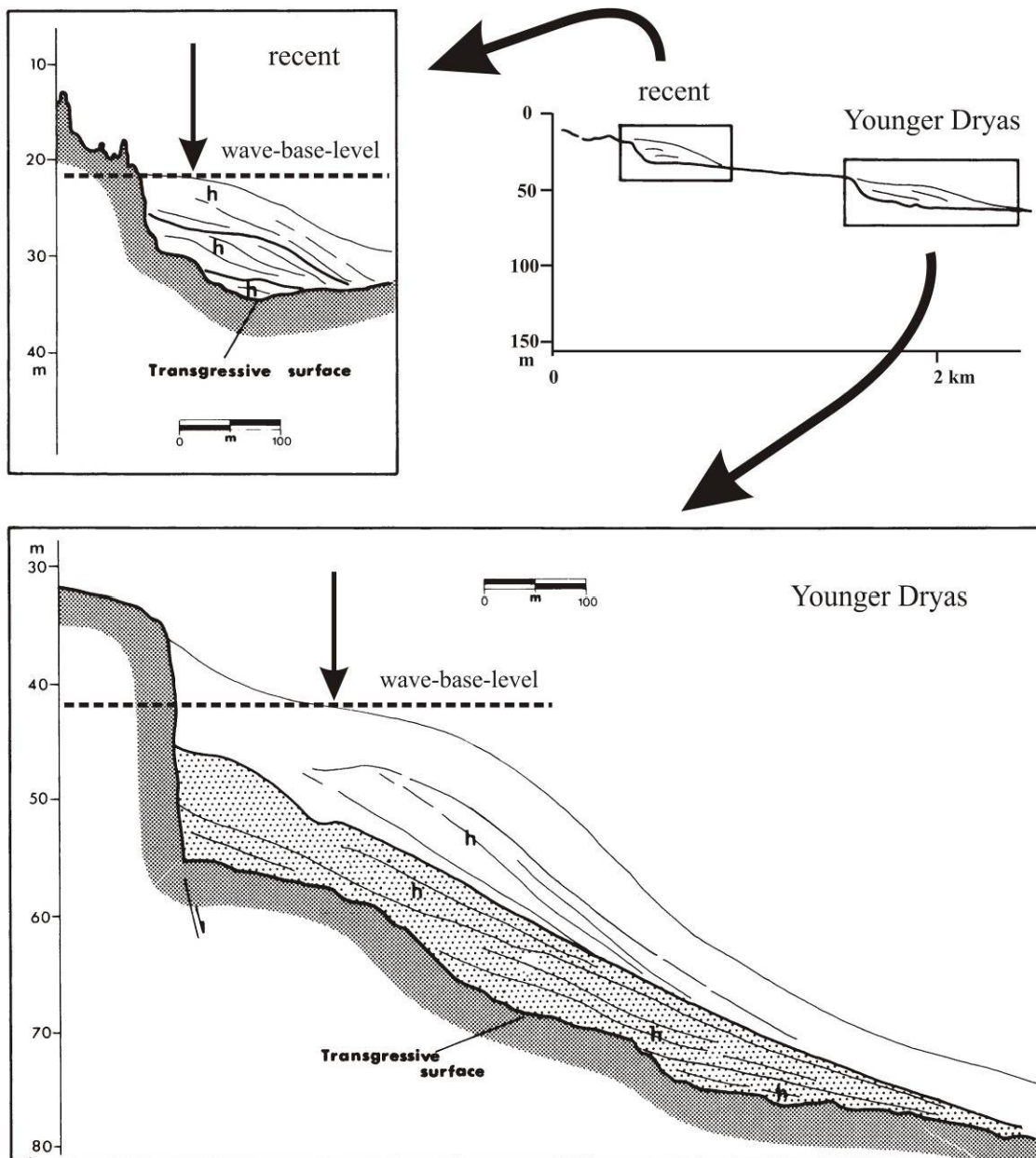
Figure 57:   Seismic interpretations of the infralittoral sedimentary prisms between Cabrera and Mallorca. Internal sedimentary bodies are marked by h (modified after Molina et al., 1994).

The comparison to the HVZ and HRZ, which were found between -10 to -23 m, reveals quite a good overlap, especially for the lower part, which is located mostly below reef core. At the section MC2-5-3 the whole part of high velocities below the reef core lies within the zone of the Younger Dryas sea level (Figure 55). Especially at MC5 the anomalous behavior below the reef core lies exactly at -18 to -23 m. Here increased borehole-scale porosity could be recorded and a mostly dense and recrystallized rock (chapter 3). Furthermore, enhanced cementation with blocky spar, sometimes patchy, has led to matrix-porosities, which are even lower than recorded within the recrystallized reef core (chapter 2). For the smallest pore classes on thin sections even higher anisotropy was found than for the larger pore classes, which uniquely was observed at that depth. In this earlier study about the rock-matrix-scale porosity structure it was suggested already that a directed cementation of the pore space, which is due to a paleo-water level could be the reason for the inversed trend of the pore size/anisotropy-relationship. At section MC2-5-3 the part, which lies above -18 m is mainly

located within the reef core. Within the reef core several processes led to a dense and well recrystallized rock, such as neomorphism of aragonitic corals to calcite and occlusion of the framework porosity by blocky spar cementation. Furthermore, large primary pores between the coral colonies and large secondary pores, such as leached out coral heads could act as nucleus for karstic channels, which interconnected the primary and secondary pores and enhanced the fluid circulation within the reef core. The activity of fluids and the production of dense sinter within the karst system influenced the host rock as well as the internal sediment and parts of the adjacent lithofacies types. Thus, parts of the HVZ and the HRZ, which lie above -18 m could be due to these processes, e.g. on section MC5-4-7 the zone, which is bounded by the two karstified layers A on top and B at the bottom (Figure 53). In this section the zone between B and C, which is characterized by both high velocity and high resistivity exactly fits with the Younger Dryas event. Thus, it arises, that mainly the zones below reef core, which cannot be explained by karsting or dense recrystallized reef rock are due to the sea level stillstand of the Younger Dryas event, which lasted for about 1500 years. Nevertheless one has to consider, that after the Messinian, sea level has been fluctuating during the Pliocene and during the Pleistocene, progressively increasing the amplitude. During some of these fluctuations sea level-stabilization has occurred as is documented in vadose and phreatic caves (Gines and Gines, 1995).

Many authors have stressed, that diagenesis is controlled by both the depositional system and the sea level history (e.g., Eberli et al., 2001; Melim et al., 2001b). The complex post-depositional sea level history of the Llucmajor platform suggests that the rock mass has been subjected to alteration by numerous freshwater lenses and their corresponding mixing-zone. Within the mixing-zone alteration of aragonite to calcite was reported from the Bahama Bank (Melim et al., 2004). Effects at the mixing-zone are physical mixing, organic carbon oxidation and sulfur oxidation/reduction processes. Geochemical investigations at the present-day mixing-zone on Mallorca have shown that no dissolution is occurring (Price and Herman, 1991). The same authors state that dissolution together with neomorphism rather occurs below the water table. Kerans (1988) reported signatures of karst and dissolution voids in the geological record, which could be due to degassing at the vadose/phreatic interface or alternatively due to carbonate dissolution in the mixing-zone. Past sea level stillstand positions are represented by phreatic dissolution voids, which occur at discrete horizons (Mylroie and Carew, 2003). According to these authors the more time a carbonate body has spent in the freshwater lens, the more permeable it will become as dissolutional pathways develop. The rate at which sea level changes and the duration of stillstands at any given sea level position will control the distribution of karst porosity and permeability produced by the freshwater lens.

The patterns of the HVZ and the high resistivity zone found in the present study thus are most probably remnants of these former water levels, which at a stillstand of longer duration could develop larger voids and karstic chambers, as observed for the zones A and B of section MC5-4-7 (Figure 53). According to Lucia et al. (1992), in many reservoirs with massive dissolution there is some indication that cave formation occurred at freshwater lenses that developed during exposure of high frequency sequences. Thus, the freshwater lens, which could develop during such events, seems to be more important for the formation of caves than the exposure surface above. Observations on the test site near Campos confirmed this and furthermore showed that karstic horizons could develop much easier in rock of high primary and secondary porosity like in the reef core, where dm-scale primary and secondary pores were present already before initiation of karst. Karst-processes are always related to dissolution and recrystallization processes, which as well affect the non-karstified host rock and build a dense halo of low porosity and intense cementation, following sedimentary

patterns and anisotropies. Sonic logs as well as induction logs together with thin section analysis support this statement (chapters 2 and 3). Processes along sedimentary patterns and anisotropies include variable thickness of the capillary fringe due to laterally and vertically changing sedimentary texture and the uneven distribution of cements through layering and crossbedding at the vadose/phreatic interface. Recently Pomar et al. (2004b) published results from a study, which has been carried out on the Tortonian ramp of Menorca. They describe calcite concretions, which built during former sea level stillstands within the freshwater lens. According to the authors these concretions followed preferably high permeability zones within the primary sedimentary structures or grain fabric and originate from extraformational fluids of unknown origin.

The lower part of HVZ respectively HRZ, which is located below or at the basis of the reef core, as mentioned is characterized by low matrix porosity, which to a large extent is due to patchy to pervasive cementation with blocky spar. Furthermore, vuggy porosity consisting of larger molds is abundant in this zone. The secondary anisotropy in the smallest pore classes suggests (chapter 2), that the top of a slightly oscillating freshwater lens, most likely of the Younger Dryas sea level stillstand, with intermittently changing conditions from freshwater phreatic to vadose was located at that position. According to Lucia (1999) blocky spar cements form preferably near the undulating sea level within the capillary fringe. However, in this study low matrix porosity and the abundance of large moldic pores are additionally controlled by the sedimentary environment. Directly below the reef core it is characterized by high amounts of aragonitic reef rubble, which was leached out or neomorphosed to calcite. Especially in the karstified reef core epiphreatic cements, like observed in caves, could furthermore play an important role in producing more or less planar HVZ respectively HRZ.

With the Younger Dryas event especially parts of the HVZ below the reef core between -18 to -23 m below present-day sea level could be explained. The higher part of the HVZ is either due to karstified and thus recrystallized rock or neomorposed coral patches, occurring mostly within the reef core. Thus, the irregular and partly layered shape of HVZ and HRZ is the result of its composite origin, which is controlled by several sea level stillstands, the internal heterogeneity of the reef core with the unevenly distributed primary and secondary megapores and its interconnecting karstic channeling with all its related recrystallization and precipitation processes.

4.5.2.   Crosshole geometry at the test site and implications for reservoir behavior

In this study most of the permeable features recorded by the IFM could be correlated horizontally between individual boreholes. From the tomographic data it is evident that at least three distinct levels occur, where karstic processes led to an interconnected channel system. The channeling was mainly driven by sea level stillstands, which at the vadose/phreatic interface led to the enlargement and interconnection of dm-scale primary and secondary pores. These channels, which lie approximately at -21, -17 and -11 m, thus are the most productive zones of the whole reef complex at the test site. Even large pumping tests, which have been conducted on the test site did not yield measurable drawdown in closely spaced observation boreholes, illustrating the high transmissivity of the aquifer (Van Meir et al., 2005).

Unlike reported from the coast (Ardila and Pomar, 2000), at Ses Sitjoles no collapsed karst-structures could be found in the AST of reef core or outer lagoon implying, that at the interior

of the platform karst-collapse structures are rather seldom. Like observed by Lucia (1999) the diagenetic events that follow dissolution and which require fluid flow, such as recrystallization and cementation, spatially are controlled by the touching-vug pore system. Thus, karst-processes as well affect the pore structure of the rock matrix, building a dense halo of low porosity and intense cementation. The halo is proven by the HVZ/HRZ and rock samples out of this zone. Measurements on 1inch mini-cores have shown that the rock within the halo is characterized by low porosity and low permeability at the rock-matrix-scale. Residual clays at the bottom of the cavities of the test site seem to be abundant, especially at borehole MC3, where the highest degree of karstification has been reported. In chapter 3 we have shown by IFM logs that the clays at least locally are acting as seals, which could lead to a compartmentalization of the carbonate reservoir as reported in an early study by Kerans (1988). However, the karst is not very mature at the test site and thus residual clays are only very locally acting as a seal.

A further sealing is built by sequence boundaries, which according to Melim et al. (2001a) can play an important role within carbonate reservoirs. Sequence boundaries consist of wackestones with a low matrix-porosity of 10-20%, built of small and non-connected moldic pores. They have a long range and are rather continuous. Furthermore, sequence boundaries are known to be important controls on reservoir anisotropy (Anderson et al., 1994). Pomar & Ward (1999) state, that at the coastal parts of the platform minor zones of dolomite are associated with boundaries of high-frequency-sequences (HFS), which proves that at least certain sequence boundaries are relevant for fluid flow. At Ses Sitjoles SB1, which is well developed at MC5 approximately 5 m below the reef core, builds an important control on the fluid flow (Figure 50). IFM logs revealed a vuggy zone right on top of the sequence boundary, which could be identified as a permeable feature and at the same time marked the lowermost recordable inflow of this borehole (chapter 3). At MC2 two further important sequence boundaries SB2 right at the bottom of reef core and SB3, which is located about 7 m above reef core are present. At MC2 both sequence boundaries are clearly marked by pronounced gamma excursions, which cannot be recognized anymore near MC5, where SB2 has been eroded (Figure 50). SB3 again appears within outer lagoon at MC3, where it is marked by a prominent gamma excursion. The lateral changes in the character of the sequence boundaries illustrate, that although they are continuous, their sealing potential might not be continuous at all. Especially near MC5 no sealing can be expected from SB2 and SB3. The sealing character of SB3 near MC2 and MC3 is proven by abrupt changes in seismic velocity and resistivity right there, which on core material was identified as enhanced cementation of the rock matrix by blocky spar. Most probably the sealing sequence boundaries led to longer residence times of saturated fluids resulting in enhanced cementation of the rock as observed in sandwiched sections between sequence boundaries and reef core. Furthermore, the mixing with less saturated fluid-species out of the reef core leads to local dissolution. For example near MC3 a fractured zone is sandwiched between SB3 on top and the reef core below of which some fractures are solution enlarged and yielded flow in the IFM (Figure 52). The pore space of the rock matrix in the vicinity of these fractures is partially occluded with blocky spar.

The HVZ/HRZ was built by fluid-rock interactions, such as neomorphism and cementation with blocky spar, which led to a remarkable reduction of porosity at the rock-matrix-scale. It could be shown that the zone, where resistivity and seismic velocity are high, especially within the reef core is dominated by karstic channels, which are occurring on distinct planar horizons. From the lateral continuity of the HVZ/HRZ, which at the same time marks a zone of low matrix porosity- and permeability, it could be assumed that the karstic horizons are not connected vertically. However, ERT and seismic tomography are not capable of resolving

local heterogeneities, like solution enlarged fractures or thin vertical channels at the intersection of two individual coral colonies, which could be of eminent importance for the vertical hydraulic connection between larger karstic horizons. Furthermore, observations made with IFM logs suggest channel-systems of a large extent. The undulating HVZ with reef core of variable thickness at different depths at the dip-section MC2-5-3 (Figure 55) indicates that for a high productivity of the planar karstic horizons as well vertical connections must occur. Nevertheless the karstic system developed at different times on different levels rather in the horizontal than the vertical direction. The vertical interconnection of the karstic levels is mainly controlled by the high degree of internal heterogeneity within the reef core.

All the made observations lead to the typical hydraulic properties of karstic systems, where at a large scale the fluid flow is mainly concentrated in a touching-vug pore system of interconnected, solution enlarged molds, which is very permeable but contributes only minor amounts to total porosity. The partly occluded intergranular and moldic pores of the rock matrix yield the major contribution to the total porosity, but are much less important for the productivity of the formation, as could be shown by permeability measurements on 1inch mini-cores out of the HVZ/HRZ near tertiary pores (chapter 2).

At the lower and the upper limit of reef core, seismic and especially resistivity-tomograms confirmed observations made on core material and wireline logs (chapter 3). The upper limit is not sharp, since internal sediment, which fills up the space between the coral colonies originates mostly from outer lagoon and thus is not different in texture and grain composition. Resistivity and velocity generally are higher than in proximal talus, indicating higher cementation and affection through fluids. Permeable features are recorded at fractured zones, sometimes in association with sequence boundaries like in MC3 (Figure 52) or within intensively burrowed horizons, which are building local anisotropies. The lower limit of reef core, where it is interfingering with the grainstones and rudstones of proximal talus, is much sharper, however, not always on the tomograms. At MC5 HVZ and HRZ are blurring the lithofacies boundary. Qualitatively for most boreholes the boundary RC/PT builds a remarkable hydraulic boundary, since at borehole- and crosshole-scale the permeability contrast is high, as has been demonstrated in chapter 3 by IFM logs. At rock-matrix-scale the contrast is high as well, but the other way round. Whereas in proximal talus for rock-matrix-scale permeability a mean of 185 md was evaluated, at the overlying reef core a mean of only 9 md was found (chapter 2).

For ERT it has been demonstrated, that the LRZ can be highly permeable like lateral continuous karstic horizons or low permeable, if isolated as primary or secondary dm-scale pores within rock of low matrix-porosity. Furthermore, isolated LRZ's can occur within karstified sections, where parts of the tertiary porosity are separated by residual clays. In general no statement about porosity and permeability can be made from seismic tomograms, since seismic velocity is strongly affected by pore structure, which leads to different V_P at similar total porosity and especially for larger borehole spacing within the HVZ karst cannot be distinguished on tomograms due to low resolution and overestimation of low-velocity anomalies.

Proximal talus is an anisotropic lithofacies, which is built of clinobeds, which show internal and overall coarsening upward (chapter 3). The progressive flattening of the clinobeds from MC3 over MC5 to MC2 is indicated by a reduction of the cycle-thickness and confirms the geological model, which was derived in this study by the analysis of sequence stratigraphy. From seismic tomography no indication is given about the internal structure of proximal talus. The clinobeds together with the lenticular coarse grained storm deposits in between build a

large scale anisotropy, which most probably is affecting the hydraulic behavior within the talus. The anisotropy is also observed at the rock-matrix-scale, where large and elongated fossil fragments were deposited in a preferred orientation. These fossil fragments later on were dissolved and form now an important moldic porosity, which due to its connectivity exhibits a high permeability (chapter 2). However, compared to the permeability of the karstic conduits within reef core, the impact for the whole reefal complex is small.

Within the seismic tomogram MC2-5-3 the transition PT/DT could be traced laterally (Figure 55). At this transition seismic velocity increases towards distal talus by about 200 m/s. This contrast has already been recorded by sonic logs (chapter 3). There it was found that rather than a reduction in total porosity, a change of the predominant pore type from large and elongated moldic pores to small and round shaped molds within a micritic matrix, forming a framework-like porosity structure is responsible for the recorded velocity contrast. Permeability measurements on 1inch mini-cores showed, that at the rock-matrix-scale distal talus is much less permeable than proximal talus, despite comparable total porosity.

4.6. Conclusions

Geology observed on cores and the associated sequence stratigraphical model, which is mainly based on the outcrop analogues from the cliff coast, are important factors for the understanding of reef geometry, genesis and heterogeneity. Architectural concepts and diagnostic features for the determination of the systems tracts, derived from the outcrops at the cliff coast, were indispensable for building a reliable sequence stratigraphical model, which made it possible to correlate between individual cored boreholes. From the observed geometry it can undoubtedly been stated that the reefal complex at the test site is comparable to the Cap Blanc reefs, however, two main differences can be pointed out: The occurrence of patch reefs in the outer lagoon of the test site, which have been hit in four of the five boreholes and the lack of stromatolites within inner lagoon lithofacies.

ERT and seismic tomography proved to be indispensable tools for imaging resistivity- and velocity heterogeneity at the crosshole-scale. In general HRZ and HVZ roughly correlate (Table 5). HRZ and HVZ were observed within reef core, where neomorphosed corals and the well cemented rock matrix near karstic horizons build dense rock of low porosity at the rock-matrix-scale. However, the zones in most cases are not restricted to the reef core only and are as well present in the uppermost proximal talus, where former sea level stillstands led to incomplete occlusion of the pore space with blocky spar.

LRZ's can be correlated with karstified horizons, which vertically are separated by HRZ/HVZ. Thus, on the ERT's, karstic horizons can be traced laterally between boreholes. The sharp boundaries and the uniform resistivity, which is not interrupted by higher values, suggest the existence of an interconnected channel network on these horizons. A further indication about the existence of interconnected channel networks, which are located within several horizontal planes, is given by the fact that even permeable features were measured by the IFM, not for every continuous LRZ at the boreholes large karstic cavities could be observed. Electric and seismic crosshole data furthermore proved that permeable features observed with IFM logs on three different levels at individual boreholes can be correlated horizontally and thus are connected to each other. Consequently a channeling is present, which interconnects larger primary and secondary pores. These pores are unevenly distributed on the karstified horizons, which leads to complex traces of the channels in the horizontal direction.

It has been shown, that the sea level during the Younger Dryas event was located exactly within the lower part of HVZ/HRZ. At the vadose/phreatic transition, parts of the pore space were occluded with blocky spar. Here directed cementation led to the development of a secondary anisotropy, which predominately affected small pores (chapter 2). With the Younger Dryas event the lower part of the HVZ/HRZ between -18 to -23 m below present-day sea level could be explained, however, since the deposition of the reefal complex numerous freshwater lenses have passed through the whole platform, with unknown positions and durations of sea level stillstands. The higher part of the HVZ/HRZ is either due to karstified and thus recrystallized rock or neomorphosed coral patches, which occur mostly within the reef core. Thus, the irregular and partly layered shape of the HVZ/HRZ is the result of its composite origin, which is most probably controlled by several sea level stillstands, the internal heterogeneity of the reef core with the unevenly distributed primary and secondary megapores and its interconnecting karstic channeling, with all the accompanying recrystallization- and precipitation-processes.

The combined analysis of ERT and seismic tomograms together with core material has shown, that karst is always related to dissolution and recrystallization processes, which at the rock-matrix-scale build a dense halo of low porosity and intense cementation, following preexisting sedimentary patterns and anisotropy. In addition to tomographic evidence, sonic logs as well as induction logs together with thin section analysis support this statement (chapters 2 and 3).

The high resistivity contrasts observed at several levels in the reef core display the complexity of the distribution of large scale primary and secondary porosity, which acted as a nucleus for karstic processes at certain levels. The system of karstic channels, which is the most permeable feature of the reefal complex, could be displayed and traced easily with ERT. Seismic tomography proved to be useful in displaying HVZ for large borehole spacing. Lithofacies boundaries are only exceptionally displayed by tomograms, since generally secondary and tertiary processes blur the primary sedimentary texture. The transition PT/DT is displayed on the seismic tomogram as a velocity step of 200 m/s. Here a change of the predominant pore type from large and elongated moldic pores to small and round shaped molds within a micritic matrix, forming a framework-like porosity structure is responsible for the recorded velocity contrast.

5.   Synthesis – Conclusions and perspectives

5.1.   Evolution and development of the pore structure at Ses Sitjoles

Depositional

During Upper Tortonian and Lower Messinian, the reefal carbonate complex prograded about 20 km over the Tortonian ramp until the Late Messinian salinity crisis, where the carbonate production was abruptly shut down and the reefal complex exposed. During reef-progradation, mainly intergranular porosity formed through deposition of bioclastic sediment within lagoon and talus. Framework porosity within corals was the predominant pore type of the reef core. In between the coral framework internal sediment with a significant amount of intergranular porosity was present. Furthermore, large scale cavities were built in between individual coral colonies. Some of these large scale cavities were not filled up by internal sediment from the outer lagoon and thus preserved. Primary megapores reaching man size have been reported from the cliff coast. However, at the test site single pores did not exceed a few dm in diameter.

The energy milieu and exact location within the former carbonate factory significantly defines the primary parameters like grain size distribution, sorting, sedimentary anisotropy and mud content. Water dynamics within outer lagoon removed carbonate mud through winnowing. The bioclastic carbonate sands within outer lagoon were reworked and the mud was shed at distal parts of the talus. The distribution of microporosity to a large extent is dependent on the amount of mud. Mud-dominated packstones with highest amounts of microporosity are found within distal talus. Grain-dominated sediments are typical for the upper part of talus and the outer lagoon. Measurements on 1inch mini-cores have shown, that a mud-dominated fabric like observed in distal talus results in high porosity and a low permeability, whereas grain-dominated fabrics like observed in outer lagoon in general show high porosity and permeability. Lots of sedimentary deposits, which are recognized on the stratigraphical column, were deposited during storm events, when the wave base level was low and pulses of bioclastic sediments from high zones, such as outer lagoon and the reef core, were transported to distal parts of the reef.

It could be shown, that within proximal talus primary anisotropy of the pore distribution is important, resulting from a combination of both, depositional cyclicity of clinobeds and storm induced rudstone lenses. Clinobeds show a coarsening upward, which is mostly controlled by high frequency sea level changes. At Ses Sitjoles cycle thickness varies between 1.4 and 2 m, as could be shown with the ATS. Studying the variations of cycle thickness between individual boreholes allows for cross-checking the sequence stratigraphical model. It could be shown, that the trend of diminishing cycle thickness is consistent with the direction of reef-progradation, resulting from sequence stratigraphy on boreholes. Storm induced rudstone lenses and the clinobeds both are causing depositional anisotropy, which as well could be observed at the outcrop analogues near Cap Blanc.

Primary porosity and its distribution within a lithofacies type are controlled by the local reef geometry and the evolutionary stage of the reef complex. The averaged porosity trends

between individual lithofacies types remain the same for each borehole, however on different absolute levels. Whereas the differences of porosity between individual reef core parts can clearly be explained by reef geometry and subsequent diagenetic overprint, in outer lagoon differences in porosity are rather of depositional and thus primary origin.

Syndepositional

Burrowing was observed throughout the entire reefal complex. It is a primary process, which occurred during deposition. The burrows are characterized by a network of non-cemented sediment with increased grain size and sorting, building zones of slightly enhanced permeability at the rock-matrix-scale. With the ATS primary porosity caused by extensive burrowing could be recorded and locally values up to 50% have been measured.

In outer lagoon and proximal talus several inflow zones, recorded by the IFM are related to sequence boundaries, which can either act as a seal or which facilitate the formation of secondary permeable features like vuggy zones in the overlying rock. At Ses Sitjoles sequence boundaries evoke important heterogeneity within bioclastic lithofacies types, such as outer lagoon and proximal talus. They can hardly be recognized on core material within reef core, where the recrystallized coral framework and the internal sediment in between display an even more pronounced heterogeneity. Consequently sequence boundaries within reef core do not exhibit a sealing potential.

Early post-depositional

Right after deposition and especially through the influence of freshwater lenses during several sea level changes, the formation of secondary porosity began. Moldic porosity is the most important pore type of the whole reefal complex. It formed through the complete dissolution of aragonitic constituents, such as corals and coral fragments and shells of bivalves and gastropods. Large and elongated moldic pores are interconnected through the intergranular pore space in outer lagoon and proximal talus. It was found, that towards the bottom of proximal talus small and round shaped molds are more and more common. There molds formed through fabric-selective dissolution of peloids and other well rounded bioclasts. Packstones and grainstones of distal talus are mud-dominated and round-shaped small moldic pores, originating from the dissolution of peloids, are the most important pore type. We found that micritic crusts, which enclose the small moldic pores, impede a productive connection between individual pores and most of the interparticle pore space is filled with microspar. In distal talus diagenesis led to the recrystallization of mud to micrite or microspar. Here highest values of microporosity have been recorded, which is mostly ineffective for permeability. At the boundary PT/DT a remarkable reduction in sonic porosity was recorded, which can be explained by the change of the pore structure. In distal talus the small and round shaped molds are surrounded by micritic crusts, micrite and microspar and thus barely interconnected. The small and round shaped molds are building a framework-like pore structure within micritic sediment with a high amount of ineffective microporosity.

The bimodal pore size distributions of outer lagoon and proximal talus were mainly built by large and elongated moldic pores within smaller molds and intergranular pores. For samples with a bimodal pore size distribution no pore size dependent correlation of porosity versus permeability could be observed like proposed by many authors (Hearst et al., 2000; Lucia, 1983; Serra, 1984). High permeability was recorded in outer lagoon and proximal talus, which is mainly due to well connected moldic porosity, which consists of large and elongated molds with large shape factors, leading to a prominent primary anisotropy.

The formation of moldic pores through leaching of coarse grained aragonitic layers within proximal talus led to the detection of clinobeds by the ATS. Clinobeds show a coarsening upward, which reflects the sea level fall of the high frequency cycle (Pomar et al., 1996). At the top coarse grained aragonitic reef rubble was leached, forming moldic porosity. The origin of clinobeds is primary, however, the porosity there was build by the subsequent diagenesis. Within reef core the ATS mainly records karstic cavities. Within talus and outer lagoon it is the moldic porosity, which controls the recording. Variography on ATS-data has shown that within distal talus the REV is smallest, which is consistent with the high degree of homogeneity observed on core material.

A further secondary process, which significantly affected heterogeneity of the reefal complex, is neomorphism. This process predominantly occurred within the coral framework of reef core and the patch reefs of outer lagoon. Here coral colonies originally built of aragonite neomorphosed to the more stable calcite. Later on especially through the influence of oscillating freshwater lenses, blocky spar cements partially occluded the coral framework porosity. HVZ and HRZ recorded from seismic respectively electric tomography are a consequence of these fluid-rock interactions. At these locations neomorphism and cementation with blocky spar led to a remarkable reduction of porosity at the rock-matrix-scale. At the rock-matrix-scale reef core is not a reservoir rock. From measurements on 1inch mini-cores we found, that about 80% of all samples from reef core exhibit porosities lower than 25%, which is opposite to the two adjacent lithofacies types, outer lagoon and proximal talus. Thus, there is a remarkable porosity-contrast at the upper and the lower boundary of the reef core. However it could be shown, that permeability within the karstified reef core is strongly scale-dependent, since despite the lowest matrix-porosity, permeability at larger scales is highest due to extensive channeling on several levels.

Tectonic activity

During lower to middle Pleistocene minor tectonic activity affected the reefal platform (Jenkyns et al., 1990). The platform was slightly deformed by tectonic flexure. Consequently at Cap Blanc the reef core emerged, whereas it submerged in the north western part of the platform. The tectonic activity led to some fractures, however as investigations at Ses Sitjoles have shown, they are rather rare and in many cases seem to be parallel to the local bedding and thus directly related to reefal geometry. Sporadic closed sub-vertical fractures could be related to the slight tectonic flexure and tilting of the carbonate platform. Some fractures are solution enlarged and hydraulically active, as logs with the IFM have shown. At the borehole-scale these fractures are not significantly contributing to total porosity and within outer lagoon and proximal talus they build permeable features. These productive factures typically are sandwiched between a sequence boundary and the reef core. The sealing potential of sequence boundaries, which mainly consist of wackestones, in combination with the fluid circulation within reef core, led to those solution enlarged fractures. In addition it has been found in this study, that the rock matrix at that sandwiched position is well cemented by blocky spar, which leads to increased seismic velocity and electrical resistivity on the tomograms.

Pleistocene sea level changes

During Pleistocene several major sea level fluctuations took place, which built terraces at the exposed Miocene rocks near the south-eastern coast of Mallorca. Several sea level stillstands are documented as epiphreatic calcite cements in caves, which occurred during middle to

upper Pleistocene (Gines and Gines, 1995). The younger record of Upper Pleistocene to Holocene sea level changes is documented by infralittoral sedimentary prisms, which have been recorded on the continental shelf (Hernandez-Molina et al., 1994). The complex post-depositional sea level history of the Llucmajor platform suggests that the rock mass has been subjected to alteration by numerous freshwater lenses and their corresponding mixing-zones. It has been found, that the reefal complex was mainly subjected to meteoric diagenesis. Some of the processes, such as blocky spar cementation, which occluded most of the growth-framework porositiy within reef core, have already been mentioned. HVZ and HRZ within reef core can be explained by neomorposed coral colonies, and blocky spar cementation, which was intensified through the oscillating freshwater lenses.

Sea level stillstands play a major role in the diagenetic history of the reefal platform. Especially at the vadose/phreatic interface within the reef core, dissolutional pathways could develop on certain horizons, where a high internal heterogeneity was present, such as dm-scale primary and secondary pores and recrystallized rock matrix. The interconnection of primary and secondary pores and the occlusion of the pore space in the adjacent rock matrix are common in zones of karst influence. The karstic system within reef core is doubtless the most productive zone of the whole reef complex. Karstic cavities are associated with residual clays, which can have a certain sealing potential as has been demonstrated by IFM logs. However, considering the size and maturity of the karst system observed, their lateral continuity might be in the order of several meters and thus limited. Karst-related dissolution and recrystallization processes affect the adjacent host rock as well and build a dense halo of low porosity and intense cementation, following sedimentary patterns and anisotropies.

The best documented sea level stillstand is the Younger Dryas-event. At that time sea level was about 18-23 m lower than at present. The patchy to pervasive cementation of the pore space by blocky spar at that depth results in increased values for electrical resistivity and seismic velocity within a coarse grained bioclastic sediment, which is not directly affected by karst like in the reef core above. According to Lucia (1999) cementation and occlusion of the pore space forms preferably near the undulating sea level within the capillary fringe. The different initial pore structure within the upper part of proximal talus with no preexisting dm-scale pores and a relatively low permeability at larger scales, results in a rather closed system, where fluid flow mainly occurs in the vertical direction, e.g. by capillary forces. Consequently past sea level stillstands are not always characterized by dissolution processes. Furthermore, the intermittently changing conditions from vadose to phreatic right at the sea level led to the development of a secondary anisotropy. It has been found, that below reef core in MC5, smaller pore classes are more anisotropic than larger ones. The smaller pores are more sensitive to directed occlusion of the pore space, as could be shown by digital image analysis. Since among other controlling factors there is a clear dependence on the absolute pore size, whether a pore was subjected to secondary anisotropy or not, we assume that mainly sedimentary anisotropy can significantly determine the fluid flow within the rock matrix.

5.2. Karst and implications for its regional distribution

Within the reef core we found prominent low resistivity anomalies, which can be traced horizontally between boreholes. Those revealed the existence of at least three distinct karstic horizons. Several observations, such as the lateral correlation of permeable features between boreholes, suggest that a horizontally interconnected channel network is present, which communicates between the different levels. The channeling was mainly driven by sea level stillstands, which at the vadose/phreatic interface led to the enlargement and interconnection

of dm-scale primary and secondary pores within the coral framework. It has been found, that karst processes furthermore affect the pore structure of the rock matrix, building a dense halo of low porosity and intense cementation. The halo is proven by the HVZ/HRZ, which was recorded by seismic respectively electric crosshole tomography and measurements on thin sections and 1inch mini-cores out of this zone. It could be shown, that residual clays cause a certain influence on the productivity of karstic zones. However at the test site, 6 km off the coast, the karst is not very mature and thus residual clays are only very locally acting as a seal. The karstic system developed at different times on different levels rather in the horizontal than in the vertical direction and at least at the test site is restricted to the heterogeneous reef core. The small dimensions of the karstic channels suggest a young system, which developed stepwise during the influence of freshwater lenses, intermittently moving up and down the stratigraphical column.

It was found that microkarst within outer lagoon is related to exposure surfaces. However at our test site it is not abundant and less important for the fluid flow compared to the karstified reef core. From the coast Ardilla et al. (2000) reported karst, which formed within the AST of the reef core and led to the collapse of the overlying lagoonal sediments. At Ses Sitjoles no collapse structures could be recorded and the karstic system is well developed within the lower part of the reef core. It has been observed within all 5 cored boreholes, in form of three horizontal layers, which are rather connected in the lateral than in the vertical direction. Larger karstic cavities within the reef core are furthermore known from other wells in the vicinity of the test site. A direct hydraulic coupling to karst observed within reef core at Cap Blanc is not possible, since there the entire reef core is located within the vadose zone. Main subsidence of the Campos basin during lower to middle Pleistocene led to a slight tectonic flexure of the platform, which results in a relative tilt of the reefal unit from the coast near Cap Blanc towards the test site near Ses Sitjoles. Consequently there is a certain zone along the southern coast, where the reef core is above present-day sea level and a zone, where it is submerged (Figure 58). We suppose that from the coast east of Cap Blanc, where the reef core is submerged till the test site 6 km landward, a rather direct connection though karstic channeling within the reef core is present. This hypothesis is supported by a study, which recently has been carried out by Keith Evans and Nathalie Van Meir of ETH Zurich (pers. comm.), who found that pressure signals recorded within the wells at the test site showing tides of the sea require a nearly direct connection between the sea and the test site at Ses Sitjoles.

The karst system of the Llucmajor platform is important for the aquifer. Karst mainly occurs within the approximately 20 m thick freshwater part. At least at Ses Sitjoles the mixing-zone is located below the karstified reef core. Thus, water circulating within the karstified reef core is fresh water. An upconing test was performed in 2004 and showed that heavy pumping during 13 days changed the salinity of the pumped water by only 5%. Furthermore, no measurable drawdown could be generated in a closely spaced observation well nearby. The well mainly produced water out of the karstified reef core and consequently flow occurred rather in the horizontal than vertical direction. The drawdown from the pumping could not produce pronounced vertical flow, which harms the quality of freshwater. The high productivity of the karstic system thus protects the partially penetrating well from upconing and the resulting salinization. This large scale pumping test furthermore proved that the karstic system extends within the freshwater lens beyond the range of the pumping test. Consequently the karstic system within the lower part of the reef core seems to extend laterally and its good interconnection protects pumping-wells from upconing despite the high porosity and permeability of the underlying talus sediments. Karstic collectors, which end at the coast below sea level, forming submarine freshwater springs, are known from the northern

coast of Mallorca. The outlets of these collectors for the Llucmajor platform might be located at its southern margin, where the karstified reef core is submerged (Figure 58).
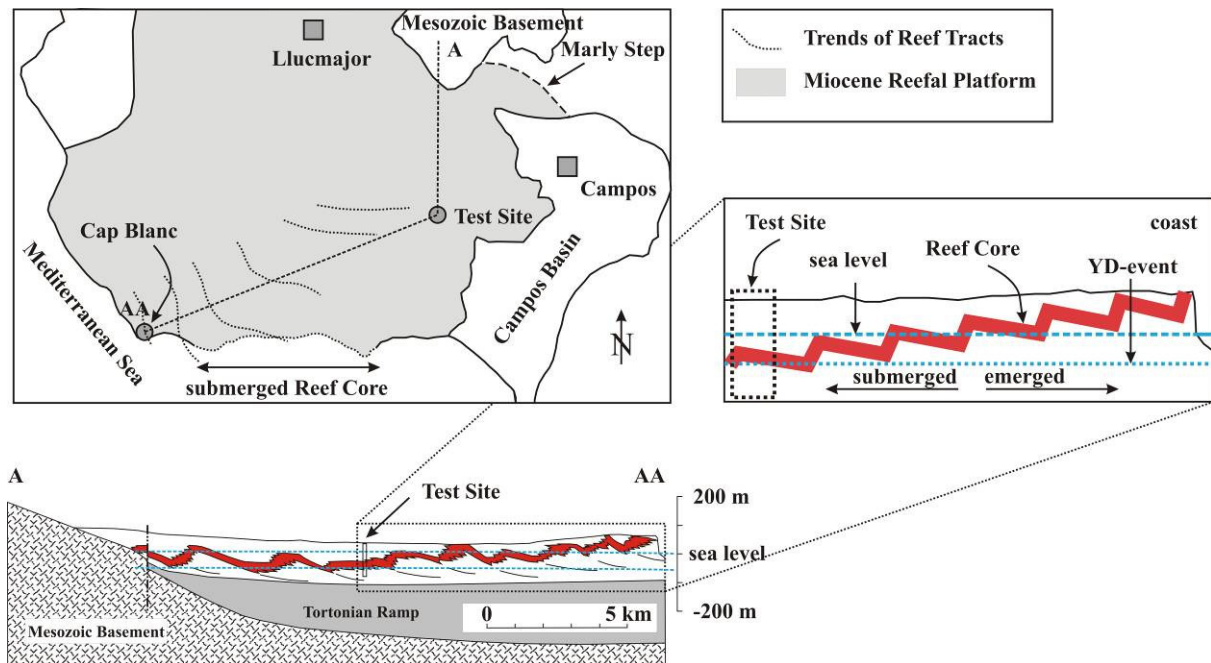
Figure 58:   Map view and dip-section of the Llucmajor platform. Along the southern margin of the platform, the reef core is submerged and there the karstic system accesses the sea (modified after Pomar and Ward, 1995).

5.3.   Perspectives

The results of this thesis form a basis for modeling transport and fluid flow within reefal carbonate reservoirs. With the knowledge about the porosity structure from this thesis, it is possible to build reliable models, which for example could simulate push-pull tests or other hydraulic tests performed on the test site. The multiscalar approach, which considers the entire rock mass from micrometer- up to decameter-scale, comprising as well evolutionary stages and processes, significantly supports the evaluation of modeling parameters and puts them on a well constraint basis. Furthermore, without going too deep into modeling, the present thesis provides important information for an enhanced water management on the Llucmajor platform and comparable coastal carbonate aquifers. The information of hydraulic interactions between karstified reef core and the adjacent lithofacies types as well as for example the change of the pore structure at the transition proximal/distal talus, build an important information for the design of new pumping wells. Furthermore, the hypothesis that the Llucmajor platform mainly discharges along the submerged reef core at the southern coast should be verified, which furthermore would explain the direct karstic connection between the sea and the test site at Ses Sitjoles.

The thesis as well has shown uncertainties and some preexisting questions still remain unanswered or new questions arise through this study. Future research on the platform must concentrate on the impact of sea level stillstands on the regional-scale pore structure. The Younger Dryas event was observed at Ses Sitjoles but absolutely no data about this feature is available from other boreholes of the platform. Furthermore, it should be verified, whether at other locations as well 3 distinct karstified levels occur within the AST of the reef core and whether there is an increase in the dimensions of the karstic cavities towards the coast or not.

At the test site the interconnection between karst within AST and karst within LST or OST could be verified with another borehole between MC5 and MC3. Here additional electrical crosshole tomograms would provide valuable additional information about the evolution of the karstic system.

Further field work should be carried out at the well exposed cliff coast, with a special emphasis on the pore structure and the interaction between individual lithofacies types. Larger datasets of thin sections and 1inch mini-cores should be acquired from other boreholes of the test site for the evaluation of differences between individual boreholes, which are part of different evolutionary reef stages. Especially for the investigations at the rock-matrix-scale, larger data sets would eliminate uncertainties about the reliability of statistical trends.

This thesis is the first comprehensive reservoir characterization, which has been carried out on the Llucmajor platform. Together with the publications from Luis Pomar and other authors about the fantastic outcrops near the well exposed cliff coast, it builds a further step towards the overall understanding of Miocene reefal carbonate systems, for which the Llucmajor platform got a world reputation among sedimentologists, petroleum geologists and reservoir engineers.

F) Appendix

A I. Permeability measurements on 1inch mini-cores
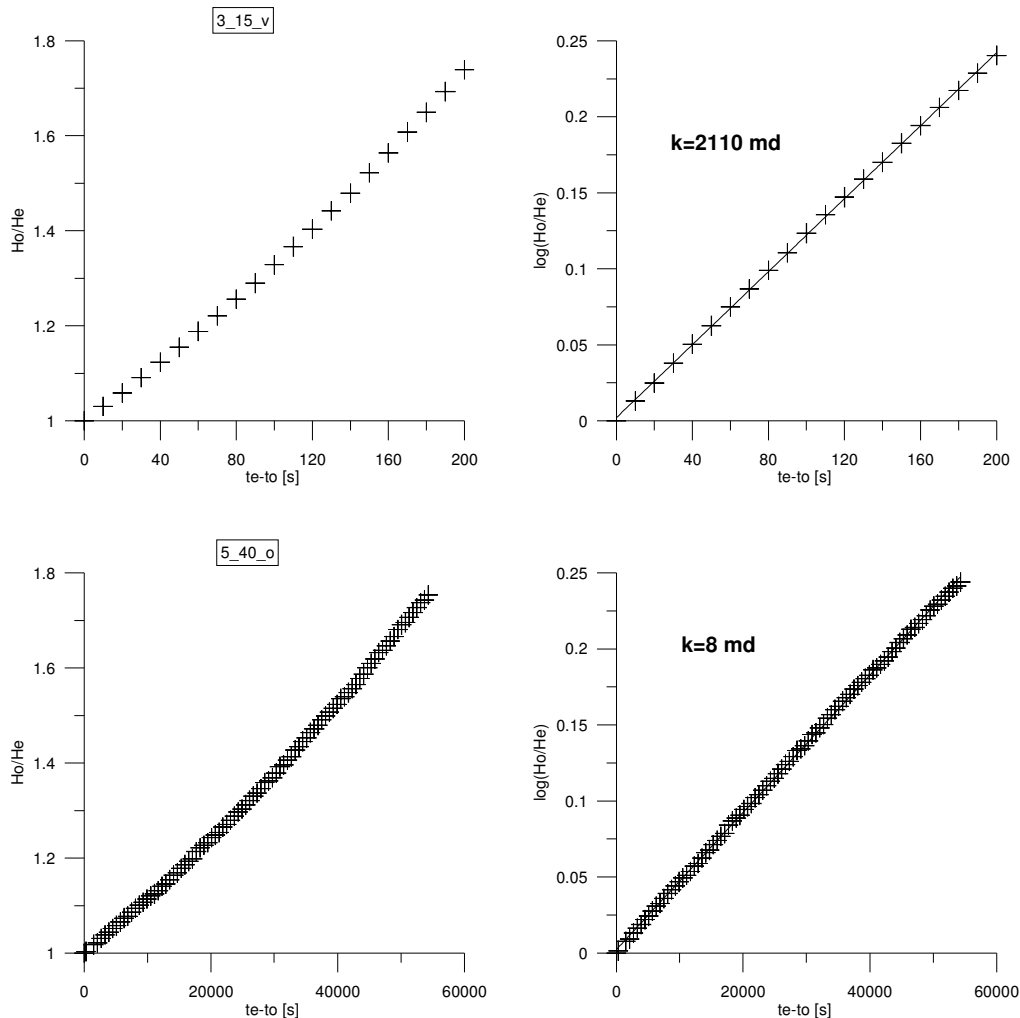
Figure 59:   Results from two standard falling head permeability tests, obtained for a sample of high permeabiliy (3_15v with k=2110 md) and a sample of rather low permeability (5_40o with k=8 md).

Permeability measurements were performed after the standard falling head permeability test (e.g., Lang et al., 2003). The self-made cell used in this study consists of two caps, which act as inlet and outlet of the water and which are together with the sandwiched rock-sample in between, sealed by an enveloping soft PVC-hose-piece. In order to avoid water escaping along the walls, this cell is put into an aluminum tube. This tube can be mechanically pressurized. The inlet is connected to a burette, which is equipped with a valve. Before putting the samples into the sleeve, they were saturated during 3 days with tap water. In order to avoid air bubbles within the samples, saturation took place by capillary forces, thus the samples were not fully immersed. The outlet of the cell is connected to an overflowing container in order to keep the hydraulic head constant. Carbonates in general exhibit a large range of permeability, which is difficult to assess with a single setup only. Thus, depending on the permeability of the sample, long and narrow or rather short and thick burettes were

used in order to optimize the test. Some samples were measured overnight by using a camcorder, shooting an image of the falling water column every 10 minutes. The following relationship provides permeability from the falling head test:

$$k = 2.3 \frac{C}{(t_e - t_0)} \log \frac{H_0}{H_e}$$

C is a geometrical factor containing the diameters of the sample and the burette and the length of the sample. The time t_e corresponds to the height H_e of the water level in the burette, with respect to the constant head at the outlet. Permeability for each sample was determined by graphically fitting a straight line through (t_e-t_0) versus $\log(H_0/H_e)$ on a semilog-plot (Lang et al., 2003). The good fits for high permeable as well as for low permeable samples indicate, that no losses occurred between sample and the enveloping sealing (Figure 59).

A II.   Sample preparation and preprocessing of the digital images

The blocks for thin sections have been cut out in such a manner that the rectangular plane represents a vertical section through the formation with the length vertical to the borehole axis and the width parallel to the borehole axis. In the horizontal plane, the thin section is not oriented. The vertical section allows for studying the porosity structure and sedimentary fabric, which occur between the bedding planes and is not considering features occurring on a bedding plane as much. The thin sections were cut in the lab of the Geological Institute at ETH Zurich with special micro-saws, in order to produce artifact-free slices. Samples with very low cementation were rigidified by using an inviscid epoxy resin. Some samples were stained with blue epoxy under vacuum in order to highlight the accessible pore space. However, the intrusion of the colored resin in most cases remained incomplete and could not provide any additional information about the 3D-pore structure. The thin sections were then polished with a 3 µm special grinding powder in order to make the samples available for the ESEM as well.

Several tests with polarized and non-polarized scans revealed, that the latter is much more precise in displaying the exact 2D-pore structure at that scale of investigation. Thus, for the thin section scans (TSS) a commercially available flatbed scanner from Epson was used, which yielded sufficient resolution for pores with sizes down to 20 µm. ESEM-images in turn were obtained with and FEI Quanta 600, located at the Institute for Building Materials of ETH. The composition contrast images yielded a non-destructive display of the micropores (<20 µm). In order to produce comparable results for both image types, size and resolution were standardized. The TSS covers an area of 15x20 mm at a resolution of 2400 dpi and the ESEM-image exhibits a size of 110x130 µm at a resolution of 399'000 dpi.

For digital image analysis on pc-systems, two main software packages are available in the public domain, namely *ImageJ* and *ScionImage*. For mac-based systems *NIHimage* or *SXM175* are available. The user friendly *ImageJ* has been chosen for standard DIA like segmentation, pore size distribution and orientation imaging. *SXM175* is very useful for the autocorrelation function (ACF) for which several macros were available. Below the segmentation of the images is described in detail.

The images were first scaled in order to obtain real metric values for the output. Then they were set to 8-bit, which is necessary for the threshold process. The threshold proved to be a critical process for the assessment of the pore space. In order to extract the porosity

information from the original Tiff-image correctly, a simultaneous manual comparison of the true image and the thresholded image at a high magnification (300%) was necessary. When the representation of the pore boundaries was satisfying, the threshold was applied, which converts the original image into a binary image, with the pore space in black and the matrix in white. For the porespace of 15x20 mm TSS, automated procedures did not yield reliable results. In a plane polarized image the pore space appears in a dark color. Here special attention has to be paid on the Mg-calcite-fossils, like for example red algae and forams, which as well appear quite dark and which should not account for porosity. This problem does not occur if non-polarized images are analyzed. The pores appear white and most of the matrix is much darker. However, for some samples only an incomplete staining with blue dyed epoxy has been achieved, which caused serious difficulties in capturing the whole pore space, since the contrast of the stained pores compared to the non-stained pores is not as optimal anymore. Thus, the thresholding had to be divided into two parts, the white non-stained pores and the blue stained pores have been thresholded individually and the resulting binary images were finally stacked. The precision of the above described thresholding is in the order of ±10%.

For ESEM-images the approach had to be adapted a little bit in order not to capture too much badly resolved background information. Again the image is thresholded in a conservative manner from low to high but without any zoom into the image. The main problem of precisely hitting the pore boundaries is caused by the depth information (3D-effect), which results in gradual matrix-pore transitions and therefore in a disturbing haziness. This effect leads to a lower precision of the TOP-values in the order of ±15%. The brightness distribution histogram of TSS is usually bimodal or at least shows a flat, followed by a clear rise of the curve. The brightness distribution histogram of ESEM-images in contrast is usually very flat and in most cases no real peak can be recognized. This is the main reason for the differences in precision. Thus, in order to mitigate the problem of inappropriate thresholds for ESEM-images, finally an overall threshold value, coupled with the integrated TOP and plug porosity proved to be the best choice. The automated approach for ESEM-images yielded a much better fit for the cross-correlation plug porosity versus TOP and will be presented below in AIII.

The next step after thresholding consists in filtering the binary image appropriately. In general at least a median filter with a radius of 1 pixel is applied, which reduces the noise by replacing each pixel with the median of the neighboring pixel values. The resulting effect is that isolated single pixels within a larger pore or within the matrix are eliminated. Additionally the pore boundaries are smoothed this way. In order not to cause too many artifacts by excess filtering, the median is applied only once. After the filtering, a complete suite of measurements has been performed on the pores, such as pore area, perimeter, orientation and axial ratio of the fitted ellipse and Feret's diameter.

A III.   Comparison of integrated TOP and plug porosity and the consequential automated assessment of microporosity

The first approach was to assess macroporosity from plane polarized images and with individual thresholding for TSS and ESEM-images both. The result of the crossplot total plug porosity versus TOP seems to be quite confusing (Figure 60A). Till about 35% porosity the samples follow quite well the ideal straight line - they rather lie a bit too high. An overestimation of the optical porosity can be explained by too high thresholding values for the solid. Above 35% TOP is remarkably underestimated, compared to the physically measured total porosity on 1inch mini-cores, it even seems that TOP cannot exceed 35%. If no scale

effects occur and the thin sections would originate from exactly the same location as the plugs, the two porosities should plot approximately on a 1:1-line. Of course the optical and the physical method are measuring different properties, which should finally lead to the same prospected value. Since insufficient resolution of ESEM-images and immobile water, which despite the drying at 80° remained within the 1inch mini-cores both lead to an underestimation in total porosity, the observed scattering on the graph cannot be explained this way. A scale effect can be dismissed, since the thin section and the 1inch mini-core are covering a similar scale of investigation and furthermore a scaling effect would most probably result either in a constant under- or overestimation of the values. Thin section and 1inch mini-core are not from exactly the same location but at least from the same half core piece, which covers a certain rock type within a lithofacies type. Thus, no lithological or significant structural changes should occur within a set of thin section and corresponding 1inch mini-cores. The systematical error, which appears for higher porosity, must be due to an inappropriate segmentation procedure. Back-checking the thresholding procedure for macroporosity revealed a clear underestimation of the TOP under plane polarized light, since the polarized pores, especially the smaller ones, appeared smaller than with non-polarized light only. Furthermore, under plane polarized light thin sections, which are partially stained with blue epoxy, caused some problems in incorporating the colored pore space into the complete binary image.
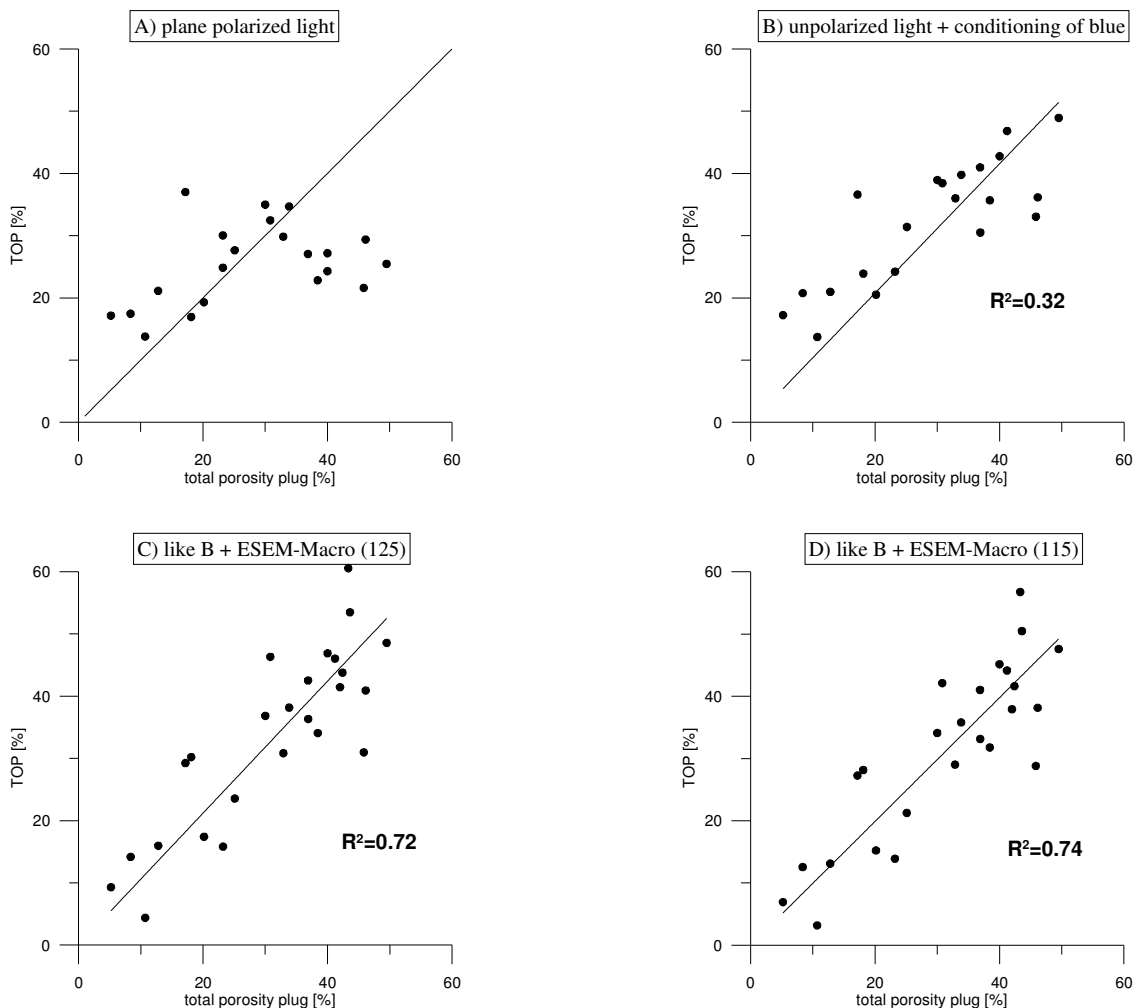

Figure 60:   Determination of TOP by using thin section scans of plane polarized light (A), by using scans of non polarized light and conditioning of the blue component (B), as before but with an automated procedure for microporosity and an overall threshold of 125 (C) or 115 (D).

Thus, a more appropriate approach of assessing the optical pore space on thin sections was developed. The thin sections preliminarily are scanned on the Epson scanner Photo 3200 under non-polarized conditions and at a resolution of 2400 dpi. Then the white and the blue stained pore space are thresholded separately and stacked. In order to extract the blue color from the thin section, the scanned image has to be preconditioned with *Photoshop* first, where the original image is put into 8-bit mode. Then the blue color range is selected, the image inverted and overlain with a quick mask. If the blue color exhibits a sufficient contrast, the background can already be subtracted from the image. Otherwise the blue color can be highlighted by selecting it and enhancing its density and again the blue color range is selected. This procedure goes on, till the contrast of the blue color is high enough. Normally one or two cycles are required. The blue image extracted this way exactly represents the pore space of the thin section, which is stained with blue epoxy and it can be thresholded in the same way, like the white pore space. The two resulting binary images are then stacked within *ImageJ*, creating the real binary image of the porosity. The resulting images revealed to be much closer to the real pore space, since the incomplete staining was not a restriction of the method any more.

The cross-plot plug porosity versus TOP shows that the right approach has been chosen (Figure 60B). The points plot much better on a straight line, which goes through the origin and the systematical error has gone. However, there still seems to be a slight overestimation of TOP at low porosities and an underestimation at high porosities. This phenomenon has also been observed by Anselmetti et al. (1998) who explained it by non-representative fields of view under the microscope. In that study thin sections have been taken from the plugs directly, however the spread of the data is not significantly lower than in the present study. Here the fit has been forced through the origin and exhibits a slope of a=1.04, which is acceptable but the covariance R^2=0.32 is rather low. Note that the ESEM-images still have been thresholded manually in this plot. The way to do it better could be found in a better assessment of the ESEM-microporosity, which till now caused some problems due to the inherent depth information of the composition contrast images. The uncertainty in where to set the threshold in combination with the fact that the raw ESEM-images exhibit the same illumination and are in an 8-bit gray-level format, calls for an overall threshold. Furthermore, digital image analysis on ESEM-images exhibits a low reproducibility, being a further reason for a more reliable technique.

A simple macro has been written within *ImageJ* in order to automate and unify the segmentation process of the ESEM-images:

```
run("Set Scale...", "distance=2027 known=130 pixel=1 unit=Mm global");
setAutoThreshold();
//run("Threshold...");
setThreshold(0, 125);
run("Threshold", "thresholded remaining black");
run("Median...", "radius=2");
run("Select All");
run("Set Measurements...", "area perimeter fit circularity feret's redirect=None decimal=4");
run("Analyze Particles...", "minimum=1 maximum=999999 bins=20 show=Nothing display exclude clear");
run("Histogram");
```

The ESEM-image is scaled, thresholded at gray-level 125 (value between 0 and 255) and filtered with a Median radius of 2. The threshold has been chosen from several runs on different images. The Median radius was set to 2, since a higher scattering is present on these images and most of the boundaries are transitional and quite fuzzy. Then a similar analysis is carried out, like for macroporosity. The database is generated in μm, considering 4 decimal

places and excluding edge particles. It is used for shape analysis and pore size distribution. For the calculation of anisotropy by rose plots, particles smaller than 16 pixels (0.3 μm pore size) have been removed in advance from the raw file, in order to avoid anomalous angle calculations.

From several runs visually a threshold of 125 has been evaluated (Figure 60C). The slope of the fit is a=1.06 and the R^2=0.72, which stress the much better fit than before. However, the average for the x-values (plug porosity) is 31.0% and the average for the y-values (TOP) 33.5%. Ideally both averages would lie at 31.0%. If we assume that the optical macroporosity was evaluated correctly and that the plug porosity and the TOP theoretically should plot on a straight line with slope a=1, the ESEM-threshold can be adjusted in a manner, that both averages lie at 31.0%. Several iterations resulted in a threshold of 115 for which R^2 increases slightly to 0.74 (Figure 60D). The visual comparison of the two cross-plots C and D does not reveal a significant difference, but the choice of the threshold has now a clear meaning and is not chosen arbitrarily any more. Although there is a certain scatter of the data, the optical method fits the physical data reasonably well. Most part of the misfit between plug and thin section data is likely to be caused by the heterogeneity of the rock on the dm- and cm-scale. With the described method even at highest porosities of 40% or more, no clear under- or overestimation of TOP can be recognized. This data set thus provides a well defined and thoroughly elaborated basis for further data analysis.

A IV.   Assessment of anisotropy and heterogeneity by using the ACF

The ACF is a two dimensional function, related to the average shape that occurs in the fabric. This function is a portrait of how well the image correlates with itself. Visual textures show a clear signal in the ACF, which is a powerful tool for doing shape analysis and assessment of isotropy, symmetry, size, shape and orientation. As described in Heilbronner (1992) the ACF is defined by an equation, which contains the brightness function and the discrete coordinates x and y of an image and it is calculated using the Fast Fourier Transform (FFT). In order to make use of the FFT algorithms, the image has to be transformed to a square matrix of 2^nx2^n size. In the original image a given coordinate point (x,y) denotes a position, whereas in the ACF, a given coordinate point (x',y') denotes the endpoint of a neighborhood vector, and the value of the ACF at a given (x',y') denotes the correlation of all image points (x,y) with all neighborhood points that are located at (x+x',y+y'). It is common practice to represent the ACF with the origin placed in the center. Thus, the ACF-image is showing maximum correlation in the center, which is expressed by a peak (gray-level 255). The correlation decreases from the center towards all directions. For circles or isotropic fabrics in general the rate of decrease of the ACF values away from the origin is the same in all directions, thus the contour lines are circular.

We first consider the central peak inside the lowest contour line, which already grades into the background correlation. The resulting image shows a peak in the center, because for short distances (if we start in the center) the correlation is best. If the nucleus in the center is circular the pores of this shape are isotropic, therefore no preferred orientation is present in the pore structure. The concentric shape shows the anisotropy behavior for different pore sizes. It can occur that at smaller pore sizes the structure is isotropic, but not at larger pore sizes. A dominance of elongated and oriented larger pores is expressed in the ACF-image as an elliptical shape of the nucleus in the outer region. The size of the nucleus is already a hint for the dominant pore size (DPS), which is more or less an average pore size and shape within the image. At 8x magnification the nucleus can be studied in more detail. Since porosity and matrix correlate to each other, they also show the same autocorrelation. If the image is set to

gray-scale, it can be thresholded continuously, which revealed, that an isotropic behavior on the overall scale can be the integrated result of several anisotropies for different pore sizes. Thus, it shows as well the scale-dependency of anisotropy.

Especially for non-elliptical pores, the shape of the contours may not always represent correctly the average pore shape. For rectangular pores for example, rhombic contour shapes can occur due to the better correlation parallel to the sides of the rectangles. The identical effect can be observed on rhombic pores, where rectangular contour shapes can occur. Thus, for non-elliptical shapes, the relation between ACF contours and shapes of fabric components ceases to be one of geometrical similarity. However, the axial ratios and diameters derived from the ACF contours are still correct. In the discussion of the ACF data, the shapes of the pores thus should not be considered.

If a profile through the center of the ACF-image is taken, the width of the peak at 39% of the 255 gray-levels yields qualitatively the diameter of the DPS (Figure 61). According to Heilbronner (1992), this is the appropriate level for closely packed spheres. The contour for which the diameter is exactly equal to the diameter of the circle is at 39% of the maximum ACF. The DPS can also be determined exactly by thresholding the ACF at 39%. The particle in the center of the resulting image is characteristic for the dominant pore size and under the aforementioned circumstances as well for the pore shape of the considered area. The axial ratio b/a and the orientation Φ of the contour at 39% are a measure for the axial ratio and the preferred orientation of the fabric anisotropy.
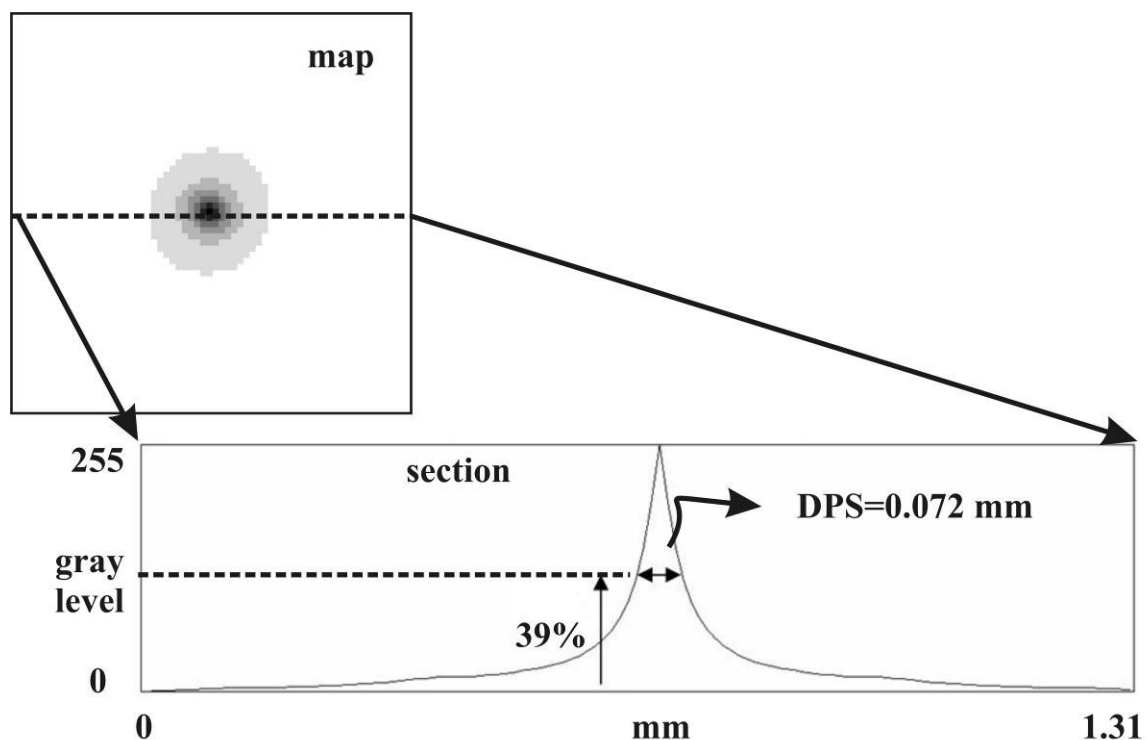

Figure 61:   DPS is determined from the ACF-image by thresholding at 39% of the whole gray-level spectrum, which is the appropriate level for closely packed spheres. Alternatively a profile through the nucleus can be sliced at 39%, which as well yields shape and size of the dominant pore size. The width of the peak at 39% is equal to DPS.

A V.   StripStar for assessing the volumetric pore size distribution

With *StripStar* the 3D volumetric histogram V(R) is calculated, a representation, which is much more useful for physical interpretation, than a numerical density histogram only (Figure 62A). The underlying concept of *StripStar* is simple and it will be briefly introduced here. For more details the reader is referred to Heilbronner (2002b). The measured size distribution of sectional circles h(r) is compared to one that would be obtained, if the size distribution of spheres h(R) were the uniform distribution, which means equal probability for each sphere (Figure 62B). The uniform distribution h(R) is composed of lots of individual monodisperse distributions with the same probability, which summed up yield the distribution of sectional circles h(r). The hump-shape of the distribution h(r) arises from the fact that larger spheres are more likely to be cut than smaller ones, and for an individual sphere, which is randomly cut by planes, the probability of large sectional circles with a radius close to the sphere radius is higher. This "ideal" size distribution will be denoted $h(r)_u$. The measured distribution h(r) is worked off from the largest to the smallest class. The largest size class of spheres is at the same time the largest possible class of sectional circles ($r_{max}=R_{max}$). Starting at the largest value of h(r), a unit starting proportion of spheres is created with a radius $R_k = R_{max}$. The size distribution of sectional circles $h(r_k)$ pertaining to this largest class of spheres is calculated and "stripped" from the measured (total) distribution h(r). As a result the remaining h(r) is zero for $r=r_k$. The remaining h(r), in particular, the remainder of h(r) in the next lower class, r_{k-1}, is analyzed next (Figure 62C). The value $h(r_{k-1})$ is divided by the theoretical value of the "ideal" $h(r)_u$ at this point and a proportional fraction of R_{k-1} is set aside. Again the size distribution pertaining to the proportion of R_{k-1} is stripped off the remaining h(r). By repeating this procedure down to the last, smallest size class, the entire distribution h(r) is stripped to zero. Classes, which dropped below zero are denoted as antispheres and are a hint for the reliability of the calculated distribution of spheres. Note that after each stripping, the measured distribution of circles is slightly modified and the former r_{max} becomes zero.
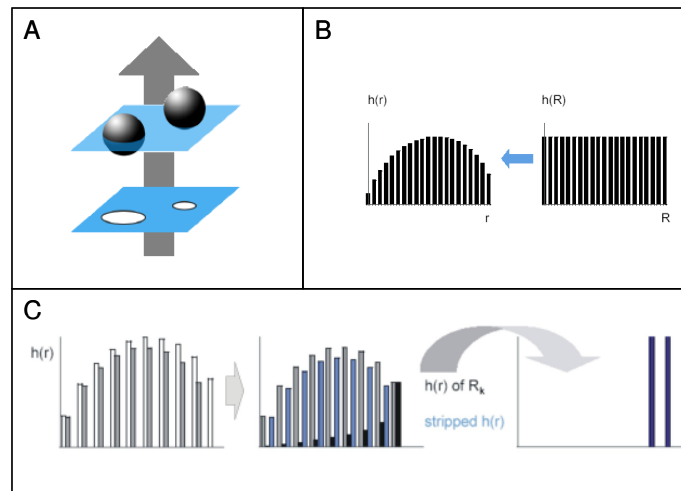

Figure 62:   Basic concept of StripStar – from 2D sectional circles to spheres (A), comparison of uniform distribution of spheres to measured distribution of sectional circles (B), functioning of stripping process for second step (C), (after Heilbronner, 2004)
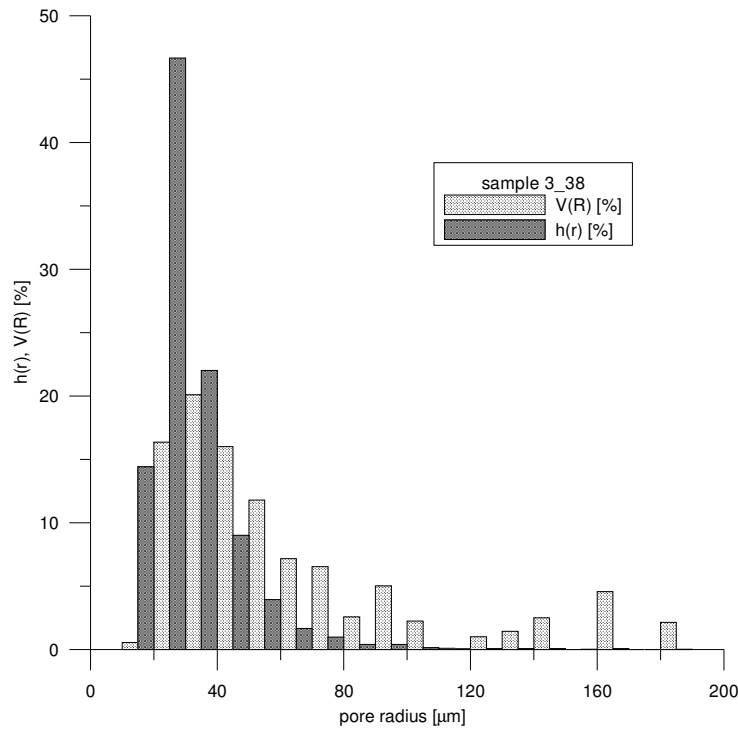
Figure 63:   Example for effect of program StripStar with original distribution of sectional circles h(r) on thin section and calculated volumetric distribution of spheres V(R) in the rock.

An example of how different the distribution of sectional circles and the volumetric distribution of the spheres can be is given in Figure 63. The combined graph stresses the importance of analyzing the volumetric distribution for petrophysical interpretation of the rock matrix. A small number of large pores can have a significant effect on the volumetric distribution. The procedure for evaluating the pore size distribution of the samples will be described and discussed in the following paragraph.

First of all the binary image has to be scaled to pixels. Perimeter and Area are measured with the software *ImageJ* for all pores of the TSS, except for edge particles and pores smaller than four pixels. For each individual pore the equivalent radius r_{eq} is calculated adding up area and perimeter in pixels, since the perimeter-ring is missing in the measured area. Consequently the equivalent radius calculates to:

$$r_{eq} = \sqrt{\frac{A + P}{\pi}}$$

where A is the area of the pore and P the perimeter, both in pixels. Then within *Grapher* the dataset of r_{eq} is grouped within a histogram into 20 classes of constant width (1, 2 or 4 pixels). Depending on the range of the equivalent radius, the data is grouped into a histogram and the frequencies are the input data for *StripStar*. The output of *StripStar* yields for each class of r_{eq} the frequency of particles in the thin section h(r)(%), the frequency of particles in the rock h(R)(%) and the volumetric percentage in the rock V(R)(%). Additionally the numeric, respectively the volumetric density of the antispheres in the rock (h*(R)(%) respectively V*(R)(%)) are calculated, which are a measure for the reliability of the calculated distribution. The data of biggest interest is V(R)(%), which represents the 3D volumetric pore size distribution in the rock matrix. This data is again imported into *Grapher*, where r_{eq} is scaled from pixels to µm.

The above described procedure has been performed on all available samples. The whole range of pore sizes (>20 µm) has been analyzed by adapting the number of bins for each individual sample. For all distributions always the midpoint of each class was taken as a reference. For example class 0-2 is referred to the midpoint of 1, class 2-4 is referred to the midpoint of 3 and so on. Data from microporosity (pores<20 µm) has not been incorporated into the dataset, since it would disturb the distribution in a non convenient way - such as total overflow of the small pore classes! Thus, data from microporosity has been analyzed in a similar way like macroporosity but separately.

A VI.   Statistical parameters of volumetric pore size distributions

Despite the fact that for carbonates no general distribution model can be found, the statistical parameters can have a certain meaning without the basis of a statistical model. In this paragraph the statistical parameters, which describe the volumetric pore size distributions, are presented and the weighted formulas will be given.

The mean is the arithmetic average of the data values. For the distribution it has to be weighted:

$$m = \frac{\sum (V(R)_i\, r_i)}{\sum V(R)_i}$$

where $V(R)_i$ designates the volumetric percentage of the pore class within the rock and r_i is the corresponding equivalent radius. The median describes where 50% of the data lies and is not dependent on the values. The median is much more pronouncing unequal distributions concerning the abundance than the mean. The mean is weighted with the frequency and therefore much more sensitive to high values at high r_i. However, a high mean in most cases correlates with a high median, since high means are generally obtained if high frequencies are abundant at high r_i, but a high mean can also be produced by high frequencies at lower r_i.

The dispersion or the width of a distribution is given by the standard deviation σ. The standard deviation is the square root of the variance and yields information about the spread of the data. It is given by the following equation, where m designates the mean:

$$\sigma = \sqrt{\frac{1}{n\sum V(R)_i} \sum V(R)_i\,(r_i - m)^2}$$

In geologic terms a grain size distribution with a relatively small standard deviation is called well sorted. One with a large standard deviation, e.g. with a wide spectrum of grain sizes is called poorly sorted or well graded. Porosity in general decreases as sorting becomes poorer, since the large pores, which would result from densely packed grains of equal size only are filled up with smaller grains. The main assumption for siliziclastic sediments is that grain size distribution correlates to porosity distribution, thus a rock with a well graded grain size distribution presumably is less permeable than one with a well sorted grain size distribution. This assumption is not valid for carbonates, where the pore system is controlled by secondary processes, like dissolution and cementation, rather than by grain size only.

The coefficient of skewness designated here as CS, is a statistic used for summarizing the symmetry of a distribution. It suffers from its sensitivity to erratic high values. More

important than the absolute value is the sign, which if positive indicates a flat slope of the distribution towards the right and if negative indicates a flat slope towards the left:

$$CS = \frac{\frac{1}{n\sum V(R)_i} \sum V(R)_i (r_i - m)^3}{\sigma^3}$$

A negative CS indicates that the lognormal distribution is not the correct model for this type of rock. It furthermore indicates that there is a population of large macropores, which do not follow the usual pore size distributions. These pores in most cases are of moldic or vuggy origin.

The coefficient of variation CV is a statistic that is often used as an alternative to skewness in order to describe the shape of the distribution. It is more or less a normalized measure of spread:

$$CV = \frac{\sigma}{m}$$

This measure of spread combines the effects of standard deviation and mean and is supposed to show a behavior, which is inverse proportional to the permeability of the rock matrix.

A VII. Induction sonde - correction for skin effect and the geometric factor
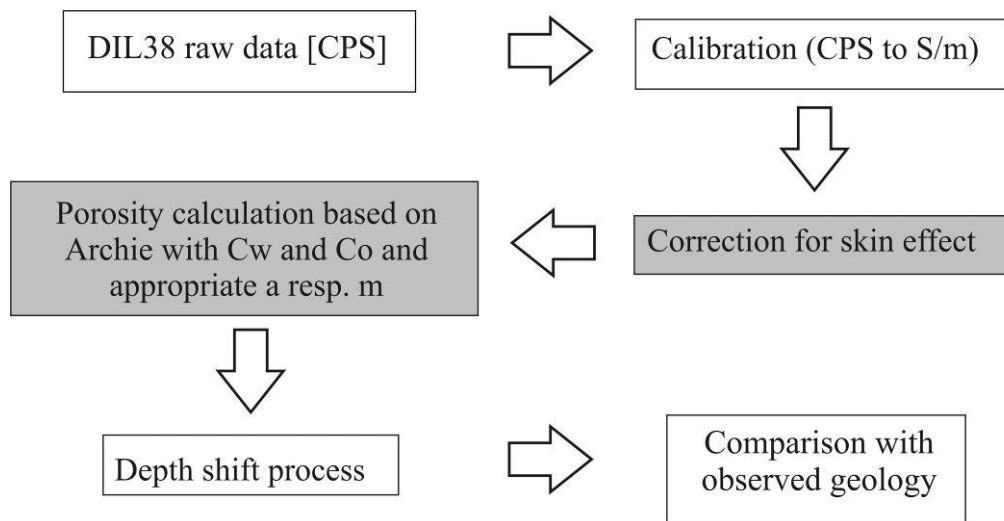
Figure 64:   Flowchart of log-processing for DIL38 induction logs.

Several steps have to be performed for the analysis of logging data from the DIL38 induction sonde on porosity of which only the correction for skin effect and the method for the porosity evaluation will be presented in the appendix (Figure 64). The correction of the induction signal for the skin effect is in fact a propagation correction for the electromagnetic waves, which travel through the formation and has nothing to do with the mud cake or hydrogeological skin effects. In order to understand the correction, one first has to know the skin depth. Skin depth δ is defined as:

$$\delta = \left(\frac{2}{\mu\omega C} \right)^{\frac{1}{2}}$$

where $\mu = 4\pi\text{E-7}$ H/m is the magnetic permeability, ω the circle frequency ($\omega = 2\pi f$) and C the conductivity in S/m. The skin depth is a measure of distance to which an electromagnetic wave will penetrate. It is defined as the depth at which 63% (1-1/e) of the emitter signal amplitude has been attenuated. The more conductive the medium, the larger the currents and the shorter the distance over which the disturbance can propagate. For a two-coil tool in a homogeneous medium, the solution of Maxwell's equations in the simplified form (first term of series expansion) is:

$$C_a = C\left(1 - \frac{2L}{3\delta} + ... \right)$$

where C_a denotes the apparent or measured conductivity and L the spacing of the coils. This correction is fairly insensitive to variation in resistivity of the invaded zone (Hearst et al., 2000). The correction remains valid within 5% of the measured signal for $L/\delta <= 0.65$. The used DIL38 has a coil spacing L for short spaced of 0.51 m and an operating frequency f of 39'063 Hz. On our site at Mallorca, measured values are ranging from 2'000 µS/cm to 8'000 µS/cm. If we calculate skin depth and- correction for these values, we get the following:

C_a [µS/cm]	δ [m]	C [µS/cm]	C_a/C	correction %
2'000	5.69	2'128	0.94	6
8'000	2.85	9'091	0.88	12

L/δ is much smaller than 0.65 and therefore the first order correction is valid and enough precise. The table shows clearly that at higher conductivities more of the signal is lost and thus a higher correction is required.

The important question, from which part of the formation the signal originates is answered by the geometric factor. For a two coil tool in a homogeneous isotropic formation of infinite extent, every sector contributes 0.1 to the total signal (Figure 65A). The resulting total signal is weighted through the geometrical factor. The geometrical factor for each elemental loop (g) can be expressed in terms of radial (r) and vertical (z) distance relative to a plane passing through the mid point between emitter and receiver:

$$g = \frac{L}{2} \frac{r^3}{[r^2 + (\frac{L}{2} - z)^2]^{3/2}[r^2 + (\frac{L}{2} + z)^2]^{3/2}}$$

The multiplier L/2 is introduced to normalize the integration of g from $z = -\infty$ to $+\infty$ to a dimensionless unity. The total receiver signal E is then:

$$E = K[C_A G_A + C_B G_B + ...]$$

where

$$G_A = \iint_A g \, dr \, dz$$

$$G_B = \iint_B g \, dr \, dz$$

K is a constant for the sonde configuration (Serra, 1984). The induction log is a measurement of E/K, which is the apparent conductivity of the formation C_a. The signal from each elemental loop will be proportional to its conductivity, weighted according to a geometrical factor, which depends on the position of the loop relative to the tool. The geometrical factor G is the fraction that each zone contributes to the total signal:

$$C_a = C_A G_A + C_B G_B + ...$$

where

$$G_A + G_B + ... = 1$$

In the radial direction the major part of the electromagnetic field propagates within a radius L/4 to L, L being the coil spacing (Figure 65B). For the DIL38 sonde the short spacing is 51 cm, consequently the signal originates mainly from the zone between 12 and 51 cm. Out of 1 m from the sonde axis the contribution is already very small. The vertical definition is in the same order of magnitude as the spacing. Therefore beds thicker than 50 cm are hardly affected by the adjacent formations. These relationships are only valid for coil spacing much less than skin depth (L/δ <<1).
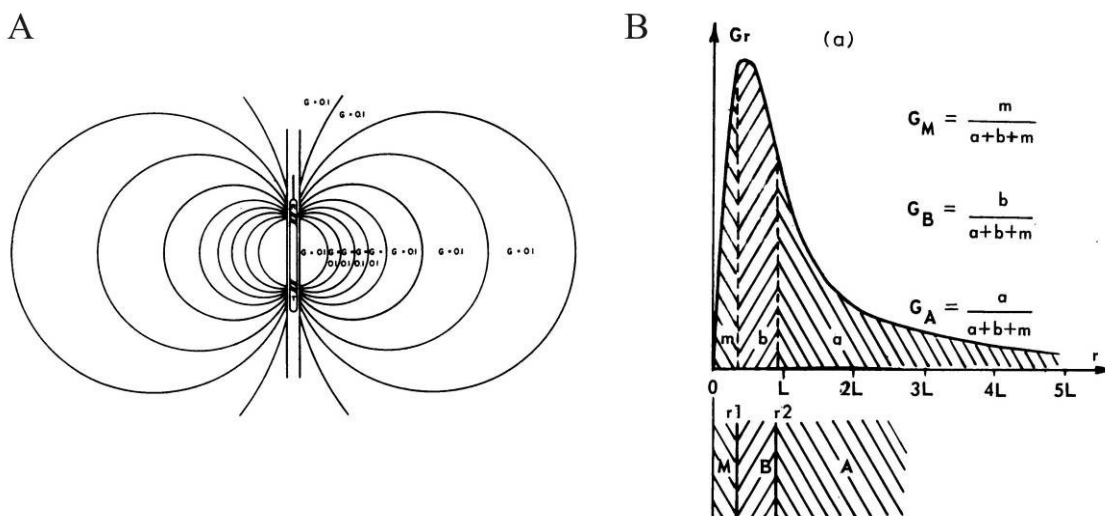

Figure 65:   For a two coil tool in a homogeneous isotropic formation of infinite extent every sector contributes 0.1 to the total signal (A). In the radial direction the major part of the electromagnetic field propagates within a radius L/4 to L, L being the coil spacing (B).

A VIII.   Porosity evaluation from induction logs

Total porosity can be determined in the water saturated part of the borehole, where induction log and fluid conductivity log both are available. If we know the formation and fluid resistivity or conductivity, porosity can be determined using Archie's law:

$$F = \frac{R_0}{R_w} = \frac{a}{\phi^m}$$

where F is the formation factor, R_0 the specific resistivity of the formation and R_w the specific resistivity of the fluid. The parameters a respectively m are to determine empirically; m is also designated as cementation factor. Nowadays the factor "a" is not used anymore and commonly set to 1. Therefore especially the cementation factor is crucial and porosity reacts extremely sensitive to this factor. According to Schlumberger, the proper choice is best determined by laboratory measurements or experience in the area. In the absence of this knowledge, a possibility in finding an appropriate cementation factor m is provided by the mixing rules. If we combine the spectra for water with the dielectric properties of dry rock, we should be able to predict the resulting properties of saturated rock. At present there exist two generally accepted mixing models for complex conductivity, the equivalent medium model and the complex refractive index model. Both models reduce to Archie's equation at low frequencies (Hearst et al., 2000). Here we just have a quick look at the first model. An approximated form of the original Bruggeman-Hanai-Sen (BHS) equation, which describes the equivalent medium model is given by Bussian (1983), which is:

$$C_o = mC_{ma}(1-\phi^m) + \phi^m C_w$$
$$\text{for}$$
$$C_w > C_o > C_{ma}$$

where C_o is the formation-, C_{ma} the matrix- and C_w the fluid conductivity. The factor m is comparable to the cementation factor of Archie's equation. Thus, if we know porosity from lab tests and have measured values for C_o and C_w at a certain depth, with the C_{ma} given from literature, we can calculate an appropriate m-value. C_{ma} for calcite lies between 0.1-50 μS/cm, which is the whole range, found in several references. We rewrite the equation above:

$$C_{ma}m - C_{ma}m\phi^m + C_w\phi^m = C_o$$

Due to the low C_{ma}, the first two terms only contribute less than 1% to the m-value. Consequently they can be neglected and the determination of m simplifies to:

$$m \approx \frac{\log\left(\frac{C_o}{C_w}\right)}{\log\phi}$$

This is exactly Archie's equation with a=1. This approximation is valid for high formation conductivities. As a preliminary conclusion the m-value can be determined this way but only accurate enough in the high conductivity range, which at the test site is accomplished for the lower parts of the talus. Calculations with plug porosities in the distal talus, where no mixing-zone-effects occur anymore and where porosity at the rock-matrix-scale is homogeneous and

comparable to the scale of investigation, as the induction probe records the formation, yielded cementation factors around 1.8.

A IX.   FWS logs - first arrival picking and porosity evaluation

There exist three different ways for the first arrival picking of the p-waves. One possibility is the automated picking built in the logging tool. The advantage is that it yields data every two centimeters on the four transmitter-receiver pairs and thus the probe can be used in a compensated manner. The disadvantage is that there is no control on the picking quality and on the picking algorithms. Another possibility is the manual picking of the p-wave transit time on the full-waveform record. The advantages are the picking in a fully controlled manner and the possibility to visually compare the waveform of both transmitter/receiver pairs. The disadvantages are the time consumption of this procedure and the use of the tool in a non-compensated manner. The third way is the automated picking within the software *WellCAD*, using features of the p-wave transit-time on the full-waveform record. The advantages are the low time consumption and the control on the picking algorithm. The disadvantages are the inherent uncertainty of such an automated picking and the not considered information about the tool-compensation.

The coherence of the automated picking included in the logging tool has been checked for the TX1-RX1 transit time and TX1-RX2 transit time by a visual comparison with the full-waveform. The curves of first arrivals did not well correspond to each other on MC4 and MC5. The manual picking has been performed by comparing both full-waveforms (RX-3 and RX-5) and by picking similar features on both waves. The chosen picked feature is the first compressive peak on both waves that not necessarily coincides with the first deviation of the non-vibrating state. This picking is not trivial at all and it is often hard to determine a coherent transit-time for both waves. For the automated picking within *WellCAD*, an advanced threshold pickup algorithm has been chosen, with a blanking of 200 μs, a small window width of 20 μs, a large window width of 200 μs and ratio threshold of 2.

For the velocity calculation transit-time values from manual picking and values from automated picking have been used and compared. For the two boreholes MC3 and MC5 the two picking methods yielded comparable velocity profiles. Confidence for large peaks is not as high as in zones with moderate values. Manual picking in such zones is complicated by diffuse first arrivals and a high noise level.

Before starting to calculate porosities, the scale of investigation should be evaluated in order to know exactly, where the signal comes from. The signal, which arrives first at the receiver, is the fastest and it is linked with the longitudinal waves refracted at the critical angle. Thus, intuitively the depth of investigation should be in the order of few centimeters. However, lab experiments have shown that a thickness of at least 3λ is needed to propagate a pressure wave through several dm of formation (Serra, 1984). The sonic probe used in the present study operates at a frequency of 23 kHz. For carbonates velocities ranging from 1500 m/s for water up to 6500 m/s for the mineral calcite can be supposed theoretically, however the values for a young unburied reefal carbonate hardly reach this maximum. Thus, depth of investigation d is calculated as follows:

$$d = 3\lambda = \frac{3V_P}{f}$$

For the present study values ranging between 20 and 100 cm are obtained. The horizontal resolution is generally about the spacing between emitter and receiver, which in our case would be 40 cm. Thus, the sonic tool yields an averaged signal, which depending on the medium measured, originates from 20 to 100 cm from the borehole axis and it is capable to resolve layers down to a minimum thickness of 40 cm.

Due to high variability in texture, porosity and pore types, carbonates show a wide range of V_P-values. Calcite velocity at zero porosity is around 6500 m/s and changes to around 2000 m/s at porosities of 50% or higher (Anselmetti and Eberli, 1999). The measured velocities can be compared with the time average equation of Wyllie:

$$\frac{1}{V_{rock}} = \frac{1-\Phi}{V_{matrix}} + \frac{\Phi}{V_{fluid}}$$

This empirical equation states that the travel-time of an acoustic signal through the rock is the sum of the travel-time through the volumetric percentage of a pore phase filled by pore fluid plus the travel-time of volumetric percentage of the solid phase represented by a matrix velocity.

Sonic velocities in general have to be corrected for clay content and compaction of the clays, since clays lead to too low V_P or too high porosity. Within the saturated zone at the test site no clay occurs, except at karstified zones and sequence boundaries. Clay content of karstified zones is not measurable due to extensive core losses at these zones and sequence boundaries are thin and well constraint through gamma logs. Thus, no clay correction has been performed. As a consequence velocity, respectively porosity values at karstified zones and sequence boundaries might be biased. In the vadose zone clays and marls of inner lagoon are abundant, but the dry part anyway cannot be logged by the sonic tool.

A X.   The method of ATS and its resolution

The acoustic travel-time scan as described is operated at a resolution of 1-2 cm, depending on the data quality of the individual boreholes. Thus, for every borehole a specific threshold has been chosen, which is much easier to determine for high quality acoustic images than for data with a lot of noise. The shape of the histogram of normalized gray-level values versus frequency was the main criteria for the evaluation of the threshold (Figure 66). For boreholes MC2 and MC3 it was an easy task to separate the solid-rock-peak from the porosity peak. Good data quality is characterized by narrow and pronounced porosity peaks, which lack further populations of gray-levels and which are clearly separated from the solid gray-levels by a zone of zero frequency. The solid peak in turn is slim as well, with a median between 0.2 and 0.3 for the normalized gray-level values. Thus, for MC5 it can already be seen on the histogram, that data quality is much lower. The solid peak is wider, with a median around 0.4 and it was already quite difficult to find an appropriate threshold value, since the porosity peak is not separated anymore from the solid peak by a zone of zero frequency. Furthermore, the part right of the threshold belonging to the pore space is significant and a consequence of fuzzy transitions, which do not allow for an optical evaluation. For borehole MC7 additionally the distribution of the solid gray-levels became very wide and frequencies are low. The comparison with the optical televiewer revealed, that a processing with the ATS-technique for the dataset of borehole MC7 is not reasonable.
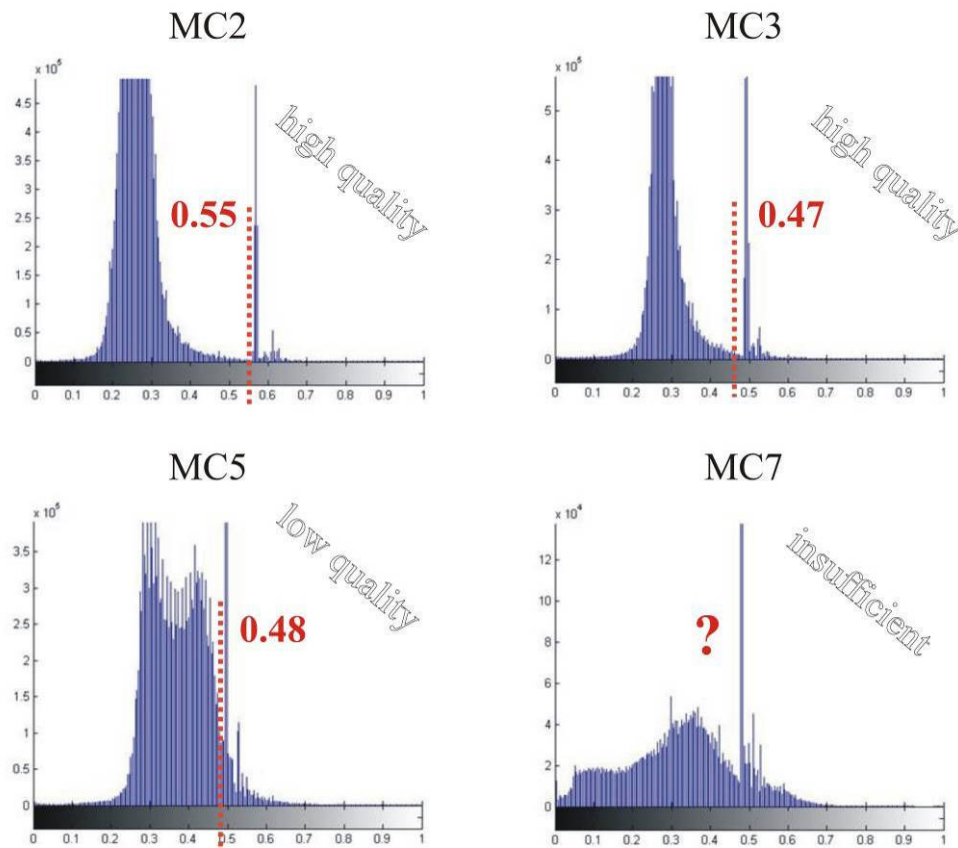
Figure 66:   Histograms of normalized gray-level values (x) versus frequency (y), illustrating the data quality of each individual borehole. For MC7 the distribution is too flat for a reliable automated procedure and thus has not been considered.

The advantage of this optical technique is, that many parameters like resolution, which is linked with the penetration depth, window size and sampling interval, can be adjusted and chosen quite freely providing a full control of what is recorded. However, as shown above, in order to record a reasonable porosity, the resolution of the scanning procedure has to be chosen appropriately on the histograms of the gray-level distribution. Here we want to evaluate the meaning of the threshold value, which depending on the borehole varies between 0.47 and 0.55. Furthermore, the accuracy of the method is illustrated by comparing the acoustic image to core and data from the optical televiewer.

For the evaluation of the resolution we recall the formula, which builds the basis within the *Matlab* script for the calculation of the threshold value (log):

$$\log = \frac{tt_{measured} - tt_{min}}{tt_{max} - tt_{min}}$$

For borehole MC3 tt_{min} is 90 µs and tt_{max} 201.9 µs, which at a threshold of 0.47 yields a $tt_{measured}$ of 142.6 µs. The tool-specific time window of 75 µs has to be subtracted, which finally yields 67.6 µs for distance 2b, b being the threshold distance (Figure 67). The borehole diameter (105 mm) and the tool diameter d (20 mm) define the ideal distance a from transmitter/receiver to the borehole wall. With the given fluid slowness of 672 µs/m, the acoustic wave needs 43.7 µs for the distance 2a. Distance c is the real depth of investigation. For this method it is more or less equal to the resolution. From the two-way travel-times of a

respectively b, c can be calculated, which is equal to 11.95 µs. Within the fluid this value corresponds to a distance of 18 mm. Thus, if the tool is ideally centered, features smaller than 18 mm cannot be resolved anymore. The advantage of this concept is that scattered noise, which is due to de-centered tool and artificial borehole roughness due to out-washing and scratches from the rotation of the drill bit, is mostly suppressed. Fortunately the next lower scale of investigation, represented by thin section scans (15x20 mm) or by 1inch mini-cores (25.4x40 mm), seamless hooks up to the ATS and thus the relatively low resolution is not a real disadvantage. As the cross-check to core and optical televiewer has shown, the larger features are precisely displayed on the binary image (Figure 67). The mold, which is clearly visible only on core but hardly on the optical BHTV, is not recorded accurately anymore with the acoustic BHTV and consequently is missing on the binary image. The large and the small open fracture above are both accurately displayed. The maximum caliper was deduced from the acoustic travel-times and provided a hint about the depth of the individual signals. It furthermore shows, which impact a shift of the threshold value has on the resolution of the ATS.
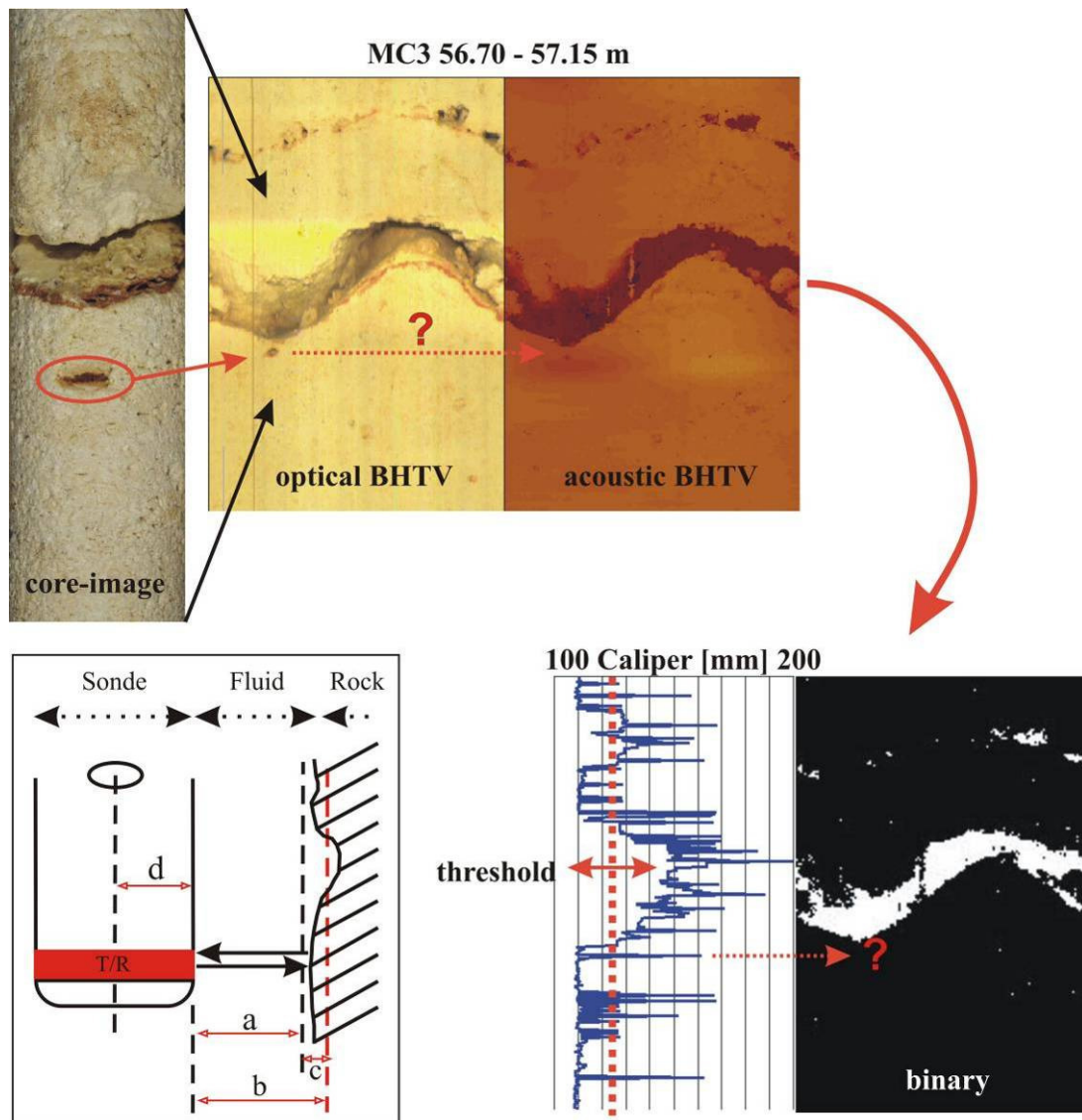

Figure 67:   Comparison of core image with BHTV-images and the resulting binary image. Fracture is open and covered with red stained sinter. For MC3 a penetration depth of 18 mm has been applied, illustrated in red at the calliper. The moldic pore (encircled) was not deep enough to be recorded by the ATS.

G)   Bibliography

Al-Hanai, W., S. D. Russell, and B. Vissapragada, 2004, Carbonate Rocks, p. 10.

Anderson, B., I. Bryant, M. Lüling, B. Spies, and K. Helbling, 1994, Oilfield anisotropy: its origins and electrical characteristics: Oilfield Review, v. 6, p. 48-56.

Anselmetti, F., and G. Eberli, 1993, Controls on sonic velocity in carbonates: Pure and Applied Geophysics, v. 141, p. 287-323.

Anselmetti, F., and G. Eberli, 1999, The Velocity-Deviation Log: A Tool to Predict Pore Type and Permeability Trends in Carbonate Drill Holes from Sonic and Porosity or Density Logs: AAPG Bulletin, v. 83, p. 450-466.

Anselmetti, F., and G. Eberli, 2001, Sonic velocity in carbonates - a combined product of depositional lithology and diagenetic alterations, *in* R. N. Ginsburg, ed., Subsurface Geology of a Prograding Carbonate Platform Margin, Great Bahama Bank: Results of the Drilling Project, v. 70: Tulsa, SEPM, p. 193-216.

Anselmetti, F., S. Luthi, and G. Eberli, 1998, Quantitative characterization of carbonate pore systems by digital image analysis: AAPG Bulletin, v. 82, p. 1815-1836.

Ardila, P. R., and L. Pomar, 2000, Upper Miocene Karst Collapse Structures of the East Coast, Mallorca, Spain: Acta carsologica, v. 29/2, p. 177-184.

Armstrong, A. K., P. D. Snavely, and W. O. Addicott, 1980, Porosity Evolution of Upper Miocene Reefs, Almeria Province, Southern Spain: AAPG Bulletin, v. 64, p. 188-208.

Baron, A., and C. Gonzalez, 1987, Hydrogeologia de la Isla de Mallorca, Palma de Mallorca, IV Simposio de Hidrogeologia. Servicio Hidraulico de Baleares, Palma de Mallorca (Spain), p. 83.

Baron, A., C. Gonzalez, and A. Rodriguez-Perea, 1995, Karst Hydrology of Mallorca, *in* A. Gines, and J. Gines, eds., Karst and Caves in Mallorca: ENDINS federacio Balear d'espeleologia, v. 20: Palma de Mallorca, p. 216.

Bear, J., 1979, Hydraulics of groundwater: New York, N.Y., United States, McGraw-Hill, 567 p.

Beard, D. C., and P. K. Weyl, 1973, Influence of texture on porosity and permeability of unconsolidated sand: AAPG Bulletin, v. 57, p. 349-369.

Bliefnick, D. M., and J. G. Kaldi, 1996, Pore geometry: control on reservoir properties, Walker Creek field, Columbia and Lafayette counties, Arkansas: AAPG Bulletin, v. 80, p. 1027-1044.

Brie, A., D. L. Johnson, and R. D. Nurmi, 1985, Effect of spherical pores on sonic and resistivity measurements: Society of professional well log analysts twenty-sixth annual logging symposium abstracts, p. 17.

Bristow, C. S., and B. J. Williamson, 1998, Spectral gamma ray logs:core to log calibration, facies analysis and correlation problems in the Southern North Sea, Core-Log Integration, v. Special Publications 136: London, Geolgical Society, p. 1-7.

Bussian, A. E., 1983, Electrical conductance in a porous medium: Geophysics, v. 48, p. 1258-1268.

Carozzi, A. V., 1995, Depositional models and reservoir properties of miocene reefs, Visayan islands, Philippines: Journal of Petroleum Geology, v. 18, p. 29-48.

Corbett, P. W. M., J. L. Jensen, and K. S. Sorbie, 1998, A review of up-scaling and cross-scaling issues in core and log data interpretation and prediction, Core-Log Integration, v. Special Publications 136: London, Geolgical Society, p. 9-16.

de Marsily, G., 1986, Quantitative hydrogeology: groundwater hydrology for engineers: Orlando, Academic Press, 440 p.

Eberli, G., F. S. Anselmetti, J. A. M. Kenter, D. F. McNeil, and L. A. Melim, 2001, Calibration of seismic sequence stratigraphy with cores and logs, *in* R. N. Ginsberg, ed., Subsurface Geology of a Prograding Carbonate Platform Margin, Great Bahama Bank: Results of the Bahamas Drilling Project, v. 70: Tulsa, SEPM special publication, p. 241-265.

Eberli, G., and R. N. Ginsburg, 1989, Cenozoic progradation of northwestern Great Bahama Bank, a record of lateral platform growth and sea-level fluctuations, *in* D. Crevello Paul, J. Wilson James, J. F. Sarg, and J. F. Read, eds., Controls on carbonate platform and basin development.: Special Publication - Society of Economic Paleontologists and Mineralogists, v. 44: Tulsa, OK, United States, SEPM (Society for Sedimentary Geology), p. 339-351.

Ehrlich, R., S. J. Cabtree, K. O. Horkowitz, and J. P. Horkowitz, 1991a, Petrography and Reservoir Physics I: Objective Classification of Reservoir Porosity: AAPG Bulletin, v. 75, p. 1547-1562.

Ehrlich, R., and S. Crabtree, 1984, Petrographic image analysis, 1. Analysis of reservoir pore complexes: Journal of Sedimentary Petrology, v. 54, p. 1365-1378.

Ehrlich, R., E. L. Etris, D. Brumfield, L. P. Yuan, and S. J. Carabtree, 1991b, Petrography and Reservoir Physics III: Physical Models for Permeability and Formation Factor: AAPG Bulletin, v. 75, p. 1579-1592.

Enos, P., and L. H. Sawatsky, 1981, Pore networks in Holocene carbonate sediments: Journal of Sedimentary Petrology, v. 51, p. 961-985.

Esteban, M., 1979, Significance of the upper Miocene coral reefs of the western Mediterranean: Palaeogeography, Palaeoclimatology, Palaeoecology, v. 29, p. 169-188.

Esteban, M., F. Calvet, C. Dabrio, A. Baron, J. Giner, L. Pomar, R. Salas, and A. Permanyer, 1978, Aberrant features of the Messinian coral reefs, Spain.: Acta Geologica Hispanica, v. 13, p. 20-22.

Flint, L. E., and J. S. Selker, 2003, Use of porosity to estimate hydraulic properties of volcanic tuffs: Advances in water resources, v. 26, p. 561-571.

Freeze, R. A., and J. A. Cherry, 1979, Groundwater: Englewood Cliffs, Prentice Hall, 604 p.

Fricke, S., and J. Schön, 1999, Praktische Bohrlochgeophysik: Stuttgart, Enke Verlag, 254 p.

Friedel, S., H. R. Maurer, M. Herfort, and N. Van Meir, 2004, Application of geoelectrical single-hole tomography to characterize a coastal aquifer, Zurich, ETH Zurich, p. 4.

Gines, J., and A. Gines, 1995, Speleochronological aspects of karst in Mallorca, *in* A. Gines, and J. Gines, eds., Karst and caves in Mallorca: ENDINS federacio Balear d'espeleologia, v. 20: Palma de Mallorca, p. 216.

Gingras, M. K., S. G. Pemberton, K. Muelenbachs, and H. Machel, 2004, Conceptual models for burrow-related, selective dolomitization with textural and isotopic evidence from the Tyndall Stone, Canada: Geobiology, v. 2, p. 21-30.

Gueguen, Y., P. Gavrilenko, and R. M. Le, 1996, Scales of rock permeability: Surveys in geophysics, v. 17, p. 245-263.

Haq, B. U., J. Hardenbol, and P. V. Vail, 1987, Chronology of fluctuating sea levels since the Triassic: Science, v. 235, p. 1156-1167.

Hearst, J. R., P. H. Nelson, and F. L. Paillett, 2000, Well logging for physical properties - a handbook for geophysicists, geologists and engineers: Chichester, John Wiley and sons, 483 p.

Heilbronner, R., 1988, Distortion of orientation data introduced by digitizing procedures: Jounal of Microscopy, v. 149, p. 83-96.

Heilbronner, R., 1992, The autocorrelation function: an image processing tool for fabric analysis: Tectonophysics, v. 212, p. 351-370.

Heilbronner, R., 2000, Automatic grain boundary detection and grain size analysis using polarization micrographs or orientation images: Journal of Structural Geology, v. 22, p. 969-981.

Heilbronner, R., 2002a, Analysis of bulk fabrics and microstructure variations using tesselations of autocorrelation functions: Computers & Geosciences, v. 28, p. 447-455.

Heilbronner, R., 2002b, How to derive size distributions of particles from size distributions of sectional areas, Basel, University of Basel, p. 21.

Heilbronner, R., and D. Bruhn, 1998, The influence of three-dimensional grain size distributions on the rheology of polyphase rocks: Journal of Structural Geology, v. 20, p. 695-705.

Hernandez-Molina, F. J., L. Somoza, J. Rey, and L. Pomar, 1994, Late Pleistocene-Holocene sediments on the Spanish continental shelves: Model for very high

resolution sequence stratigraphy: Journal of marine geology, geochemistry and geophysics, v. 120, p. 129-174.

Isaaks, E. H., and R. M. Srivastava, 1989, Applied Geostatistics: New York, Oxford University Press, 561 p.

Jackson, P. D., P. K. Harvey, M. A. Lovell, D. A. Gunn, C. G. Williams, and R. C. Flint, 1998, Measurement scale and formation heterogeneity: effects on the integration of resistivity data, Core-Log Integration, v. Special Publications 136: London, Geolgical Society, p. 261-272.

Jenkyns, H. C., B. W. Sellwood, and L. Pomar, 1990, A field excursion guide to the island of mallorca: Geologists' Association Guide: London, The geologists' association, 93 p.

Kenter, J. A. M., R. N. Ginsburg, and S. R. Troelstra, 2001, Sea-level-driven sedimentation patterns on the slope and margin, *in* R. N. Ginsburg, ed., Subsurface Geology of a Prograding Carbonate Platform Margin, Great Bahama Bank: Results of the Drilling Project, v. 70: Tulsa, SEPM, p. 61-100.

Kenter, J. A. M., and M. Ivanov, 1995, Parameters controllin acoustic properties of carbonate and volcaniclastic sediments at Sites 866 and 869, *in* J. Winterer, ed., Proceedings of the Ocean Drilling Program: Scientific Results, v. 143, p. 287-303.

Kerans, C., 1988, Karst-Controlled Reservoir Heterogeneity in Ellenburger Group Carbonates of West Texas: AAPG Bulletin, v. 72, p. 1160-1183.

Kerans, C., J. F. Lucia, and R. K. Senger, 1994, Integrated characterization of carbonate ramp reservoirs using permian san andres formation outcrop analogs: AAPG Bulletin, v. 78, p. 181-216.

Khalifah, H., and M. Makkawi, 2002, The impact of data integration on geostatistical porosity modelling: A case study from the Berri Field, Saudi Arabia: Journal of Petroleum Geology, v. 25, p. 485-498.

Lang, H. J., J. Huder, and P. Amann, 2003, Bodenmechanik und Grundbau - Das Verhalten von Boden und Fels und die wichtigsten grundbaulichen Konzepte: Berlin, Springer, 317 p.

Lovell, M. A., P. Harvey, P. D. Jackson, S. Brewer, G. Williamson, and C. G. Williams, 1998, Interpretation of core and log data - integration or calibration?, *in* P. L. Harvey, K., ed., Core-Log Integration, v. 136: London, Geological Society, London, p. 39-51.

Lucia, F. J., C. Kerans, and G. W. Vander-Stoep, 1992, Characterization of a karsted, high-energy, ramp-margin carbonate reservoir; Taylor-Link West San Andres Unit, Pecos County, Texas.: Austin, University of Texas at Austin, Bureau of Economic Geology, 46 p.

Lucia, J. F., 1983, Petrophysical parameters estimated from visual descriptions of carbonate rocks: A field classification of carbonate pore space: Journal of Petroleum Technology, v. 35, p. 629-637.

Lucia, J. F., 1999, Carbonate Reservoir Characterization: Heidelberg, Springer Verlag, 226 p.

Lucia, J. F., C. Kerans, and F. P. Wang, 1994, Fluid-flow characterization of dolomitized carbonate ramp reservoirs; San Andres Formation (Permian) of Seminole Field, and Algerita Escarpment, Permian Basin, Texas and New Mexico, *in* E. L. Stoudt, and P. M. Harris, eds., In: Hydrocarbon reservoir characterization; geologic framework and flow unit modeling., v. SEPM short course 34: Tulsa, SEPM, p. 129-153.

Mace, R. E., and S. D. Hovorka, 2000, Estimating porosity and permeability in a karstic aquifer using core plugs, well tests, and outcrop measurements, *in* I. Sasowsky, and C. Wicks, eds., Groundwater flow and contaminant transport in carbonate aquifers: Rotterdam, Balkema, p. 93-111.

Manfrino, C., and R. N. Ginsberg, 2001, Pliocene to Pleistocene depositional history of the upper platform margin, *in* R. N. Ginsberg, ed., Subsurface Geology of a Prograding Carbonate Platform Margin, Great Bahama Bank: Results of the Bahamas Drilling Project, v. 70: Tulsa, SEPM special publication, p. 17-39.

Maurer, H. R., S. Friedel, D. Jaeggi, and S. Loew, 2004, Geophysical characterization of a coastal aquifer - initial results, Zurich, ETH Zurich, p. 4.

McCreesh, C. A., R. Ehrlich, and S. J. Cabtree, 1991, Petrography and Reservoir Physics II: Relating Thin Section Porosity to Capillary Pressure, the Association Between Pore Types and Throat Size: AAPG Bulletin, v. 75, p. 1563-1578.

Melim, L. A., F. Anselmetti, and G. Eberli, 2001a, The importance of pore type on permeability of neogene carbonates, Great Bahama Bank, *in* R. N. Ginsburg, ed., Subsurface Geology of a Prograding Carbonate Platform Margin, Great Bahama Bank: Results of the Bahamas Drilling Project, v. 70: Tulsa, SEPM Special Publication, p. 217-238.

Melim, L. A., P. K. Swart, and G. Eberli, 2004, Mixing-zone diagenesis in the subsurface of Florida and the Bahamas: Jounal of Sedimentary Research, v. 74, p. 904-913.

Melim, L. A., P. K. Swart, and R. G. Maliva, 2001b, Meteoric and marine-burial diagenesis in the subsurface of Great Bahama Bank, *in* R. N. Ginsburg, ed., Subsurface Geology of a Prograding Carbonate Platform Margin, Great Bahama Bank: Results of the Bahamas Drilling Project, v. 70: Tulsa, SEPM Special Publication, p. 137-161.

Molz, F. J., R. H. Morin, A. E. Hess, J. G. Melville, and O. Guven, 1989, The impeller meter for measuring aquifer permeability variations; evaluation and comparison with other tests: Water Resources Research, v. 25, p. 1677-1683.

Montgomery, S. L., 1996, Cotton Valley Lime Pinnacle Reef Play: Branton Field: AAPG Bulletin, v. 80, p. 617-629.

Montgomery, S. L., R. Karlewicz, and D. Ziegler, 1999, Upper Jurassic Reef Play, East Texas Basin: An updated overview Part 2 - inboard trend: AAPG Bulletin, v. 83, p. 869-888.

Montoto, M., 2004, Petrophysics at the rock matrix scale: hydraulic properties and petrographic interpretation: publicaciones tecnicas: Madrid, Enresa, 297 p.

Muldoon, M. A., J. A. Simo, and K. R. Bradbury, 2001, Correlation of hydraulic conductivity with stratigraphy in a fractured-dolomite aquifer, northeastern Wisconsin, USA: Hydrogeology Jounal, v. 9, p. 570-583.

Mylroie, J. E., and J. L. Carew, 2003, Karst development on carbonate islands: Speleogeneisis and Evolution of Karst Aquifers, v. 1, p. 1-21.

Nelson, P. H., 1994, Permeability-porosity relationships in sedimentary rocks: The Log Analyst, p. 38-62.

Pézard, P., P. Gaillot, Y. Maria-Sube, P. Gouze, and G. Lotz, 2004, Quantification of Meso-Scale Porosity From Borehole Wall Images. Example From the ALIANCE Campos Experimental Site, Mallorca, Spain.: Eos Trans. AGU Fall meeting.

Pomar, L., 1991, Reef geometries, erosion surfaces and high-frequency sea-level changes, upper Miocene reef complex, Mallorca, Spain.: Sedimentology, v. 38, p. 243-269.

Pomar, L., 1993, High resolution sequence stratigraphy in prograding miocene carbonates: Application to seismic interpretation: AAPG Bulletin, v. 57, p. 389-407.

Pomar, L., 2001a, Ecological control of sedimentary accommodation: evolution from a carbonate ramp to rimmed shelf, Upper Miocene, Balearic Islands: Palaeo, v. 175, p. 249-272.

Pomar, L., 2001b, Types of carbonate platforms: a genetic approach: Basin Research, v. 13, p. 313-334.

Pomar, L., M. Brandano, and H. Westphal, 2004a, Environmental factors influencing skeletal grain sediment associations: a critical review of Miocene examples from the western Mediterranean: Sedimentology, v. 51, p. 627-651.

Pomar, L., M. Esteban, F. Calvet, and A. Baron, 1983, La unidad arrecifal del mioceno superior de mallorca, El terciario de las Baleares (Mallorca-Menorca) Guia de las excursiones X congresso nacional de sedimentologia: Menorca, grupo espanol de sedimentologia, p. 139-175.

Pomar, L., and W. C. Ward, 1995, Sea-Level Changes, Carbonate Production and Platform Architecture: The Llucmajor Platform, Mallorca, Spain, *in* B. U. Haq, ed., Sequence Stratigraphy and Depositional Response to Eustatic, Tectonic and Climatic Forcing, Kluwer Academic, p. 87-112.

Pomar, L., and W. C. Ward, 1999, Reservoir-Scale Heterogeneity in Depositional Packages and Diagenetic Patterns on a Reef-Rimmed Platform, Upper Miocene, Mallorca, Spain: AAPG Bulletin, v. 83, p. 1759-1773.

Pomar, L., W. C. Ward, and D. G. Green, 1996, Upper Miocene reef complex of the Llucmajor area, Mallorca, Spain, Models for carbonate stratigraphy from Miocene reef complexes of Mediterranean regions, v. 5: Tulsa, SEPM, p. 191-225.

Pomar, L., H. Westphal, and A. Obrador, 2004b, Oriented calcite concretions in Upper Miocene carbonate rocks of Menorca, Spain; evidence for fluid flow through a heterogeneous porous system: geologica acta, v. 2, p. 271-284.

Price, R. M., and J. S. Herman, 1991, Geochemical investigation of salt-water intrusion into a coastal carbonate aquifer: Mallorca, Spain: Geological Society of America Bulletin, v. 103, p. 1270-1279.

Renssen, H., and R. F. B. Isarin, 2001, Data-model comparison of the Younger Dryas event; discussion.: Canadian Journal of Earth Sciences, v. 38, p. 477-478.

Russell, S. D., M. Akbar, B. Vissapragada, and G. M. Walkden, 2002, Rock types and permeability prediction from dipmeter and image logs: Shuaiba reservoir (Aptian), Abu Dhabi: AAPG Bulletin, v. 86, p. 1709-1732.

Saller, A. H., J. A. D. Dickson, and F. Matsuda, 1999, Evolution and Distribution of Porosity Associated with Subaerial Exposure in Upper Paleozoic Platform Limestones, West Texas: AAPG Bulletin, v. 83, p. 1835-1854.

Serra, O., 1984, Fundamentals of well-log interpretation, 1. The acquisition of logging data: Amsterdam, Elsevier, 423 p.

Stafleu, J., A. Everts, and J. A. M. Kenter, 1994, Seismic models of a prograding carbonate platform; Vercors, South-east France: Marine and Petroleum Geology, v. 11, p. 514-527.

Teutsch, G., 1991, An extended double-porosity concept as a practical modelling approach for a karstified terrain, *in* G. Gunay, A. I. Johnson, and W. Back, eds., Hydrogeological processes in karst terranes.: IAHS-AISH Publication, v. 207: [Louvain], International, International Association of Hydrological Sciences, p. 281-292.

Tiab, D., and E. C. Donaldson, 2004, Petrophysics, Gulf Professional Publishing, 881 p.

Tsourlos, P., R. Ogilvy, P. Meldrum, and G. Williams, 2003, Time-lapse monitoring in single boreholes using electrical resistivity tomography.: Journal-of-Environmental-and-Engineering-Geophysics., v. 8, p. 1-14.

Underwood, E. E., 1970, Quantitative stereology: Philippines, Addison Wesley, 274 p.

Van der Berg, E. H., V. F. Bense, and W. Schlager, 2003, Assessing textural variations in laminated sands using digital image analysis of thin sections: Journal of sedimentary research, v. 73, p. 133-143.

Van Meir, N., D. Jaeggi, M. Herfort, S. Loew, P. Pezard, P. Gouze, and G. Lods, 2005, Development of a European test site in a coastal limestone aquifer at Campos (Mallorca, Spain), *in* L. Araguás, E. Custodio, and M. Manzano, eds., Groundwater and saline intrusion. Selected papers from the 18th Salt Water Intrusion Meeting.: Hidrogeología y aguas subterráneas, v. 15: Madrid, Instituto geológico y minero de España.

Warzeski, E. R., L. A. Melim, and R. N. Ginsburg, 2001, Geophysical log responses to variations in lithology in borings clino and unda, Great Bahama Bank, *in* R. N.

Ginsberg, ed., Subsurface Geology of a Prograding Carbonate Platform Margin, Great Bahama Bank: Results of the drilling project, v. 70, p. 189-192.

White, W. B., 2003, Conceptual models for karstic aquifers: Speleogeneisis and Evolution of Karst Aquifers, v. 1, p. 1-6.

Wilkens, R. H., G. F. Fryer, and J. Karsten, 1991, Evolution of porosity and seismic structure of upper oceanic crust; importance of aspect ratios: Journal of geophysical research, v. 96, p. 17981-17995.

Worthington, P. F., 1998, Conjunctive interpretation of core and log data through association of the effective and total porosity models, Core-Log Integration, v. Special Publications 136: London, Geolgical Society, p. 213-223.

Worthington, P. F., D. C. Ford, and J. D. Gareth, 1999, Quantification of matrix, fracture and channel contributions to storage and flow in a Paleozoic carbonate, *in* C. a. S. Wicks, I., ed., Approaches to understanding groundwater flow and contaminant transport in carbonate aquifers, Geological Society of America, p. 113-128.

Worthington, S. R. H., 2003, A comprehensive strategy for understanding flow in carbonate aquifer: Speleogeneisis and Evolution of Karst Aquifers, v. 1, p. 1-8.

Worthington, S. R. H., and D. C. Ford, 1997, Borehole tests for megascale channeling in carbonate aquifers: Proceedings of the 12th International Congress of Speleology, p. 195-198.

H)   Curriculum Vitae

David Jaeggi

Dipl. Geologe ETH
Ringmatt 120
5063 Wölflinswil
SWITZERLAND

Phone: +41 (0)62 877 14 14

Email: dj@pnpmu.ch

Personal Details

Date of Birth	September 2nd 1974
Nationality	Swiss (Mümliswil-Ramiswil, SO)

Education

2001 to 2005	Swiss Federal Institute (ETH) (www.ethz.ch)
	Engineering Geology, ETH Hönggerberg, (www.erdw.ethz.ch)
	PhD-student
2000 to 2001	Dr. von Moos AG, Zürich (www.geovm.ch)
	Consultant in geotechnics, tunnelling, hydrogeology and waste repository
1995 to 2000	Swiss Federal Institute (ETH), (www.ethz.ch)
	Study in earth science
1991 to 1995	Alte Kantonsschule Aarau (www.alte-kanti-aarau.ch)
	Maturity type C

Language Skills

German	mother tongue
English	fluent in speaking and writing
French	fluent in speaking, medium experience in writing
Spanish	intermediate

Practical Experience

July 04	Image Analysis in Earth Sciences and Optical Orientation Imaging, course given by R. Heilbronner at University of Basel (Switzerland)
June 03	Sequence Stratigraphy and Carbonate Platforms (with a special emphasis on the Llucmajor Platform), course given by L. Pomar and B. Haq in Palma de Mallorca (Spain)
Mai – Okt. 02 & 03	Site geologist and supervisor for the Aliance-(Advanced logging investigations of aquifers in coastal environments) drilling campaign on Mallorca (Spain)
Jan. 02	Gemcom for Windows, course given by M. Polliand at University of Geneva (Switzerland)
April 00 – Oct. 01	Consultant at Dr. von Moos AG in Zürich with skills in geotechnics, tunnelling, hydrogeology and waste repository (Switzerland)
Aug. 99	Term paper including extensive field work about the groundwater situation of a pumping station near Bubendorf, Baselland in collaboration with ETH Zürich and Pfirter, Nyfeler & Partner AG in Muttenz (Switzerland)
Sept. 98	1 month traineeship at Pfirter, Nyfeler & Partner AG in Muttenz (Switzerland)